

Optimizing Covalent Immune Recruiter Antibody Labelling Kinetics with Sulfur Fluoride
Exchange Chemistry

Sarah Eisinga, Anthony Rullo*

Department of Chemistry and Chemical Biology & Department of Medicine,
McMaster University

August 9th, 2022

McMaster University

© Copyright by Sarah Eisinga, August 2022

Abstract

Covalent antibody recruiting molecules (cARMs) are synthetic chemical tools that direct antibodies naturally present in human serum to tumor receptors leading to immune recognition and elimination. cARMs have three general features: an antibody binding domain (ABD), an antibody labelling domain (ALD), and a tumor binding domain. Proximal to the ABD, the ALD contains an electrophilic group which is attacked by a nucleophilic amino acid residue on the target antibody upon cARM binding. Previous cARMs use an acyl-imidazole (AL) ALD to successfully covalently recruit anti-dinitrophenyl IgG validated via fluorescence SDS-PAGE, and form immune complexes with PSMA+ HEK cells in ADCP flow experiments.¹ Through MS analysis, AL cARMs were demonstrated to target lysine-59 of antiDNP.¹ Problematically, there are several properties associated with AL chemistry that limit the therapeutic potential of associated cARMs. These limitations include limited stability *in vivo*, single amino acid (lysine) selectivity, and modest intramolecular protein labelling rates (10^{-5} s^{-1}).¹ To target novel antibody residues and possibly improve the rate of antibody labelling, a second generation of cARMs has been developed using sulfur fluoride exchange (SuFEx) chemistry as the ALD. Sulfur fluorides have been broadly used in academic and industrial applications due to intrinsically high stability and broad amino acid reactivity.² SuFEx cARMs are hypothesized to have enhanced hydrolytic stability compared to AL cARMs. This thesis explores the synthesis, stability, binding, and labeling kinetics of SuFEx cARMs to advance cARM design and development for *in vivo* applications. This research contributes collectively to the design and development of novel therapeutics in chemical biology and immune-oncology research.

Acknowledgements

I would like to thank Dr. Anthony Rullo for his support and mentorship during my graduate studies. I am grateful for the time and effort he has put into my project over the past two years, and for the opportunity to work in his laboratory.

Thank you to members of the Rullo lab who supported me in my journey: Rebecca Turner, Sissi Yang, Akshaya Raajkumar, Harrison McCann, Eden Kapcan, Benjamin Lake, and Nick Sernuick. A special thanks to Mateo Vendramini who helped as an undergraduate student on my project for 8 months and made wonderful contributions to my thesis.

Thank you, Dr. Giuseppe Melacini & Dr. Sara Andres for your input and guidance as committee members during my graduate studies.

Table of Contents

<i>Abstract</i>	<i>ii</i>
<i>Acknowledgements</i>	<i>iii</i>
<i>List of Figures</i>	<i>vi</i>
<i>List of Tables</i>	<i>ix</i>
<i>List of Abbreviations</i>	<i>x</i>
1.0 Introduction	1
1.1 Immunotherapy	1
1.2 Tumor immunotherapeutic function of antibodies	1
1.3 Antibody recruiting molecules	3
1.4 Covalent immune recruitment	5
1.5 Important kinetic parameters for CIR binding.....	7
1.6 Effective Molarity	8
1.7 Conditions for Covalent Immune Recruitment	10
1.8 Sulfur Fluoride Exchange.....	11
1.9 Relevance of SuFEx in chemical biology	14
2.0 Overall objectives	16
2.0 Synthesis & Stability of SuFEx cARMs	17
2.1 Objectives	17
2.2 Results	18
2.2.1 Synthesis.....	18
2.2.2. Hydrolytic Stability.....	20
2.3 Discussion	24
3.0 Kinetics of SuFEx cARMs	28
3.1 Objectives	28
3.2 Results	28
3.2.1. Intramolecular labelling	28
3.2.2. Intermolecular labelling	31
3.3 Discussion.....	33
3.3.1. Pseudo-first order conditions	33
3.3.2. Intramolecular rate constants.....	35

3.3.3. Second-order rate constants	39
3.3.4. Intermolecular rate constants	40
<i>4.0 Peptide Mapping of SuFEx cARMs</i>	<i>43</i>
4.1 Objectives	43
4.2 Results	44
4.2.1. Top-down analysis	44
4.2.2. Bottom-up analysis.....	47
4.3 Discussion.....	51
4.3.1 Preparation of MS samples.....	51
4.3.2 Top-down analysis	52
4.3.3 Bottom-up analysis.....	54
<i>5.0 Conclusion</i>	<i>59</i>
5.1.1 Future directions	60
<i>6.0 References</i>	<i>63</i>
<i>7.0 Appendix.....</i>	<i>67</i>
<i>8.0 Supplemental.....</i>	<i>70</i>
8.1 Synthesis.....	70
8.2 Hydrolytic Stability	140
8.2 Mass Spectrometry	143
8.2.1 Sample calculations	144
8.3 SDS-PAGE.....	146
8.3.1 Intramolecular rate constants.....	147
8.3.2. Intermolecular rate constants.....	153

List of Figures

Figure 1. General structure and composition of an antibody.	3
Figure 2. Fc-dependent mechanisms of cell death facilitated by components of the innate immune system. ¹⁰	3
Figure 3. Non-covalent antibody recruiting mechanism. ¹	5
Figure 4. Mechanism of covalent antibody labelling with acyl-imidazole cARMs.	6
Figure 5. Enzymatic inhibition mechanisms ¹⁶	7
Figure 6. Observed labelling rate equation ¹⁶	8
Figure 7. Effective molarity of a biomolecular interaction ¹⁷	9
Figure 8. Effective molarity study of kinase-substrate complex ¹⁹	10
Figure 9. Bio-orthogonal protein labelling strategies. ²¹	11
Figure 10. Classification of sulfur fluorides.	12
Figure 11. Mechanisms of covalent antibody labelling with sulfur fluoride cARMs.	12
Figure 12. Formation of bifluoride ion from SuFEx reaction ²²	13
Figure 13. Chemical cross-linker NHSF. ²⁸	15
Figure 14. General design of SuFEx cARMs.	18
Figure 15. Structure of prostate specific SuFEx cARMs.	19
Figure 16. General scheme used to synthesize fluorescent SuFEx cARMs.	19
Figure 17. Hydrolytic stability test of SuFEx cARMs via ¹⁹ F NMR.	21
Figure 18. Integrations of fluorine peaks for sCIR1 glutamate derivatives over time.	22
Figure 19. Hydrolytic stabilities of sulfur fluoride probes. ³⁰	25
Figure 20. Resonance structures of aromatic sulfonyl fluorides.	26
Figure 21. Fluorescent intensities of sCIR1-5fluor incubated with SPE7 Fab.	29
Figure 22. Fluorescent of sCIR1-3fluor and acyl-imidazole CIR incubated with SPE7 Fab.	29
Figure 23. Fluorescence of sCIR1-5 fluorophores incubated with BSA for 24-120 hours.	33
Figure 24. Pseudo first-order assumption of labelling rates ³⁴	34
Figure 25. Acceleration of covalent inhibition by sulfonyl fluoride inhibitor targeting HSP72. ³⁵	37
Figure 26. First-order labelling constants of sulfonyl fluoride probes. ³⁶	38
Figure 27. Comparison of SuFEx and acyl-imidazole labelling domains of cARMs.	39

Figure 28. Second-order rate constant of various click chemistries in current literature. ²¹	40
Figure 29. Liquid-chromatography mass-spectrometry of deglycosylated forms of antiDNP incubated with sCIR4fluor for 24 hours.....	44
Figure 30. Peak intensities of mass species of antiDNP conjugated with sCIR4fluor.	45
Figure 31. Liquid-chromatography mass-spectrometry of deglycosylated forms of antiDNP incubated with sCIR5fluor for 96 hours.....	45
Figure 32. Peak intensities of intact mass species in sCIR5fluor conjugated sample.....	46
Figure 33. Identification of post-translation modification by sCIR4fluor on antiDNP.	48
Figure 34. Peptide mapping of sCIR4-Fab sample.....	48
Figure 35. Identification of post-translation modification by sCIR5fluor on antiDNP.	49
Figure 36. Peptide mapping of sCIR5-Fab sample.....	50
Figure 37. Auto-docking of acyl-imidazole CIR with antiDNP SPE7 (PBD 1O AQ). ¹	55
Figure 38. Structure of fluorescent acyl-imidazole CIR, sCIR4, and sCIR5.	56
Figure 39. Pymol structure of antiDNP SPE7 (1O AU) with key residues for CIR binding.	57
Figure 40. Mechanism of covalent antibody labelling with N-acyl-N-sulfonamide cARM.	60
Figure 41. Mechanism of covalent antibody labelling with azirine cARM.	61
Figure 42. Bi-specific labelled antibody with AL and SuFEx cARM.....	62
Figure 43. Comparison of top down and bottom-up approaches for post-translational modification analysis. ⁵¹	67
Figure 44. Ligation of tetrazine and trans-cyclooctene functional groups. ³⁷	68
Figure 45. Incubation of sCIR4fluor with isotype IgG and antiCD38.	68
Figure 46. Blank runs on orbitrap LC-MS.	69
Figure 47. LC-MS analysis and sample calculations for the heavy chain of sCIR4fluor sample after reduction.....	144
Figure 48. LC-MS analysis and sample calculations for the light chain of sCIR4fluor sample after reduction.....	144
Figure 49. LC-MS analysis and sample calculations for the heavy chain of sCIR5fluor sample after reduction.....	145
Figure 50. LC-MS analysis and sample calculations for the light chain of sCIR5fluor sample after reduction.....	145

Figure 51. Fluorescent and protein bands of SPE7 Fab incubated with sCIR1.....	147
Figure 52. Fluorescent and protein bands of SPE7 Fab incubated with sCIR2.....	148
Figure 53. Fluorescent and protein bands of SPE7 Fab incubated with sCIR3.....	149
Figure 54. Pre-treatment of DNP-gly with sCIRfluor 1-3 and SPE7 Fab.	150
Figure 55. Fluorescent and protein bands of SPE7 Fab incubated with sCIR4.....	150
Figure 56. Fluorescent and protein bands of SPE7 Fab incubated with sCIR5.....	151
Figure 57. Relative fluorescent units of sCIR3 samples incubated with SPE7 Fab over 24 hours.	152
Figure 58. Fluorescent and protein bands of SPE7 Fab incubated with CIR3AL.	152
Figure 59. Fluorescent and protein bands of BSA incubated with sCIR1.....	153
Figure 60. Fluorescent and protein bands of BSA incubated with sCIR2.....	154
Figure 61. Fluorescent and protein bands of BSA incubated with sCIR3.....	155
Figure 62. Fluorescent and protein bands of BSA incubated with sCIR4.....	156
Figure 63. Fluorescent and protein bands of BSA incubated with sCIR5.....	157

List of Tables

Table 1. Preparation of sCIRs for fluorine-stability studies.....	20
Table 2. Half-life of SuFEx cARMs from hydrolytic stability studies.	23
Table 3. Pseudo-first order labelling rates of antibody labelling from SDS-PAGE studies.....	30
Table 4. Intermolecular rate constants of sCIRfluors.....	33
Table 5. Preparation of sCIRs for hydrolytic stability studies.....	140
Table 6. Integration of Fluorine Peaks for sCIR1 stability.....	141
Table 7. Integration of Fluorine Peaks for sCIR2 stability.....	141
Table 8. Integration of Fluorine Peaks for sCIR3 stability.....	142
Table 9. Integration of Fluorine Peaks for sCIR4 stability.....	142
Table 10. Integration of Fluorine Peaks for sCIR5 stability.....	142
Table 11. Relative fluorescence units of sCIR1fluor samples incubated with SPE7 Fab over 24 hours.....	147
Table 12. Relative fluorescent units of sCIR2 samples incubated with SPE7 Fab over 24 hours.....	148
Table 13. Relative fluorescent units of sCIR3 samples incubated with SPE7 Fab over 24 hours.....	149
Table 14. Relative fluorescent units of sCIR4 samples incubated with SPE7 Fab over 24 hours.....	151
Table 15. Relative fluorescent units of CIR3AL samples incubated with SPE7 Fab over 24 hours.....	152
Table 16. Relative fluorescent units of sCIR1 samples incubated with BSA over 24 hours... ..	153
Table 17. Relative fluorescent units of sCIR2 samples incubated with BSA over 24 hours... ..	154
Table 18. Relative fluorescent units of sCIR3 samples incubated with BSA over 24 hours... ..	155
Table 19. Relative fluorescent units of sCIR4 samples incubated with BSA over 24 hours... ..	156
Table 20. Relative fluorescent units of sCIR5 samples incubated with BSA over 24 hours... ..	157

List of Abbreviations

ABD	antibody binding domain
AL	acyl-imidazole
ALD	antibody labelling domain
ARM	antibody recruiting molecule
ACN	acetonitrile
ADCC	antigen dependent cellular cytotoxicity
ADCP	antigen dependent cellular phagocytosis
BSA	bovine serum albumin
cARM	covalent antibody recruiting molecule
CIR	covalent immune recruiter
DNP	dinitrophenyl
DMF	dimethylformamide
DMSO	dimethyl sulfoxide
FA	formic acid
Fab	fragment antigen binding
Fc	fragment crystallizable
FcR	Fc receptor
FcγRIIA	
Fv	fragment variable
GUL	glutamate urea lysine
HEK	human embryonic kidney 293 cells
IgG	immunoglobulin G
mAb	monoclonal antibody
MW	molecular weight
SDS-PAGE	sodium dodecyl sulfate-polyacrylamide gel electrophoresis
SuFEx	sulfur fluoride exchange
SF	sulfonyl fluoride
FS	fluorosulfate
PSMA	prostate specific membrane antigen
SuFEx	sulfonyl fluoride exchange
TBD	tumor binding domain

1.0 Introduction

1.1 Immunotherapy

There are a variety of factors that contribute to cancer development and progression including cellular proliferation, resistance to cell death, metastasis, and evasion of immune signalling cascades³. Developing effective therapies to selectively target and killing cancer cells is particularly challenging when translating basic research into clinical practices, as an ideal therapeutic typically exhibits high potency and minimal off-target effects⁴. The idea to leverage the immune system to target growing malignancies wasn't proposed until the 1980's when the first vaccine was developed against hepatitis B⁵. Since then, researchers have developed a variety of immunotherapies using vaccines, viruses, antibodies, and T-cells. These therapies exploit a mechanism or function of the adaptive immune system, while targeting an over-expressed or unique tumor receptor/antigen. Over the past two decades, one class of immunotherapy that has grown exponentially in market value is monoclonal antibodies (mAbs). mAbs are engineered proteins that affected targeted cancer cell death through several mechanisms that include recruitment of host immune cells to the tumor site. There are currently 80 clinically approved mAbs, used to treat a variety of cancers including non-Hodgkin's lymphoma, neuroblastoma, multiple myeloma, and breast cancer.⁶

1.2 Tumor immunotherapeutic function of antibodies

The structure of both endogenous and artificial antibodies plays a crucial role in immune cell engagement and the induction of cell-death pathways. There are five naturally occurring immunoglobulin isotypes, each composed of two smaller domains stemming from a longer domain resembling the shape of a Y (Figure 1). The smaller domains are variable regions (Fv) which contain a sequence that is highly specific to an epitope on its targeted antigen. These fragments,

also known as Fabs, are composed of heavy and light chains that mediate antigen binding. The second domain of the antibody is the constant fragment (Fc) which regulates interactions with immune cells through Fc receptors. Antibodies initiate cell death through this interaction by inducing one of three mechanisms (Figure 2): antibody-dependent cellular phagocytosis/cytotoxicity (ADCP/ADCC) or complement-dependent cytotoxicity (CDC)⁷. In ADCP, the Fc of the antibody is targeted by CD32A/CD64, Fc-gamma receptors expressed on a monocyte, macrophage, or dendritic cell. This induces a signalling pathway which causes the cell to undergo phagocytosis of the targeted cell. In ADCC, cell death is induced through the release of cytotoxic granules through interaction of CD16A ligands on natural killer cells which engages the Fc of the target antibody. CDC involves activating the complement pathway, a component of the innate immune system. This response is orchestrated through immobilization of complement proteins to the target antigen expressed on the cell surface or through an opsonizing antibody bound to the antigen. Engagement of complement proteins activates a proteolytic cascade, which ultimately leads to cell death via phagocytosis, lysis of the cell membrane, or recruitment of inflammatory molecules.⁸ In addition to these effector mechanisms, mAbs can induce cell death by blocking receptor binding and/or dimerization of their target receptors. For example, epidermal growth factor receptor plays a key role in the homeostasis of cell growth and proliferation. EGFR is over-expressed on a variety of tumor cells and initiates a cascade through receptor dimerization that leads to loss of cell differentiation, angiogenesis, and cancer cell survival by blocking apoptosis.⁹

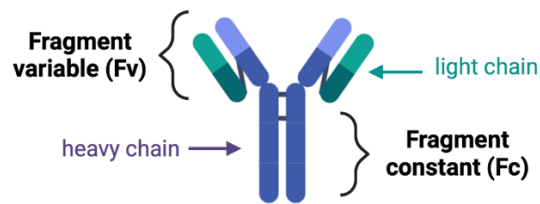


Figure 1. General structure and composition of an antibody. Light chains are coloured in green and heavy chains are coloured in purple.

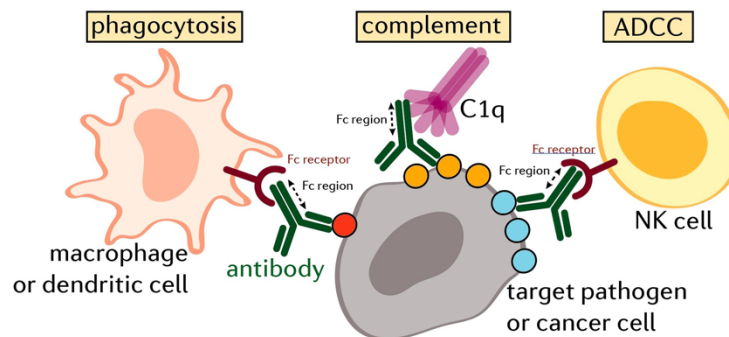


Figure 2. Fc-dependent mechanisms of cell death facilitated by components of the innate immune system.¹⁰

Although mAbs represent one of the fastest growing therapeutic platforms, they are associated with key limitations that arise in part due to their structure and molecular weight. In some cases, life-threatening inflammatory responses can occur if a portion of the antibody's protein sequence is identified as "non-self"¹¹. Furthermore, F_c receptor expression varies between individuals which can change the efficacy of the administered antibody. Due to their high molecular weight, mAb have limited ability to cross the intestinal epithelium which significantly limits oral bioavailability administration¹². In addition to these barriers, mAb administration requires large doses by continuous infusion at the bedside, coupled with tumor trafficking complications from the site of administration.

1.3 Antibody recruiting molecules

As an alternative to monoclonal antibody immunotherapeutics, organic chemists have developed a small molecule strategy which leverages the recruitment of endogenous antibodies in human serum to selectively kill cancer cells. These small molecules, known as antibody recruiting molecules (ARMs), offer many advantages including an easier and more cost-effective preparation over manipulation of vaccines or antibody-based therapies.¹³ Furthermore, ARMs are easy to administer and nonimmunogenic unlike mAbs which have caused hypersensitivity issues.¹³

Over the past decade, researchers have developed ARMs that target a broad range of endogenous antibodies and tumor receptors. The most common antibody epitopes used for ARMs include 2,4-dinitrophenyl (DNP), and carbohydrates L-Rhamnose and alpha-gal¹¹. DNP is one the easiest to incorporate synthetically in ARM design, as the starting material is commercially available, inexpensive, and easier to manipulate in comparison to carbohydrate derivatives. Although the origin of DNP epitope is unknown, it is proposed approximately 1% of antibodies in human serum recognize nitroarene groups¹². For the tumor binding domain, ARMs have been developed to target the urokinase receptor, prostate-specific membrane antigen (PSMA), vascular endothelial growth factor, folate receptor and integrins.

Most ARMs are designed with two domains which facilitate antibody recruitment and tumor cell-killing. Due to the high abundance of the targeted antibody in serum, the first binding event to occur is between the Ab and the antibody-binding domain (ABD) of the ARM. The ARM-Ab complex then localizes to a specific tumor receptor guided by the tumor binding domain (TBD) of the ARM. When the ARM is attached to both its Ab and tumor target, cell death is induced through ADCP or ADCC. Initially, these molecules were designed to bind non-covalently to their

antibody target, imposing a minimal four-partner binding equilibrium for cell death to occur. Achieving maximal quaternary formation is unfortunately challenging *in vivo* as endogenous antibody concentrations can be quite low, requiring the affinity of the ARM to be very high (pM-nM)¹. Additionally, the non-covalent complex is highly susceptible to dissociation that cannot be recovered by increasing ARM concentration due to simultaneous occupancy of both antibody and tumor binding sites by separate ARMs inducing autoinhibition (Figure 3).

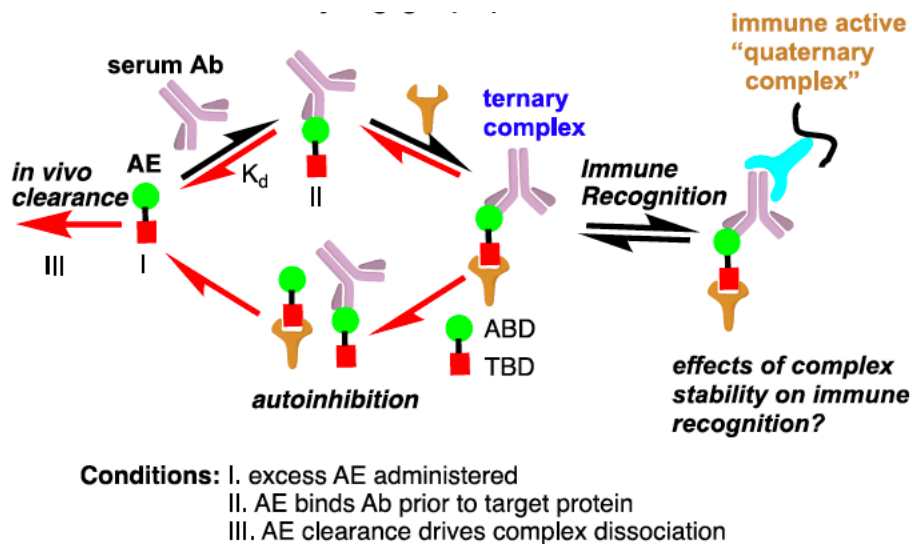


Figure 3. Non-covalent antibody recruiting mechanism.¹

Ternary complex formation of antibody engager (AE) and serum antibody (Ab). Autoinhibition occurs when excess AE is administered driving dissociation.

1.4 Covalent immune recruitment

In efforts to simplify quaternary complex formation and enhance antibody recruitment to the tumor cell surface, the Rullo lab has developed covalent ARMs (cARMs), *i.e.*, ARMs that covalently bind to their Ab target (Figure 4). cARMs were designed with three domains: an antibody-binding domain (blue star), an antibody labelling domain (green circle), and a tumor binding domain (purple square). In the first step of the mechanism, the ABD guides the cARM

to the endogenous antibody in human serum through a conserved recognition site on the target antibody. At this point a nucleophilic residue close to the ALD, attacks the electrophilic group forming a covalent bond between the cARM and antibody. The cARM-Ab complex is then directed to a tumor receptor via the binding ligand on the TBD.

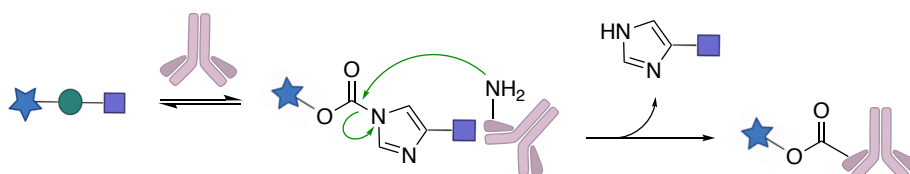


Figure 4. Mechanism of covalent antibody labelling with acyl-imidazole cARMs.

Adapted from *ACS Chem. Biol.* 2020, 15, 4, 1089–1095.

An acyl-imidazole (AL) moiety was the first reactive chemistry used in the synthesis of cARMs and was found to label lysine 59 of a monoclonal dinitrophenyl-specific antibody (anti-DNP)¹. The SPE7 antibody is an immunoglobulin E protein which has a well-defined recognition site for 2,4-dinitrophenyl.¹⁴ These molecules successfully labelled anti-DNP with a pseudo intramolecular rate constant of $8.1 \times 10^{-4} \text{ s}^{-1}$ and induced ADCP/ADCC of PSMA-positive HEK cells. While these results are extremely promising as a proof of concept of the cARM platform, acyl-imidazole cARMs were found to be hydrolytically labile with stability half-lives on the orders of hours.¹ Preliminary *in vivo* studies conducted in the Rullo lab have posed significant challenges due to hydrolysis of the acyl-imidazole group which led to autoinhibition of the cARM. In addition to intrinsic stability, AL chemistry limits the cARM platform due to its modest reaction rates and its selective nature for lysine residues which may not be present close to the target immune receptor/antibody binding site. Literature reports on acyl-imidazole labeling kinetics show second-order rate constant on the order of $10^1 \text{ M}^{-1}\text{s}^{-1}$, which is 10-1000 times slower than other labelling chemistries such as tosylate and N-acyl-N-alkyl sulfonamide chemistry.¹⁵ Fast

labelling kinetics is critical in maximizing the number of cARM-Ab complexes that bind with their targeted tumor receptor.

1.5 Important kinetic parameters for CIR binding

Current cARMs form an irreversible covalent bond with the target antibody, with reaction rates that can be described using established enzyme inhibition kinetic models. Since enzymatic inhibition involves irreversible bond formation, many kinetic parameters used to describe an inhibitor can also be used to describe a small molecule that covalently binds to a protein. However, not all protein binding constants can be used to describe an enzyme-inhibitor relationship. Covalent bond formation may occur in a one or two step mechanism (Figure 5), with the latter involving the formation of a non-covalent complex before an irreversible bond is formed.¹⁶

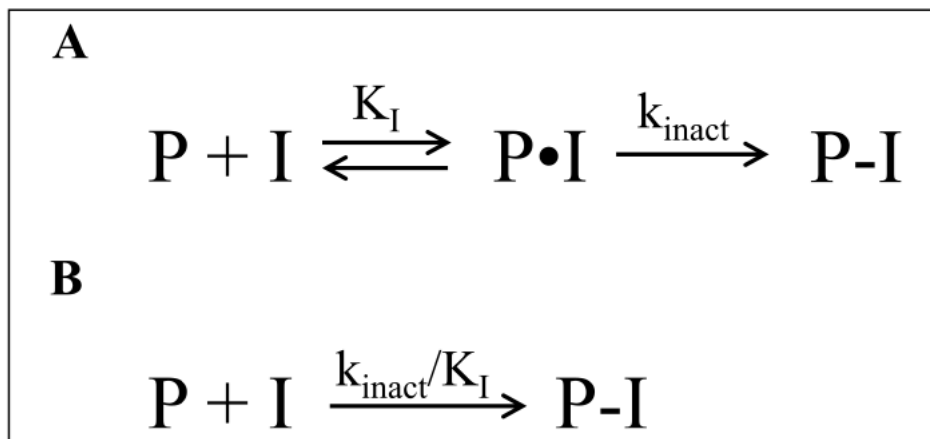


Figure 5. Enzymatic inhibition mechanisms¹⁶

P = target protein, I = inhibitor, P-I = covalent bond, P•I = reversible protein complex

In enzymatic inhibition, K_i and k_{inact} are important terms used to describe the efficiency and potency of an inhibitor.¹⁶ In a two-step enzymatic mechanism, the first binding event is the reversible complex formed between a target protein (P) and the inhibitor (I). The inhibitor

constant (K_i) is defined as the concentration required to achieve half maximal inhibition of the enzyme (k_{inact}).¹⁶ k_{inact} is a first-order rate constant with units of inverse time, which describes the covalent binding event of the inhibitor to the enzyme. In general, the higher k_{inact} is, the better the inhibitor. The efficiency of inhibition or covalent bond formation is described by the second-order rate constant, k_{inact}/K_i . With units of $M^{-1}s^{-1}$, this second-order rate constant is helpful in describing the potency of an inhibitor towards its intended target. The equation in Figure 6 describes the relationship between k_{inact} , K_i , and the observed labelling rate (k_{obs}) at a given concentration of inhibitor (I).¹⁶

$$k_{obs} = \frac{k_{inact} + [inhibitor]}{K_I + [inhibitor]}$$

Figure 6. Observed labelling rate equation¹⁶

The most relevant kinetic terms for CIR-Ab binding are the dissociation constant (K_D) and the rate of intramolecular labeling reaction (k_{intra}). K_D is used in protein dynamics to describe the affinity of a protein for its ligand. The smaller the K_D , the higher the binding affinity. For cARMs, covalent bond formation occurs intramolecularly via a two-step mechanism, with the formation of a non-covalent complex prior to the irreversible reaction. The first binding event of the cARM is guided by the affinity of the ABD to a known DNP-recognition site on anti-DNP. In 2020, this value was approximated at 63.6 nM.¹ Covalent modification ultimately occurs via irreversible intramolecular attack of a nucleophilic residue on anti-DNP to the ALD of the cARM.

1.6 Effective Molarity

Effective molarity is a term used to describe the enhancement of a bimolecular reaction between its intramolecular rate and intermolecular rate.¹⁷ To accelerate the speed at which a protein binds to its ligand, two species (grey circle and purple triangle in Figure 7) can be brought closer together in the right orientation through a linker (see arrow). This linker can increase the speed and spontaneity of a reaction, favourable for efficient and high yielding protein labelling strategies.¹⁸ cARMs are designed to covalently label anti-DNP in an intramolecular reaction which is facilitated by the association of the ABD to the DNP-binding site of anti-DNP. By bringing the small molecule near the target antibody, covalent bond formation is expedited. In a covalently tethered kinase system (Figure 8), the reaction rate was optimized with a four-residue linker between the kinase and SpyTag.¹⁹

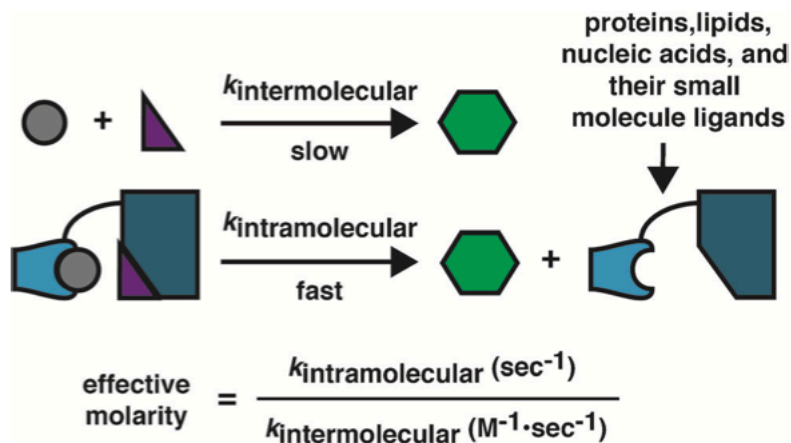


Figure 7. Effective molarity of a biomolecular interaction¹⁷

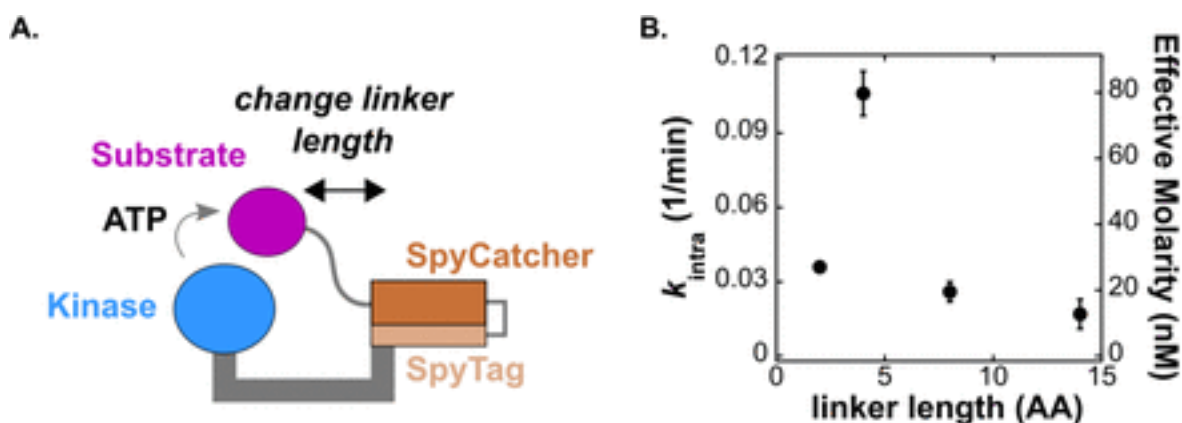


Figure 8. Effective molarity study of kinase-substrate complex¹⁹

1.7 Conditions for Covalent Immune Recruitment

Fast and selective antibody labelling is key to achieving the maximal binding and target effect of cARMs. In human serum cARMs need to label the target antibody efficiently and covalently in the presence of abundant off target proteins. This is also important in a therapeutic context where the cARM can be rapidly eliminated from systemic circulation. To achieve efficient target antibody labeling, cARMs require a combination of a sizable enhancement in reaction EM and somewhat stable pre-equilibrium binding complex. In this way, the number of ternary complexes formed on the cancer cell surface can be maximized.

While some traditional organic reactions are fast and selective, most are not suitable for covalent immune recruitment due to biological incompatibility. The ideal labelling chemistry needs to be non-toxic in a cellular environment, stable under physiological conditions, and favourable in aqueous media.²⁰ The introduction of bio-orthogonal reactive handles such as alkynes or azides have become popular ways to selectively label endogenous proteins, although these require a method such as genetic modification to first substitute the target protein with the reactive handle (Figure 8a).²¹ Affinity labelling (Figure 8b) is an alternative strategy which takes advantage of a

protein-ligand interaction to induce proximity-driven labelling of a natural amino acid on the surface of the protein.²¹

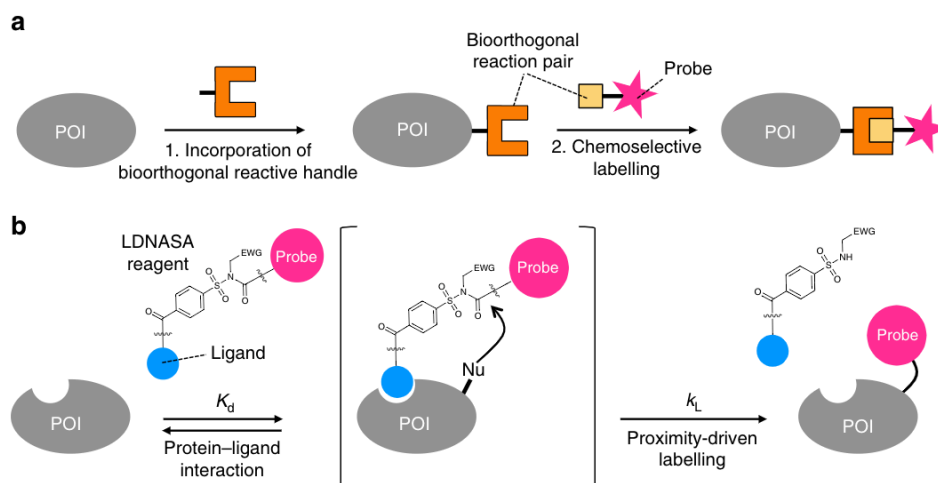


Figure 9. Bio-orthogonal protein labelling strategies.²¹

1.8 Sulfur Fluoride Exchange

One recently developed affinity labelling chemistry with promise in cARM applications is known as sulfur fluoride exchange (SuFEx). Sulfur fluorides refer to the general class of compounds that contain a sulfur-fluorine bond (Figure 9). Sulfonyl fluorides and fluorosulfates are aryl derivatives of sulfur fluorides and are the two most common sub-classes found in the SuFEx literature. SuFEx is a type of bio-compatible reaction which has been shown to covalently modify a broad range of nucleophilic amino acids including Lys, Tyr, Ser and His, Arg and Thr²². Due to the strong covalent interaction between sulfur and fluorine, sulfur fluorides are remarkably stable in aqueous conditions and only react when activated by a nucleophilic residue in close proximity (Figure 10). Since *Sharpless et al.* established the chemistry in 2014, SuFEx has been used in the development of chemical cross-linkers for mass spectrometry, targeted covalent inhibitors, and activity-based protein profiling agents.

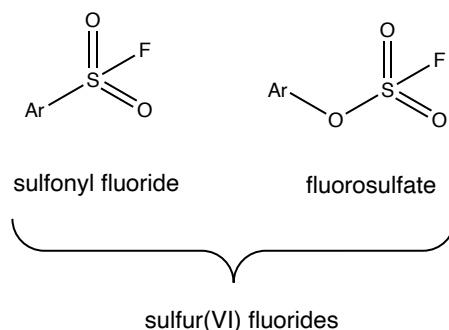


Figure 10. Classification of sulfur fluorides.
Ar represents an aromatic group.

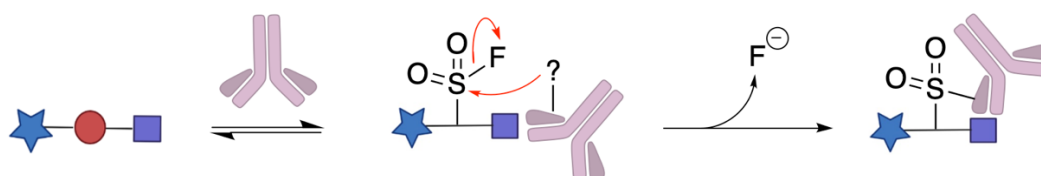


Figure 11. Mechanisms of covalent antibody labelling with sulfur fluoride cARMs.
Adapted from *Jour. of Fluor. Chem.* 2018, 213, 87–112.

SuFEx chemistry has been widely used for protein labelling due to the physical-chemical properties of the sulfur-fluoride bond, H-bonding properties of fluoride, and oxidation state at sulfur²². Fluorine is a highly electronegative atom, making the S(VI) center sulphur electrophilic. The electronics of this bond allow for exclusive reaction to occur at the sulfur center, in comparison to sulfur chlorides which also generate chlorinated products. This is partly due to the high bond energy that exists between sulfur and fluorine, reported at 84 kcal/mol in comparison to the energy of S-Cl bond at 43 kcal/mol.² The high oxidation state of sulfur further confers properties of high thermodynamic and kinetic stability.^{2,23} With six valence electrons and four binding partners, sulfur (VI) fluorides have no available electrons for additional bonding interactions. Sulfur compounds with an oxidation state of 4 or below have an extra lone pair available for bonding, making them highly susceptible to substitution, hydrolysis, and

decomposition.² Because of the stability of sulfur (VI) fluorides, the S-F bond can only be broken if the fluorine atom is supported by a silicon catalyst or protons of surrounding water molecules²². In an aqueous environment, protons of water molecules form H-bonds with the leaving fluorine molecule forming a very stable by-product, bifluoride, (HF₂)⁻ (Figure 11). Without activation of the fluorine leaving group, sulfur fluorides are non-reactive to acidic, basic, and in most cases hydrolysis. These features make SuFEx is an excellent chemistry for covalent modification of proteins, with nucleophilic substitution encouraged in cellular conditions. Particularly for aryl sulfur fluorides, reactivity can be enhanced through the introduction of electron-withdrawing groups (Figure 11) in the aromatic ring which increases electrophilicity of the sulphur atom²⁴. In contrast, fluorosulfates tend to be less nucleophilic and more resistant to hydrolysis through resonance stabilization with the oxygen atom and phenyl ring²⁵.

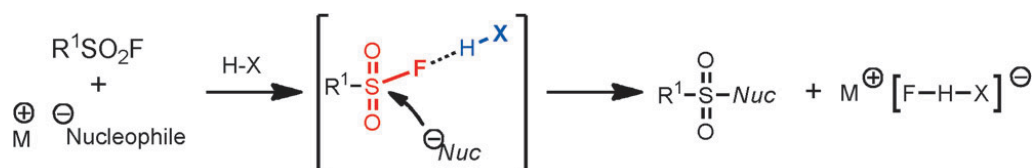


Figure 12. Formation of bifluoride ion from SuFEx reaction²²

Like other “click” reactions, SuFEx reactions are high-yielding, water, and oxygen compatible, catalyst-free, and have simple preparation and isolation protocols. There are a variety of well-established reaction conditions and synthetic routes to develop sulfur fluorides.^{2,23–25} One of the first ways SFs were produced was using sulfuryl fluoride gas (SO₂F₂), a common insect fumigant. This reagent converts a variety of phenols and amines at room temperature, and even shows selectivity towards phenols to generate fluorosulfates²⁴. The risks and costs of purchasing sulfuryl fluoride gas has fortunately led to the production of shelf-stable sulfuryl salts, which also

have good precedent for generating diverse connections between sulfonyl groups and other nucleophiles.²⁴

1.9 Relevance of SuFEx in chemical biology

Many chemical biologists have used SuFEx in their chemical labelling strategies due to their high stability and favourable reactivity in water. These features allow sulfur fluorides to remain unreactive in aqueous conditions until appropriate activation, which can be facilitated by hydrogen-bond donors and acceptors in the binding pocket of a protein.² One group of researchers refer to this as the "sleeping beauty" phenomenon, where SuFEx only occurs in an optimal protein configuration which stabilizes the fluorine leaving group.²⁶ While the application of SuFEx chemistry is rapidly evolving, the covalent modification of proteins by sulfur fluorides has been known for several decades. Two well-known serine protease inhibitors, PMSF and ABESF are commonly used in the preparation of cell lysates to inhibit trypsin and chymotrypsin (see Figure 12).² Another area of research that has leveraged the advantages of SuFEx is activity-based protein profiling. SuFEx is often used as the "warhead" of protein profilers, to identify novel targets and interactions in the drug discovery process. An inverse drug discovery study highlighted the significance of SuFEx in the rapid development of large sulfur fluoride libraries, while exploring proteome reactivity of an anti-cancer target, poly(ADP-ribose) polymerase 1.²⁷ In a similar way, SuFEx has been employed in chemical cross-linking mass spectrometry (CXMS) techniques to identify proximal amino acid residues within intrinsically disordered proteins. One of these reagents, NHSF, has expanding the amino acid selectivity of cross-linkers between lysine and other residues such as histidine, serine, threonine, tyrosine, and lysine (Figure 10).²⁸ Collectively, these examples highlight the significance of sulfur fluoride

in chemical biology research and the ways SuFEx probes can be used to monitor protein interactions.

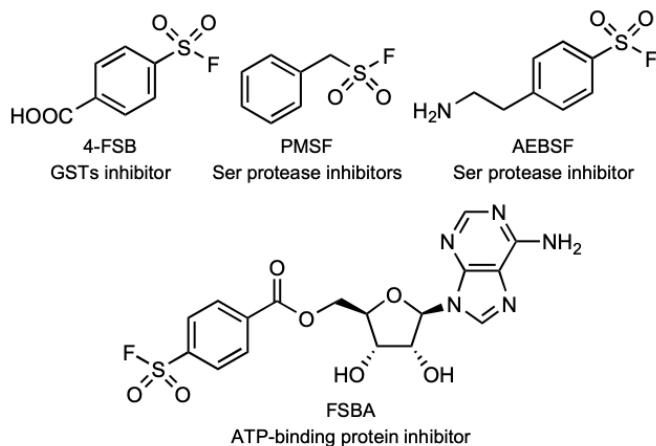


Figure 13. Sulfur fluoride protease inhibitors²

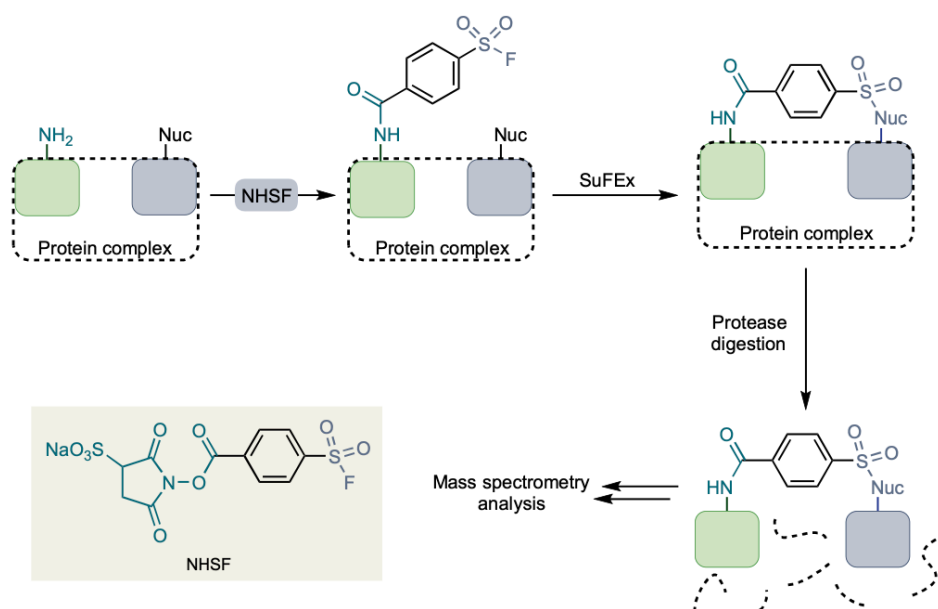


Figure 13. Chemical cross-linker N-HSF.²⁸

2.0 Overall objectives

The overarching aim of this research project is to gain mechanistic insight into SuFEx chemistry for the purposes of covalent immune recruitment. This thesis addresses the question “does SuFEx chemistry enhance the stability, selectivity, and labelling rates of current acyl-imidazole cARMs?” We hypothesized that SuFEx cARMs will improve these critical factors and be advantageous for recruitment of dinitrophenyl specific antibodies. This hypothesis was based on chemical biology literature and the use of SuFEx probes in drug discovery, protein labelling, and proteomics. Specific examples will be used to contextualize results of this thesis and highlight the ways SuFEx chemistry can advance covalent labelling of endogenous antibodies. Four objectives of this project are as follows:

1. Synthesize a small collection of SuFEx cARMs specific for anti-iDNP
2. Test the hydrolytic stability of SuFEx cARMs via ¹⁹F-NMR
3. Determine key labelling rates of SuFEx cARMs with anti-DNP through fluorescent SDS-PAGE
4. Experimentally determine the site of cARM modification on antiDNP IgG using mass spectrometry

2.0 Synthesis & Stability of SuFEx cARMs

2.1 Objectives

The first two objectives of this thesis were to synthesize and assess the stability of a small collection of sulfur fluoride compounds that were specific for dinitrophenyl antibodies (Figure 14). Keeping the ABD consistent from the first generation of cARMs allowed for a direct and fair comparison between SuFEx and AL labelling chemistries. Based on literature precedent, we hypothesized the best sulfur fluorides to make were sulfonyl fluorides and fluorosulfates. Aryl sulfur fluorides have well-documented high stability in a variety of environments, in comparison to their alkyl counterparts.²² The SuFEx ALD was designed to branch off the main backbone of the cARM, which allows the entire compound to be covalently linked to the Ab target. This differs from AL cARMs, where the ALD is incorporated within the backbone of the cARM, resulting in a portion of the molecule being cleaved upon target antibody labeling or hydrolysis to liberate binding inhibitors of both antibody and tumor antigen (Figure 4). The placement of the SuFEx ALD was styled in a similar manner to AL cARMs, with an alkyl linker short enough to keep the ALD and ABD close to facilitate covalent attachment yet long enough to prevent steric clash of aryl rings. The polyethylene glycol linker of eight repeating units ensured a great distance between antibody- and tumor-targeting regions of the cARM. For the tumor binding domain, SuFEx cARMs were synthesized with the same ligand as AL cARMs, glutamate urea, which binds to prostate-specific membrane antigen (PSMA) on tumor neovasculature and prostate cancer. Glutamate-specific SuFEx cARMs were used to test hydrolytic stability of SuFEx cARMs via ¹⁹F NMR. Fluorescent-sCIR derivatives were also synthesized with fluorescein in place of the TBD to measure fluorescence for kinetic analysis after SDS-PAGE.

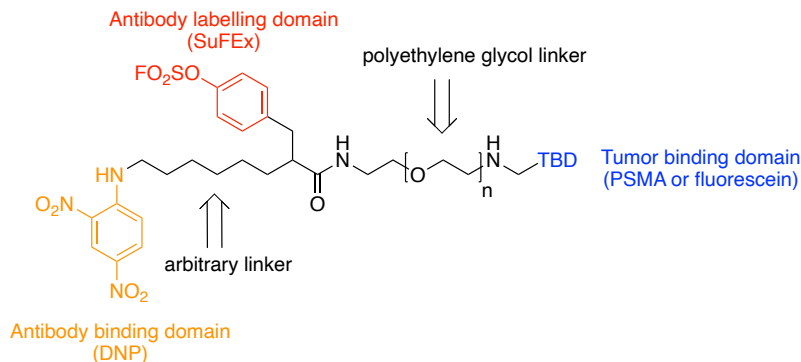


Figure 14. General design of SuFEx cARMs.

This molecule consists of three domains: antibody binding domain (orange), antibody-labelling domain (red), and tumor binding domain (blue).

2.2 Results

2.2.1 Synthesis

In total, 5 new cARMs were synthesized with varying electronic configurations as sulfonyl fluorides and fluorosulfates to probe role of electronics on the antibody labelling reaction rate and position of labeling. Named in the order they were made, Figure 15 depicts sCIR1-5 with three fluorosulfates and two sulfonyl fluorides. Meta and para derivatives of sulfonyl fluorides (2&4) and fluorosulfates (1&3) were made to compare the electronic effects between these two positions. sCIR5 was synthesized without an alkyl linker to determine if a shorter distance between the ALD and ABD was advantageous for antibody labelling by increasing reaction effective molarity. sCIR1-5 were analyzed by ^{19}F NMR to determine the stability of SuFEx chemistry.

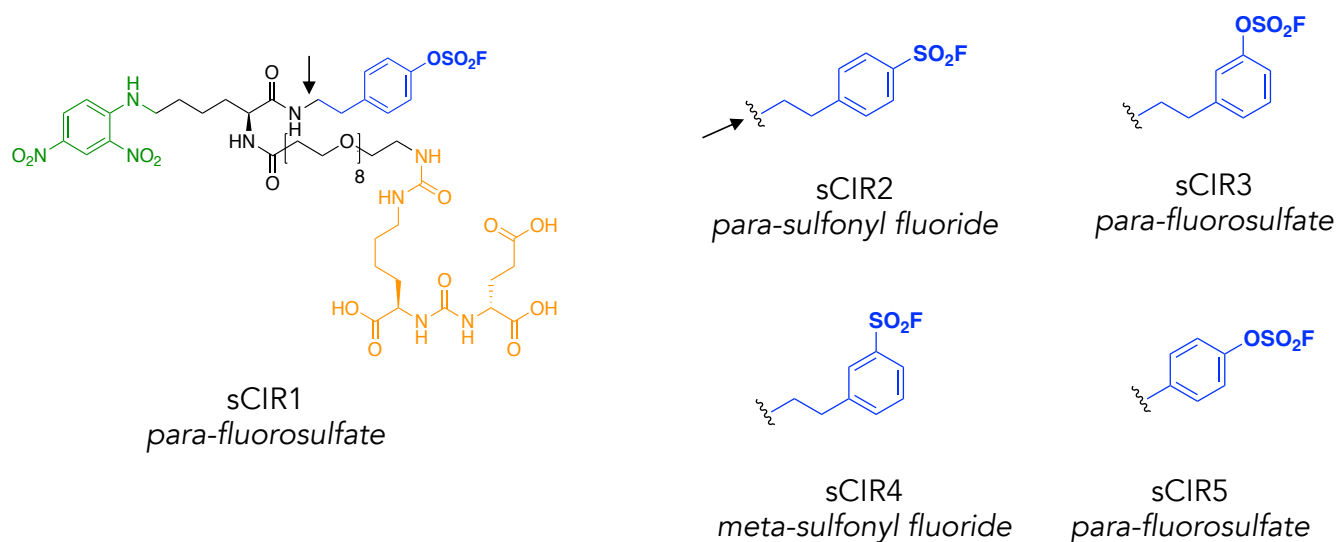


Figure 15. Structure of prostate specific SuFEx cARMs.

Synthetic routes and experimental details for all compounds can be found in the supplemental section. Structure and molecular weight of products were confirmed by LC-MS and ^1H NMR.

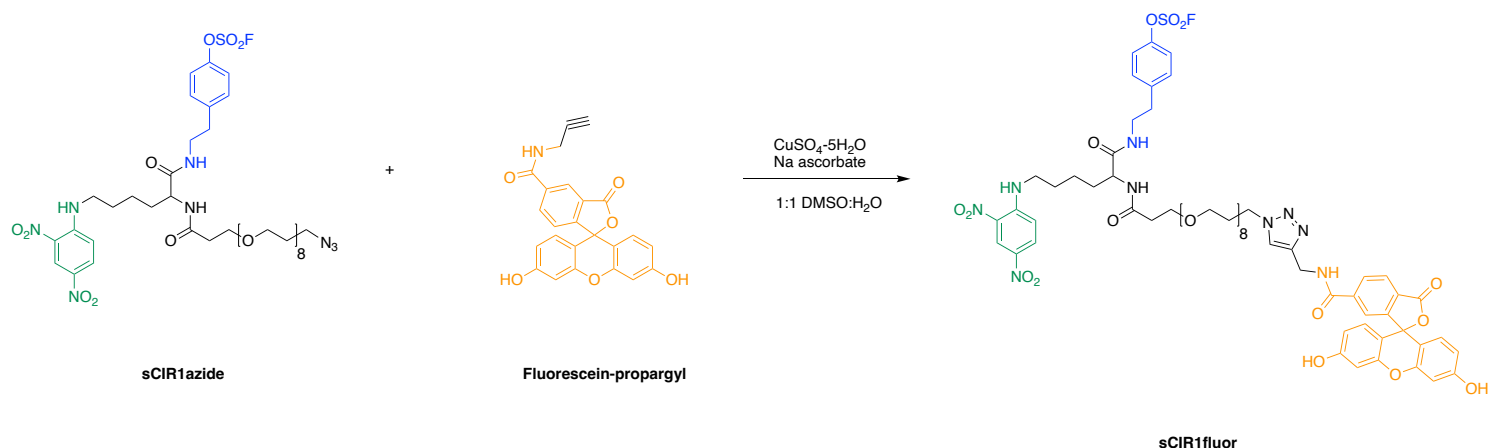


Figure 16. General scheme used to synthesize fluorescent SuFEx cARMs.

Synthetic routes and experimental details for all compounds can be found in the supplemental section. Structure and molecular weight of products were confirmed by LC-MS and ^1H NMR.

Fluorescent derivatives of the 5 SuFEx cARMs were synthesized by substituting fluorescein for glutamate area in the tumor binding domain. This was done by making azide derivatives of each CIR and clicking on fluorescein-propargyl (Figure 16) through an alkyne handle. Using standard copper-catalyzed azide-alkyne cyclo-addition (CuAAC), 5 fluorescent CIRs were made to determine antibody labelling rates through SDS-PAGE. Synthetic routes and experimental details can be found in the supplemental section. Structure and molecular weight of products were confirmed by LC-MS and ^1H NMR.

2.2.2. Hydrolytic Stability

The hydrolytic stability of each SuFEx CIR was tested by dissolving a few milligrams of each glutamate sCIR in 90:10 PBS:D₂O. Table 1 summarizes the final concentration of CIR samples used for NMR analysis. A brief overview of how the experiment can be found in the caption of Figure 17, with experimental data displayed in Figure 18.

	Final concentration (mg/mL)
sCIR1	5.47
sCIR2	3.78
sCIR3	3.83
sCIR4	4.33
sCIR5	6.1

Table 1. Preparation of sCIRs for fluorine-stability studies.

2-6 mg of glutamate sCIRs were dissolved in 0.5-1 mL of 90% PBS/10% D₂O. Specific amounts and volumes can be found in the supplemental.

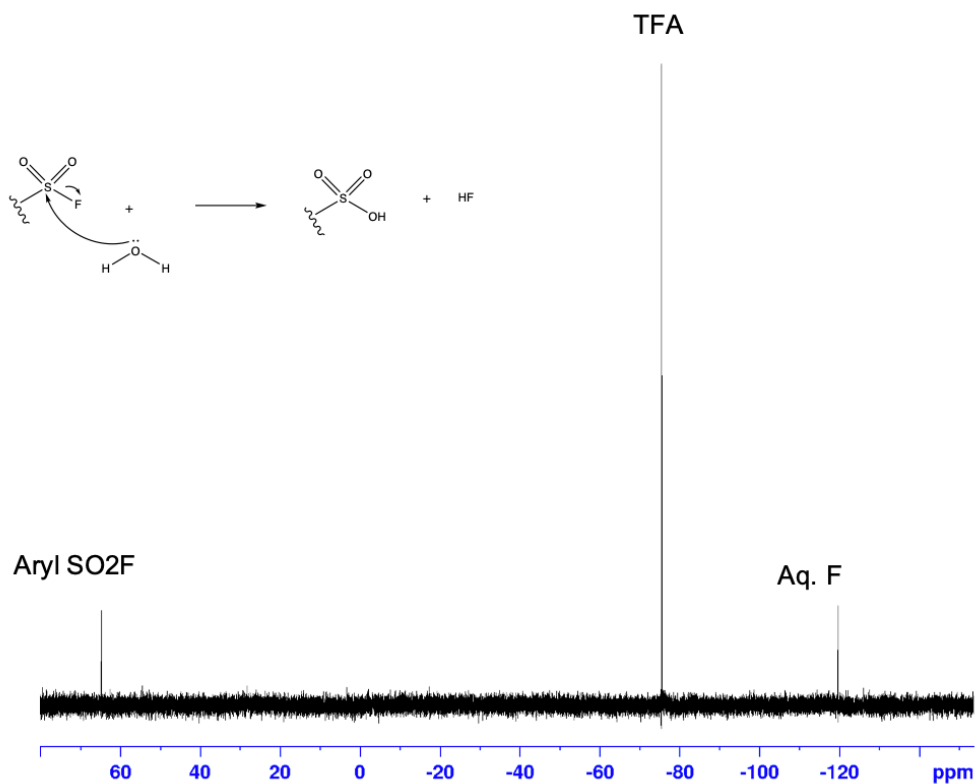


Figure 17. Hydrolytic stability test of SuFEx cARMs via ¹⁹F NMR.

sCIR samples dissolved in 90/10 PBS:D₂O and analyzed by collecting ¹⁹F spectra between 0 and 120 hours. In each sample a residual amount of TFA (-78 ppm) was present which was used as a reference value (1.00) in NMR analysis in topspin. Sulfonyl fluoride peaks of all CIRs were located between 35 and 65 ppm, and the aqueous fluoride peak was consistently located at -118 ppm²⁹. Integrations of sulfonyl fluoride and the aqueous fluorine peak were plotted over time in Figure 18.

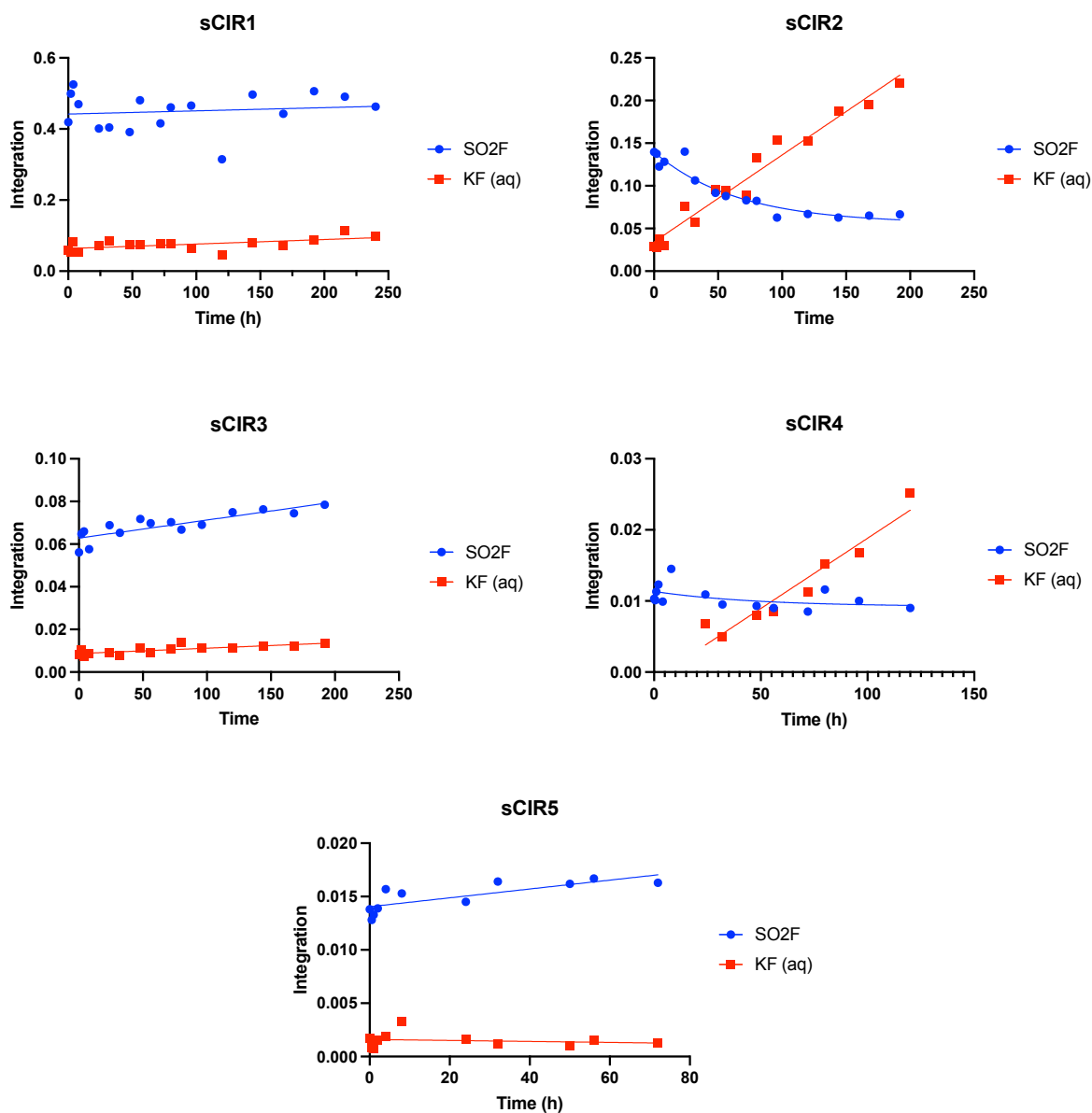


Figure 18. Integrations of fluorine peaks for sCIR glutamate derivatives over time. Dissolved sCIRs were analyzed by 700-MHz NMR spectrometer up to 250 hours. In all plots blue data points indicate integrated values for sulfonyl fluoride ($n = 1$), and red data points represent integrated values for aqueous fluorine peak ($n = 1$). A simple linear regression of each data set was computed for sCIR1, 3 & 5, and the aqueous integrations of sCIR 2 and 4. A non-linear one-phase decay of sulfonyl fluoride peaks in sCIR2 and 4 were used to determine their half-life.

In general, the integration of the aqueous fluorine peak for all fluorosulfates (sCIR 1, 3 and 5) remained consistent over the time measured. In these samples the integration of the sulfonyl fluoride increased very slightly over time.

For sCIR 2&4, the slope of the aqueous fluorine peak was dramatic, with a large linear slope that increased rapidly in comparison to the slope of the fluorosulfate aqueous peaks. The sulfonyl fluoride integrations for sCIR2 resembled a non-linear decay curve, with its half-life computed as 45.1 hours (Table 2). The non-linear fit of aryl-SO₂F integrations for sCIR4 was very close to linear, but a half-life was determined of 33.1 hours.

	Half-life (hrs)
sCIR1	Undetermined
sCIR2	45.1
sCIR3	Undetermined
sCIR4	33.1
sCIR5	Undetermined

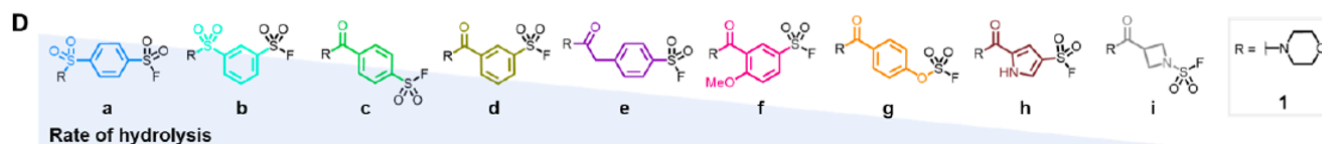
Table 2. Half-life of SuFEx cARMs from hydrolytic stability studies.

After collecting integrations of sulfur fluoride and fluorine peaks by ¹⁹F NMR, the half-life was computed through the Prism software in a one-phase decay.

2.3 Discussion

The first set of experiments conducted after the synthesis of SuFEx cARMs was an NMR time-course study used to determine hydrolytic stability of each compound. It was predicted that if hydrolysis occurred, the integration of the aryl SuFEx peak would decrease over time as the aqueous fluorine peak would increase (Figure 17). During these studies it was assumed that hydrolysis only occurred due to the loss of fluorine, since there are no other functional groups or bonds in the sCIR structure that would rapidly hydrolyze.

Based on the data presented in Figure 18, the fluorosulfate CIRs demonstrated remarkable stability over 72 hours. The integration of OSO_2F and aqueous fluorine remained steady over time with minimal fluctuations. The rate of hydrolysis is described by the half-life ($t_{1/2}$) of the compound degraded by water. This value was generated through the Prism software by computing a non-linear fit (one-phase decay) of the change in aryl SuFEx ^{19}F signal integrations over time. A half-life for sCIRs 1, 3 and 5 could not be determined as these data sets remain steady over time. In hindsight, it would have been interesting to observe the effect on hydrolysis by increasing pH of the PBS/ D_2O solution with NaOH. Many studies confirm that increasing the basicity of the solution increases the rate of hydrolysis.² Researchers at GlaxoSmithKline in the UK completed an in-depth study of the stability, reactivity, and selectivity of SuFEx compounds (Figure 19, D) to develop probes that target a greater % of the proteome. Hydrolysis of sulfonyl fluoride and fluorosulfate molecules were conducted in three different buffers and degradation was monitored by HPLC. The probe that most resembles the fluorosulfate CIRs in the study is 1g, which had a half-life of >1700 hrs in PBS at pH 7, >612 hrs in PBS at pH 8, and 4.7 hrs in bicarbonate buffer pH 10.³⁰ This data supports the finding that fluorosulfates have extraordinary stability under physiological conditions and increased levels of hydrolysis in basic conditions.



E

	1a	1b	1c	1d	1e	1f	1g	1h	1i
PBS buffer, pH 7	1.5	2.3	7.6	9.7	40.5	90.3	1700	>1700 (4700')	>1700 (1.84x10 ⁶)
Half-life / h PBS buffer, pH 8	0.6	1.0	3.1	4.3	15.3	26.9	612	>612 (1510')	>612 (4.87x10 ⁵)
Bicarbonate buffer, pH 10	<0.2	<0.2	<0.2	<0.2	<0.2	0.2	4.7	55.6	272
E(LUMO)	-0.092	-0.085	-0.080	-0.077	-0.073	-0.066	-0.055	-0.049	-0.019

Figure 19. Hydrolytic stabilities of sulfur fluoride probes.³⁰

As predicted, sulfonyl fluoride CIRs (2&4) were not as stable to hydrolysis in comparison to the fluorosulfate CIRs. In general, fluorosulfates exhibit lower rates of hydrolysis and reactivity due to the increased electron density at the sulphur atom contributed by its connecting oxygen atom.²⁵ Sulfonyl fluorides do not have this shielding effect and therefore are more susceptible to attack by hydroxide and other nucleophiles in its environment (see SDS-PAGE section). This trend is also observed in the GSK study, where the half-life of several sulfur fluoride probes was determined (Figure 19E). Based upon the compounds in panel E, sCIR4 (meta-sulfonyl fluoride) most resembles probe 1d which had a half-life of 9.7 hrs and 4.3 hrs in PBS at pH 7 and 8. The probe most comparable to sCIR2 (para-sulfonyl fluoride) was 1e which had a half-life of 40.5 hrs and 15.3 hrs in PBS pH 7 and 8. The GSK data also suggests an interesting observation that sulfonyl fluorides are more stable in the para-position than in the meta position. sCIR hydrolytic stability studies support this claim with the half-life of sCIR2 was 45.1 hrs, 12 hours longer than the half-life of sCIR4 at 33.1 hrs. To understand the chemical behaviour behind this finding, the resonance structure of both SuFEx labelling domains were drawn out (Figure 20).

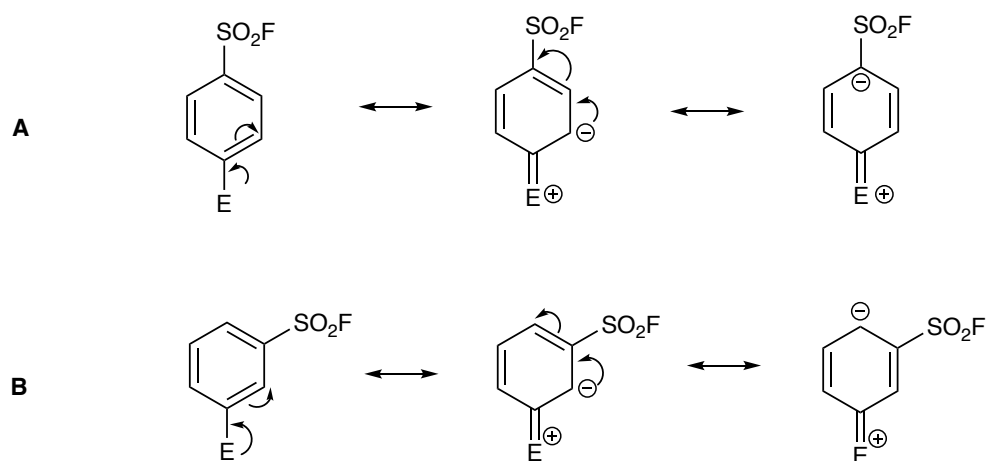


Figure 20. Resonance structures of aromatic sulfonyl fluorides.

Chemical structures of SuFEx labelling domain for sCIR2 in panel A and sCIR4 in panel B. E represents any electron-donating group.

The ALD of all SuFEx cARMs consist of an alkyl chain attached to the aryl SO_2F . An alkyl chain is a weak activating group³¹, contributing to a slight increased electron density from the s-character of the C-H bonds to the phenyl ring. In the case of the para-sulfonyl fluoride, the extra negative charge contributed to the ring can be stabilized on the carbon para to the electron donating group E (in this case the alkyl chain). This negative charge increases the electron density near the sulfur fluoride, making the sulphur atom less electrophilic. For the meta sulfonyl fluoride, the negative charge does not get stabilize on the carbon adjacent to the sulfonyl group and therefore does not impact the electrophilicity of the sulfonyl group. Based on these structures, the sulphur atom of a meta sulfonyl fluoride is more electrophilic than the sulfur of a para-sulfonyl fluoride. This helps explain why sCIR4 is more prone to hydrolysis and nucleophilic attack.

All considered, the hydrolytic stability of both fluorosulfates and sulfonyl fluoride cARMs far exceeds the half-life of acyl-imidazole derivatives reported at 10, 12 and 27 hrs.¹ This is

promising for the CIR platform, as the stability of small molecules is crucial for success of *in vivo* studies. The accuracy with which sCIR stability is measured could be improved by monitoring hydrolysis through liquid-phase chromatography or replicating the ^{19}F -NMR assay, increasing the sample size to 2 or 3.

3.0 Kinetics of SuFEx cARMs

3.1 Objectives

The second purpose of synthesizing SuFEx cARMs, was to determine the kinetic parameters describing SuFEx reaction with anti-DNP. These parameters were compared to the intramolecular rate constant calculated for AL cARMs, to determine which ALD chemistry labelled DNP antibodies the quickest relative to non-specific reactions with off target nucleophiles. While the rate constants associated with related SuFEx probes are reported in literature, this chemistry has never been used to covalently modify antibodies or anti-DNP, so the reaction rates of SuFEx cARMs was not predicted beforehand.

3.2 Results

3.2.1. Intramolecular labelling

The intramolecular rate constants were determined by incubating fluorescent SuFEx cARMs with the Fab of antiDNP SPE7, and quantifying fluorescence after separation of conjugated protein samples by SDS-PAGE. Figure 21 depicts the fluorescent data gathered for sCIR fluorophores 1-5 with rate constants listed in Table 3.

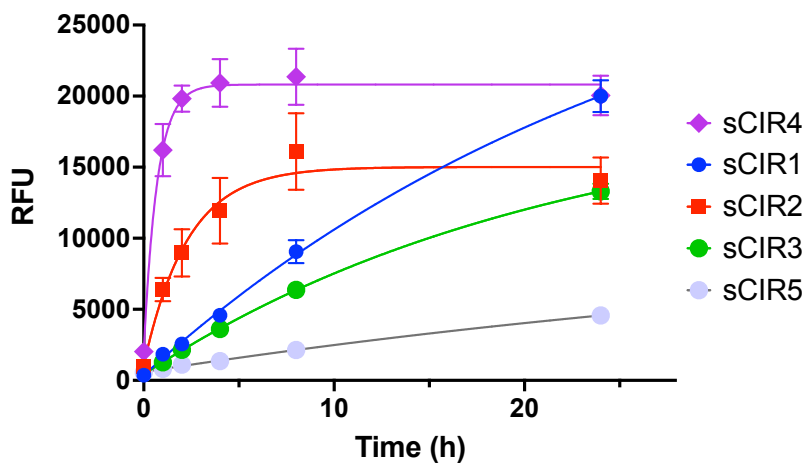


Figure 21. Fluorescent intensities of sCIR1-5fluor incubated with SPE7 Fab.

Samples were obtained by incubating equal amounts of SPE7 Fab and sCIRfluor at a final concentration of 1 μM and 2 μM respectively, over 24 hours. After separation by SDS-PAGE, protein bands were visualized by a fluorescent scan at 460 V on the GE Typhoon ($n = 2$). Relative fluorescent units were measured through densitometric analysis on ImageJ. Mean values and error bars were plotted on Prism 9, using standard deviation to quantify variability between replicates.

To compare SuFEx cARM reaction kinetics to acyl-imidazole derivatives, a fluorescent acyl-imidazole cARM was synthesized and incubated with SPE7 Fab in the same way SuFEx cARMs were. Figure 22 depicts fluorescent data gathered from this experiment, along with rate constants listed in Table 3.

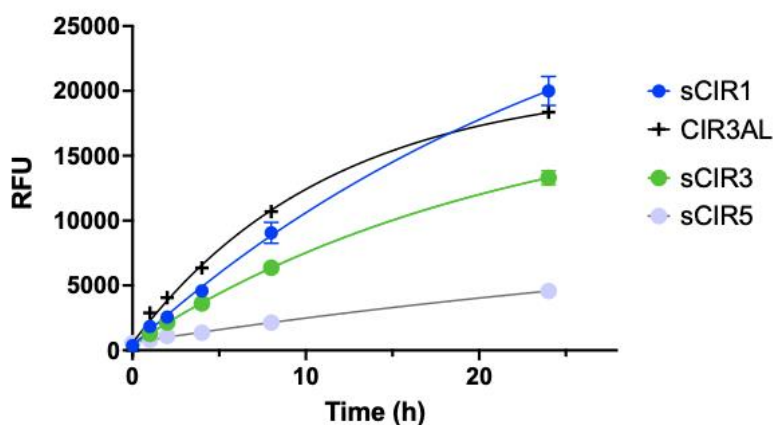


Figure 22. Fluorescent of sCIR1-3fluor and acyl-imidazole CIR incubated with SPE7 Fab.

Samples were obtained by incubating equal amounts of SPE7 Fab and sCIRfluor or aICIR at a final concentration of 1 μM and 2 μM respectively. After separation by SDS-PAGE, protein bands were visualized by a fluorescent layer at 460 V on the GE Typhoon ($n = 2$). Relative fluorescent units were measured through densitometric analysis on ImageJ. Mean values and error bars were plotted on Prism 9, using standard deviation to quantify variability between replicates.

Observed labelling rates of each sCIR were determined from the RFU vs time data (Figure 21 & 22), through non-linear one-phase association analysis on Prism 9. Since the final concentration of anti-DNP used in these experiments were in large excess (100-1000X) compared to its K_D (63.6 nM), pseudo-first order conditions were assumed. Under these conditions the rate of observed labelling (k_{obs}) is equal to the rate of intramolecular labelling (k_{inact}). Table 3 lists the intramolecular constants for sCIR fluorophores 1-5 to antiDNP. To compare sCIR-Fab labelling rates to literature values, second-order rate constants were estimated by dividing k_{inact} by the K_D of antiDNP (63.6 nM). These values are also located in Table 3. Pseudo-first and second order rate constants were also determined for the acyl-imidazole CIR. The observed labelling rate from the Rullo lab's first ACS publication was included as a reference.¹

Compound name	Electrophilic ALD	$k_{obs} = k_{inact}$ (s^{-1})	Estimated k_{inact}/K_i ($M^{-1}s^{-1}$)
sCIR1fluor	para-fluorosulfate	9.89×10^{-6}	1.56×10^2
sCIR2fluor	para-sulfonyl fluoride	1.21×10^{-4}	1.90×10^3
sCIR3fluor	meta-fluorosulfate	1.28×10^{-5}	2.01×10^2
sCIR4fluor	meta-sulfonyl fluoride	3.94×10^{-4}	6.19×10^3
sCIR5fluor	para-fluorosulfate with shorter linker	5.57×10^{-6}	8.76×10^1
alCIR	acyl-imidazole	2.45×10^{-5}	3.85×10^2
alCIR	acyl-imidazole	8.1×10^{-4} ¹	

Table 3. Pseudo-first order labelling rates of antibody labelling from SDS-PAGE studies. Observed labelling rates determined through one-phase association of fluorescence data gathered over time from each sCIR conjugated with antiDNP.

3.2.2. Intermolecular labelling

To better understand the kinetic profile of SuFEx cARMs specific to antiDNP, the intermolecular rate constants were determined by measuring non-specific labeling of bovine serum albumin (BSA). BSA is a commonly used protein in immunological assays to measure non-specific binding.³² Intermolecular rate constants were determined by incubating fluorescent SuFEx cARMs with BSA over several days at the same concentrations intramolecular constants were derived. Fluorescence of these conjugated protein samples were measured after separation by SDS-PAGE. Figure 23 depicts the fluorescent data gathered for sCIR fluorophores 1-5 with rate constants listed in Table 4. k_{inter} values were determined by calculating the slope of a simple linear regression in each data set.

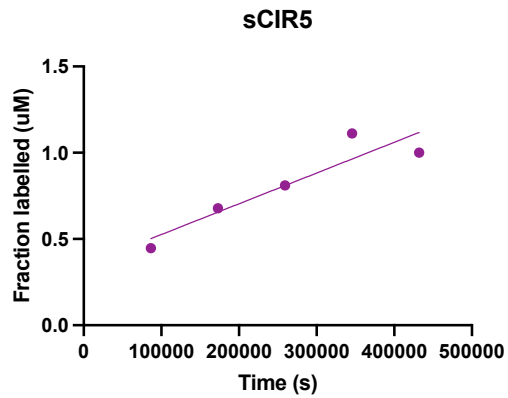
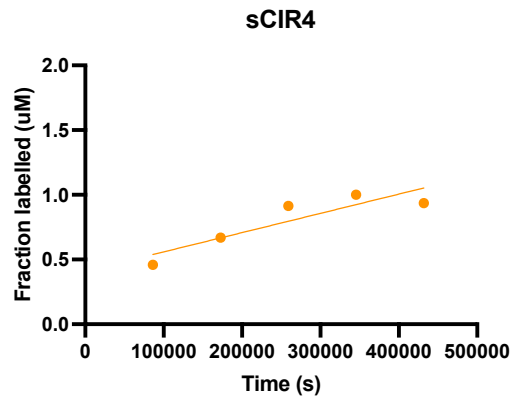
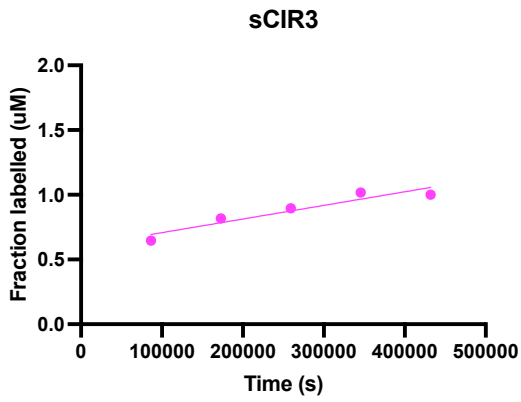
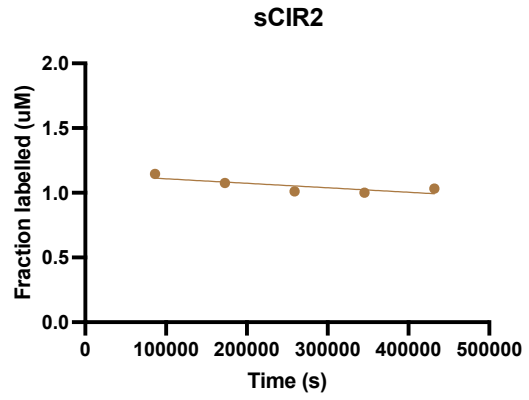
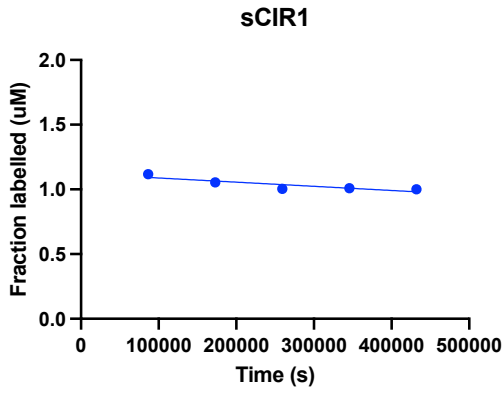


Figure 23. Fluorescence of sCIR1-5 fluorophores incubated with BSA for 24-120 hours. Samples were obtained by incubating equal amounts of bovine serum albumin (BSA) and sCIRfluor at a final concentration of 1 μM and 2 μM respectively. After separation by SDS-PAGE, protein bands were visualized by a fluorescent layer at 460 V on the GE Typhoon (n = 1 or 2). Relative fluorescent units were measured through densitometric analysis on ImageJ and fraction labelled was calculated using max fluorescent signal of each sCIR. A simple linear regression was calculated from each graph. Mean values and error bars were plotted on Prism 9, using standard deviation to quantify variability between replicates.

	$k_{\text{inter}} (\text{M}^{-1}\text{s}^{-1})$
sCIR1fluor	-0.098
sCIR2fluor	-0.149
sCIR3fluor	0.207
sCIR4fluor	0.422
sCIR5fluor	0.419

Table 4. Intermolecular rate constants of sCIRfluors.

Intermolecular rate constants were determined by completing a linear regression of fraction labelled via fluorescence of sCIR1-5 incubated with BSA.

3.3 Discussion

3.3.1. Pseudo-first order conditions

As previously mentioned, the intramolecular rate constant for the sCIR anti-DNP labeling reactions were determined under first order conditions. Any second-order reaction can be assumed to be first order when one species is present at a very high concentration in comparison to the other over the time course of the reaction.³³ In this condition, any fluctuations in concentration of the second species are minuscule and does not impact the rate of the reaction.

For CIR-Ab binding, pseudo-first order conditions were used to simplify and avoid complex kinetic calculations of a second-order reaction.

To determine the rate of covalent bond formation for SuFEx cARMs, the enzymatic equation in line 1 (Figure 24) was rearranged and simplified. Based on the relationship between enzymatic inhibition and covalent bond formation, k_{inact} was substituted for k_{intra} , and K_i substituted for K_D resulting in line 2. $[sCIR]$ was then eliminated from the right-hand side of the equation because the sCIR concentration remained constant at 2 μM during incubation with SPE7 Fab. Equation 3 was further simplified under pseudo-first order conditions because the concentration of Fab (1 μM) is well above the affinity of CIR binding to antiDNP (63.6 nM). At this concentration, the dissociation constant is extremely small and would not impact k_{intra} . This leads to the final simplification, where the observed labelling rate equals the rate of intramolecular reaction for sCIR binding (line 4).³⁴

$$k_{obs} = \frac{k_{inact} + [inhibitor]}{K_I + [inhibitor]} \quad (1)$$

$$k_{obs} = \frac{k_{intra} + [sCIR]}{K_D + [sCIR]} \quad (2)$$

when $[sCIR]$ remains constant:

$$k_{obs} = \frac{k_{intra}}{K_D} \quad (3)$$

When $K_D \ll [Fab]$, $K_D \cong 0$

$$k_{obs} = k_{intra} \quad (4)$$

Figure 24. Pseudo first-order assumption of labelling rates³⁴

3.3.2. Intramolecular rate constants

An important consideration when calculating the intramolecular rate constants of SuFEx cARMs, was that the fluorescence gathered in Figure 20 & 21 was of sCIRfluor conjugated to SPE7 Fab. Conjugation was confirmed based on the presence of fluorescence at the expected mass of the protein plus sCIR. If a portion of the sample was unconjugated, the only two fluorescent compounds that would appear when imaging the gel on the Typhoon would be sCIRfluor alone and sCIRfluor bound to the Fab. Since SDS-PAGE separates proteins by their molecular weight, the location of the sCIRfluor band would be very different from the sCIRfluor-Fab complex, which has a significantly higher molecular weight (53 500 Da Fab + 1380 Da sCIR). Therefore, any fluorescent signal from a protein band of this size of approximately 54.8 kDa was assumed to be sCIRfluor covalently labelled to the antibody. Covalency was assumed in this experiment, as non-covalent protein-small molecule complexes would be unlikely to survive denaturation by heat and treatment with sodium dodecyl sulfate (SDS) before gel electrophoresis. Samples are treated with SDS in excess to neutralize all charges on the protein surface, which would disrupt any electrostatic interactions if sCIRfluor was non-covalently bound to the Fab. Because a fluorescent band was observed at the approximate MW of the Fab + sCIRfluor, this interaction was assumed to be covalent.

To test specificity of the sCIRfluor, pre-treatments of a competitor DNP-Gly was used. In the “pre” treatment samples, a high concentration of DNP-Gly (5 mM) was incubated along with sCIRfluor and Fab. If DNP-gly out competed the sCIRfluor for the Fab, this would support binding of the sCIR is specific to the DNP-binding site of the Fab. In Figure 53, all sCIRs were pre-treated with DNP-gly over 24 hours (lanes 1 – 6). When imaged, no bands were detected in the fluorescent channel but visible when stained with Bradford reagent. This indicates DNP-Gly out

competed for Fab binding and that sCIR-fluorophores 1-3 were specific for antiDNP. If the sCIR labelled in a non-specific manner, fluorescent bands would be present and indicate binding occurred somewhere other than the DNP-binding site. While these controls were not completed for all sCIR samples, all sCIRs were synthesized and designed in the same manner so it was assumed all sCIRs were selective and interacted covalently with antiDNP.

To confirm specificity of sCIRs to DNP-antibodies over other immunoglobulin proteins, one control sample was prepared along with sCIR-Fab samples. In this control, sCIRfluor was incubated for 24 hours with isotype IgG. Isotype IgG was chosen because the engineered antiDNP SPE7 used is also an immunoglobulin G (IgG) protein, however isotypes lack specificity for dinitrophenol groups. In lane 7 of Figures 53, 54, 55, and 57 contained isotype controls for all sCIRs. No bands were detected in these lanes when imaged in the fluorescent channel, but bands were visible when stained with Bradford reagent. This indicates the sCIRfluor did not bind covalently to isotype IgG and suggests sCIRfluor are only specific to antiDNP due to proximity induced labeling.

Based on the labelling rates summarized in Table 3, the sulfonyl fluoride CIRs have the fastest intramolecular rate constants of 10^{-4} s^{-1} . This value is comparable to the k_{inact} of a lysine-targeting sulfonyl fluoride probe reported by *Pettinger et. al* in 2019.³⁵ In this study the kinetic rate of a target covalent inhibitor of HSP72 was enhanced by 108-fold from replacing the acrylamide warhead with a sulfonyl fluoride ($k_{\text{inact}} = 4.4 \times 10^{-4} \text{ s}^{-1}$ in Figure 25). In the GSK study rate constants of sulfur-fluoride probes were also measured using a fragment of carbonic anhydrase II (CAII), an enzyme previously shown to react with aryl sulfonamides via a histidine residue.³⁶

Modification of CAII was studied by LCMS and many mono-substituted sulfonyl fluoride probes (2c-e, 3e and 4c-e in Figure 26) had k_{inact} of 10^{-4} s^{-1} .

While these examples act as a good approximation for the rate of sulfonyl fluoride labelling, it is important to note that rate constants vary greatly between studies, techniques, and target proteins. Specific to SuFEx, kinetic rates can vary depending upon their target, pH in the binding site, and the electron donating/withdrawing groups attached to the aryl ring., as well as proximity to nearby amino acid nucleophiles

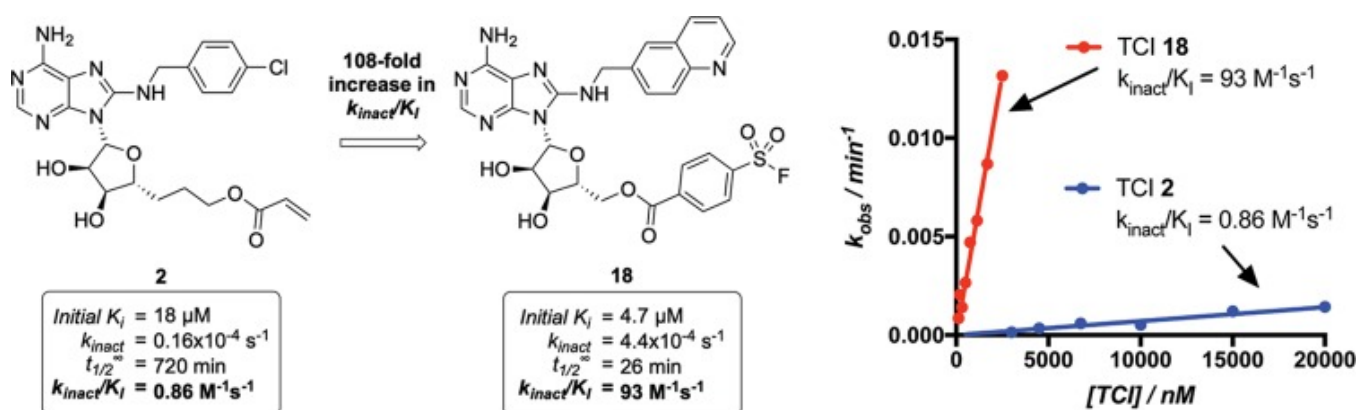
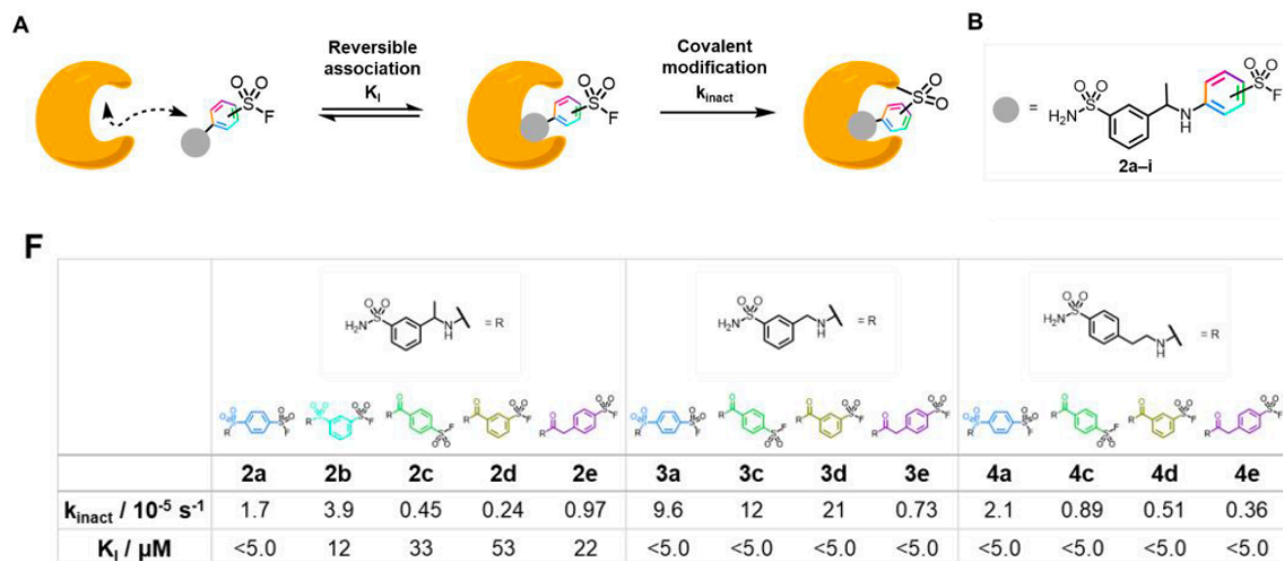


Figure 25. Acceleration of covalent inhibition by sulfonyl fluoride inhibitor targeting HSP72.³⁵ Kinetic parameters were determined through competitive fluorescent polarization assay.

Figure 26. First-order labelling constants of sulfonyl fluoride probes.³⁶

Although little information exists in SuFEx literature on the labelling rates for fluorosulfate probes, it was predicted fluorosulfate CIRs would label antiDNP at a slower rate due to the increased electron density around the sulphur atom contributed by the additional oxygen. Comparing the rates of sulfonyl fluoride CIRs to fluorosulfate CIRs, sCIRs 1, 3 and 5 were at least 10^1 s^{-1} (an order of magnitude) slower than sCIRs 2 and 4. With sCIR5 exhibiting the smallest k_{inact} , this finding suggests shortening the alkyl linker does not improve labelling of fluorosulfate by the CIR likely by moving the ALD farther from the optimal reactive amino acid. Interestingly, it seems the SuFEx CIRs in the meta position have a greater rate of inactivation than in the para position (Figure 27). With the k_{inact} of meta-SF 3.2 times greater than para-SF, and the k_{inact} of meta-FS 1.3 times greater than para-FS. This suggests that the meta position is optimal for SuFEx labelling to the target amino acid residue on antiDNP. Looping back to the hydrolysis of SuFEx CIRs, para sulfonyl fluorides were found to be more stable than meta sulfonyl fluorides. These results correlate well with the first-order rate constants, as higher stability indicates an increase

in electron density at the sulfur center which leads to decreased reactivity of the SuFEx group. Since sCIR4 is more vulnerable to hydrolysis than sCIR2, it also is more inclined to reactivity. Another surprising finding was discovered when comparing SuFEx to acyl-imidazole chemistry, as the k_{inact} of aICIR was higher than the k_{inact} of fluorosulfate CIRs. The measured value of $2.45 \times 10^{-5} \text{ s}^{-1}$ was close to the observed labelling rate of monoclonal antiDNP reported at $8.1 \times 10^{-4} \text{ s}^{-1}$.¹ This data demonstrates acyl-imidazole cARMs have modest reactivity, which correlates with their modest hydrolytic stability.

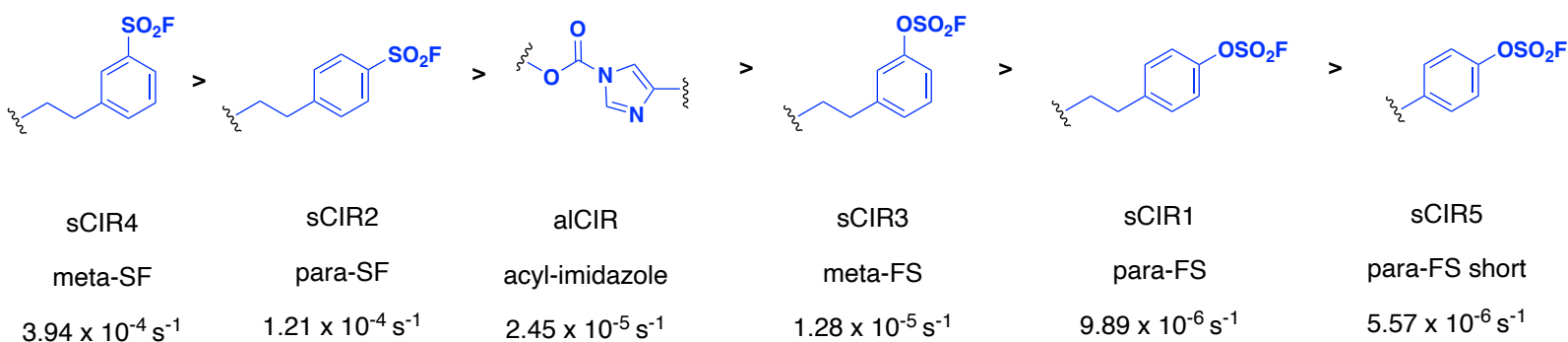


Figure 27. Comparison of SuFEx and acyl-imidazole labelling domains of cARMs.

3.3.3. Second-order rate constants

In Table 4 the second-order rate constant was estimated by dividing the k_{inact} of each CIR by the K_{D} of antibody binding (63.6 nM). As all k_{inact} values were divided by the same value (K_{D}), the second-order constants of SuFEx CIR followed a similar trend as their first-order constants (sulfonyl fluoride CIRs > acyl-imidazole CIR > fluorosulfate CIRs). Comparing these labelling rates to other click chemistries, sulfonyl fluoride CIRs exhibited a similar second-order constant

(10^4) to the tetrazine-*trans*-cyclooctene (Tz-TCO) ligation and enzymatic labelling reported at 10^4 - 10^5 $M^{-1}s^{-1}$ (Figure 28).²¹ The Tz-TCO reaction (Figure 35 in Appendix) is one of the fastest and most desirable click chemistries reported, with some reported up to 10^7 $M^{-1}s^{-1}$.³⁷ Since the development of copper-catalyzed azide-alkyne cycloaddition (CuAAC) in 2002, the generation of fast, selective, catalyst-free, and physiologically stable reactions is crucial to biochemical research.³⁷

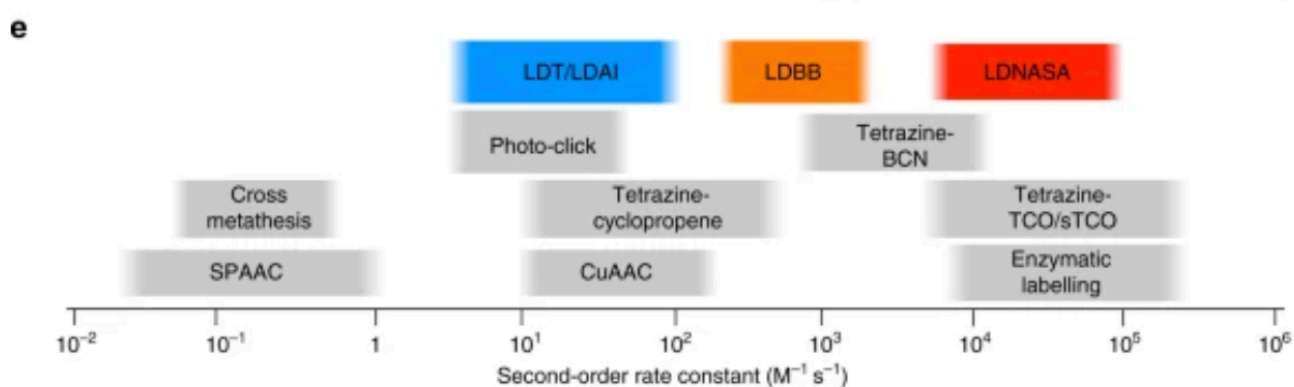


Figure 28. Second-order rate constant of various click chemistries in current literature.²¹

3.3.4. Intermolecular rate constants

Another important parameter measured in cARM labeling mechanism, is rate enhancement versus off target nucleophiles. This is calculated by dividing the rate of the catalyzed reaction by the rate of the uncatalyzed reaction. In the context of Ab labelling by CIR, the rate enhancement of antibody labelling is equal to the k_{inact} divided by the rate constant of the intermolecular reaction (k_{inter}). The rate of intermolecular reaction for sCIRs were determined by monitoring fluorescence after SDS-PAGE at $2 \mu M$ sCIR, with $1 \mu M$ of a non-specific protein. The second order rate constant of the intermolecular reaction was determined by calculating the slope of linear regression obtained from graph of fraction labelled vs time (see Figure 23).

At first, one of the SuFEx CIRs (sCIR4fluor) was incubated with isotype IgG over a 24-hour period. Non-specifically labelling would entail sCIR forming a covalent interaction with another protein aside from its intended target, antiDNP. A linear rate would be observed in this circumstance, using a fluorescent sCIR. Interestingly, we observed a rapid increase in protein fluorescence (Figure 44 in appendix), albeit low in magnitude within the first 8 hours before reaching a plateau, resembling a specific binding interaction. Because of this result, it was suspected the isotype antibody contained a small percentage of DNP-antibodies which allowed for selective labelling by the sCIRfluor. In the second attempt, fluorescence was observed of sCIR4fluor incubated with a monoclonal antibody specific for CD38 (antiCD38) as it was not known to bind to nitroarenes. Again, the fluorescence data of sCIR4fluor (Figure 44) indicated specific binding to antiCD38. Some antibodies can recognize nitroarene rings, which may explain why a small percentage of isotype IgG and antiCD38 exhibited specific labelling.³⁸ An alternative attempt to determine the intermolecular labelling rate of sCIRfluor involved incubations with BSA (Figure 23). In Figure 22, three of the five sCIRs (3, 4 and 5) exhibited an increasing linear rate over time, while data sets for sCIR1 and 2 demonstrated a slight decreasing linear rate. Since the second order rate constants were very small ($\mu\text{M}^{-1}\text{s}^{-1}$), the rate of intermolecular reaction for all sCIRs were considered negligible.

3.3.5. Limitations of CIR labelling kinetics

One aspect to consider for SDS-PAGE is the measure of fluorescence through the fluorescein-sCIRs. Fluorescein is a highly hydrophobic molecule, that has low photostability in comparison to other fluorophores like the Alexa Fluor 488 dye.³⁹ This means sCIRfluor can rapidly degrade

if exposed to prolonged periods of light, skewing the fluorescence reading of the sCIR-Fab conjugates.

Another important consideration when measuring fluorescence is the photomultiplier tube (PMT) voltage used on the Typhoon imager. The PMT converts photons acquired from fluorescence into photocurrent and amplifies the signal sent to the detector of the laser.⁴⁰ Optimization of the PMT voltage of a fluorescent laser is crucial to obtain the best quality of a fluorescent signal. The PMT voltage for detecting of sCIRfluor-antibody bands was optimized on the first gel scanned using auto PMT detection on the Typhoon imager. The value of 460V was used for the rest of the gels scanned, which allows for accurate comparison of band intensities in all sCIRfluor-Fab samples. However, the PMT voltage could have been more diligently optimized by imaging a fluorescent gel over a range of voltages to determine which value obtained the best signal-to-noise ratio.⁴⁰

4.0 Peptide Mapping of SuFEx cARMs

4.1 Objectives

The third and final objective of this project was to determine the site of covalent modification by SuFEx cARMs on antiDNP. As previously discussed, these molecules were designed and predicted to bind to one nucleophilic residue on antiDNP to form a covalent bond between the small molecule and antibody. This could be any nucleophilic amino acid; with a high probability the amino acid target would be a tyrosine or lysine. To complete this objective, fluorescent SuFEx CIRs were incubated with full-length monoclonal antiDNP IgG, synthesized from the Miller lab. Conjugated samples were sent to Bioinformatic Solutions Inc. (Waterloo, ON) to analyze post-translational modification. In brief, conjugated protein samples were analyzed using top-down and bottom-up analysis with each approach described below (also see Figure 42 in appendix). Experimental details are included in the supplemental.

4.2 Results

4.2.1. Top-down analysis

In the top-down approach, sCIR conjugated samples were introduced and analyzed by liquid-chromatography mass spectrometry. In this technique, the number of intact species in sCIR4fluor-Fab and sCIR5fluor-Fab samples were determined, along with their molecular weights (Figures 29 & 31). The percentage of conjugated was estimated from the area under the peak of the conjugated sCIR-Fab species (Figures 30 & 32).

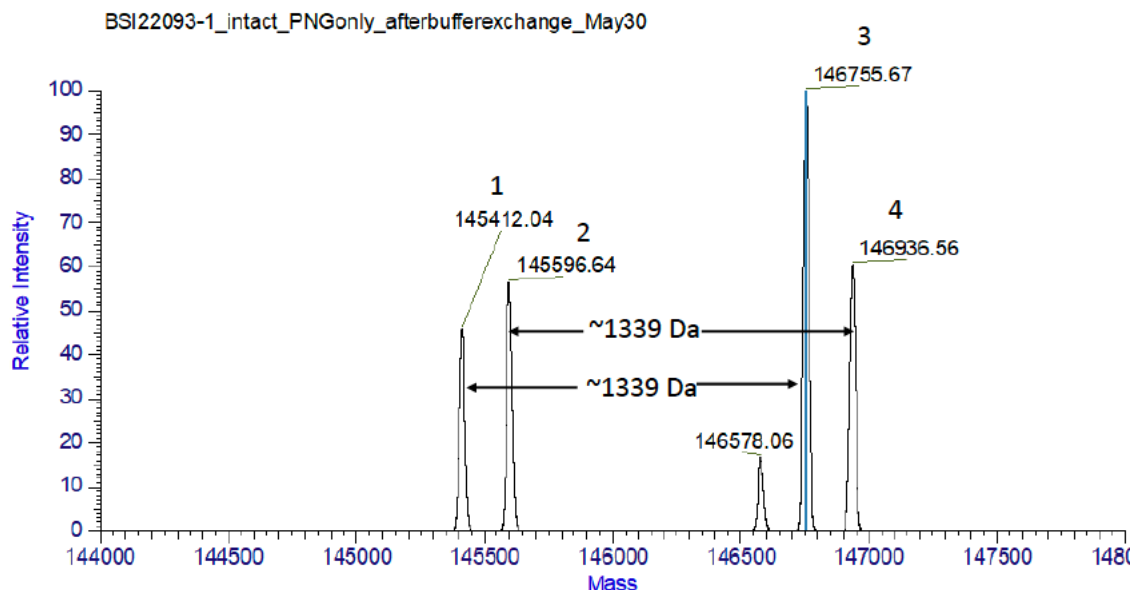


Figure 29. Liquid-chromatography mass-spectrometry of deglycosylated forms of antiDNP incubated with sCIR4fluor for 24 hours.

In this spectrum four intact species were detected, with peaks 1 and 2 representing the unconjugated forms of non-reduced antibody and peaks 3 and 4 representing the non-reduced antibody conjugated with sCIR4fluor. The mass of species 2 and 4 correspond to the predicted molecular weights of reduced antibody unconjugated (peak 2) and conjugated (peak 4). Identity of species 1 and 3 is unknown but are assumed to be proteoforms of antiDNP. There is a mass difference of 1339 Da between each conjugated and unconjugated pair (1 and 3, 2 and 4), indicating sCIR4fluor successfully labelled the SPE7 Fab.

Average Mass	Intact Species	Sum Intensity	Sum of Intact Species	Percentage of antibody species
145412.04	Unconjugated (1)	5.83E+08		
145596.64	Unconjugated (2)	7.16E+08	1.30E+09	36.99%
146755.67	1*conjugate (3)	1.27E+09		
146936.56	1*conjugate (4)	7.65E+08	2.03E+9	57.77%
146578.06	Unidentified	2.11E+08	2.11E+08	6%

Figure 30. Peak intensities of mass species of antiDNP conjugated with sCIR4fluor. Peak intensities of intact mass species in antiDNP sample conjugated with sCIR4fluor. Area under each peak was calculated from LC-MS data of Ab-sCIR4fluor and used to determine percentage of antibody species labelled.

From the data presented in Figure 30, it is calculated 57.7% of antibody is conjugated. Sample calculation is included in the supplemental section.

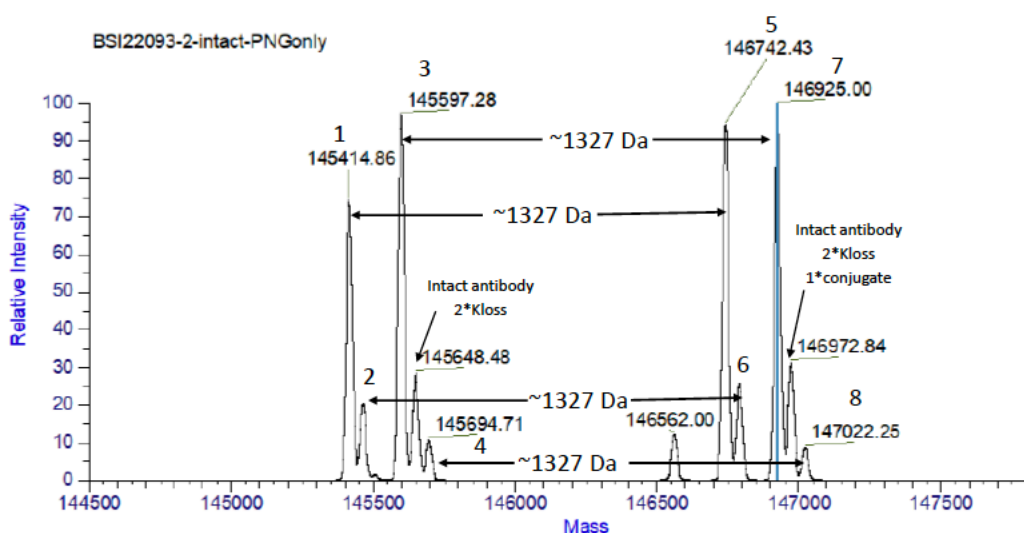


Figure 31. Liquid-chromatography mass-spectrometry of deglycosylated forms of antiDNP incubated with sCIR5fluor for 96 hours.

In this spectrum four major intact species were detected, with peaks 1 and 3 representing the unconjugated forms of non-reduced antiDNP and peaks 5 and 7 representing the conjugated forms of antiDNP with sCIR4fluor. The mass of species 3 and 7 correspond to the predicted

molecular weights of non-reduced Fab unconjugated (peak 3) and conjugated (peak 7). Identity of species 1 and 3 is unknown but are assumed to be proteoforms of antibody. There is a mass difference of 1327 Da between each conjugated and unconjugated pair (1 and 5, 3 and 7), indicating sCIR4fluor successfully labelled the DNP antibody.

Average Mass	Intact Species	Sum Intensity	Sum of Intact Species	Percentage of antibody species
145414.86	Unconjugated (1)	5.42E+07		
145462.32	Unconjugated (2)	5.92E+06		
145597.28	Unconjugated (3)	7.05E+07		
145648.48	Unconjugated with 2*Kloss	2.09E+07		
145694.71	Unconjugated (4)	7.88E+06	1.59E+8	47.05%
146742.43	1*conjugate (5)	6.88E+07		
146791.61	1*conjugate (6)	1.87E+07		
146925	1*conjugate (7)	7.28E+07		
146972.84	1*conjugate with 2*Kloss	2.29E+07		
147022.25	1*conjugate (8)	6.51E+06	1.73E+8	51.2%
146562	Unidentified	5.92E+06	5.92E+06	1.75%

Figure 32. Peak intensities of intact mass species in sCIR5fluor conjugated sample. Area under each peak was calculated from LC-MS data of Ab-sCIR5fluor and used to determine percentage of antibody species labelled.

From values in Figure 32, it is estimated 51.2% of antibody is conjugated.

Reduced samples of sCIR4fluor and sCIR5fluor conjugates were also analyzed by LC-MS, but this resulted in the loss of both sCIR compounds from antibody. Figures 46 & 47 in supplemental section depict LC-MS spectra of the heavy and light chain for sCIR4fluor. Figures 48 & 49 represent the LC-MS spectra of the heavy and light chain for sCIR5fluor. In both samples, only

Figure 33. Identification of post-translation modification by sCIR4fluor on antiDNP. MS/MS spectra of a digested protein from sCIR4fluor incubated with antiDNP. The location of lysine modification indicated by a red arrow and in row 10 in ion match table. Blue numbers represent a b-ion match and red indicate y-ion match.

Peptide Mapping of Heavy Chain-Sample 1

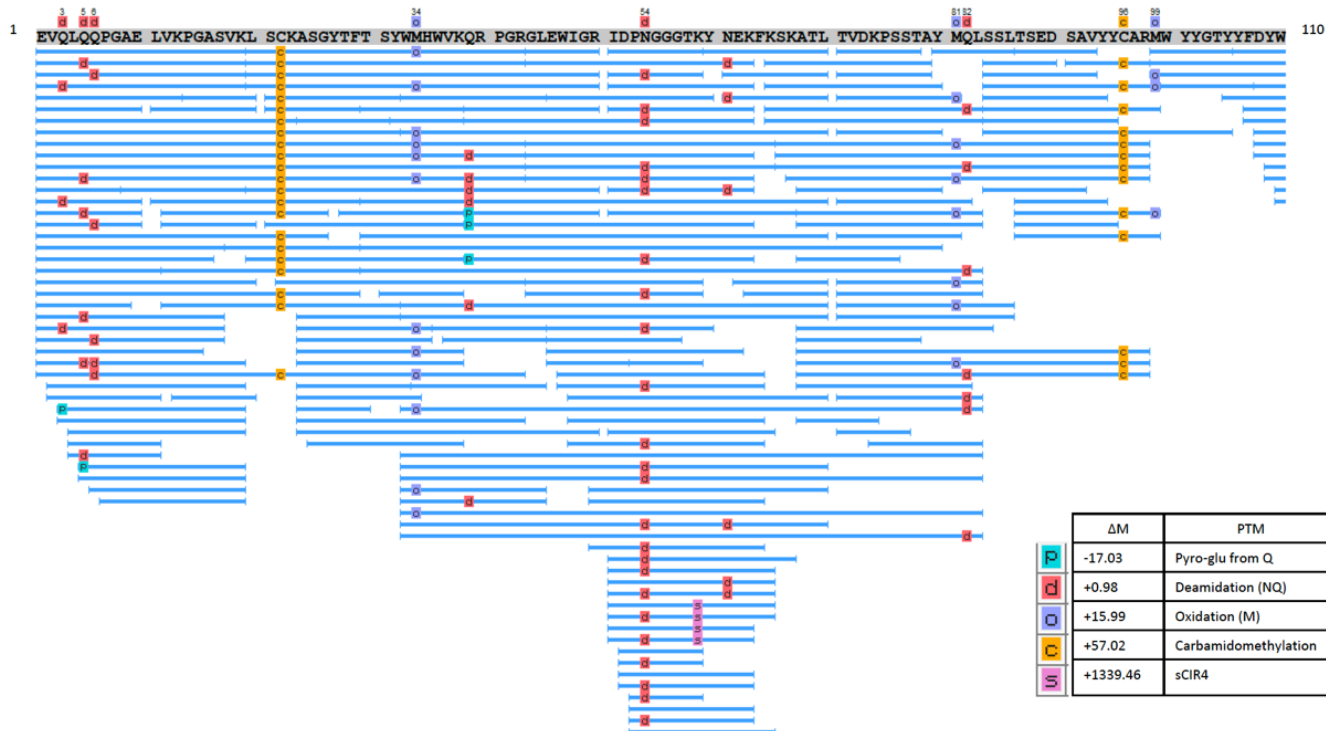


Figure 34. Peptide mapping of sCIR4-Fab sample.

Sequences of sCIR4fluor peptide fragments generated after protein digestion were mapped onto known antiDNP sequence of the heavy chain. One PTM of sCIR4fluor was found with a molecular weight of 1339.46 g/mol.

From PTM analysis of sCIR4fluor with antiDNP, the site of covalent modification was determined to be lysine 59 of the heavy chain (red arrow in Figure 33).

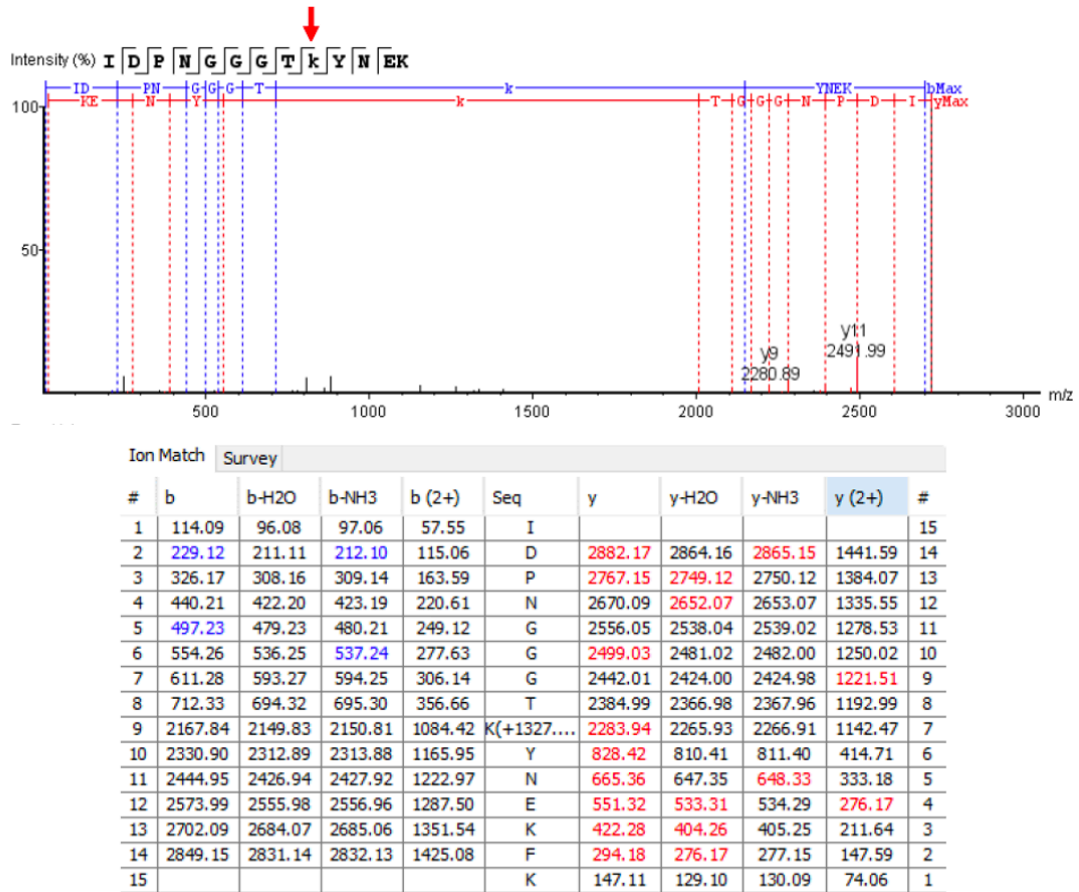


Figure 35. Identification of post-translation modification by sCIR5fluor on antiDNP. MS/MS spectra of a digested protein from sCIR5fluor incubated with antiDNP. The location of lysine modification indicated by a red arrow and in row 10 in ion match table. Blue numbers represent a b-ion match and red indicate y-ion match.

Peptide Mapping of Heavy Chain-Sample



Figure 36. Peptide mapping of sCIR5-Fab sample.

Sequences of sCIR5fluor peptide fragments generated after protein digestion were mapped onto known antiDNP sequence of the heavy chain. One PTM of sCIR5fluor was found with a molecular weight of 1327.42 g/mol.

Based on the peptide fragments matched to the known sequence of antiDNP, the site of covalent modification of sCIR5fluor was also lysine 59 of the heavy chain (red arrow in Figure 35).

4.3 Discussion

4.3.1 Preparation of MS samples

Based on the chemical properties and recent papers of SuFEx, the target of sCIRs were assumed to be any nucleophilic residue on antiDNP including lysine, tyrosine, serine, threonine, histidine, and cysteine.⁴¹ Many papers indicate the reactivity of sulfur fluorides can be tuned towards their target, depending on the positioning and interactions between other residues in a binding pocket or stable protein confirmation. We predicted that SuFEx cARMs would target a lysine or tyrosine residue on antiDNP but had no way of testing this claim before peptide mapping of the sCIR-Ab complex was performed. Some papers suggest that fluorosulfates preferentially react with tyrosine residues^{42–44}, which is one of the reasons sCIR5fluor was sent for PTM analysis. Along with this sample, sCIR4fluor was sent for sequencing to identify the target of sulfonyl fluoride and fluorosulfates cARMs.

The major reason sCIR4&5fluor were chosen for mass spectrometry analysis was due to their intramolecular rate derived from Figure 20 & 21. This data revealed sCIR4 had the largest k_{inact} of $3.94 \times 10^{-4} \text{ s}^{-1}$, and sCIR5 was the slowest to label antiDNP at $5.57 \times 10^{-6} \text{ s}^{-1}$. To ensure the highest % of labelling in the conjugated samples, sCIR4 was incubated with the Fab for 24 hours and sCIR5 was incubated for 96 hours. In Figure 20, fluorescence reached a plateau at 24 hours which led to the assumption sCIR4 labelling was complete in this time. 96 hours was an arbitrary length of time chosen for sCIR5 incubation since its fluorescent output never reached a plateau. Both sCIR4&5fluor were incubated and prepped at the same final concentration as SDS-PAGE analysis ($1 \mu\text{M}$ sCIR, $2 \mu\text{M}$ Fab) to ensure consistency.

4.3.2 Top-down analysis

The first part of MS analysis involved treatment of sCIR4fluor and sCIR5fluor samples with PNGase F, to determine the intact mass of deglycosylated proteoforms. The LC-MS spectra in Figure 28 identified an unusual number of intact species. Based on the molecular weight of the intact antibody, accounting for terminal and reduction modifications, peaks 2 and 4 correspond to the expected masses of the deglycosylated unconjugated and conjugated Ab. While intact mass cannot confirm which residue was labelled, sCIR4fluor is expected to be conjugated to the antibody as peaks 2 and 4 have a mass difference of 1339 Da, the exact MW of sCIR4fluor. There are two unexpected peaks present in the LC-MS spectra, 1 and 3, that also have a mass difference of 1339 Da. This mass shift suggests species 1 is a proteoform of the deglycosylated antibody which has labelled by sCIR4fluor to produce peak 3. The difference between the unconjugated and conjugated species is very close, with a mass difference of 184.6 g/mol between peaks 1 and 2, and 180.89 g/mol between peaks 3 and 4. LC-MS of deglycosylated reduced antibody reduced, was also completed and the mass difference of ~180 g/mol was also observed between species. The most likely cause of this modification was from the loss of a glucose molecule (180.16 g/mol) due to incomplete deglycosylation of the antibody. O- and N-glycans are common post-translational modifications found on antibodies like antiDNP IgG, to help with receptor binding and Fc receptor function.^{45,46} PNGase F, the enzyme used in MS analysis, deaminates asparagine residues into aspartic acid, cleaving most N-glycans.⁴⁷ Since the mass difference of ~180 g/mol is observed by in both non-reduced and reduced samples of sCIR4fluor, it is suspected a O-glycan modification present on the antibody was not cleaved before LC-MS analysis.

A similar observation was observed in the LC-MS spectra of sCIR5fluor sample with four major mass species detected and a mass shift of 1327 Da corresponding to the MW of sCIR5fluor. In this sample there were many minor proteoforms that also had a mass difference of 1327 Da corresponding to peaks 2 and 4, 6 and 8 (Figure 30). A mass difference of 182.24 g/mol between peak 3 and 1, and 182.57 g/mol between peak 7 and 5. Based on a similar line of reasoning for sCIR4fluor, it is also suspected that the different mass species detected in the sCIR5fluor conjugated sample is because of different glycosylation patterns of antiDNP.

The sum of intact species detected in the LC-MS of the deglycosylated samples revealed interesting information about the % of conjugation in each sample. It was surprising only 57.7% of antiDNP was labelled by sCIR4fluor, as it was initially assumed SuFEx labelling for this CIR finished at 24 hours. It is possible the full extent of labelling was not detected by LC-MS, as a result of an instable covalent linkage that was fragmented during ionization. The percentage of labelling for sCIR5 was less surprising with approximately half (51.2 %) of sCIR5 conjugated to antiDNP. Since sCIR5fluor exhibited the slowest labelling rate and did not reach a plateau of fluorescence at 24 hours, the end point of this reaction is unknown. Based on the strong stability and slow reactivity of fluorosulfates (see hydrolytic stability section), it is unlikely sCIR5fluor can reach 100% labelling of SPE7 Fab.

4.3.3 Bottom-up analysis

In the second part of PTM analysis, protein samples were digested and analyzed by LC-MS/MS and compared to the known antibody sequence to identify the site of covalent modification. The amino acid identified of sCIR4fluor and sCIR5 labelling was K59 on the heavy chain, the same site identified for acyl-imidazole CIR attachment.¹ This is a fascinating discovery, which establishes sulfonyl fluoride, fluorosulfate, and acyl-imidazole cARMs have the same amino acid target. This finding suggests AL and SuFEx cARMs have a similar geometric positioning in the binding pocket of antiDNP, leading to the attack of the proximal lysine residue. Two factors which contribute to nucleophilic attack of the CIR include: 1. The aromatic residues in the binding pocket which “sandwiches” the ABD, and 2. The linker length between the ABD and ALD.

In the first cARM paper, key residues for DNP binding were identified through Auto-Dock (10AU, Figure 36) and peptide mapping experiments.¹ From this study, it was revealed that the residues Y105 (heavy chain) and W93 (light chain) in the variable region of the Fab aid in aromatic ring stacking of the dinitrophenyl ring. Aromatic compounds, including tyrosine and tryptophan, have “clouds” of electron density above and below their aromatic ring due to pi-systems in their structure.⁴⁸ Pi-stacking or aromatic stacking is a non-covalent force in which aromatic rings “stack” on top of each other due to alignment of electrostatic charges. In the binding pocket of antiDNP, Tyr105 and Trp93 align the aromatic ring of the ABD, which places the ALD 4.2 angstroms away from the closest nucleophilic amino acid, lysine-59. These residues help facilitate covalent bond formation by aligning the CIR in the DNP binding site.

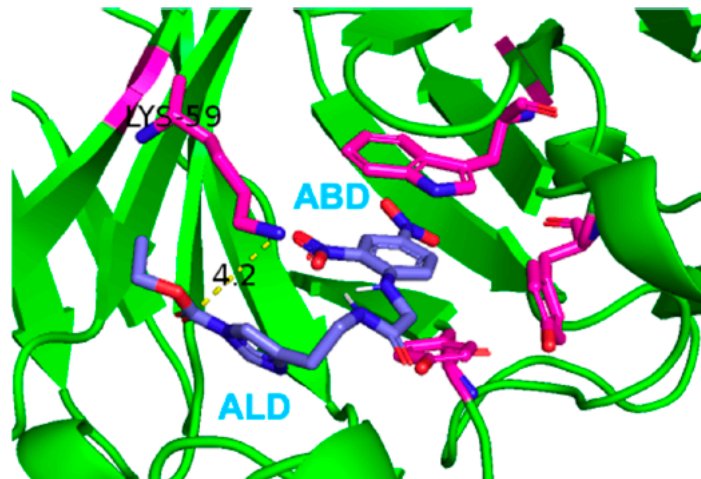


Figure 37. Auto-docking of acyl-imidazole CIR with antiDNP SPE7 (PBD 1O AQ).¹ CIR fragment coloured in purple, with acyl-imidazole labelling domain located 4.2 angstroms from the attacking residue lysine-59 on antiDNP.

The second factor that impacts amino acid selectivity is the distance between the ABD and ALD of the cARM. The acyl-imidazole CIR, sCIR4, and sCIR5 were all designed with a similar linker length between the binding-domain (green in Figure 38) and the labelling-domain (blue in Figure 38). Alkyl linkers are very flexible, which explains why the ALD of each is positioned in a similar way and subject to attack by lysine59. A future endeavour of the SuFEx cARM project could involve varying the distance between the ABD and ALD with linker of different length and rigidity, to better understand distance between these domains impact amino acid selectivity.

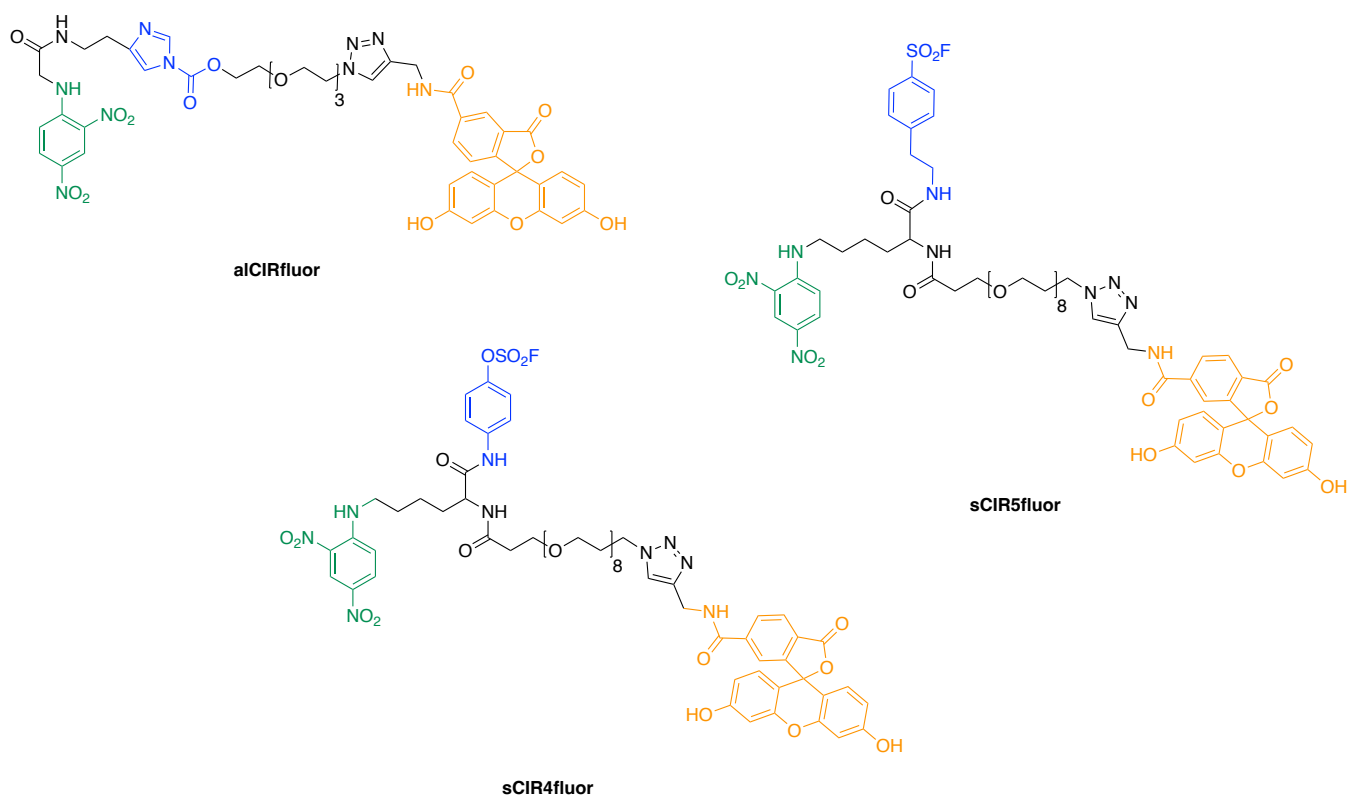


Figure 38. Structure of fluorescent acyl-imidazole CIR, sCIR4, and sCIR5.

Antibody binding domain highlighted in green, antibody labelling domain in blue, and fluorescein reporter in orange.

From the autodocking study, two other nucleophilic residues that were close to the CIR were Y34 (7.2 Å) and Y94 (13.8 Å) on the light chain (Figure 38). These residues could be a center of focus in future CIR development, as the reactivity of SuFEx probes can be tuned towards nucleophilic residues such as tyrosine. This is of keen interest for the Rullo lab, as the targeting of a novel residue could facilitate attachment of two CIRs per Fab of antiDNP.

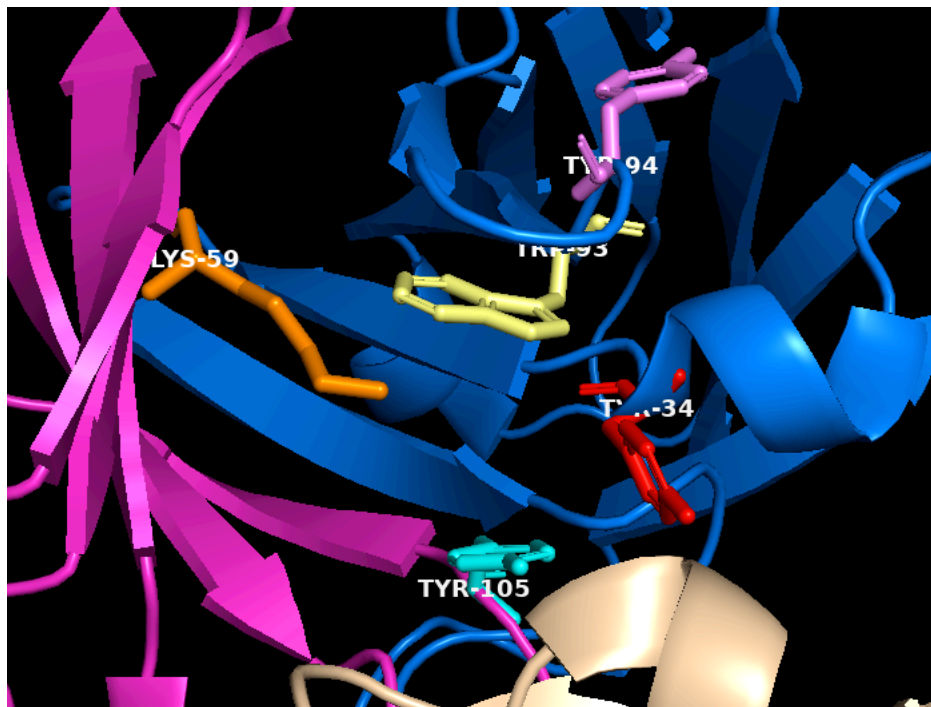


Figure 39. Pymol structure of antiDNP SPE7 (10AU) with key residues for CIR binding. Pink ribbon structure represents heavy chain of antiDNP, with blue representing the light chain and beige representing the constant region of the Fab. Key residues involved in CIR labelling include lysine59, tyrtophan93 and tyrosine105. Nearby tyrosine residues labelled are at 34 and 94 on the light chain.

PTM identification can be challenging for numerous reasons. Aside from the cost and the length of time required for peptide mapping, the identification of antibody modification is tricky due to the range of innate oxidation, deamidation, and glycosylation patterns that are present before conjugation of a small molecule.⁴⁹ In particular, the matching of peptide sequences to the known antibody sequence is challenging as peptides are fragmented in MS twice. In this way, fragments with different amino acid sequence can have a similar molecular weight introducing bias when resolving the amino acid sequence of the generated peptides.⁴⁹ Difficulties encountered in the sCIR project included finding a facility that could reliably identify PTMs at a reasonable cost, and the identification of sCIR5fluor to antiDNP. At first, conjugation of sCIR5fluor could not be

determined as no modification of 1327 g/mol was observed in the protein identification software. When the peptide fragments were scanned in a different software, the mass shift corresponding to sCIR5fluor was found. This difference could be contributed by the differences in the peptide mapping algorithm, which matches every peptide sequence against the MS/MS spectra.

5.0 Conclusion

There were three key findings in this thesis, relating to the stability, selectivity, and labelling rate of antiDNP by sulfur fluoride cARMs. Based upon the hydrolytic stability studies, PTM analysis, and fluorescent labelling experiments conducted, SuFEx chemistry has enhanced the CIR platform. Fluorosulfate (-OSO₂F) CIRs exhibited remarkable stability in the presence of 90:10 PBS and D₂O. Sulfonyl fluorides were more prone to hydrolysis but had significantly longer half-lives in comparison to acyl-imidazole CIRs. Both para derivatives, sCIR1 (fluorosulfate) and sCIR2 (sulfonyl fluoride) had a higher stability than their meta counterparts. Interestingly, the fluorescent version of sCIR4 (meta-sulfonyl fluoride) labelled lysine59 on the heavy chain of the monoclonal anti-DNP, the same site of covalent modification as acyl-imidazole CIRs. PTM analysis of antiDNP and sCIR5fluor (para-fluorosulfate short linker) was also conducted but the site of covalent modification could not be determined. Fluorescent sCIR derivatives were used to determine the intramolecular rate of antibody labelling through measuring fluorescence after SDS-PAGE. Of the five sCIRs, the meta sulfonyl fluoride (sCIR4) demonstrated the fastest pseudo-first order rate constant, while the para fluorosulfate with the shorter linker (sCIR5) demonstrated the slowest labelling rate. An interesting link was made between the rates of reaction and hydrolysis, with the increased stability of para sCIRs correlated with a slower labelling rate than their meta derivatives. Surprisingly, the rate of labelling for fluorosulfate derivatives were slower than the labelling rate measured of a fluorescent acyl-imidazole CIR. The intermolecular rate constants were deemed negligible from BSA incubated with sCIRfluors. These findings contribute to the overall conclusion that SuFEx is advantageous for the stability, selectivity, and labelling of endogenous antibodies.

5.1.1 Future directions

While there is still much to discover about the selectivity and reactivity of SuFEx cARMs, there are a few other labelling chemistries of interest for covalent antibody recruitment (Figure 39 & 40). A novel *N*-acyl-*N*-alkyl (NASA) sulfonamide probe reported in 2018²¹, covalently modified a lysine residue on Hsp90, a chaperone protein expressed on cancer cells. While its target is the same as SuFEx and acyl-imidazole reactive chemistry, the second-order rate constant of the NASA inhibitor was found to $10^4 - 10^5 \text{ M}^{-1}\text{s}^{-1}$ which is comparable to the fastest biorthogonal click reaction²¹. Another ligand-directed chemistry of current interest to the Rullo lab is use of a 3-phenyl-2*H*-azirine alkyne derivative, which was used to selectively label carboxylic acids⁵⁰. Due to the high nucleophilicity of the three-membered ring with a C=N group, azirines are highly reactive towards intramolecular nucleophilic addition and ring expansion to form a very stable *N*-phenylacetamide adduct.

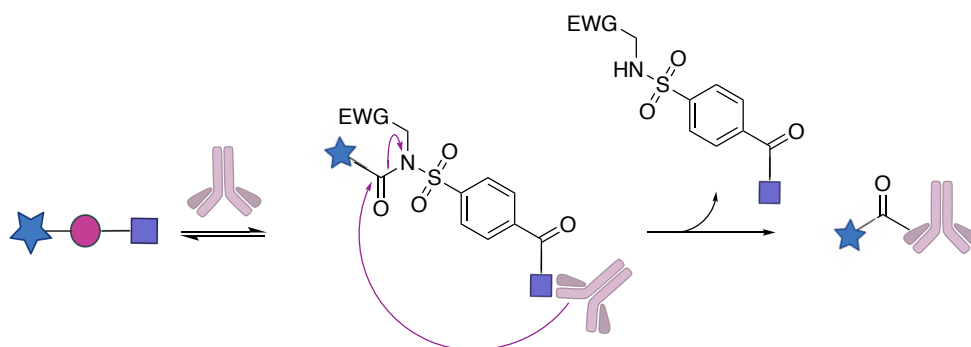


Figure 40. Mechanism of covalent antibody labelling with *N*-acyl-*N*-sulfonamide cARM.

Adapted from *Nat. Comm.* 2018, 9, 1870.

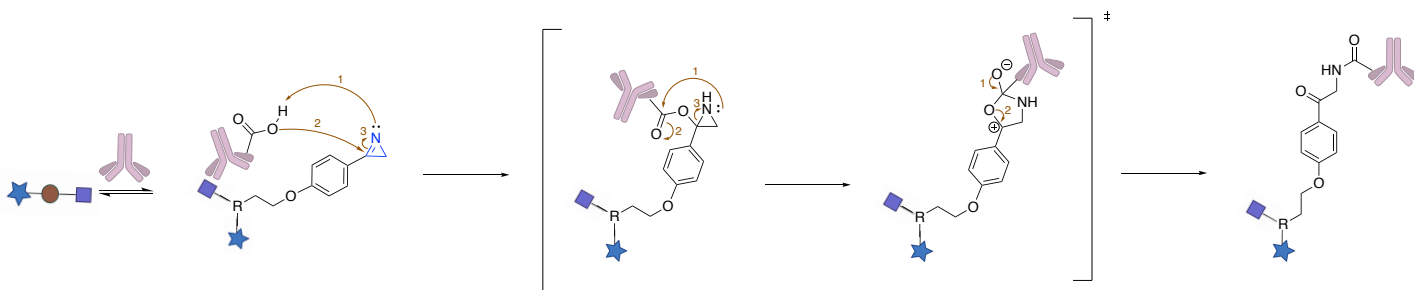


Figure 41. Mechanism of covalent antibody labelling with azirine cARM.

Adapted from *J. Am. Chem. Soc.* 2020, 142, 13, 6051-6059.

Expanding upon the results discussed in this thesis, there are several ways SuFEx chemistry can be explored in CIR development. One example includes the strategic targeting of tyrosine residue using varying linkers between the backbone and ALD of the cARM. Labelling an amino acid residue other than lysine would significantly advance the cARM platform, with the ability to target one Fab with two CIR molecules (Figure 41). The development of a bi-specific labelling strategy could enhance cell-killing of a heterogenic tumor cell. Furthermore, SuFEx could be useful in the development of cARMs that target other endogenous antibodies such as L-Rhamnose. A current endeavour of this work involves crystallization of antiDNP Fab and obtaining co-crystal structures with SuFEx cARMs to determine how position of the sulfur fluoride group impacts selectivity and effective molarity within the antibody binding pocket. All these areas of research would contribute to the understanding of covalent labelling of serum antibodies and the broad fields of protein labelling, biorthogonal reactions, and immunotherapeutic development.

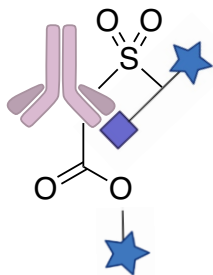


Figure 42. Bi-specific labelled antibody with AL and SuFEx cARM.

6.0 References

- (1) Lake, B.; Serniuck, N.; Kapcan, E.; Wang, A.; Rullo, A. F. Covalent Immune Recruiters: Tools to Gain Chemical Control over Immune Recognition. *ACS Chemical Biology* **2020**, *15* (4), 1089–1095. <https://doi.org/10.1021/acscchembio.0c00112>.
- (2) Lou, T. S. B.; Willis, M. C. Sulfonyl Fluorides as Targets and Substrates in the Development of New Synthetic Methods. *Nature Reviews Chemistry*. Nature Research February 1, 2022, pp 146–162. <https://doi.org/10.1038/s41570-021-00352-8>.
- (3) Abbott, M.; Ustoyev, Y. Cancer and the Immune System: The History and Background of Immunotherapy. *Seminars in Oncology Nursing*. Elsevier Inc October 1, 2019. <https://doi.org/10.1016/j.soncn.2019.08.002>.
- (4) Weiner, G. J. Monoclonal Antibody Mechanisms of Action in Cancer. *Immunologic Research*. November 2007, pp 271–278. <https://doi.org/10.1007/s12026-007-0073-4>.
- (5) Dobosz, P.; Dzieciatkowski, T. The Intriguing History of Cancer Immunotherapy. *Frontiers in Immunology*. Frontiers Media S.A. December 17, 2019. <https://doi.org/10.3389/fimmu.2019.02965>.
- (6) Lu, R. M.; Hwang, Y. C.; Liu, I. J.; Lee, C. C.; Tsai, H. Z.; Li, H. J.; Wu, H. C. Development of Therapeutic Antibodies for the Treatment of Diseases. *Journal of Biomedical Science*. BioMed Central Ltd. January 2, 2020. <https://doi.org/10.1186/s12929-019-0592-z>.
- (7) *Antibody-dependent cellular cytotoxicity & phagocytosis (ADCC & ADCP)*. [https://www.invivogen.com/adcc-adcp#:~:text=ADCC%20and%20ADCP%20are%20initiated%20when%20multiple%20IgG,activation%20motifs%20%28ITAMs%29%20and%20inhibition%20motifs%20%28ITIMs%29%2C%20respectively.\(accessed 2022-07-02\)](https://www.invivogen.com/adcc-adcp#:~:text=ADCC%20and%20ADCP%20are%20initiated%20when%20multiple%20IgG,activation%20motifs%20%28ITAMs%29%20and%20inhibition%20motifs%20%28ITIMs%29%2C%20respectively.(accessed%202022-07-02)).
- (8) Norman Phillip. *Immunobiology: The Immune System in Health and Disease*, 2nd ed.; Janeway C.A. Jr, Travers P., Eds.; Garland Science: London, 1995; Vol. 96.
- (9) Martinelli, E.; de Palma, R.; Orditura, M.; de Vita, F.; Ciardiello, F. Anti-Epidermal Growth Factor Receptor Monoclonal Antibodies in Cancer Therapy. *Clinical and Experimental Immunology*. October 2009, pp 1–9. <https://doi.org/10.1111/j.1365-2249.2009.03992.x>.
- (10) Uvyn, A.; de Geest, B. G. Multivalent Antibody-Recruiting Macromolecules: Linking Increased Binding Affinity with Enhanced Innate Immune Killing. *ChemBioChem*. Wiley-VCH Verlag November 2, 2020, pp 3036–3043. <https://doi.org/10.1002/cbic.202000261>.
- (11) McEnaney, P. J.; Parker, C. G.; Zhang, A. X.; Spiegel, D. A. Antibody-Recruiting Molecules: An Emerging Paradigm for Engaging Immune Function in Treating Human Disease. *ACS Chemical Biology*. July 20, 2012, pp 1139–1151. <https://doi.org/10.1021/cb300119g>.
- (12) Ovacik, M.; Lin, K. Tutorial on Monoclonal Antibody Pharmacokinetics and Its Considerations in Early Development. *Clinical and Translational Science* **2018**, *11* (6), 540–552. <https://doi.org/10.1111/cts.12567>.
- (13) Achilli, S.; Berthet, N.; Renaudet, O. Antibody Recruiting Molecules (ARMs): Synthetic Immunotherapeutics to Fight Cancer. *RSC Chemical Biology* **2021**, *2* (3), 713–724. <https://doi.org/10.1039/d1cb00007a>.

- (14) James, L. C.; Roversi, P.; Tawfik, D. S. *Antibody Multispecificity Mediated by Conformational Diversity*.
- (15) Tamura, T.; Hamachi, I. Chemistry for Covalent Modification of Endogenous/Native Proteins: From Test Tubes to Complex Biological Systems. *J Am Chem Soc* **2019**, *141* (7), 2782–2799. <https://doi.org/10.1021/jacs.8b11747>.
- (16) Strelow, J. M. A Perspective on the Kinetics of Covalent and Irreversible Inhibition. *Journal of Biomolecular Screening*. SAGE Publications Inc. January 1, 2017, pp 3–20. <https://doi.org/10.1177/1087057116671509>.
- (17) Hobert, E. M.; Doerner, A. E.; Walker, A. S.; Schepartz, A. Effective Molarity Redux: Proximity as a Guiding Force in Chemistry and Biology. *Israel Journal of Chemistry*. August 2013, pp 567–576. <https://doi.org/10.1002/ijch.201300063>.
- (18) Krishnamurthy, V. M.; Semetey, V.; Bracher, P. J.; Shen, N.; Whitesides, G. M. Dependence of Effective Molarity on Linker Length for an Intramolecular Protein-Ligand System. *J Am Chem Soc* **2007**, *129* (5), 1312–1320. <https://doi.org/10.1021/ja066780e>.
- (19) Shiraiwa, K.; Cheng, R.; Nonaka, H.; Tamura, T.; Hamachi, I. Chemical Tools for Endogenous Protein Labeling and Profiling. *Cell Chemical Biology*. Elsevier Ltd August 20, 2020, pp 970–985. <https://doi.org/10.1016/j.chembiol.2020.06.016>.
- (20) Tamura, T.; Ueda, T.; Goto, T.; Tsukidate, T.; Shapira, Y.; Nishikawa, Y.; Fujisawa, A.; Hamachi, I. Rapid Labelling and Covalent Inhibition of Intracellular Native Proteins Using Ligand-Directed N-Acyl-N-Alkyl Sulfonamide. *Nature Communications* **2018**, *9* (1). <https://doi.org/10.1038/s41467-018-04343-0>.
- (21) Dong, J.; Krasnova, L.; Finn, M. G.; Barry Sharpless, K. Sulfur(VI) Fluoride Exchange (SuFEx): Another Good Reaction for Click Chemistry. *Angewandte Chemie - International Edition*. Wiley-VCH Verlag September 1, 2014, pp 9430–9448. <https://doi.org/10.1002/anie.201309399>.
- (22) Abdul Fattah, T.; Saeed, A.; Albericio, F. Recent Advances towards Sulfur (VI) Fluoride Exchange (SuFEx) Click Chemistry. *Journal of Fluorine Chemistry*. Elsevier B.V. September 1, 2018, pp 87–112. <https://doi.org/10.1016/j.jfluchem.2018.07.008>.
- (23) Barrow, A. S.; Smedley, C. J.; Zheng, Q.; Li, S.; Dong, J.; Moses, J. E. The Growing Applications of SuFEx Click Chemistry. *Chemical Society Reviews*. Royal Society of Chemistry September 7, 2019, pp 4731–4758. <https://doi.org/10.1039/c8cs00960k>.
- (24) Jones, L. H. Emerging Utility of Fluorosulfate Chemical Probes. *ACS Medicinal Chemistry Letters* **2018**, *9* (7), 584–586. <https://doi.org/10.1021/acsmedchemlett.8b00276>.
- (25) Zheng, Q.; Woehl, J. L.; Kitamura, S.; Santos-Martins, D.; Smedley, C. J.; Li, G.; Forli, S.; Moses, J. E.; Wolan, D. W.; Sharpless, K. B. SuFEx-Enabled, Agnostic Discovery of Covalent Inhibitors of Human Neutrophil Elastase. *PNAS* **2019**, *116* (38), 18808–18814. <https://doi.org/10.1073/pnas.1909972116>.
- (26) Brighty, G. J.; Botham, R. C.; Li, S.; Nelson, L.; Mortenson, D. E.; Li, G.; Morisseau, C.; Wang, H.; Hammock, B. D.; Sharpless, K. B.; Kelly, J. W. Using Sulfuramidimidoyl Fluorides That Undergo Sulfur(vi) Fluoride Exchange for Inverse Drug Discovery. *Nature Chemistry* **2020**, *12* (10), 906–913. <https://doi.org/10.1038/s41557-020-0530-4>.
- (27) Yang, B.; Wu, H.; Schnier, P. D.; Liu, Y.; Liu, J.; Wang, N.; Degrado, W. F.; Wang, L. Proximity-Enhanced SuFEx Chemical Cross-Linker for Specific and Multitargeting Cross-

- Linking Mass Spectrometry. *Proc Natl Acad Sci U S A* **2018**, *115* (44), 11162–11167. <https://doi.org/10.1073/pnas.1813574115>.
- (28) *¹⁹F NMR Reference Standards*. https://www.colorado.edu/lab/nmr/sites/default/files/attached-files/19f_nmr_reference_standards_0.pdf (accessed 2022-07-02).
- (29) Gilbert, K.; Vuorinen, A.; Aatkar, A.; Pogány, P.; Pettinger, J.; Kirkpatrick, J. M.; Rittinger, K.; House, D.; Burley, G. A.; Bush, J. T. *Profiling Sulfur(VI) Fluorides as Reactive Functionalities for Chemical Bi-Ology Tools and Expansion of the Ligandable Proteome*.
- (30) Hunt, I. Substituent Effects.
- (31) Nicoya Lifesciences. *4 ways to reduce non-specific binding in surface plasmon resonance experiments*. <https://nicoyalife.com/blog/4-ways-reduce-non-specific-binding-spr/> (accessed 2022-07-23).
- (32) EMBIBE. *Pseudo First-Order Reactions: Overview, Reactions, Examples*. <https://www.embibe.com/exams/pseudo-first-order-reactions/> (accessed 2022-07-22).
- (33) McCann, H. M.; Lake, B. P. M.; Hoffman, K. S.; Davola, M. E.; Mossman, K. L.; Rullo, A. F. Covalent Immune Proximity-Induction Strategy Using SuFEx-Engineered Bifunctional Viral Peptides. *ACS Chemical Biology* **2022**. <https://doi.org/10.1021/acscchembio.2c00233>.
- (34) Pettinger, J.; Carter, M.; Jones, K.; Cheeseman, M. D. Kinetic Optimization of Lysine-Targeting Covalent Inhibitors of HSP72. *Journal of Medicinal Chemistry* **2019**, *62* (24), 11383–11398. <https://doi.org/10.1021/acs.jmedchem.9b01709>.
- (35) Gilbert, K.; Vuorinen, A.; Aatkar, A.; Pogány, P.; Pettinger, J.; Kirkpatrick, J. M.; Rittinger, K.; House, D.; Burley, G. A.; Bush, J. T. *Profiling Sulfur(VI) Fluorides as Reactive Functionalities for Chemical Bi-Ology Tools and Expansion of the Ligandable Proteome*.
- (36) Zhang, Y.; Park, K. Y.; Suazo, K. F.; Distefano, M. D. Recent Progress in Enzymatic Protein Labelling Techniques and Their Applications. *Chemical Society Reviews*. Royal Society of Chemistry December 21, 2018, pp 9106–9136. <https://doi.org/10.1039/c8cs00537k>.
- (37) Dietlin-Auril, V.; Lecerf, M.; Depinay, S.; Noé, R.; Dimitrov, J. D. Interaction with 2,4-Dinitrophenol Correlates with Polyreactivity, Self-Binding, and Stability of Clinical-Stage Therapeutic Antibodies. *Molecular Immunology* **2021**, *140*, 233–239. <https://doi.org/10.1016/j.molimm.2021.10.019>.
- (38) *Fluorescein (FITC)*. <https://www.thermofisher.com/ca/en/home/life-science/cell-analysis/fluorophores/fluorescein.html#> (accessed 2022-07-03).
- (39) *PMT Voltage Optimization*. <https://www.uth.edu/imm/service-centers/flow-cytometry/pmt-voltage-optimization> (accessed 2022-07-03).
- (40) Narayanan, A.; Jones, L. H. Sulfonyl Fluorides as Privileged Warheads in Chemical Biology. *Chemical Science*. Royal Society of Chemistry May 1, 2015, pp 2650–2659. <https://doi.org/10.1039/c5sc00408j>.
- (41) Chen, W.; Dong, J.; Plate, L.; Mortenson, D. E.; Brighty, G. J.; Li, S.; Liu, Y.; Galmozzi, A.; Lee, P. S.; Hulce, J. J.; Cravatt, B. F.; Saez, E.; Powers, E. T.; Wilson, I. A.; Sharpless, K. B.; Kelly, J. W. Arylfluorosulfates Inactivate Intracellular Lipid Binding Protein(s) through Chemoselective SuFEx Reaction with a Binding Site Tyr Residue. *J Am Chem Soc* **2016**, *138* (23), 7353–7364. <https://doi.org/10.1021/jacs.6b02960>.

- (42) Choi, E. J.; Jung, D.; Kim, J. S.; Lee, Y.; Kim, B. M. Chemoselective Tyrosine Bioconjugation through Sulfate Click Reaction. *Chemistry - A European Journal* **2018**, *24* (43), 10948–10952. <https://doi.org/10.1002/chem.201802380>.
- (43) Yang, B.; Wu, H.; Schnier, P. D.; Liu, Y.; Liu, J.; Wang, N.; Degrado, W. F.; Wang, L. Proximity-Enhanced SuFEx Chemical Cross-Linker for Specific and Multitargeting Cross-Linking Mass Spectrometry. *Proc Natl Acad Sci U S A* **2018**, *115* (44), 11162–11167. <https://doi.org/10.1073/pnas.1813574115>.
- (44) Boune, S.; Hu, P.; Epstein, A. L.; Khawli, L. A. Principles of N-Linked Glycosylation Variations of IgG-Based Therapeutics: Pharmacokinetic and Functional Considerations. *Antibodies* **2020**, *9* (2), 22. <https://doi.org/10.3390/antib9020022>.
- (45) de Haan, N.; Falck, D.; Wuhrer, M. Monitoring of Immunoglobulin N- And O-Glycosylation in Health and Disease. *Glycobiology*. Oxford University Press 2021, pp 226–240. <https://doi.org/10.1093/GLYCOB/CWZ048>.
- (46) *Rapid PNGase F*. http://wolfson.huji.ac.il/purification/PDF/Deglycosilation/NEB_RapidPNGaseF.pdf#:~:text=N-glycans%20using%20PNGase%20F%20requires%20an%20incubation%20time,addition%20C%20incomplete%20deglycosylation%20can%20lead%20to%20biased%20results (accessed 2022-07-04).
- (47) Rahman, M.; Muhseen, Z.; Junaid, M.; Zhang, H. The Aromatic Stacking Interactions Between Proteins and Their Macromolecular Ligands. *Current Protein & Peptide Science* **2015**, *16* (6), 502–512. <https://doi.org/10.2174/138920371606150702131516>.
- (48) Wang, Y. *What is peptide mapping?*. <https://www.rapidnovor.com/what-is-peptide-mapping/#:~:text=Since%20conventional%20peptide%20mapping%20does%20not%20employ%20tandem,isobaric%20or%20same-mass%20peptides%20or%20amino%20acid%20combinations> (accessed 2022-07-24).
- (49) Ma, N.; Hu, J.; Zhang, Z. M.; Liu, W.; Huang, M.; Fan, Y.; Yin, X.; Wang, J.; Ding, K.; Ye, W.; Li, Z. 2 H-Azirine-Based Reagents for Chemoselective Bioconjugation at Carboxyl Residues Inside Live Cells. *J Am Chem Soc* **2020**, *142* (13), 6051–6059. <https://doi.org/10.1021/jacs.9b12116>.
- (50) *Top-Down Proteomics vs Bottom-Up Proteomics*. <https://www.creative-proteomics.com/resource/top-down-proteomics-vs-bottom-up-proteomics.htm> (accessed 2022-07-02).

7.0 Appendix

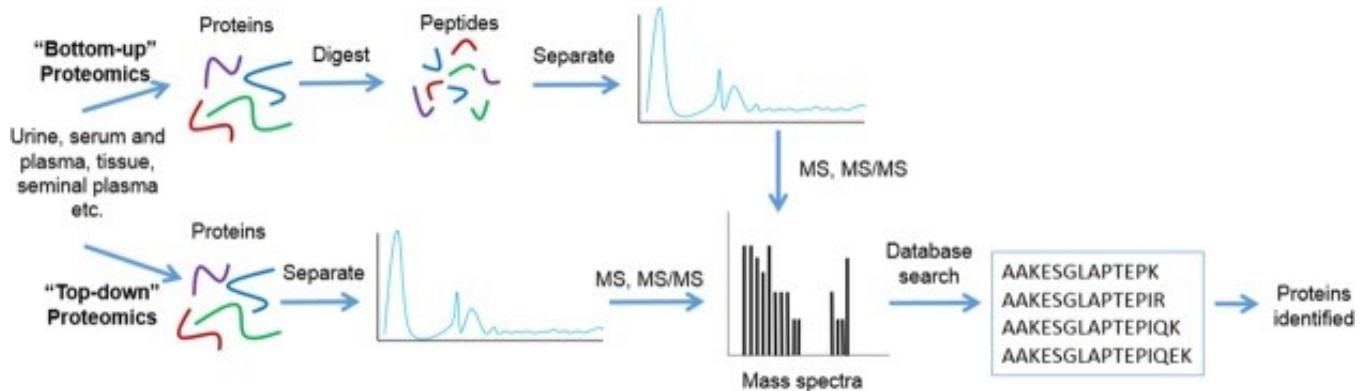


Figure 43. Comparison of top down and bottom-up approaches for post-translational modification analysis.⁵¹

In the top-down approach, the protein sample is directly introduced and ionized by a mass spectrometer. Proteins are separated by their molecular weights and further MS analysis can be conducted. For bottom-up mass-spectrometry, intact proteins are digested with an enzyme to yield varying peptide fragments. These fragments are then ionized and subjected to a mass spectrometer twice, to yield a MS/MS spectrum. Peptide sequences are then compared to the unconjugated protein sequence to determine the site of post-translational modification.

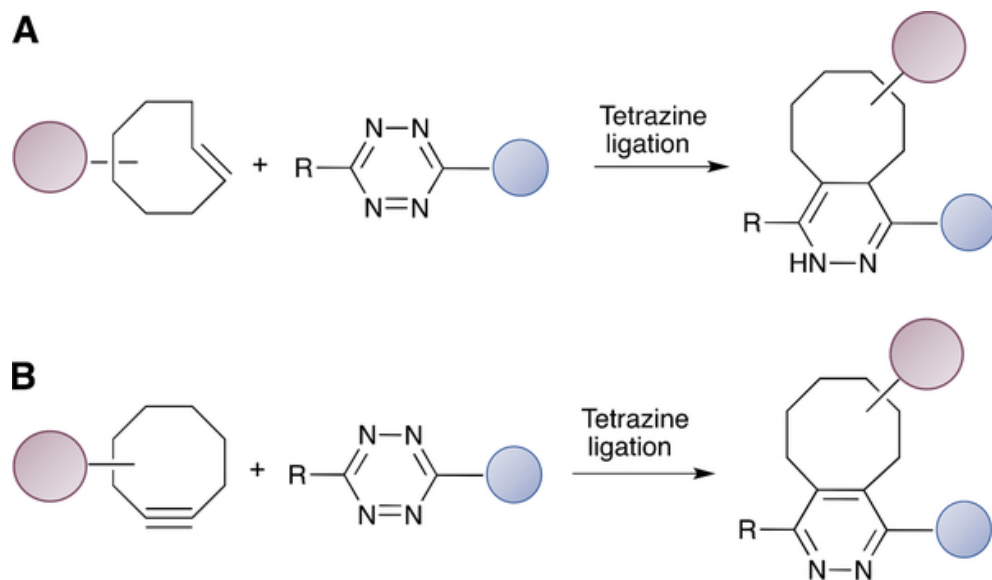


Figure 44. Ligation of tetrazine and trans-cyclooctene functional groups.³⁷

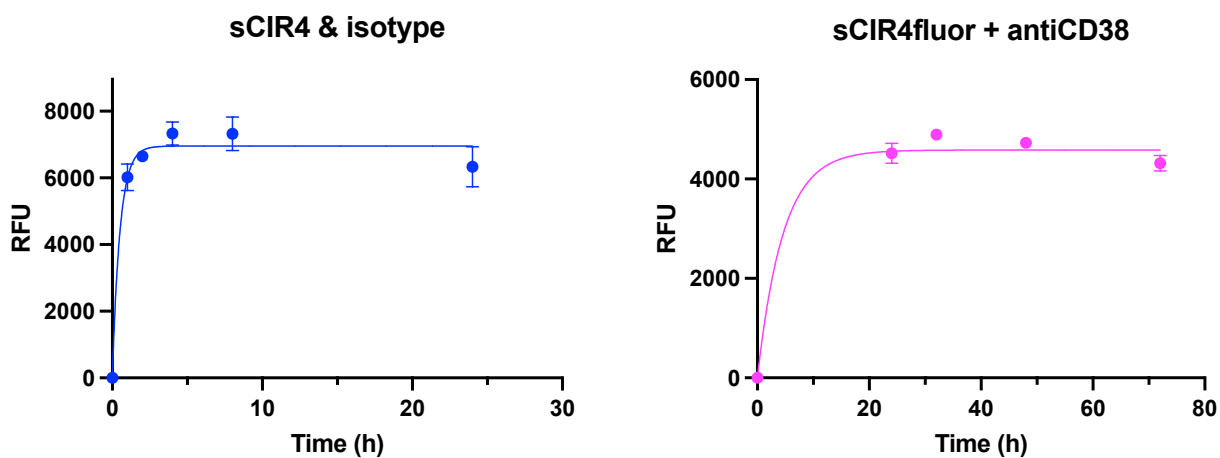
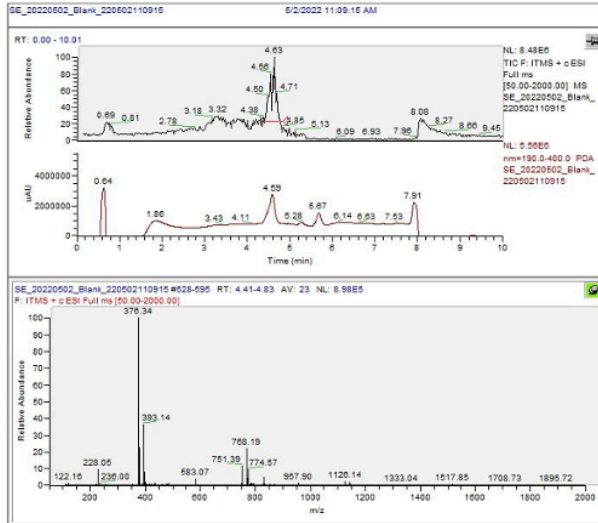


Figure 45. Incubation of sCIR4fluor with isotype IgG and antiCD38.

Blank 1. 10 min run of 20 μ L ACN



Blank 2. 5 min run of 20 μ L ACN

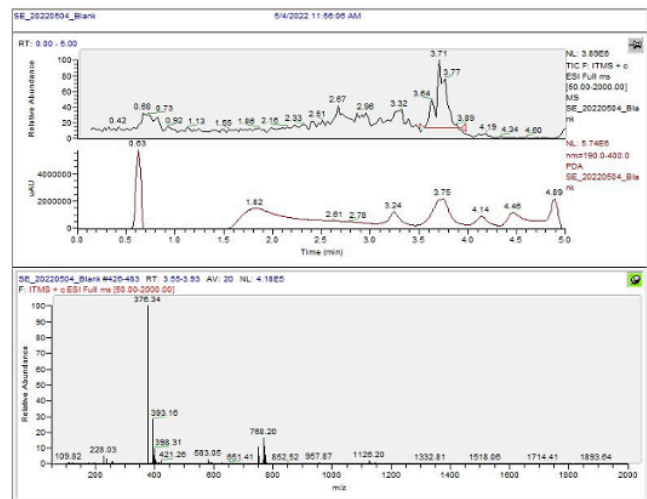
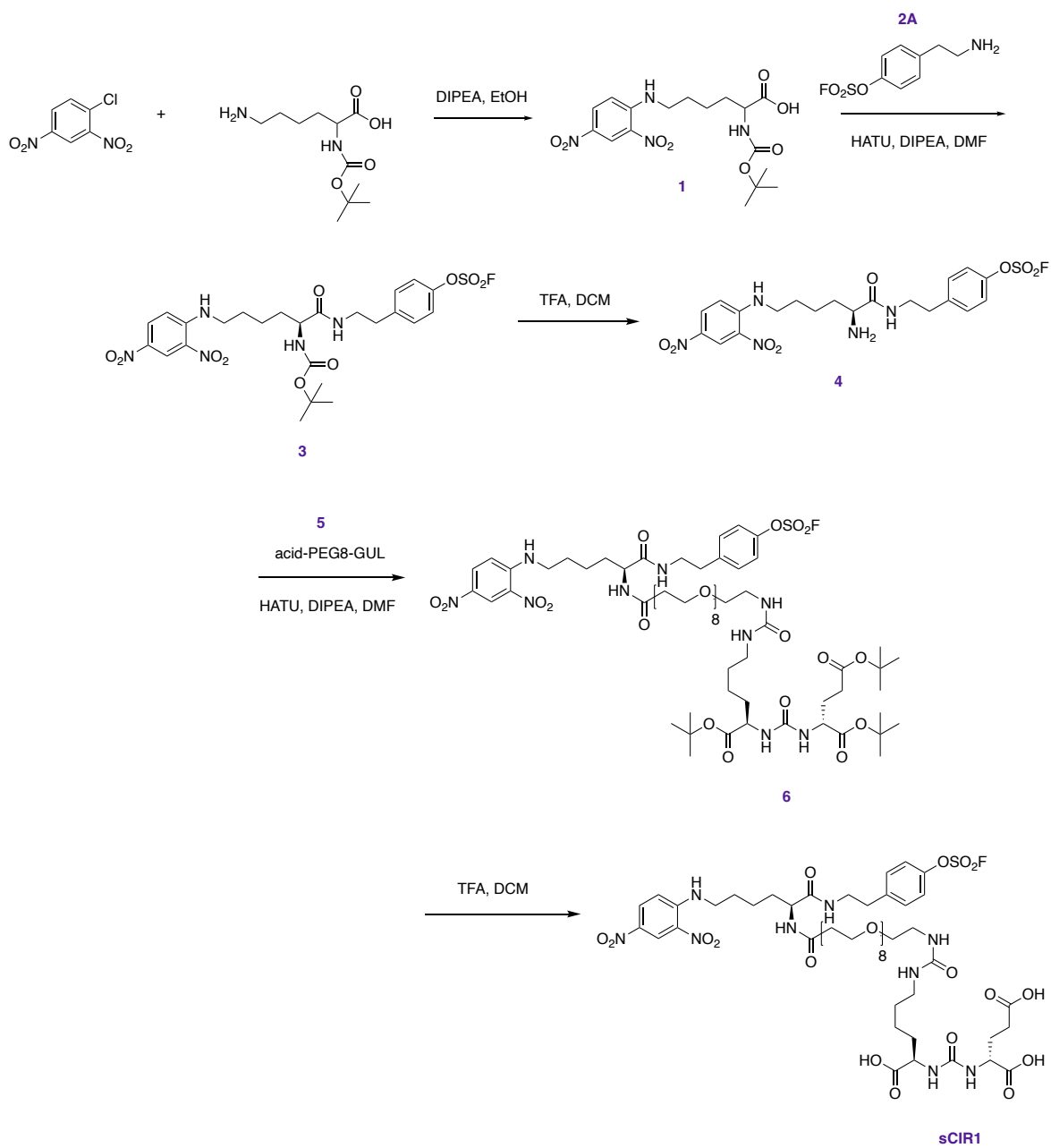


Figure 46. Blank runs on orbitrap LC-MS.

8.0 Supplemental

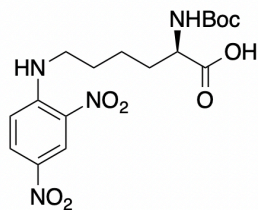
8.1 Synthesis

All chemical reagents were purchased and used without further purification from commercial suppliers (Sigma Aldrich, Broadpharm, ThermoFischer). Crude material was purified on a Buchi C-810 Flash-prep using normal phase or reverse phase C18 columns. ¹H or ¹⁹F NMR spectra were recorded in deuterated solvent on Bruker 700 MHz spectrometer. Liquid chromatography mass spectrometry data was collected on LTQ Orbitrap XL.

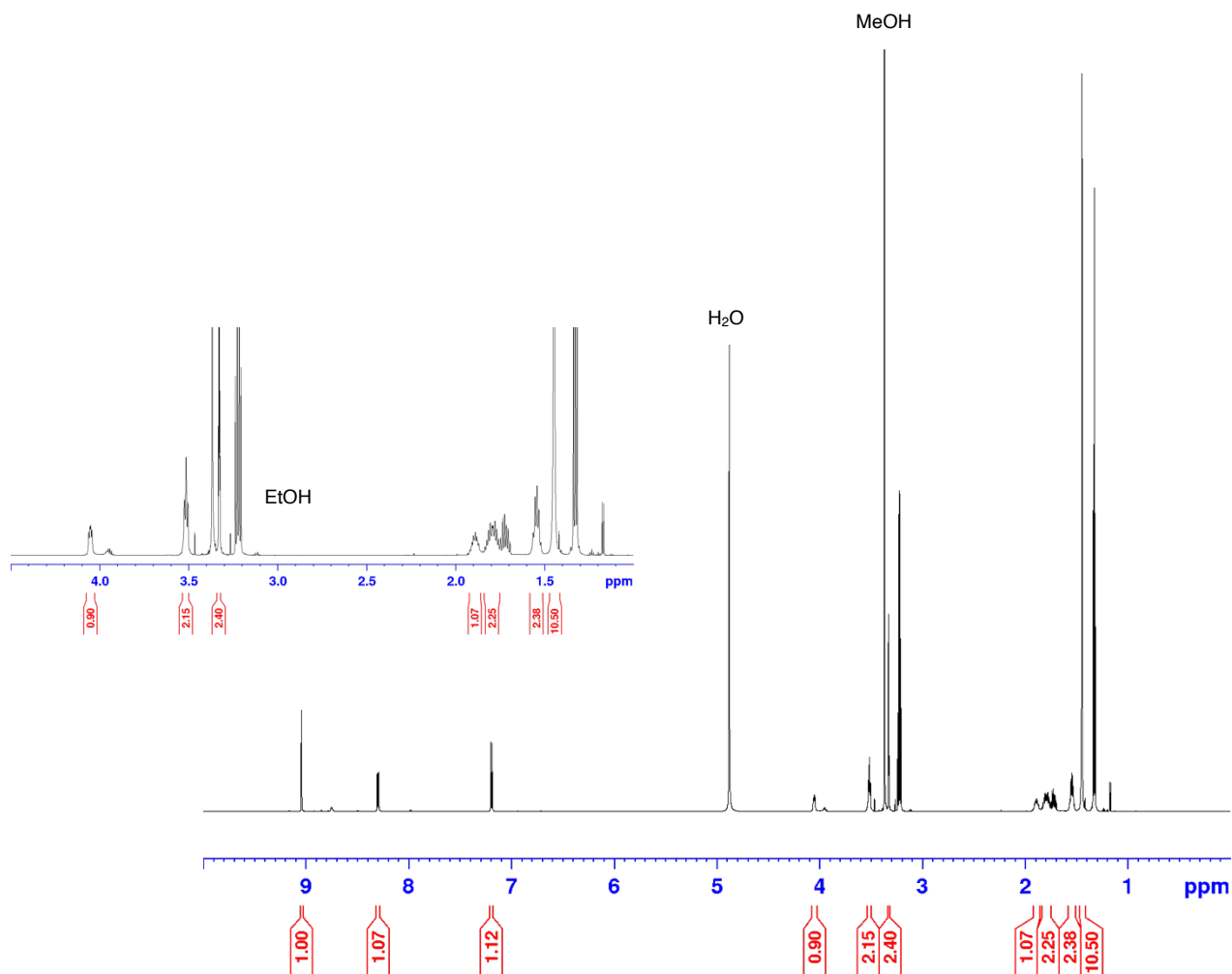


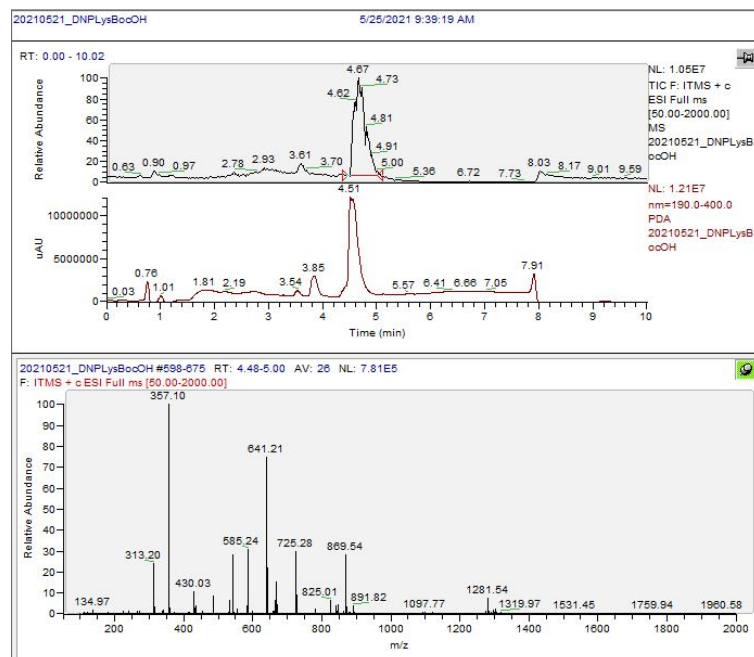
Scheme 1. General sCIR synthesis

Compound 1. DNPllysBoc

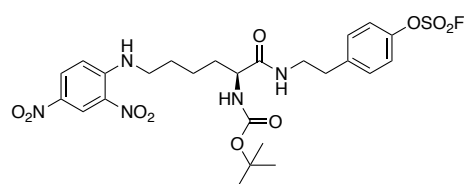


A solution of 1-Chloro-2,4-Dinitrobenzene (328 mg, 1.62 mmol), H-Lys(Boc)-OH (200 mg, 0.812 mmol) and triethylamine (0.4 mL, 2.84 mmol) was stirred in 4 mL of ethanol at room temperature overnight. Excess Boc-Lys was removed through gravity filtration, and the solvent was removed *in vacuo*. The crude material was purified by normal phase (95:5 DCM:MeOH) to yield 217.1 mg (53.3%). ^1H NMR (700 MHz, CD_3OD) δ 9.04 (d, $J = 2.7$ Hz, 1H), δ 8.30 (dd, $J = 2.7$ Hz, $J = 9.57$ Hz, 1H), δ 7.19 (d, $J = 9.6$ Hz, 1H), δ 4.05 (q, $J = 3.11$ Hz, 1H), δ 3.52 (t, $J = 7.0$ Hz, 2H), δ 3.33 (m, 2H), δ 1.89 (m, 1H), δ 1.79 (m, 2H), δ 1.55 (m, 2H), δ 1.44 (s, 10H).



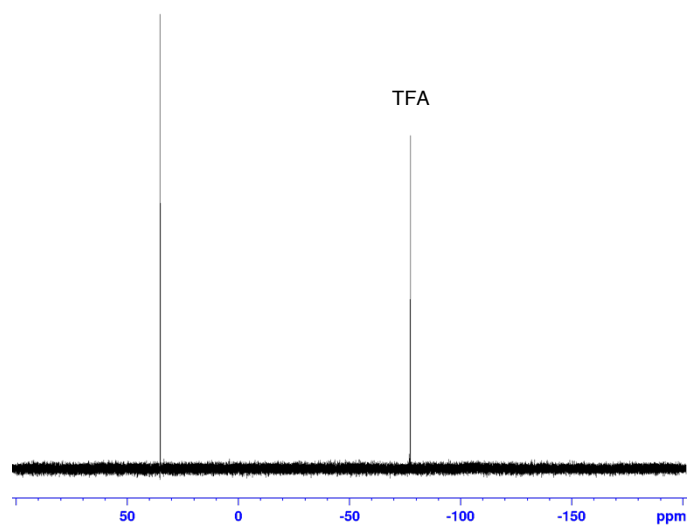
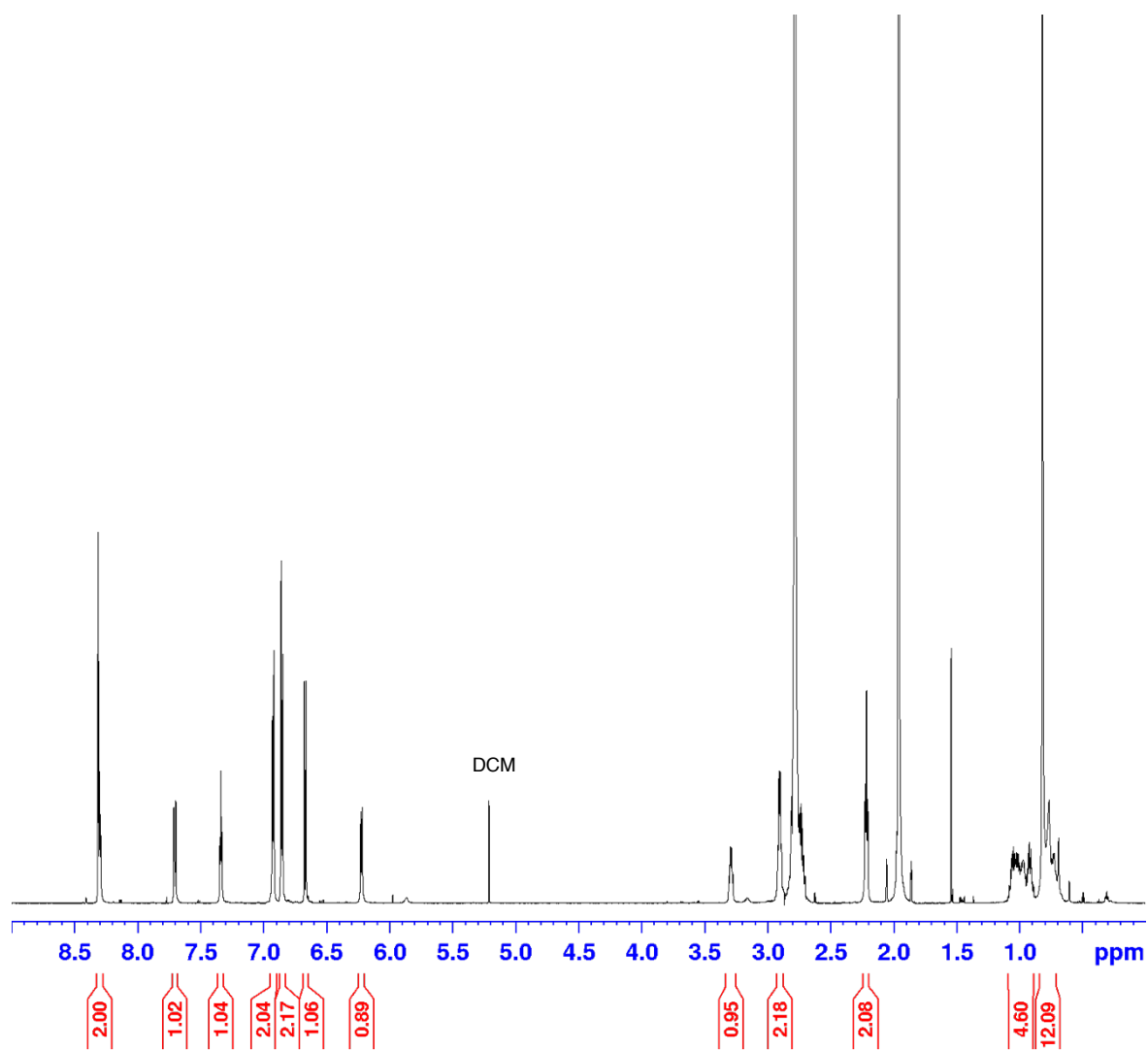


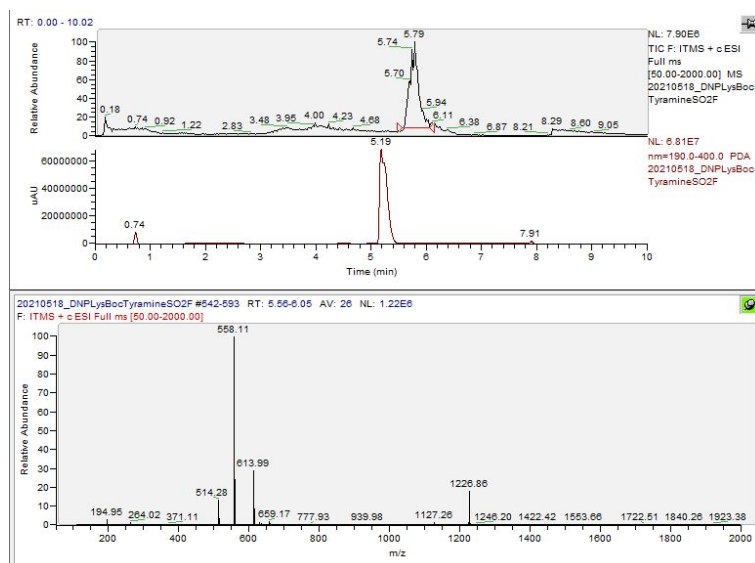
Compound 3A. DNPLysBocTyrSO₂F



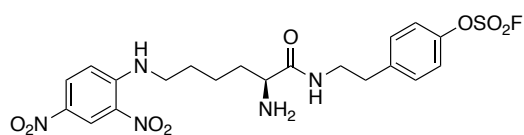
70 mg (0.1697 mmol) of compound **1** was dissolved in 2 mL of DMF and stirred with EDC-HCl (0.2036 mmol, 39 mg) at room temperature. After a few minutes HOBt-H₂O (0.2036 mmol, 31.2 mg) was added, along with compound **2A** (0.2546 mmol, 55.8 mg) and DIPEA (0.674 mmol, 120 μ L). 7 hours later DMF was

removed, and the crude material was re-dissolved in ethyl acetate. Three washes were completed with brine and the compound was purified by normal phase (DCM/MeOH) to collect 36.3 mg of product (34.9%). ¹H NMR (700 MHz, CD₃CN) δ 9.04 (m, 2H), δ 7.70 (m, 1H), δ 7.34 (t, J = 5.67 Hz, 1H), δ 6.93 (d, J = 8.52 Hz, 2H), δ 6.85 (d, J = 8.66 Hz, 2H), δ 6.67 (d, J = 8.66 Hz, 1H), δ 6.22 (d, J = 8.19 Hz, 1H), δ 3.29 (q, J = 5.17 Hz, 1H), δ 2.90 (q, J = 6.89 Hz, 2H), δ 2.21 (t, J = 6.97 Hz, 2H), δ 0.89 – 1.08 (m, 4H), δ 0.82 (s, 9H). ¹⁹F NMR (700 MHz, CD₃CN) 33.5 ppm.

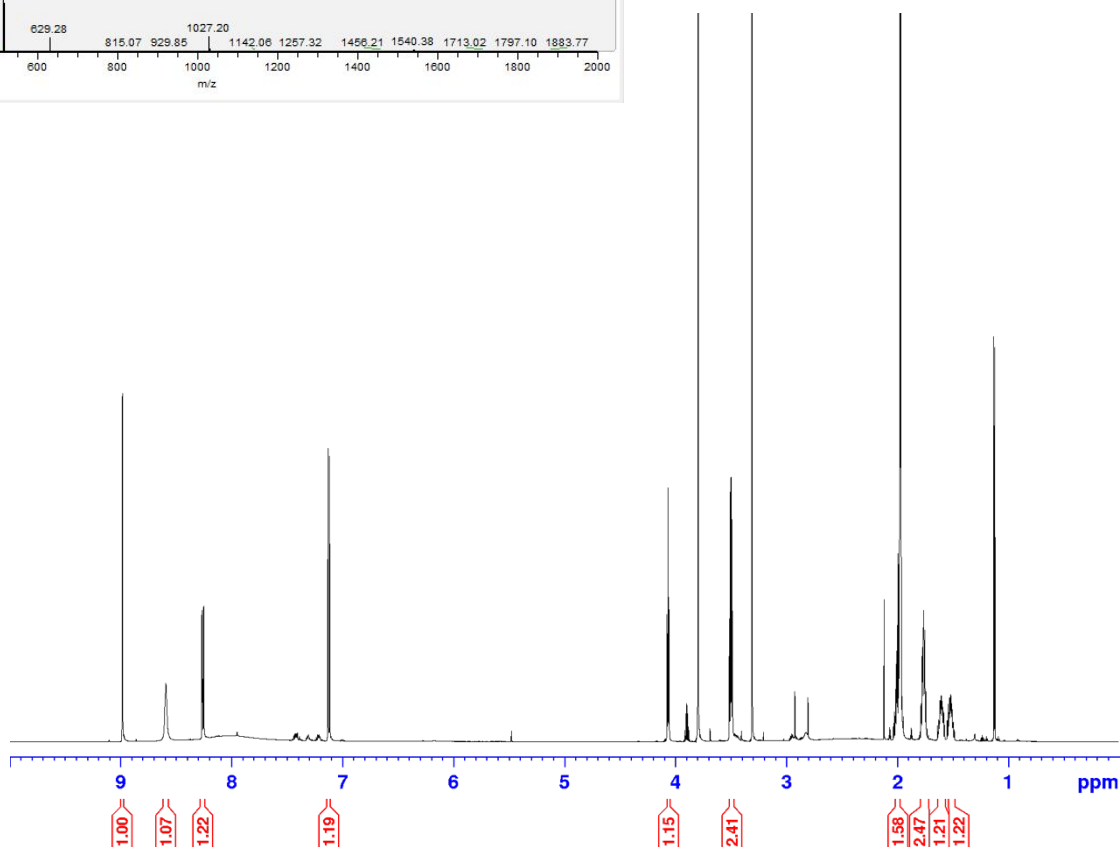
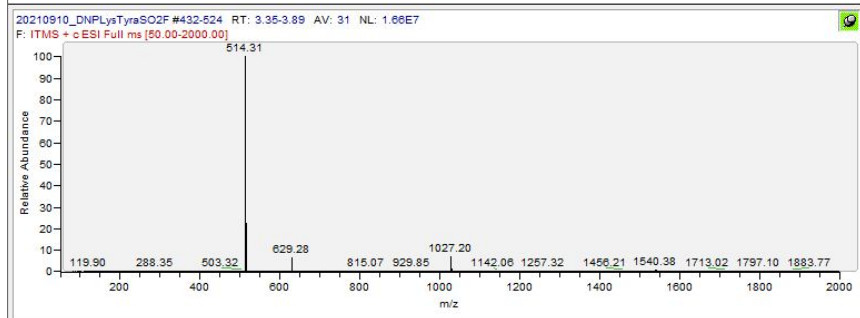
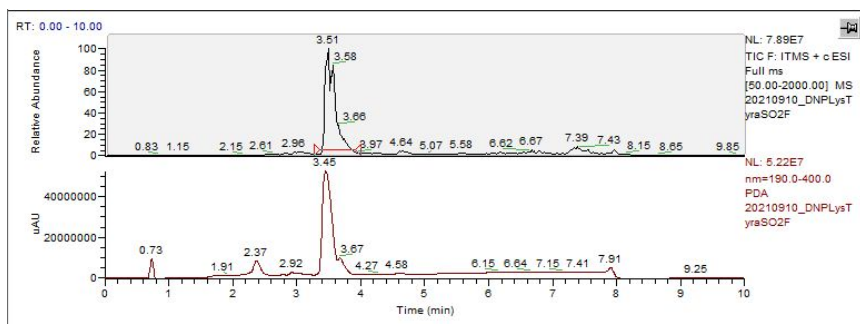


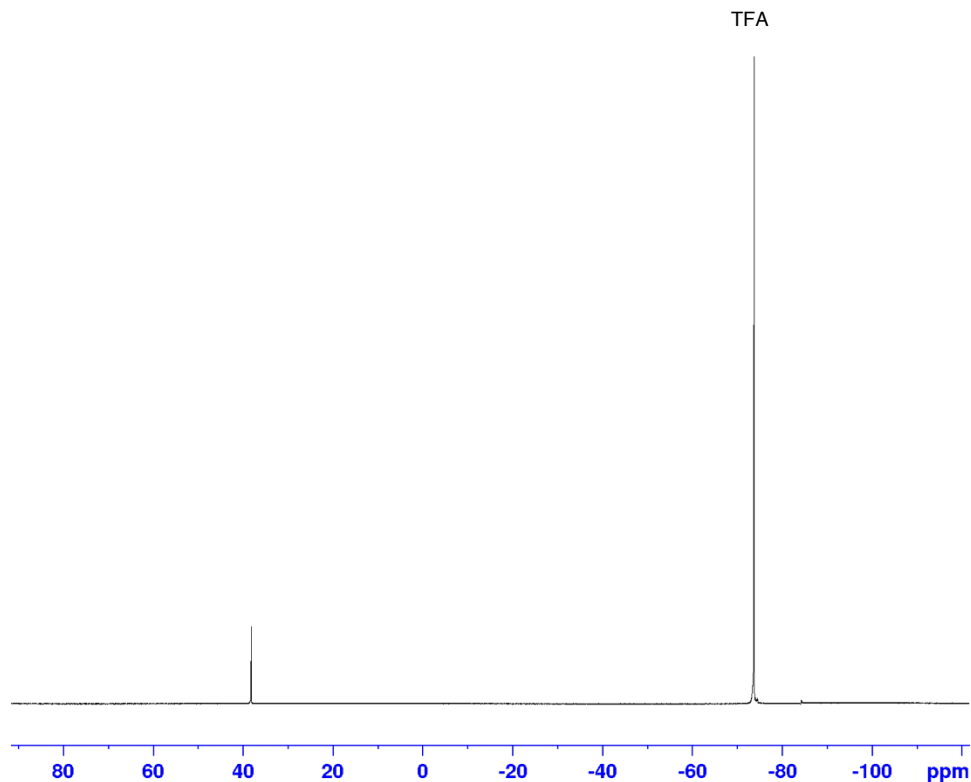


Compound 4A. DNPLysTyraSO₂F

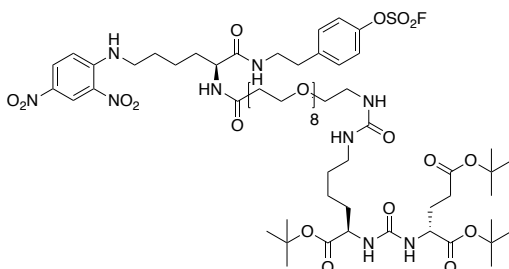


Compound **3A** (36.3 mg, 0.0591 mmol) was deprotected by dissolving the solid in 1.8 mL DCM and adding 0.2 mL TFA. After 1.25 hours the solvent was reduced under pressure. The solid was re-dissolved in 1 mL DCM and dried several times to remove residual TFA. 50.8 mg (102 %) of product was obtained. ¹H NMR (700 MHz, CD₃CN) δ 8.99 (d, J = 2.73 Hz, 1H), δ 8.60 (s, 1H), δ 8.26 (q, J = 12.95 Hz, 1H), δ 7.13 (q, J = 9.53 Hz, 1H), δ 4.06 (t, J = 6.51 Hz, 1H), δ 3.50 (q, J = 6.80 Hz, 2H), δ 1.99-2.03 (m, 1H), δ 1.73-1.78 (m, 2H), δ 1.56-1.63 (m, 1H), δ 1.48-1.54 (m, 1H). ¹⁹F NMR (700 MHz, CD₃CN) 36.4 ppm.





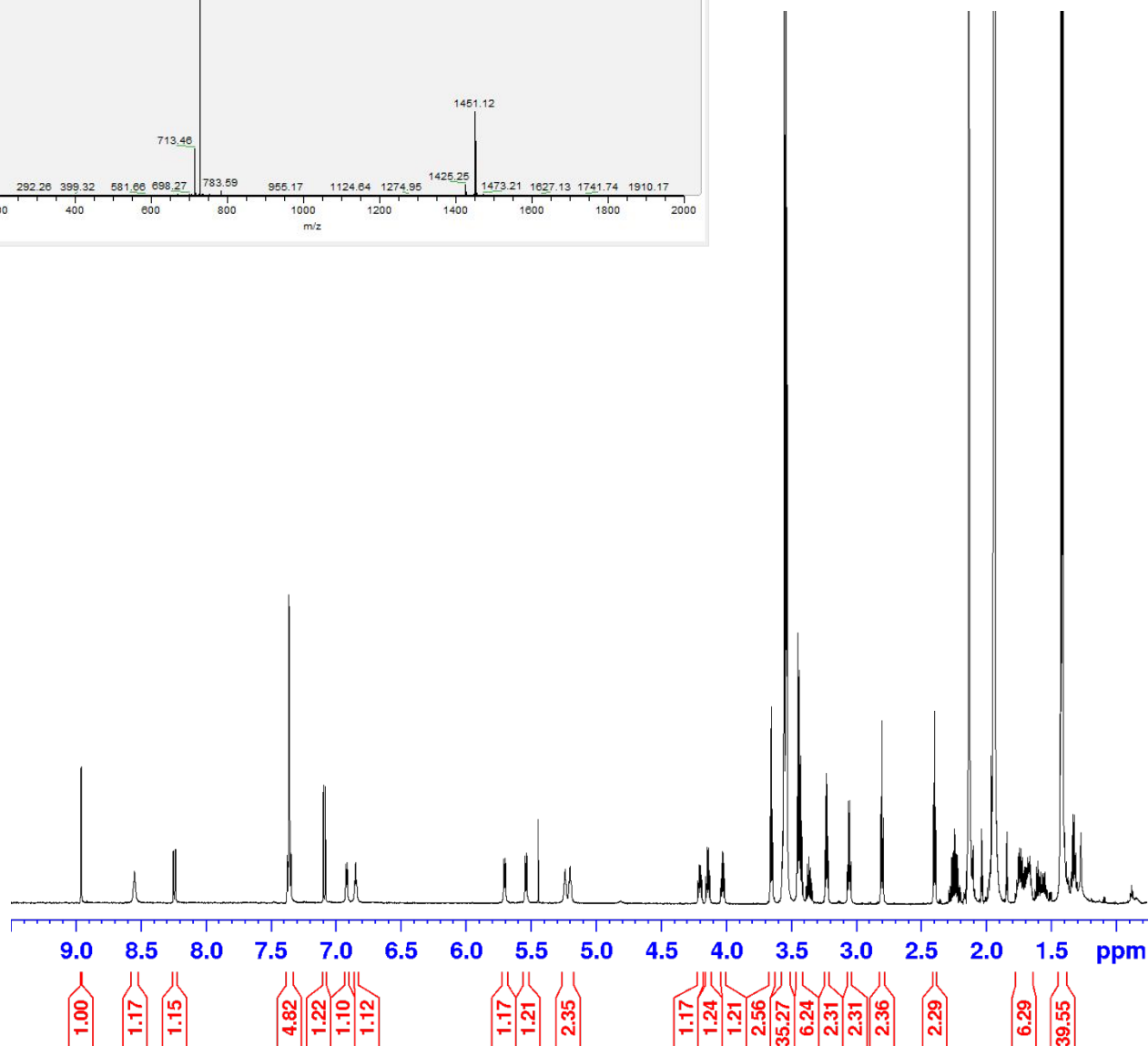
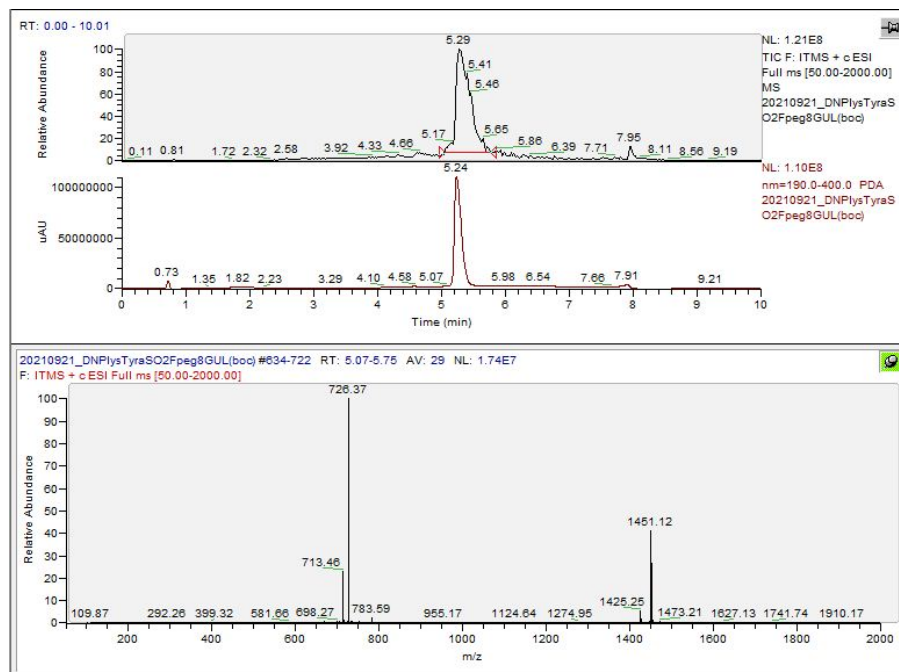
Compound 6A. DNPLysTyraSO₂Fpeg8GULboc

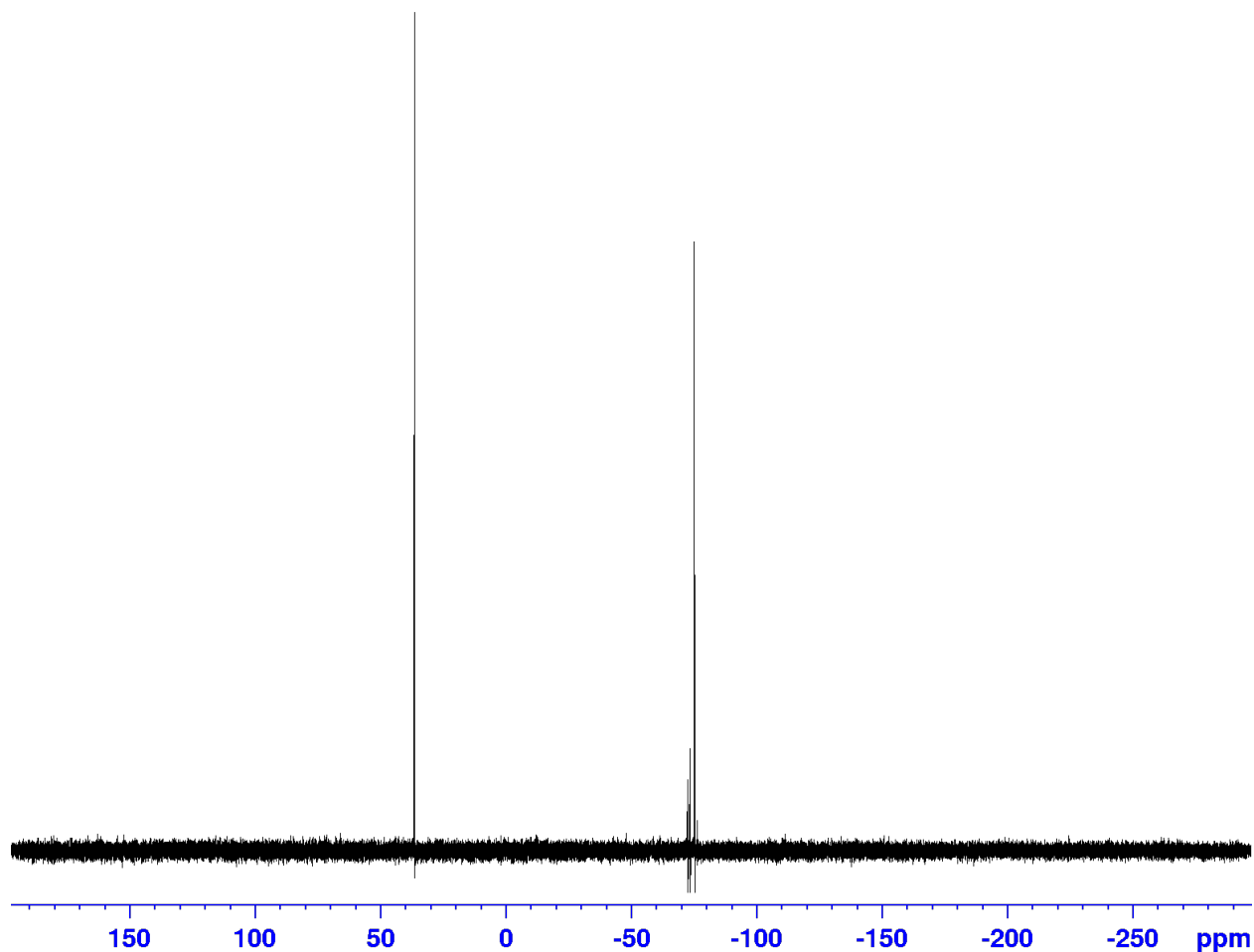


Compound 6A was synthesized by coupling compound 4A (21 mg, 0.0410 mmol) with compound 5 (46.9 mg, 0.0491 mmol) in 5 mL of DMF at room temperature. First compound 5 was stirred with EDC-HCl (0.0492 mmol, 9.4 mg) at room temperature. Then HOBt-H₂O (0.0492 mmol, 7.5 mg) and DIPEA (0.1148 mmol, 20 μ L)

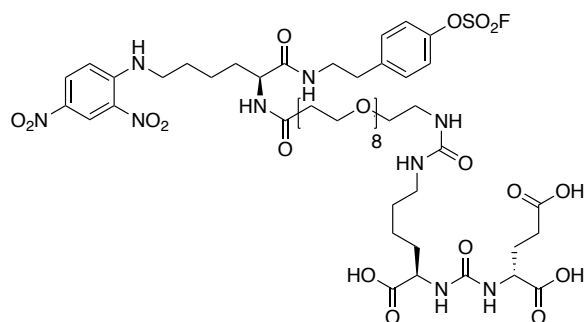
were added to the reaction, and lastly compound 4A. After 16 hours the reaction was stopped by adding ~1 mL of water and 15 mL of EtOAc. After discarding the aqueous layer, the organic layer was washed three times with saturated sodium bicarbonate and once with brine. The crude mixture was dried using MgSO₄ and the solvent was removed under vacuum before reverse phase chromatography. Total product obtained was 11.3 mg (19.0 %). ¹H NMR (700 MHz, CD₃CN) δ 8.96 (d, J = 2.70 Hz, 1H), δ 8.55 (s, 1H), δ 8.24 (q, J = 2.68, 9.63 Hz, 1H), δ 7.37 (q, J = 6.30 Hz, 4H), δ 7.09 (d, J = 9.60 Hz, 1H), δ 6.92 (d, J = 7.74 Hz, 1H), δ 6.85 (d, J = 5.83 Hz, 1H), δ 5.70 (d, J = 7.81 Hz, 1H), δ 5.54 (d, J = 8.37 Hz, 1H), δ 5.24 (s, 1H), δ 5.19 (s, 1H), δ 4.18-4.21 (m, 1H), δ 4.12-4.15 (m, 1H), δ 4.01-4.04 (m, 1H), δ 3.64-3.66 (t, J = 6.09 Hz, 2H), δ 3.53-3.55 (m, 31H), δ 3.42-3.45 (m, 5H), δ 3.21-3.23 (q, J = 5.56 Hz, 2H), δ 3.03-3.06 (q, J = 6.49 Hz, 2H), δ

2.79-2.81 (t, J = 6.99 Hz, 2H), δ 2.39-2.40 (t, J = 6.99 Hz, 2H), δ 1.64-1.78 (m, 5H), δ 1.41-1.43 (t, J = 6.82 Hz, 34H). ^{19}F NMR (700 MHz, CD_3CN) 38.2 ppm.



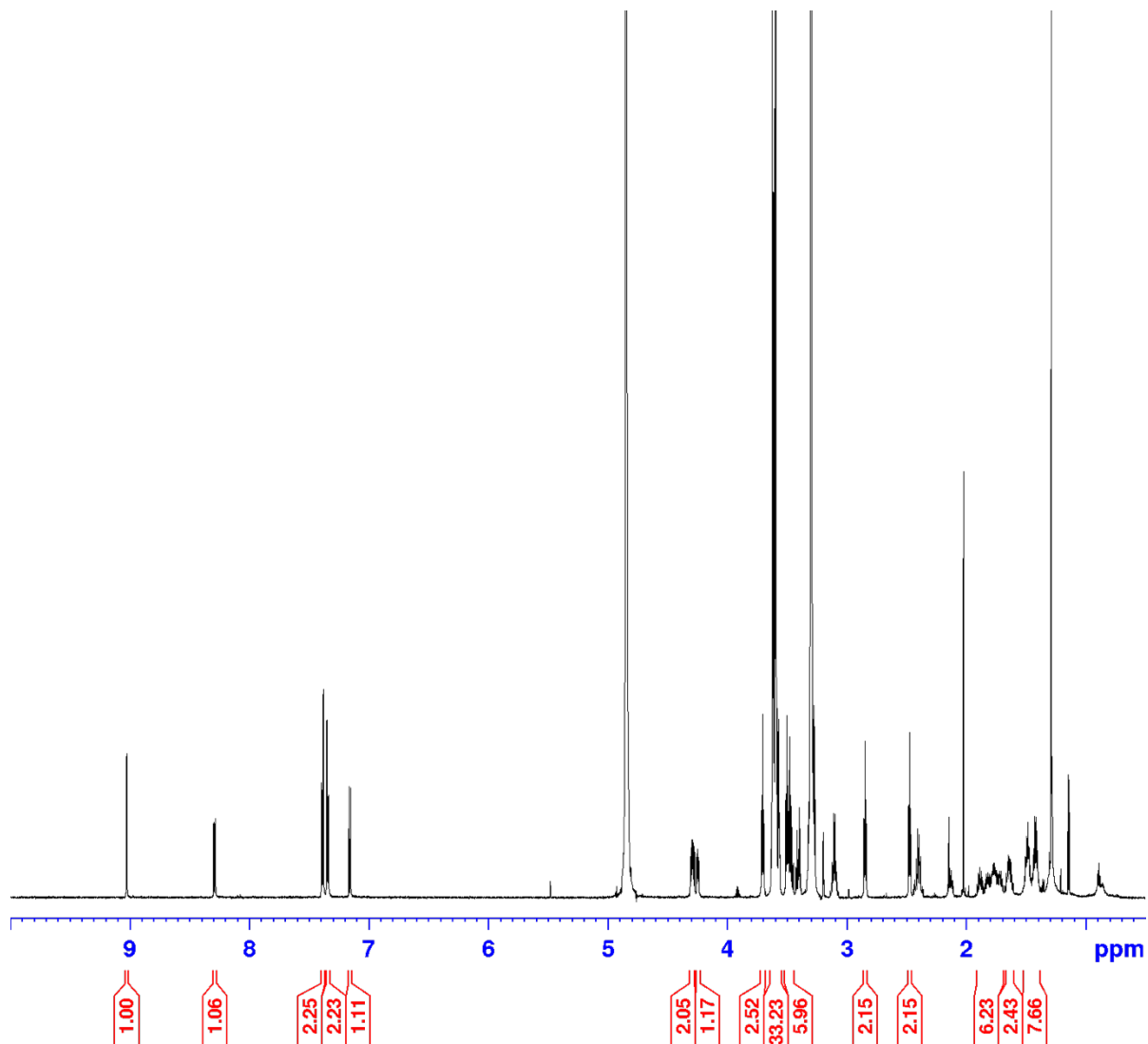
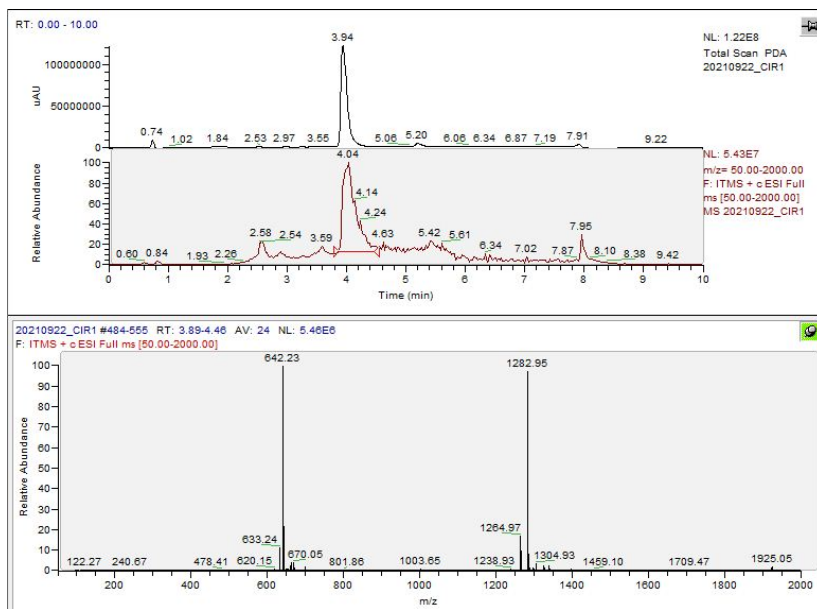


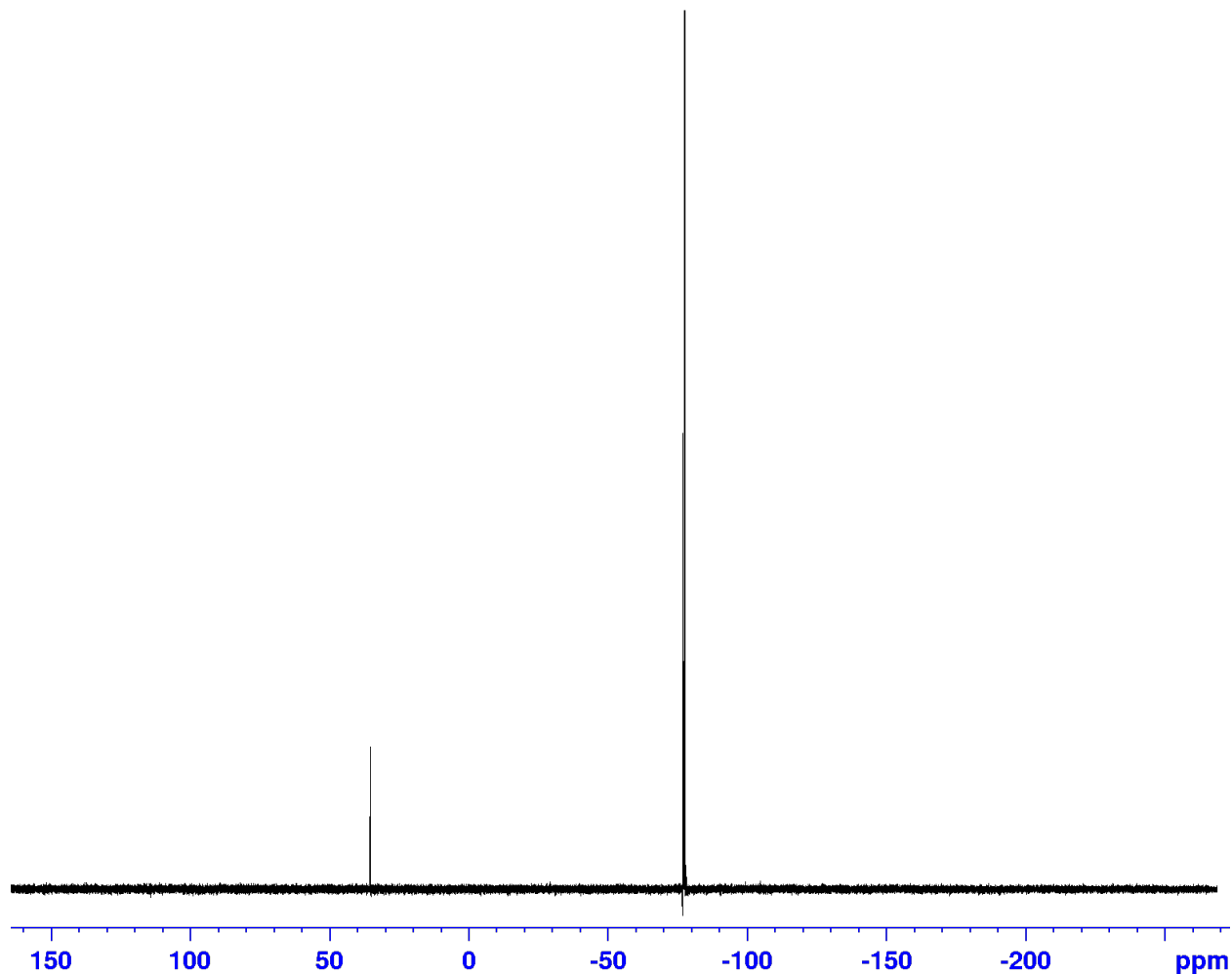
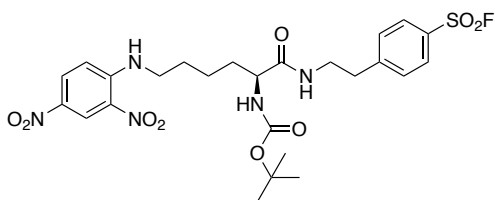
sCIR1



Compound 8 was deprotected in 25% vol/vol TFA:DCM. Reaction was stirred for 3 hours before solvent was removed *in vacuo*. 14 mg (140%) of **sCIR1** was obtained. ^1H NMR (700 MHz, CD_3CN) δ 9.03 (d, $J = 2.70$ Hz, 1H), δ 8.29 (dd, $J = 2.7$ Hz, 9.56 Hz, 1H), δ 7.37 (q, $J = 12.96$ Hz, 4H), δ 7.16 (d, $J = 9.59$ Hz, 1H), δ 4.28 – 4.30 (m, 2H), δ 4.23 – 4.25 (m, 1 H),

δ 3.70 (t, $J = 6.08$ Hz, 2H), δ 3.59 – 3.62 (m, 33H), δ 3.44 – 3.51 (m, 6H), δ 2.84 (t, $J = 6.98$ Hz, 2H), δ 2.15 (t, $J = 6.06$ Hz, 2H), δ 1.70 – 1.90 (m, 6H), δ 1.60 – 1.66 (m, 2H), δ 1.39 – 1.51 (m, 7H). ^{19}F NMR (700 MHz, CD_3CN) 35.2 ppm.

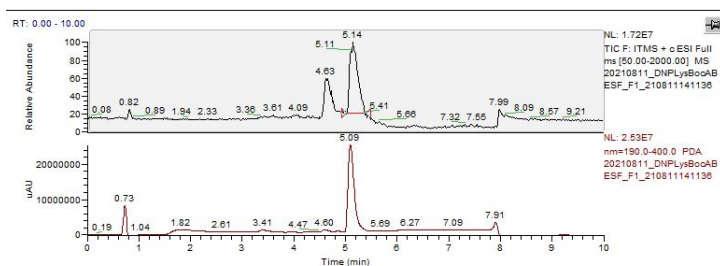


Compound **3B**. DNPLysBocABESF

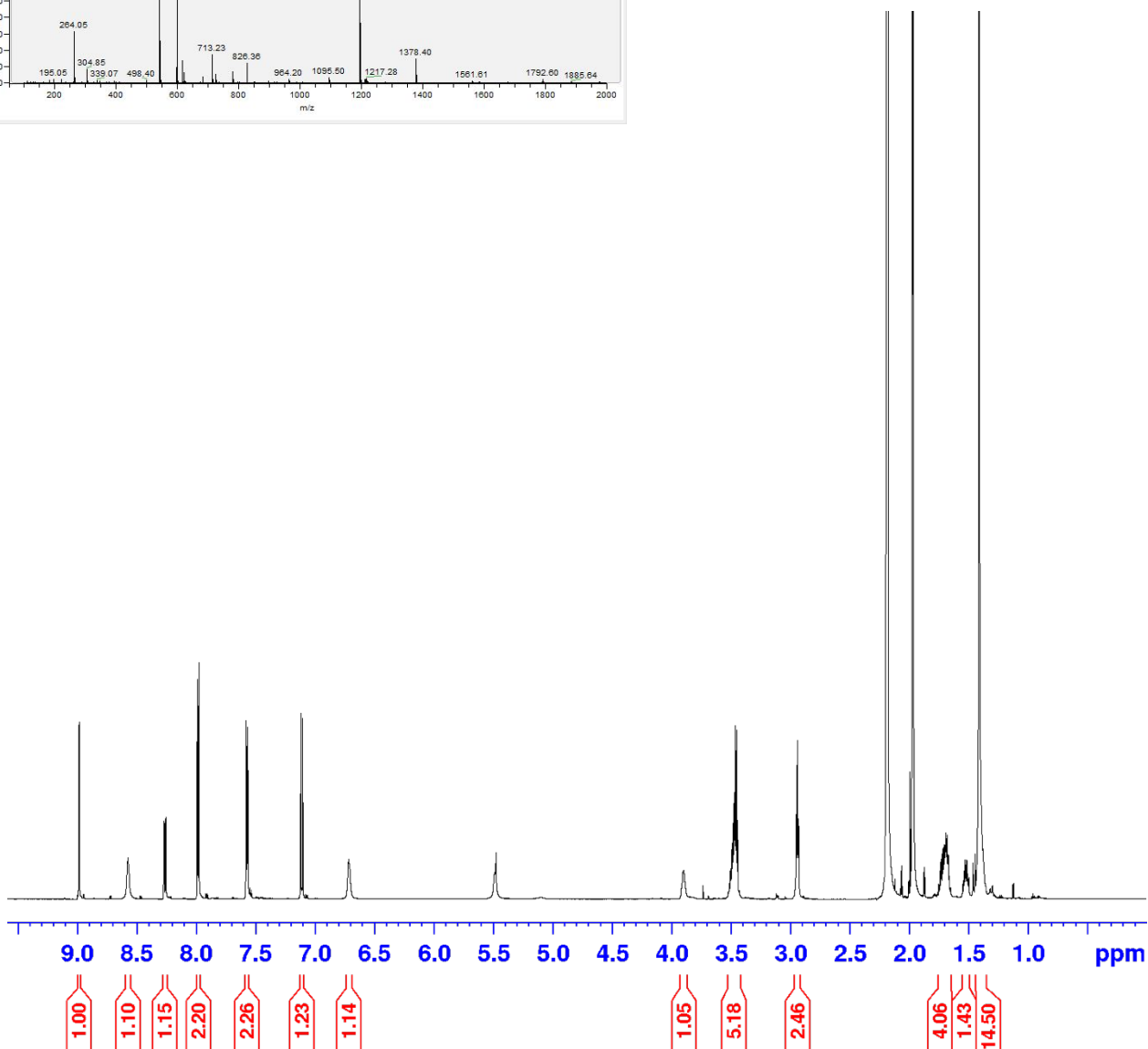
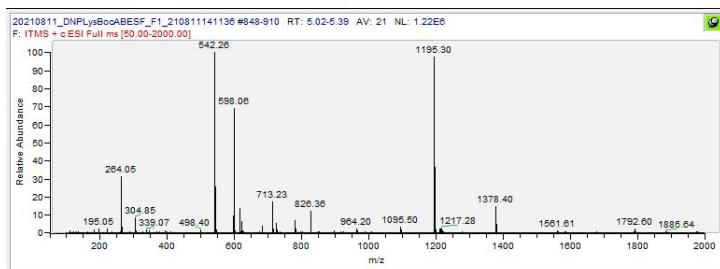
33.8 mg (0.0821 mmol) of compound **1** was dissolved in 3 mL DMF with HATU (0.0984 mmol, 18.9 mg) and DIPEA (0.287 mmol, 49 μ L). After a few minutes compound **2B** (25 mg, 0.123 mmol) was added and the reaction was stirred for three hours. The solution was removed under vacuum, and the crude material was re-dissolved in ethyl

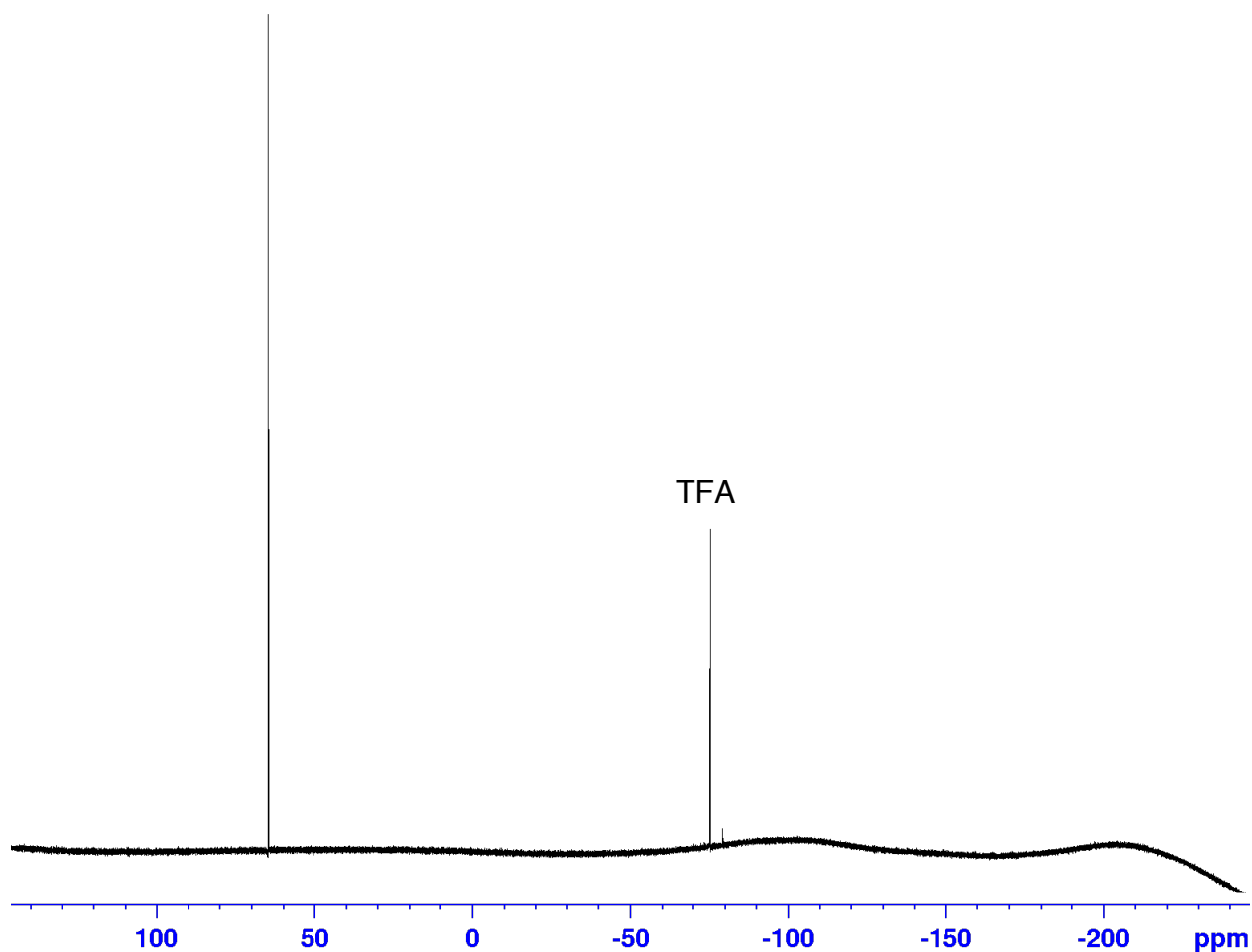
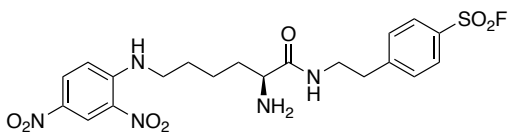
acetate. Three washes were completed, two with saturated bicarbonate and one with brine. 40.6 mg (48.9%) of product was obtained by purifying by normal phase (DCM/MeOH). ^1H NMR (700 MHz, CD_3CN) δ 8.98 (d, $J = 2.70$ Hz, 1H), δ 8.57 (s, 1H), δ 8.26 (q, $J = 4.09$ Hz, 1H), δ 7.98 (d, $J = 8.40$ Hz, 2H), δ 7.57 (d, $J = 8.25$ Hz, 2H), δ 7.11 (d, $J = 9.60$ Hz, 1H), δ 6.72 (s, 1H), δ 3.90 (s, 1H), δ 3.44 – 3.49 (m, 5H), δ 2.93 (t, $J =$

6.75 Hz, 2H), δ 1.64 – 1.75 (m, 4H), δ 1.49 – 1.54 (m, 1H), δ 1.41 (s, 14 H). ^{19}F NMR (700 MHz, CD_3CN) 64.3 ppm.



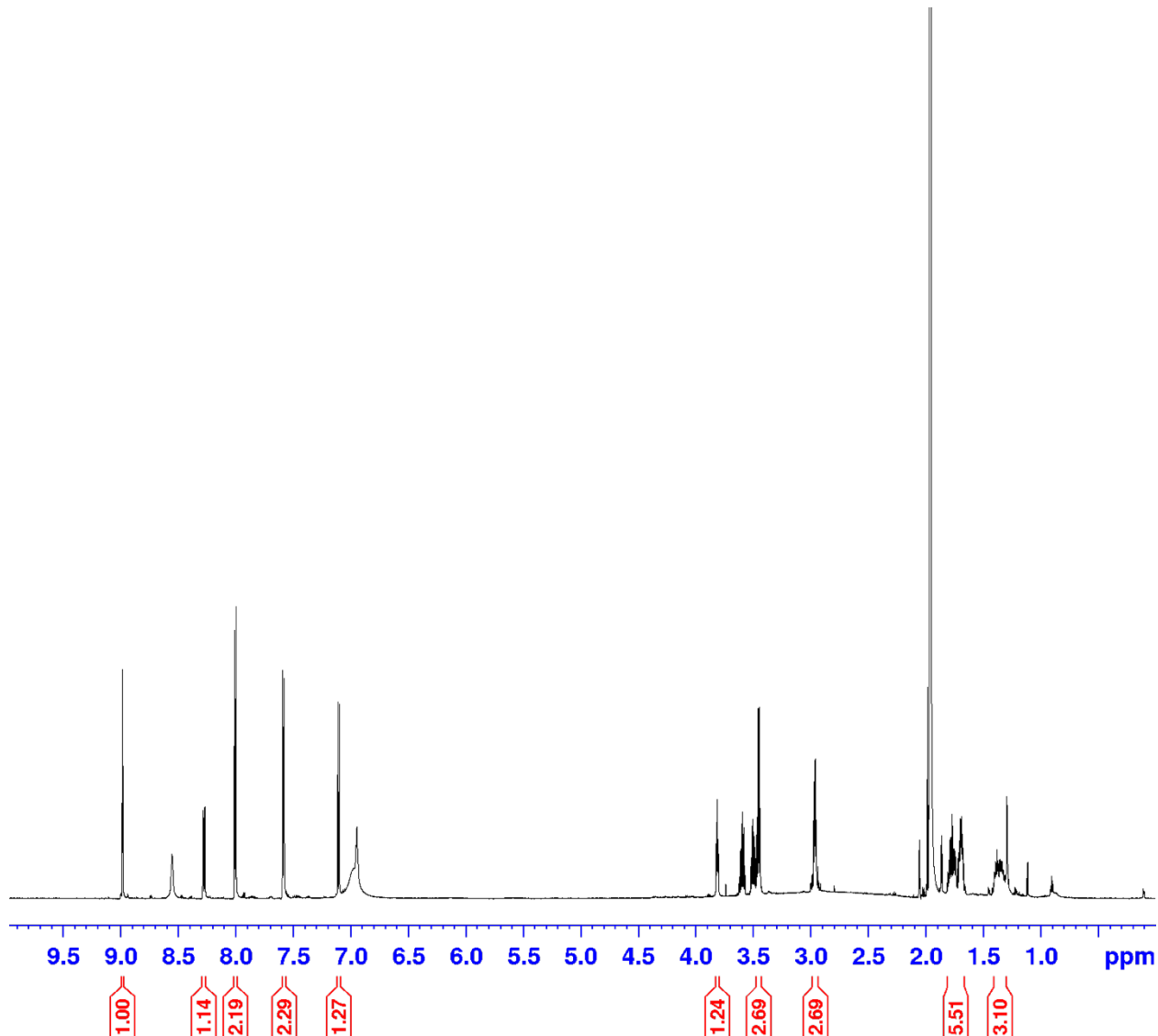
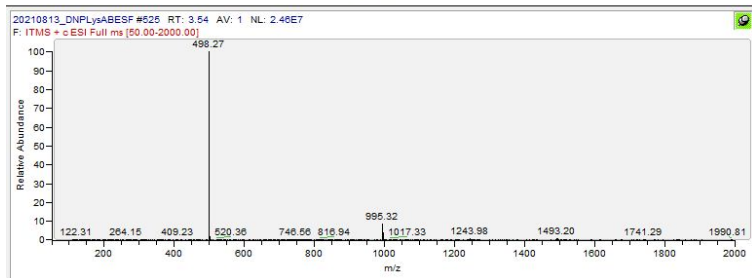
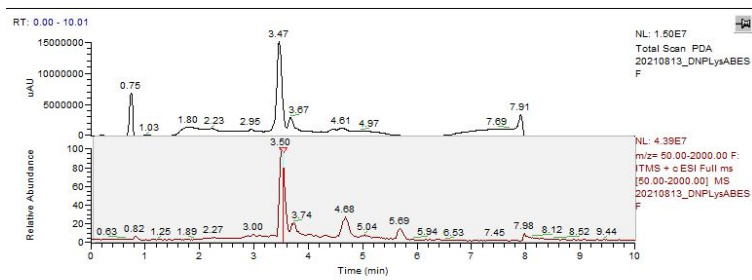
Peak at 4.63 min in ITMS spectrum is a contaminant in the MS (see appendix for blank).

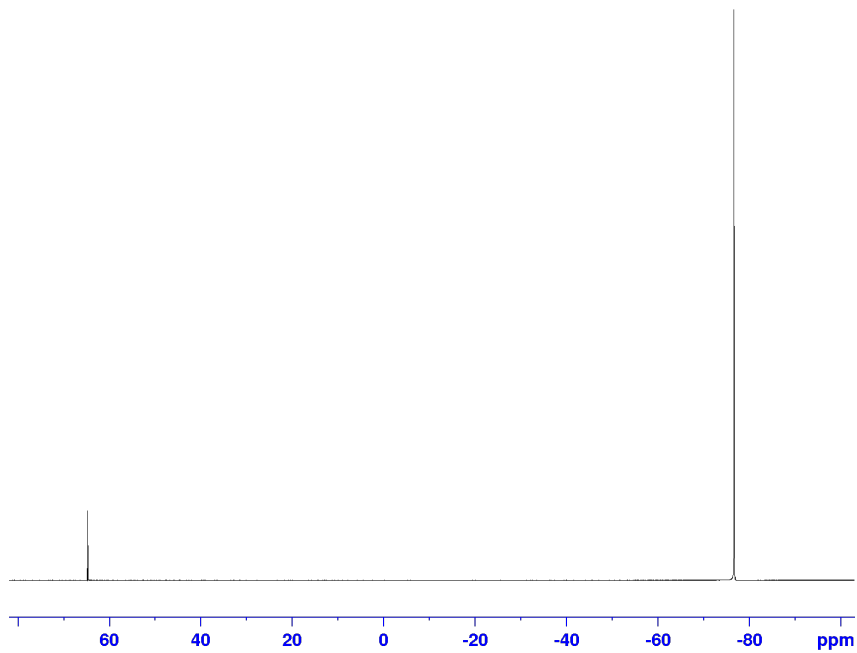


Compound **4B**. DNPLysABESF

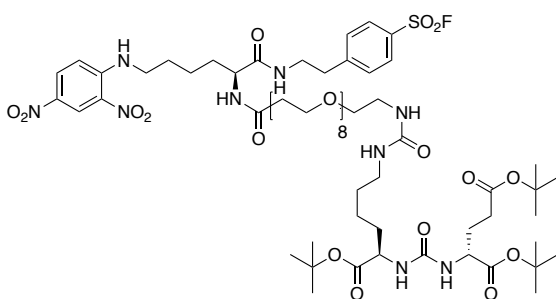
Compound **3B** was dissolved in 20% vol/vol TFA:DCM and stirred for 2.5 hours. Solvent was removed under vacuum. 48.2 mg of product was collected (121%). ^1H NMR (700 MHz, CD_3CN) δ 8.98 (d, $J = 2.70$ Hz, 1H), δ 8.55 (s, 1H), δ 8.28 (q, $J = 4.09$ Hz, 1H), δ 8.00 (d, $J = 8.42$ Hz, 2H),

δ 7.58 (d, $J = 8.28$ Hz, 2H), δ 7.10 (d, $J = 9.59$ Hz, 1H), δ 3.81 (t, $J = 6.22$ Hz, 1H), δ 3.45 (q, $J = 5.92$ Hz, 2H), δ 2.96 (q, $J = 4.00$ Hz, 2H), δ 1.66 – 1.80 (m, 5H), δ 1.31 – 1.42 (m, 3H). ^{19}F NMR (700 MHz, CD_3CN) 64.9 ppm.





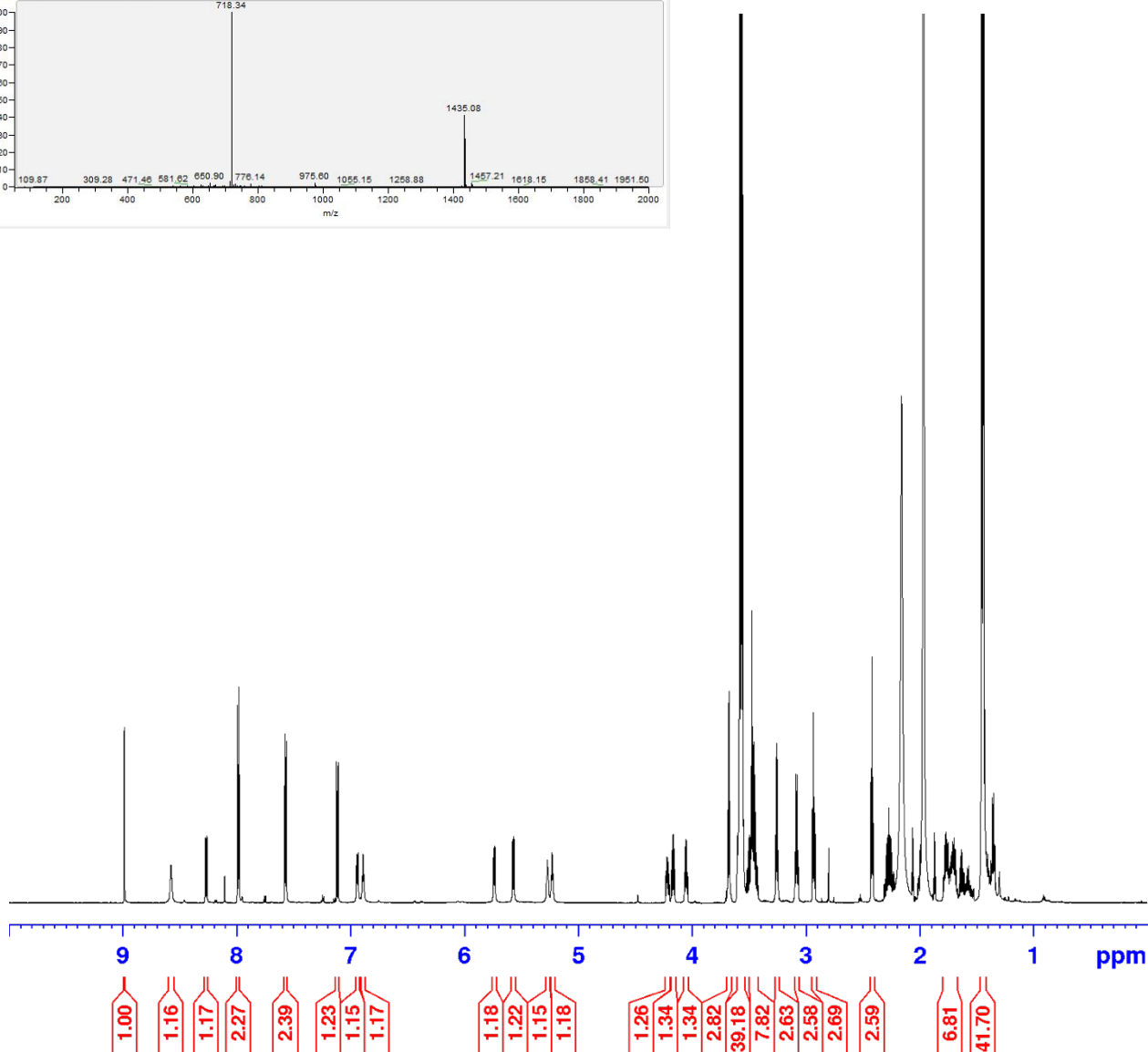
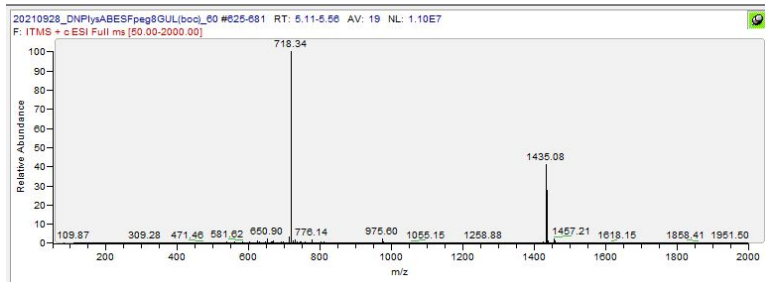
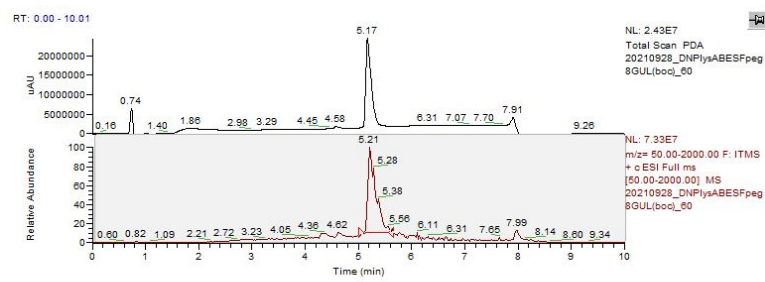
Compound **6B**. DNPLysABESFpeg8GULboc

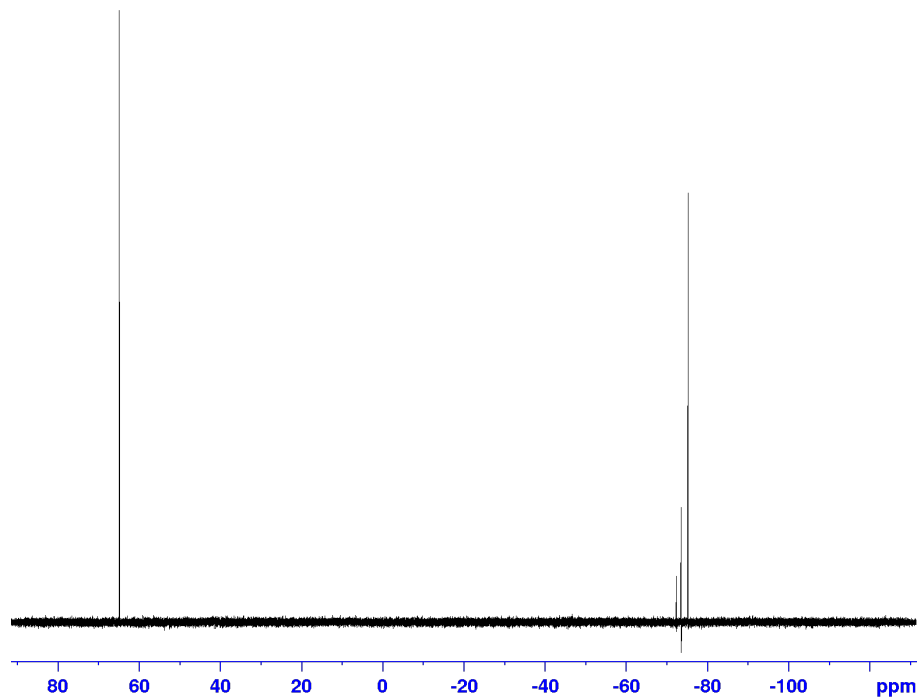


This compound was synthesized by dissolving 66.6 mg (0.06973 mmol) of Compound **5** in 3 mL DMF. HATU (33.2 mg, 0.08715 mmol) and DIPEA (30.3 μ L, 0.1743 mmol) were added to the solution, along with 29.8 mg (0.0581 mmol) of Compound **4B** a few minutes later. After 7 hours the reaction was stopped and 1 mL H₂O and 4 mL EtOAc was added. The suspension

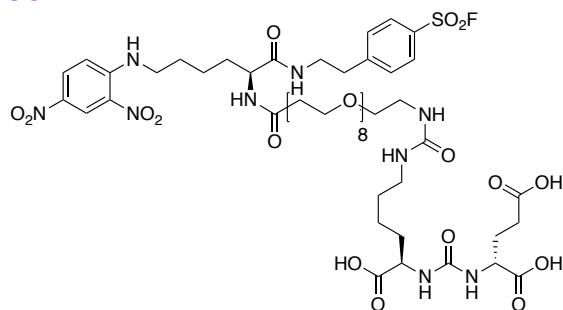
was washed three times with brine, before purification by reverse phase chromatography. 16.8 mg of product was collected, giving a 20.1% yield. ¹H NMR (700 MHz, CD₃CN) δ 8.98 (d, J = 2.70 Hz, 1H), δ 8.58 (s, 1H), δ 8.27 (dd, J = 4.10 Hz, 1H), δ 7.99 (d, J = 8.44 Hz, 2H), δ 7.57 (d, J = 8.31 Hz, 2H), δ 7.12 (d, J = 9.60 Hz, 1H), δ 6.94 (d, J = 7.77 Hz, 1H), δ 6.89 (t, J = 5.87 Hz, 1H), δ 5.74 (d, J = 7.84 Hz, 1H), δ 5.57 (d, J = 8.39 Hz, 1H), δ 5.27 (t, J = 5.40 Hz, 1H), δ 5.23 (t, J = 5.62 Hz, 1H), δ 4.20 – 4.23 (m, 1H), δ 4.15 – 4.18 (m, 1H), δ 4.03 – 4.06 (m, 1H), δ 3.67 – 3.69 (t, J = 6.10 Hz, 3H), δ 3.55 – 3.58 (m, 39H), δ 3.41 – 3.50 (m, 8H), δ 3.26 (q, J = 5.57 Hz, 2H), δ 3.08 (q, J = 6.49 Hz, 2H), δ

2.93 (q, $J = 6.12$ Hz, 2H), δ 2.42 (t, $J = 6.07$ Hz, 2H), δ 1.67 – 1.79 (m, 7H), δ 1.45 (t, $J = 5.39$ Hz, 41H). ^{19}F NMR (700 MHz, CD_3CN) 65.0 ppm.



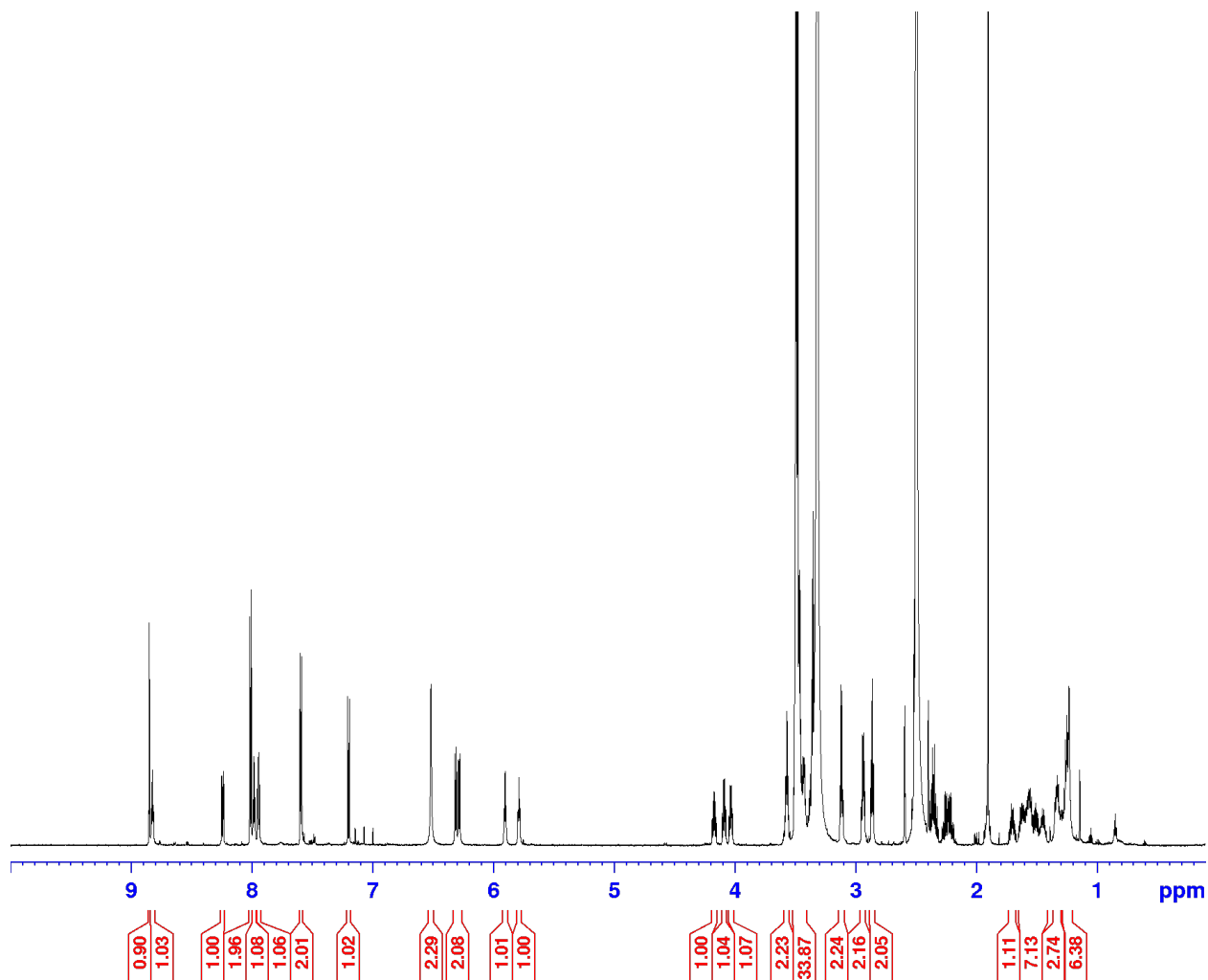
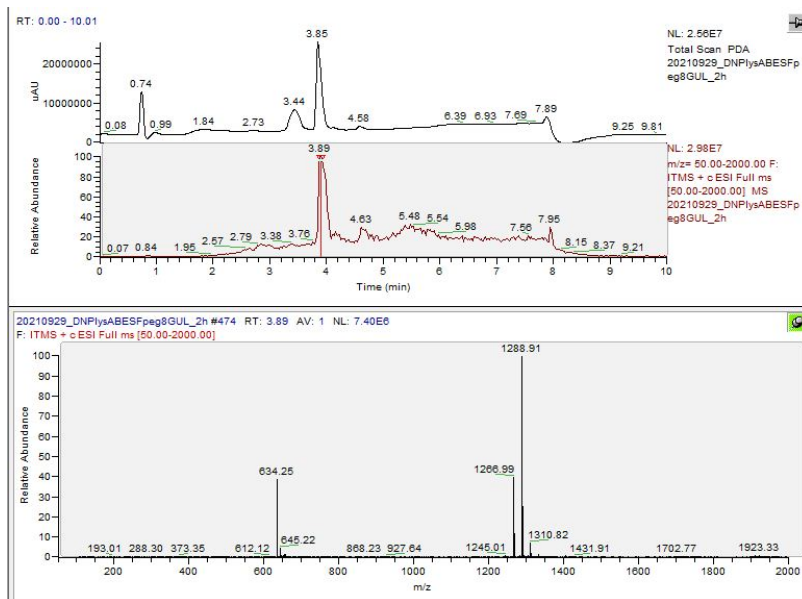


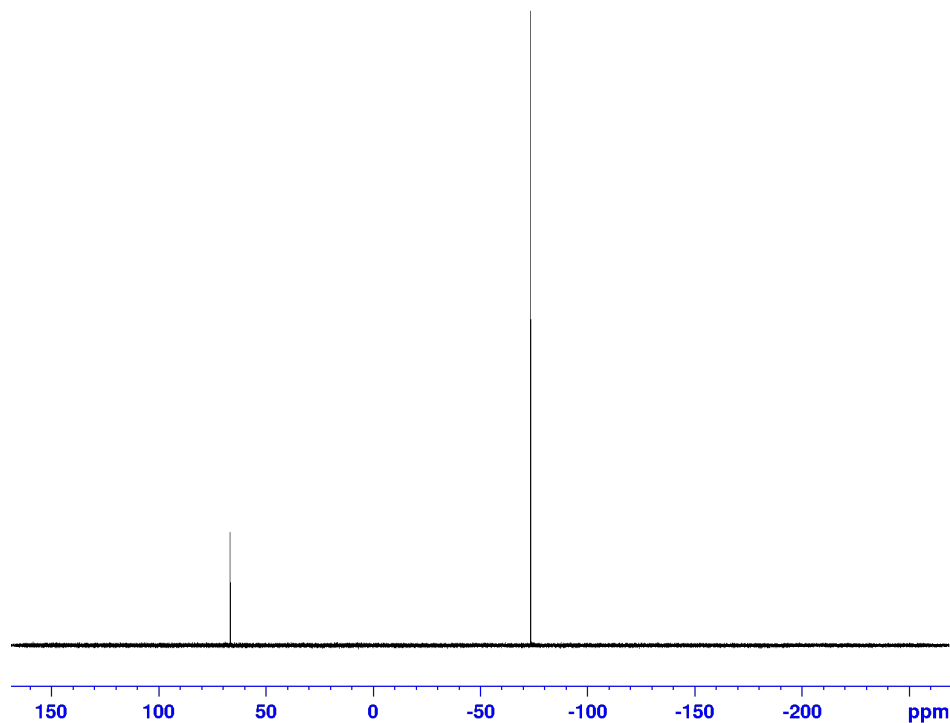
sCIR2.



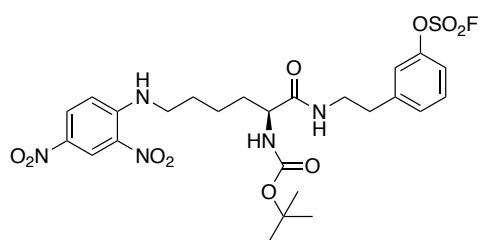
35.9 mg of Compound **6B** was dissolved in 2.5 mL DCM and 0.6 mL TFA was added. 2.5 hours later the solvent was removed under vacuum. 29.8 mg of product collected (106.4%). ^1H NMR (700 MHz, CD_3CN) δ 8.85 (d, $J = 2.76$ Hz, 1H), δ 8.82 (t, $J = 5.86$ Hz, 1H), δ 8.24 (dd, $J = 3.97$ Hz, 1H), δ 8.01 (d, $J = 8.48$ Hz, 2H), δ 7.98 (d, $J = 5.72$ Hz, 1H), δ 7.94 (d, $J = 8.18$ Hz, 1H), δ

δ 7.59 (d, $J = 8.39$ Hz, 2H), δ 7.20 (d, $J = 9.68$ Hz, 1H), δ 6.51 (s, 2H), δ 6.29 (dd, $J = 9.67$ Hz, 2H), δ 5.90 (t, $J = 5.61$ Hz, 1H), δ 5.79 (t, $J = 5.66$ Hz, 1H), δ 4.15 – 4.18 (m, 1H), δ 4.07 – 4.18 (m, 1H), δ 4.01 – 4.04 (m, 1H), δ 3.55 – 3.58 (m, 2H), δ 3.47 – 3.49 (m, 34H), δ 3.12 (q, $J = 5.74$ Hz, 2H), δ 2.94 (q, $J = 6.49$ Hz, 2H), δ 2.86 (t, $J = 6.89$ Hz, 2H), δ 1.67 – 1.72 (m, 1H), δ 1.42 – 1.65 (m, 7H), δ 1.31 – 1.35 (m, 3H), δ 1.22 – 1.27 (m, 6H). ^{19}F NMR (700 MHz, CD_3CN) 66.6 ppm.



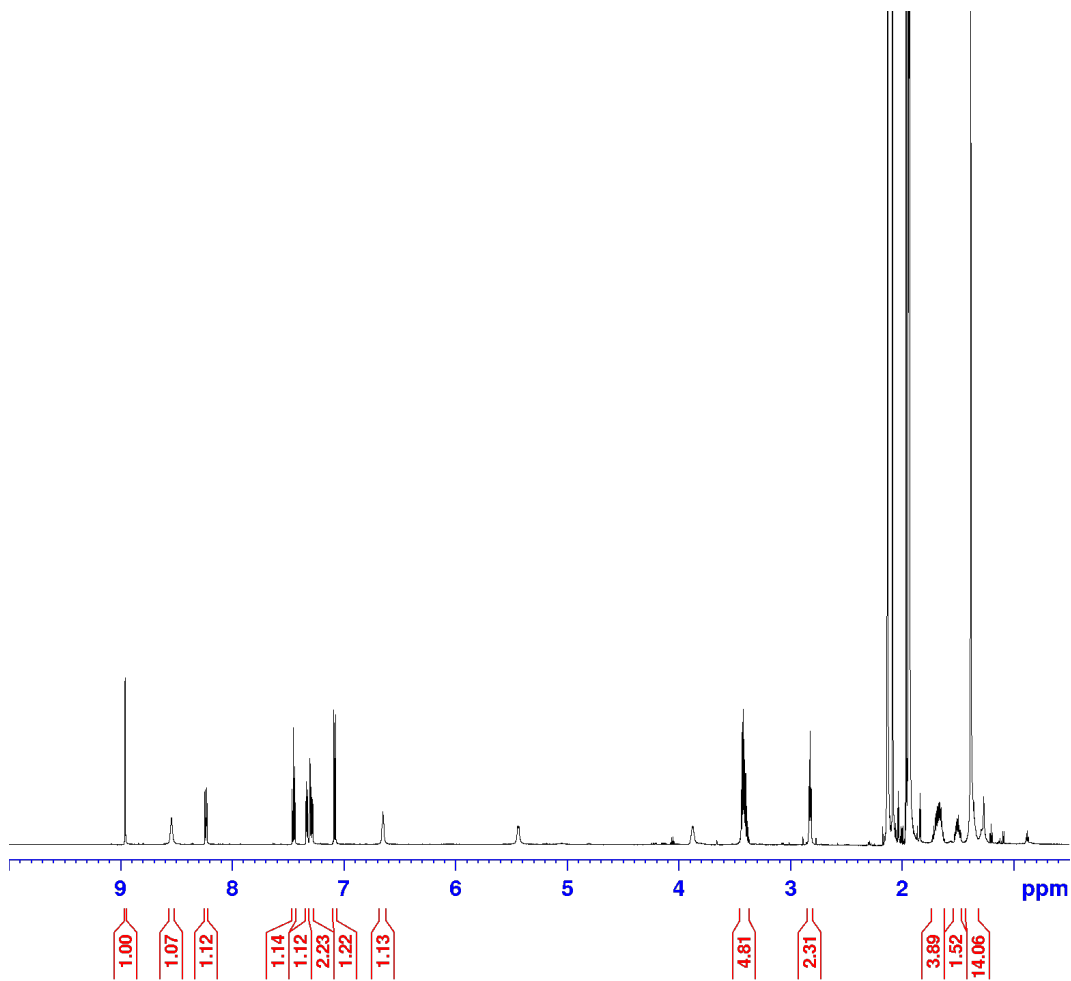
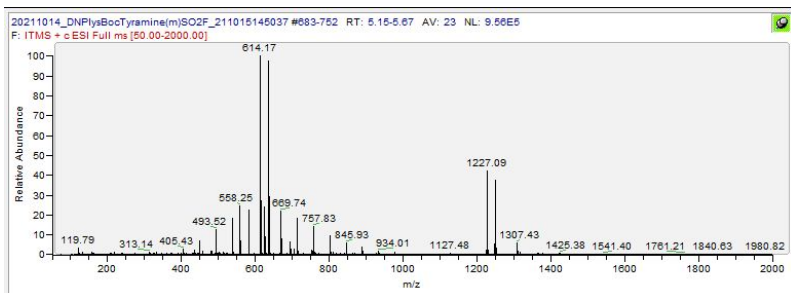
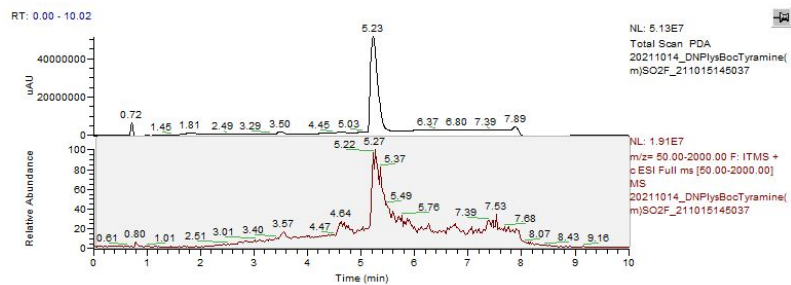


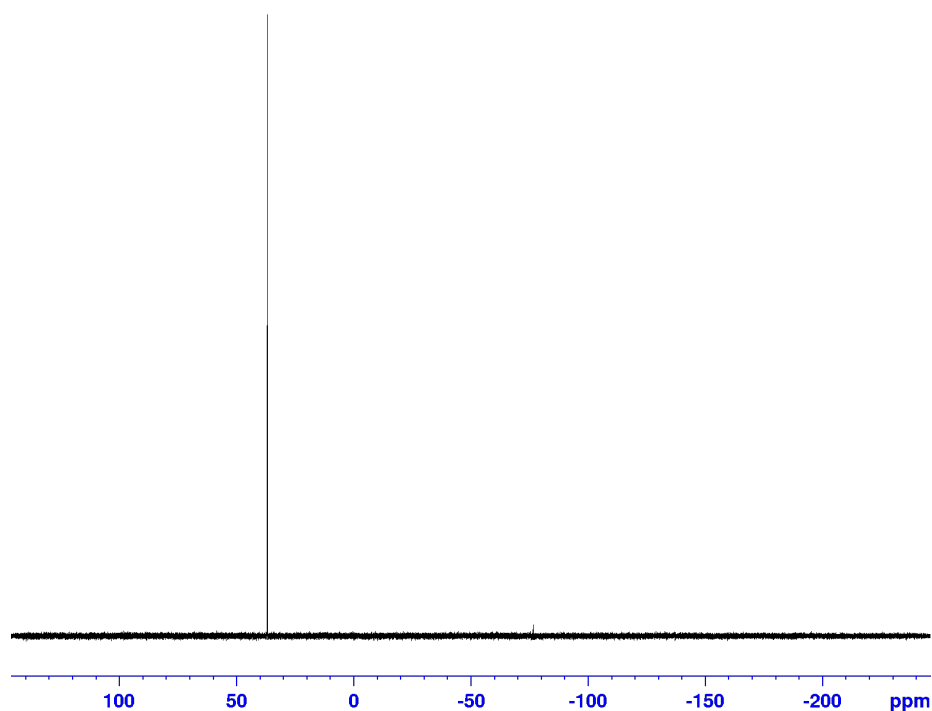
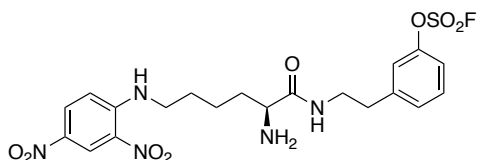
Compound **3C**. DNPLysBocTyra(m)SO₂F



A solution of Compound **1** (26.4 mg, 0.1204 mmol), HATU (52.9 mg, 0.139 mmol) and DIPEA (40.4 μL , 0.232 mmol) was made in 3 mL DMF. 47.8 mg (0.1159 mmol) of Compound **2C** was added to the flask and the reaction was stirred for 2.5 hours. An extraction was performed by adding a small amount

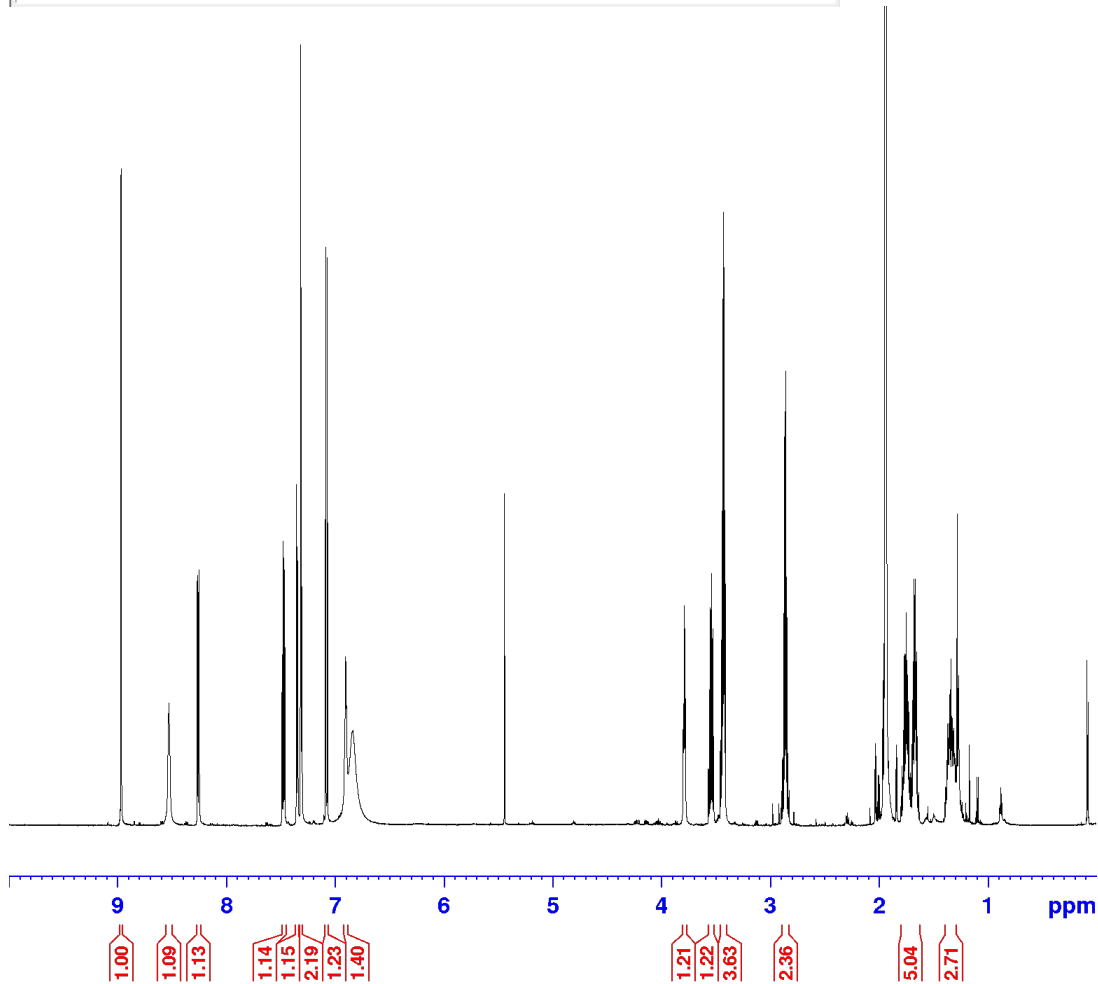
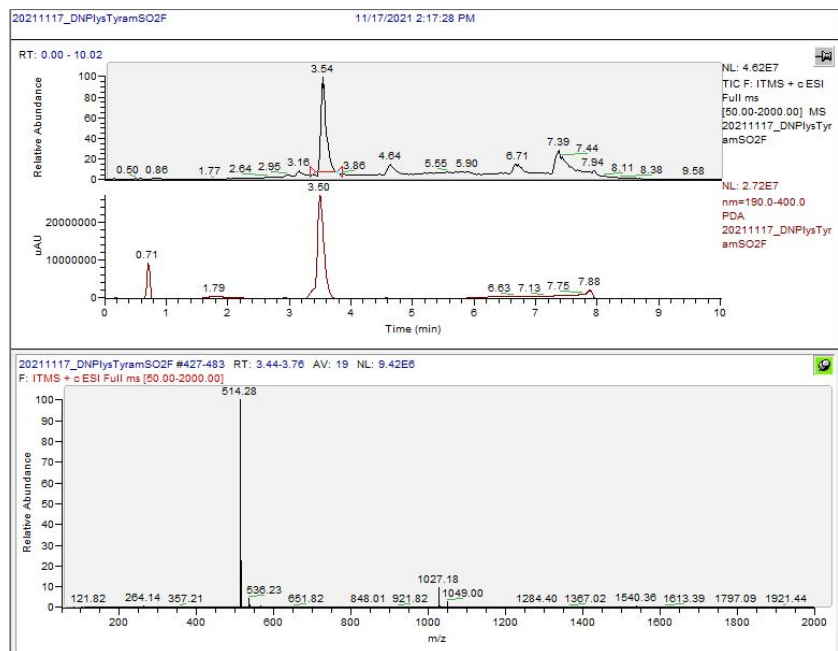
of H₂O and conducting 3 washes with saturated NaCl. Solvent was removed and the product was isolated through normal phase chromatography (DCM/MeOH) yielding 38.4 mg (54%). ^1H NMR (700 MHz, CD₃CN) δ 8.95 (dd, J = 2.71 Hz, 1H), δ 8.54 (s, 1H), δ 8.23 (dd, J = 1.84 Hz, 1H), δ 7.45 (t, J = 7.93 Hz, 1H), δ 7.27 – 7.33 (m, 2H), δ 7.08 (d, J = 9.60 Hz, 1H), δ 6.65 (s, 1H), δ 3.40 – 3.44 (m, 5H), δ 2.82 (t, J = Hz, 2H), δ 1.63 – 1.72 (m, 4H), δ 1.47 – 1.53 (m, 1H), δ 1.38 (s, 14H). ^{19}F NMR (700 MHz, CD₃CN) 36.9 ppm.

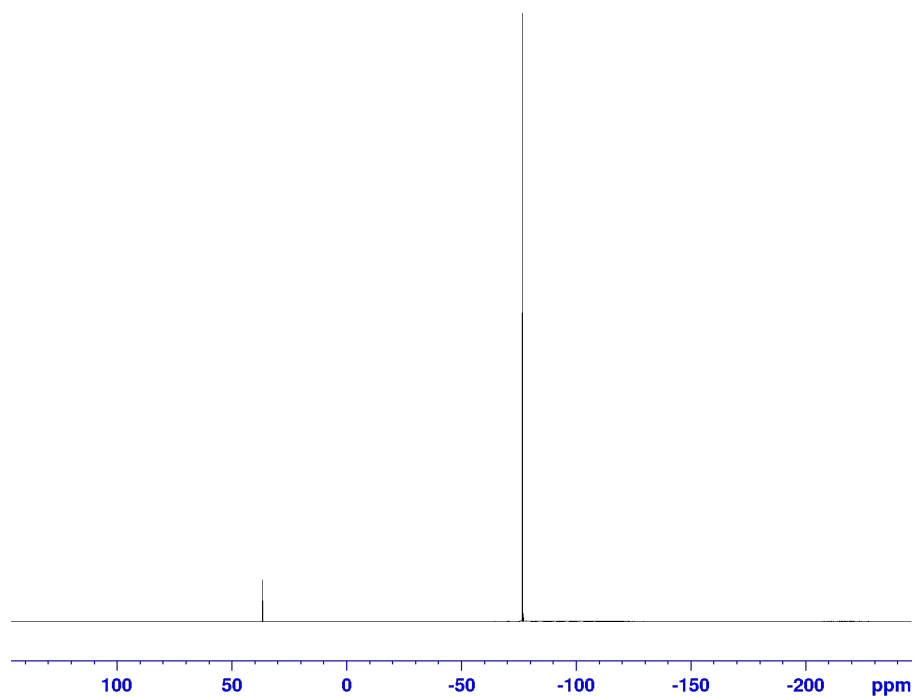


Compound **4C**. DNPLysTyra(m)SO₂F

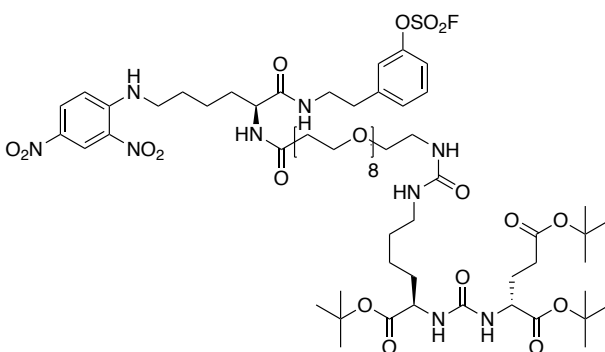
Compound **3C** was dissolved in 2 mL of 25% vol/vol DCM:TFA. This reaction was stirred for an hour and the compound was placed under vacuum. 38.4 mg was obtained (118 %). ¹H NMR (700 MHz, CD₃CN) δ 8.97 (d, J = 2.71 Hz, 1H), δ 8.53 (s, 1H), δ 8.26 (dd, J = 3.06 Hz, 1H), δ 7.46 – 7.48 (m, 1H),

δ 7.35 (d, J = 7.88 Hz, 1H), δ 7.31 (d, J = 6.83 Hz, 2H), δ 7.08 (d, J = 9.59 Hz, 1H), δ 6.90 (s, 1H), δ 3.79 (t, J = 4.13 Hz, 1H), δ 3.52 – 3.55 (m, 1H), δ 3.41 – 3.44 (m, 4H), δ 2.82 – 2.89 (m, 2H), δ 1.63 – 1.79 (m, 5H), δ 1.29 – 1.39 (m, 3H). ¹⁹F NMR (700 MHz, CD₃CN) 36.9 ppm.



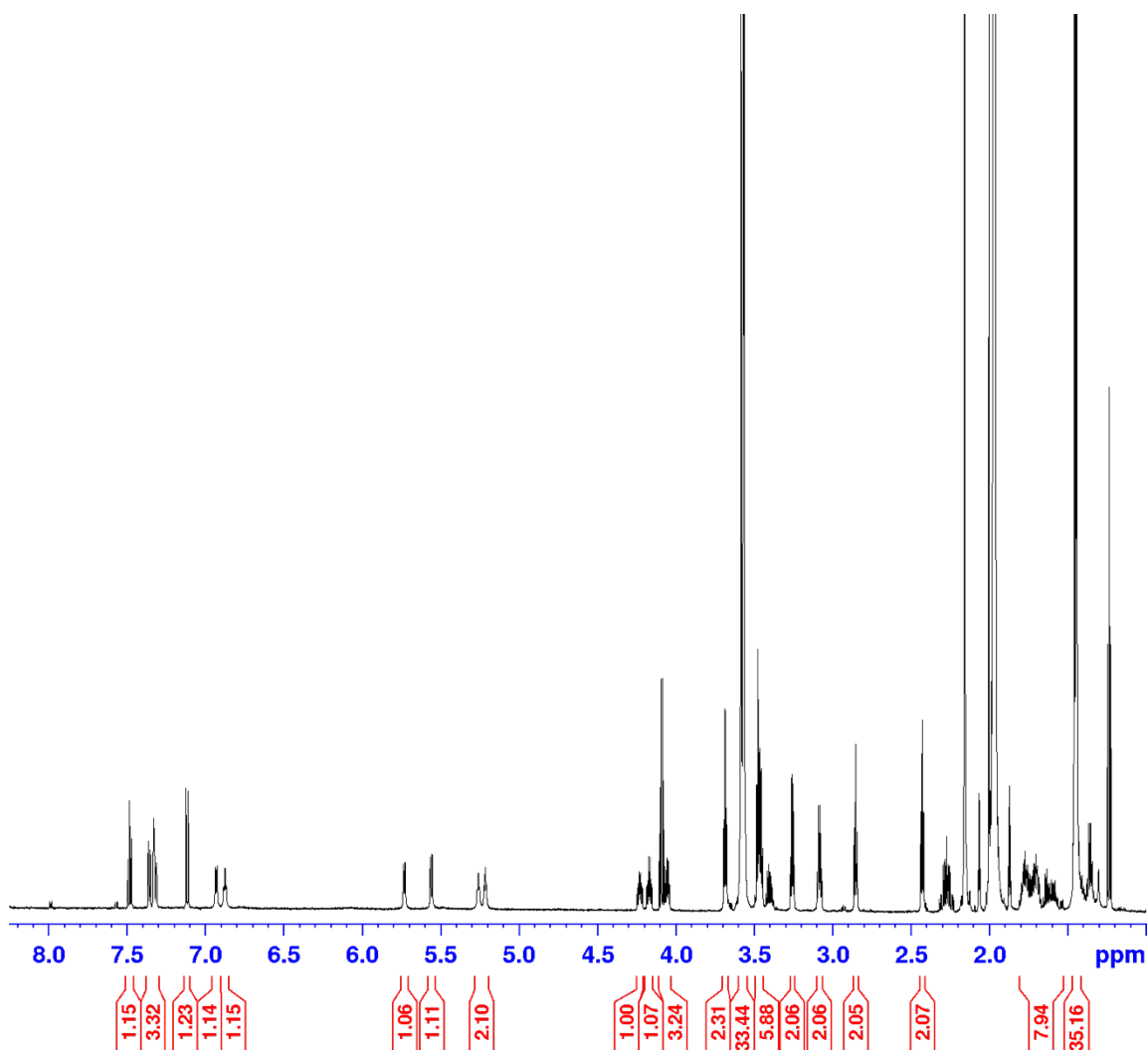
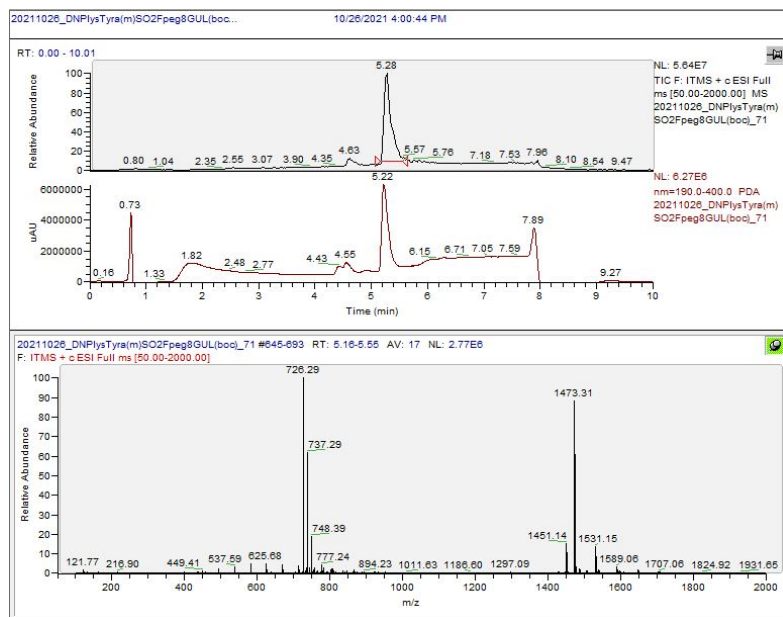


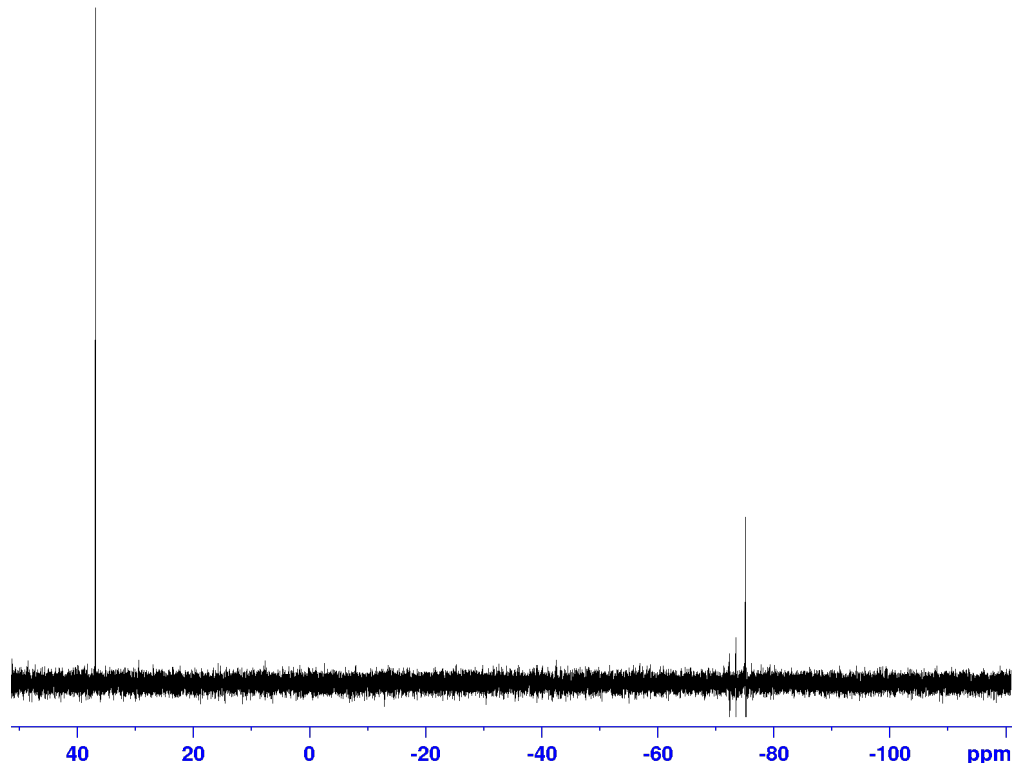
Compound **6C**. DNPLysTyra(m)SO₂Fpeg8GULboc



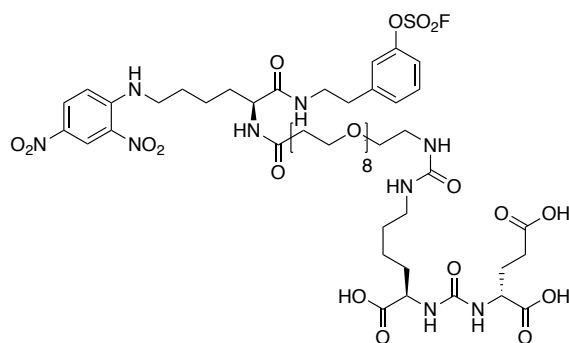
Compound **6C** was obtained by dissolving 25.6 mg (0.0268 mmol) of Compound **5** with 20.6 mg (0.0541 mmol) HATU and 11.3 μ L (0.0810 mmol) DIPEA. A few minutes later 20.8 mg (0.0405 mmol) Compound **4C**. After the reaction was stirred overnight, DMF was removed, re-dissolved in EtOAc, and washed with brine three times. 25.6 mg (66.3%) was obtained

through reverse-phase chromatography.

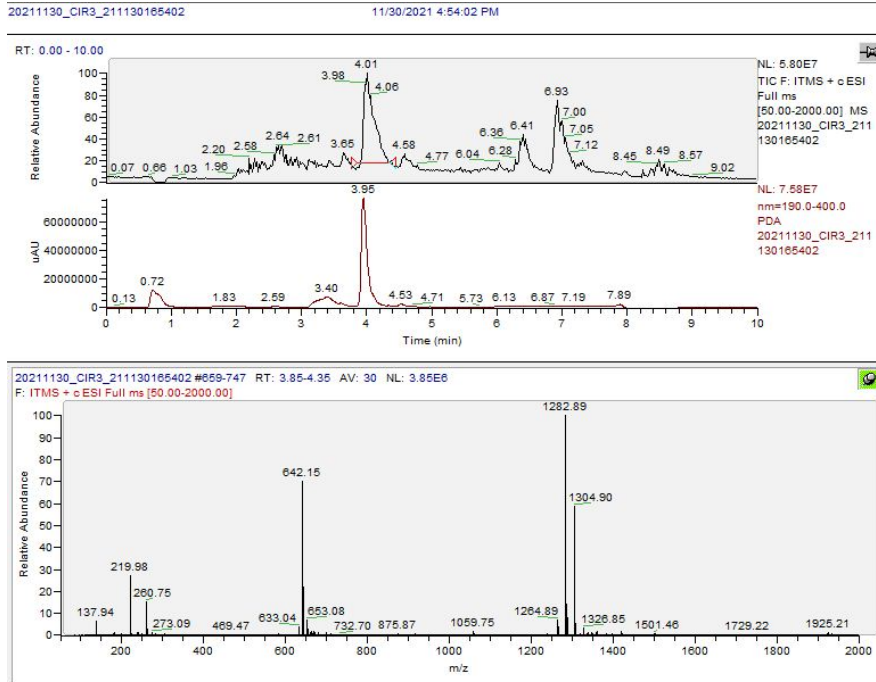


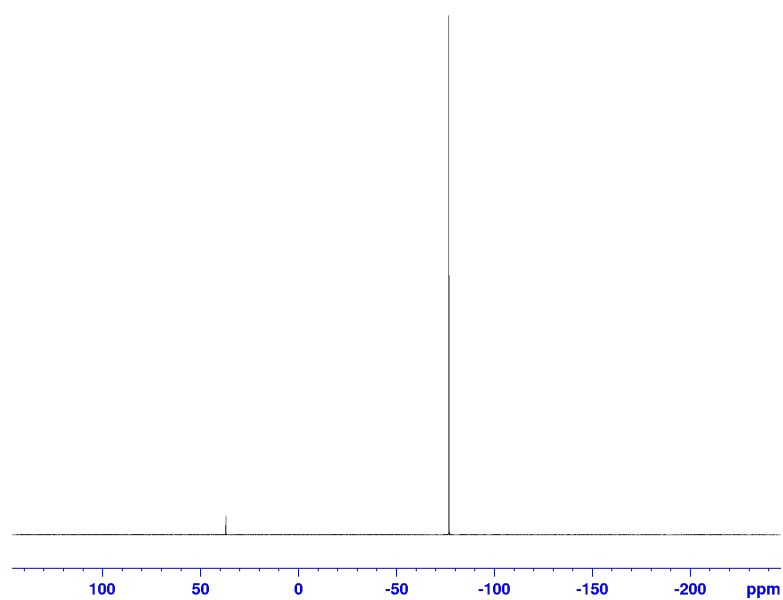
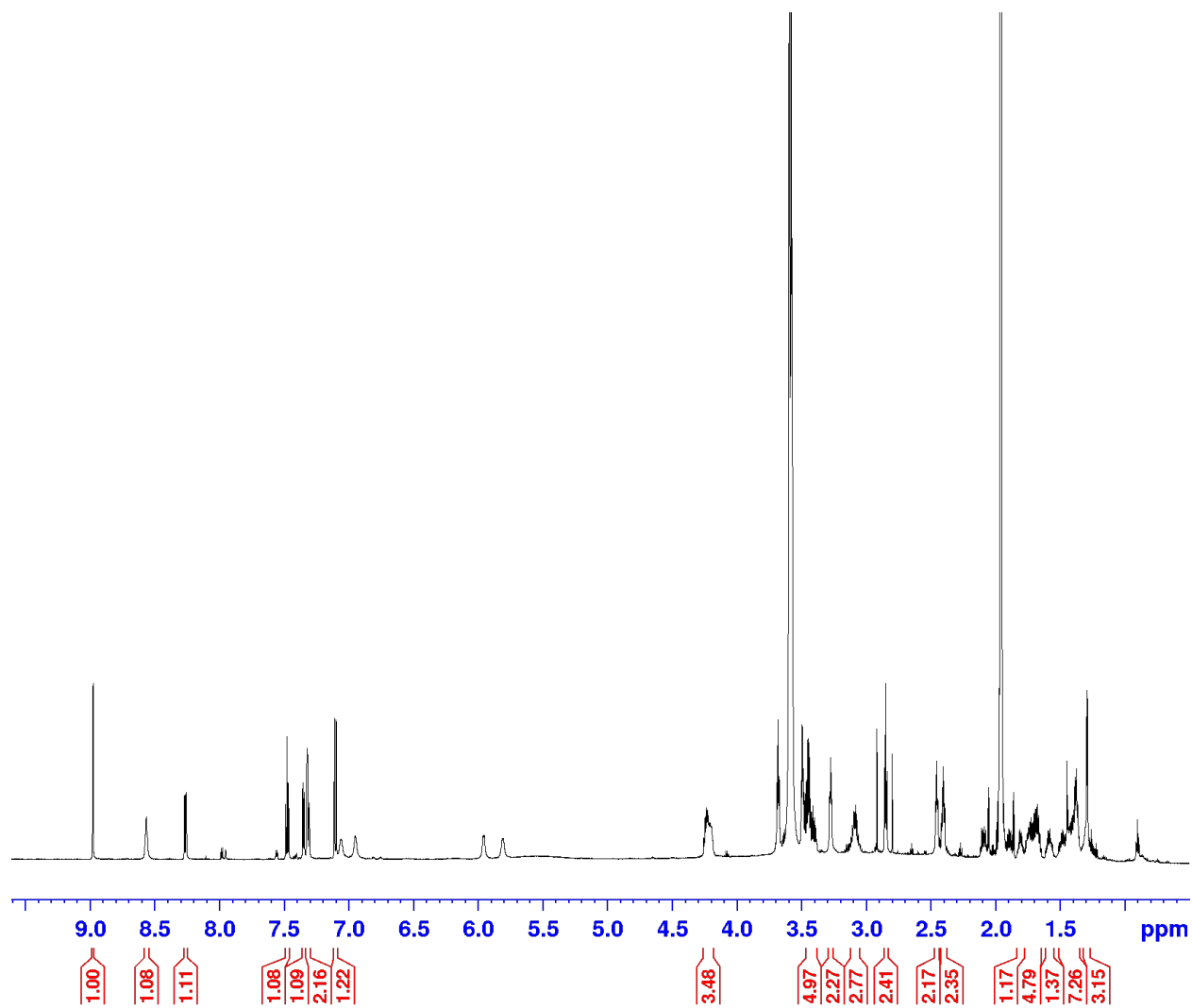


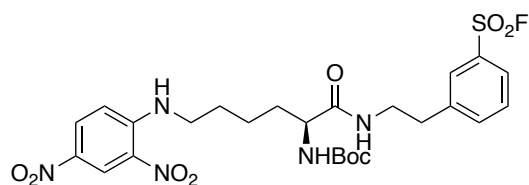
sCIR3



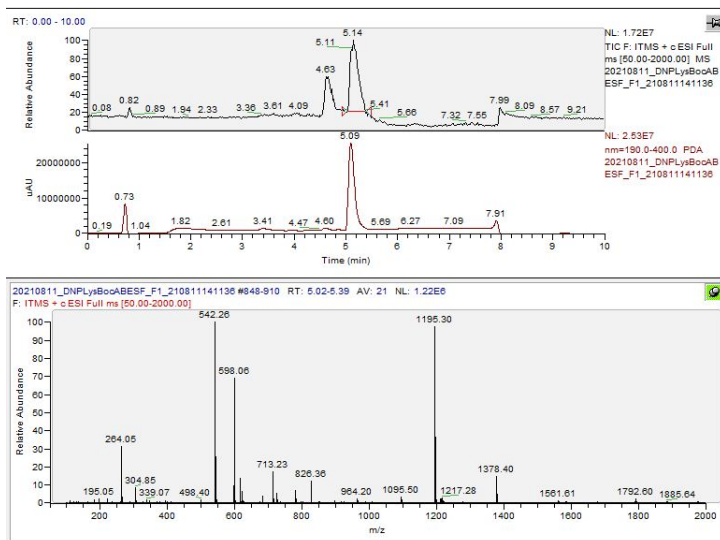
22.5 mg (125%) of **sCIR3** was obtained by dissolving 20.5 mg of Compound **6C** in 1 mL DCM and 0.3 mL TFA. After 3 hours the solvent was removed and dried under vacuum. ^1H NMR (700 MHz, CD_3CN) δ 8.98 (d, $J = 2.7$ Hz, 1H), δ 8.56 (s, 1H), δ 8.26 (d, $J = 4.07$ Hz, 1H), δ 7.48 (t, $J = 7.88$ Hz, 1H), δ 7.30 – 7.35 (m, 3H), δ 7.09 – 7.11 (d, $J = 9.60$ Hz, 1H), δ 4.20 – 4.25 (m, 3H), δ 3.39 – 3.47 (m, 5H), δ 3.27 (t, $J = 5.02$ Hz, 5H), δ 3.06 – 3.11 (m, 3H), δ 2.85 (t, $J = 6.95$ Hz, 2H), δ 2.45 (t, $J = 6.95$ Hz, 2H), δ 2.39 – 2.41 (m, 3H), δ 1.78 – 1.82 (m, 1H), δ 1.64 – 1.76 (m, 5H), δ 1.55 – 1.61 (m, 1H), δ 1.35 – 1.51 (m, 7H), δ 1.29 (d, $J = 5.08$ Hz, 3H). ^{19}F NMR (700 MHz, CD_3CN) 36.8 ppm.



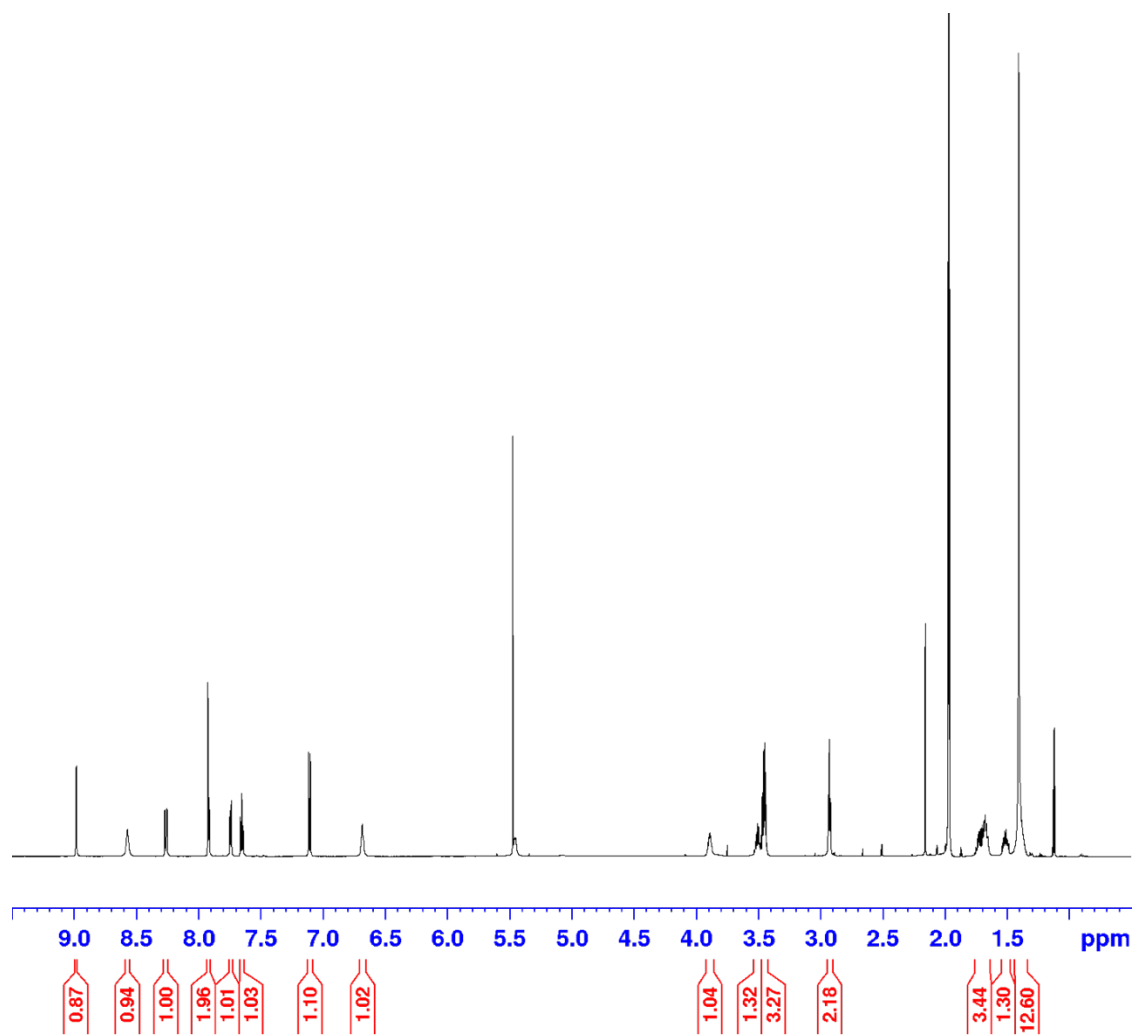


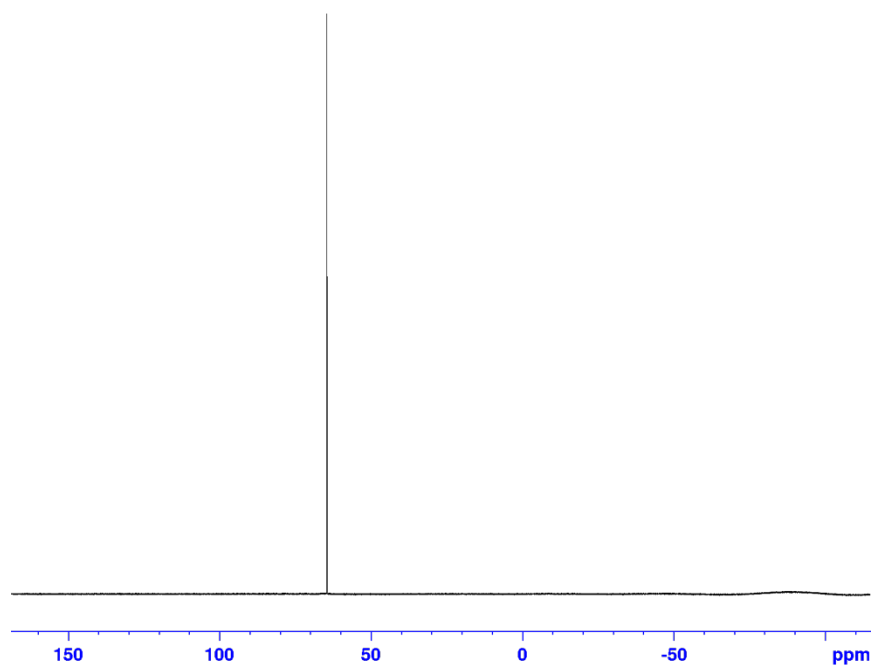
Compound **3D**. DNPLysBocTyraMetaSF

Compound **2D** (25 mg, 0.1043 mmol) was stirred with 39.7 mg (0.1042 mmol) HATU and 45.4 μ L DIPEA (0.2607 mmol) in 2 mL DMF. 35.8 mg (0.0869 mmol) of Compound **1** was added a few minutes later, then the reaction was stirred 2.5 hours. The solvent was removed, the crude material was re-dissolved in EtOAc and washed three times with brine. Purification by normal phase yielded 39.1 mg of product (90.5%). ^1H NMR (700 MHz, CD_3CN) δ 8.26 (d, J = 2.68 Hz, 1H), δ 8.57 (s, 1H), δ 8.26 (dd, J = 4.08 Hz, 1H), δ 7.92 (d, J = 3.93 Hz, 2H), δ 7.74 (d, J = 7.72 Hz, 1H), δ 7.65 (t, J = 9.60 Hz, 1H), δ 7.10 (d, J = 9.60 Hz, 1H), δ 6.68 (s, 1H), δ 3.87 – 3.91 (m, 1H), δ 3.43 – 3.52 (m, 4H), δ 2.92 (t, J = 2.92 Hz, 2H), δ 1.64 – 1.75 (m, 4H), δ 1.45 – 1.54 (m, 1H), δ 1.40 (s, 12H). ^{19}F NMR (700 MHz, CD_3CN) 64.9 ppm.

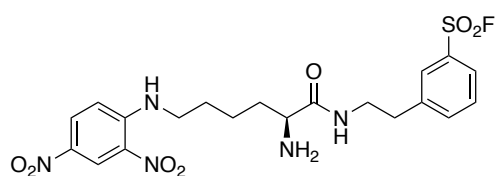


Peak at 4.63 min in ITMS spectrum is a contaminant in the MS (see appendix for blank).

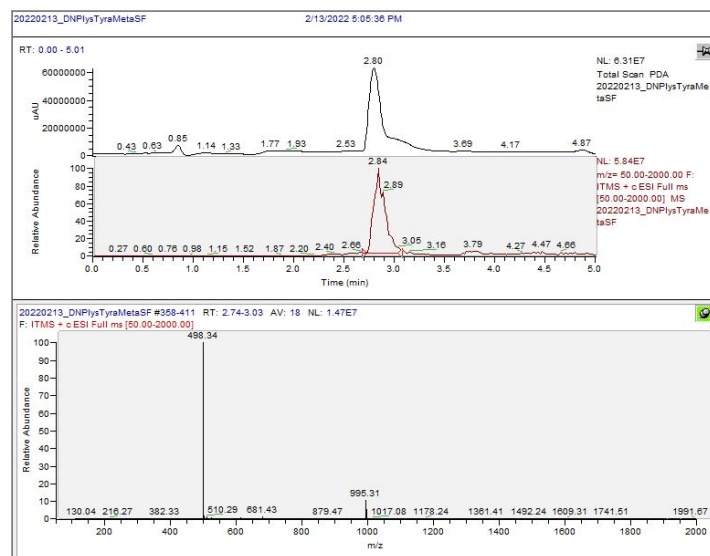


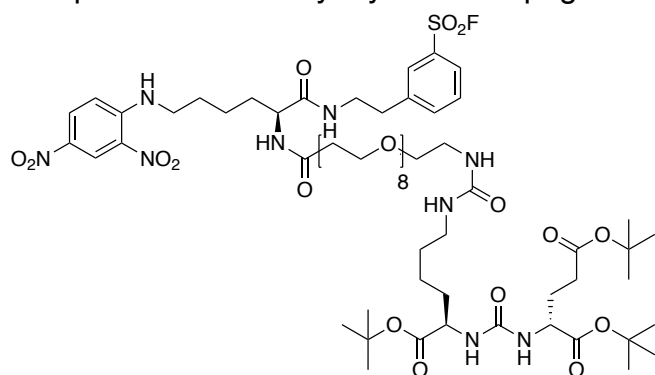


Compound **4D**. DNPLysTyraMetaSF



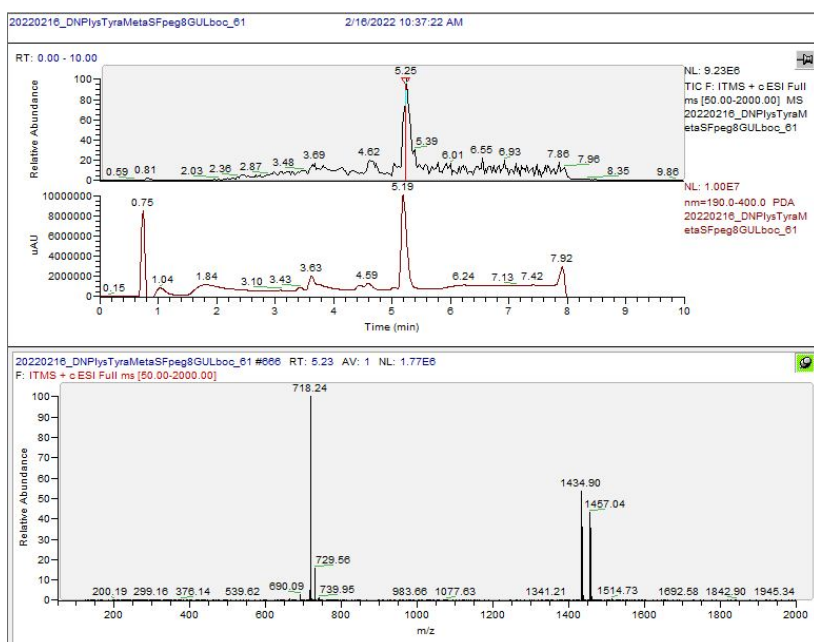
Compound **3D** was deprotected by dissolving 39.1 mg in 0.5 mL TFA and 1.5 mL DCM. After 2 hours the solvent was removed and dried under vacuum. 35.5 mg (109%) was yielded.



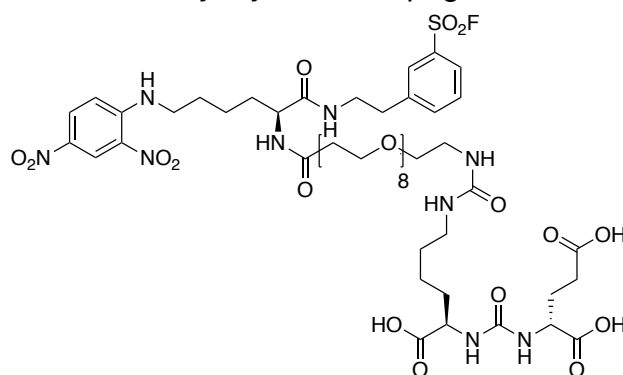
Compound **6D**. DNPLysTyraMetaSFpeg8GULboc

This compound was synthesized by adding 16.1 (0.0169 mmol) mg of Compound **5** in 2 mL DMF, along with 13.6 mg (0.0358 mmol) HATU and 5 μ L (0.0359 mmol) TEA. After 5 minutes 8.9 mg (0.0179 mmol) of Compound **2D** was added to the mixture. The next day, DMF was removed, and the crude mixture was re-dissolved in EtOAc. After

washing with brine three times, the crude material was purified by reverse phase. 2.2 mg (8.6%) was collected from the column.

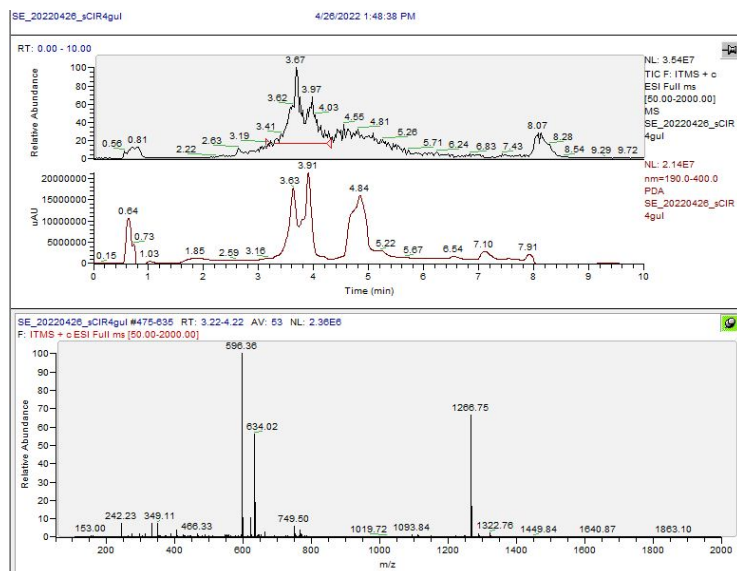


sCIR4. DNPLysTyraMetaSFpeg8GUL

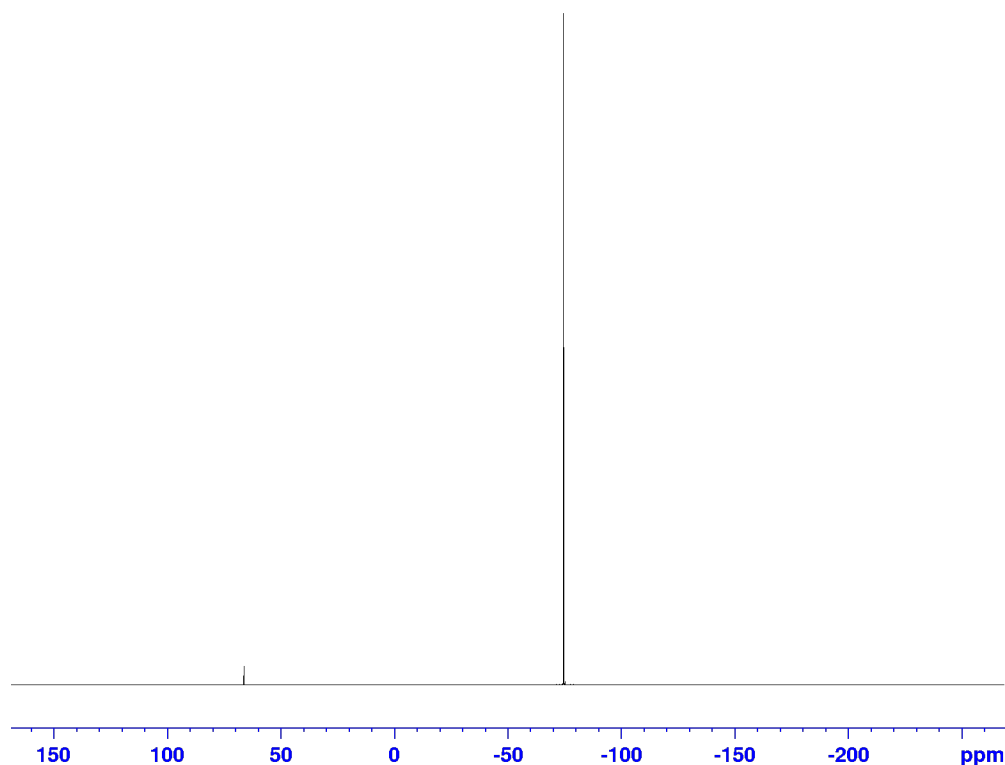


11.3 mg of Compound **6D** was deprotected using 0.4 mL TFA in 1 mL DCM. After 2 hours, solvent was evaporated. Total mass obtained was 12.7 mg (88.8%). ^1H NMR (700 MHz, CD_3CN) δ 8.79 (d, $J = 2.74$ Hz, 1H), δ 8.76 (t, $J = 5.83$ Hz, 1H), δ 8.18 (dd, $J = 3.99$ Hz, 1H), δ 7.91 (t, $J = 5.70$ Hz, 1H), δ 7.86 – 7.89 (m, 4H), δ 7.71 (d, $J = 7.84$ Hz, 1H), δ 7.62 (t, $J = 7.76$ Hz, 1H), δ

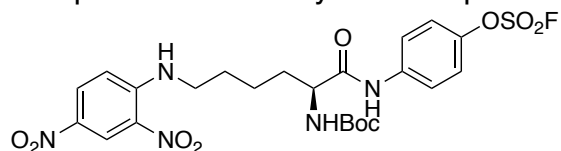
7.12 (d, $J = 9.64$ Hz, 1H), δ 6.24 (dd, $J = 9.64$ Hz, 2H), δ 4.09 – 4.12 (m, 2H), δ 4.00 – 4.04 (m, 2H), δ 3.94 – 3.98 (m, 3H), δ 3.41 – 3.43 (m, 39H), δ 3.05 (t, $J = 5.66$ Hz, 2H), δ 2.87 (t, $J = 6.84$ Hz, 2H), δ 2.78 – 2.81 (m, 2H), δ 2.24 – 2.33 (m, 3H), δ 2.12 – 2.21 (m, 3H), δ 1.82 – 1.87 (m, 1H), δ 1.61 – 1.69 (m, 1H), δ 1.34 – 1.58 (m, 9H), δ 1.24 – 1.28 (m, 3H), δ 1.16 – 1.20 (m, 10H). ^{19}F NMR (700 MHz, CD_3CN) 66.2 ppm.



Peak at 4.84 min in UV spectrum is solvent

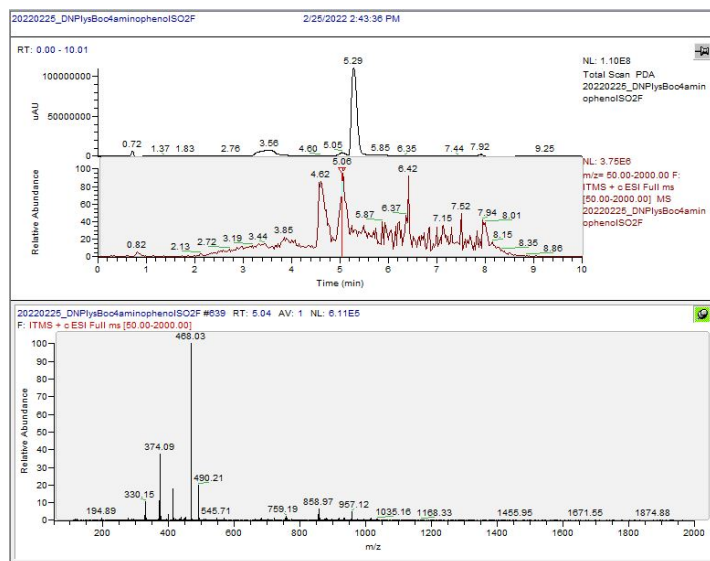


Compound **3E**. DNPLysBoc4amphSO₂F

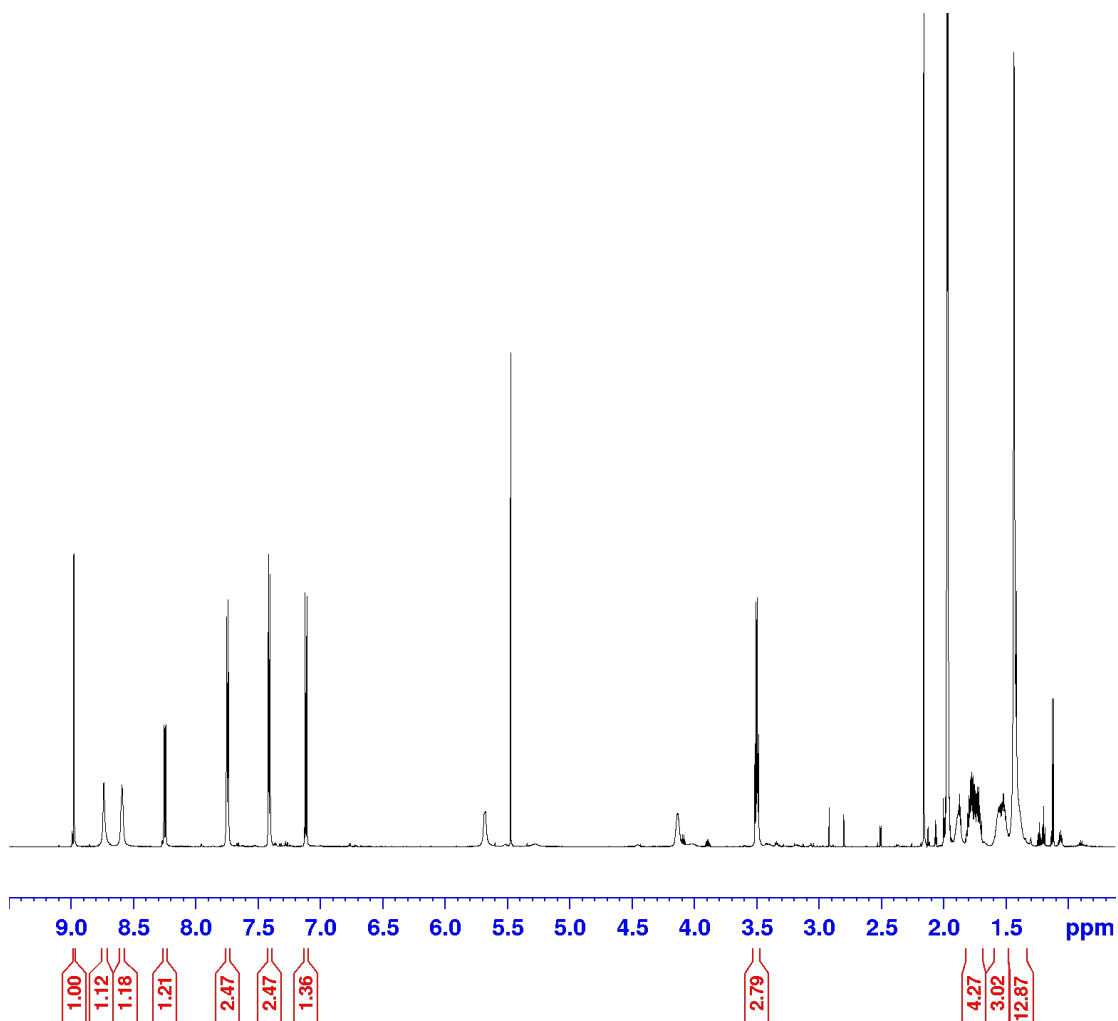


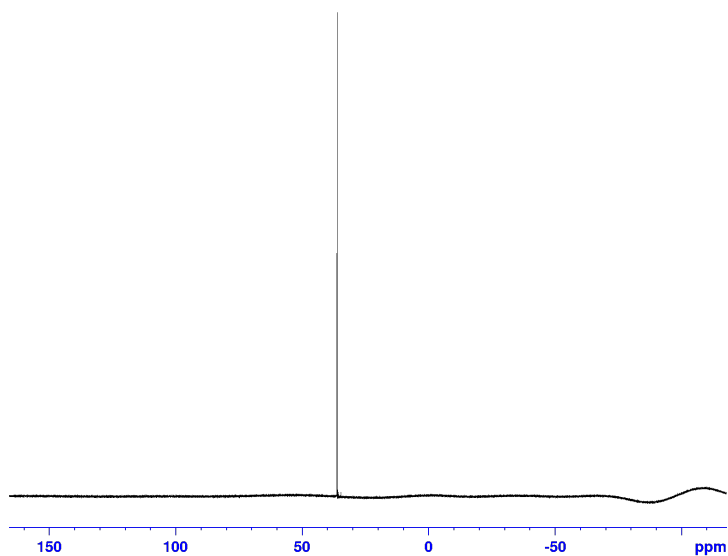
48.9 mg (0.245 mmol) of Compound **2E** was added to a solution of 121.4 mg (0.294 mmol) Compound **1**, 111 mg (0.294 mmol) HATU and 66 μL (0.49 mmol) TEA in 3 mL DMF. After

stirring overnight, the solvent was removed *in vacuo*. The crude material was dissolved in EtOAc, washed with brine, then purified by normal phase (DCM/MeOH). Total product collected was 29.8 mg (17.3 %). ^1H NMR (700 MHz, CD₃CN) δ 8.98 (d, J = 2.71 Hz, 1H), δ 8.74 (s, 1H), δ 8.59 (s, 1H), δ 8.24 (dd, J = 1.8 Hz, 1H), δ 7.74 (d, J = 9.09 Hz, 2H), δ 7.41 (d, J = 9.08 Hz, 2H), δ 7.11 (d, J = 9.60 Hz, 1H), δ 3.50 (q, J = 6.66 Hz, 3H), δ 1.69 – 1.81 (m, 4H), δ 1.50 – 1.56 (m, 3H), δ 1.43 (s, 13H). ^{19}F NMR (700 MHz, CD₃CN) 36.1 ppm.

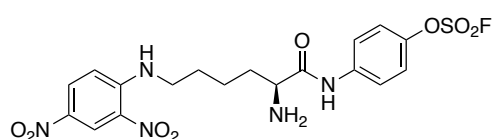


Peak at 4.62 min in ITMS spectrum is a contaminant in the MS (see appendix for blank)

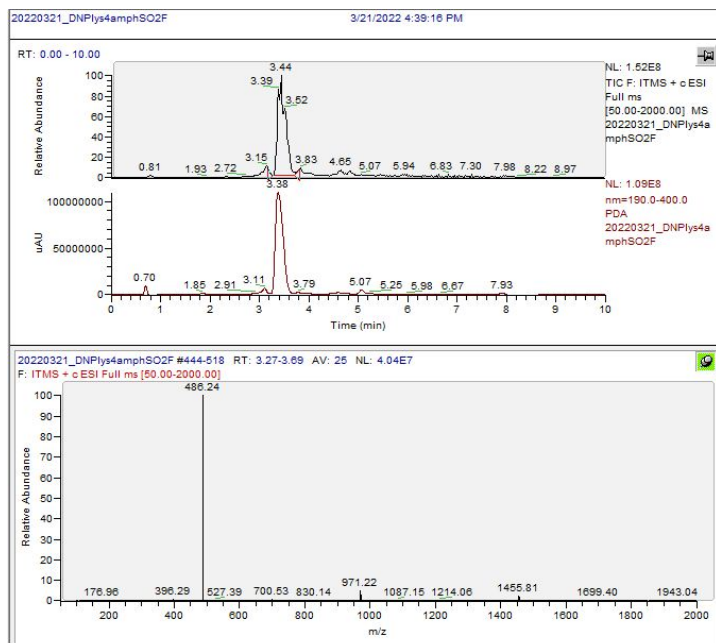


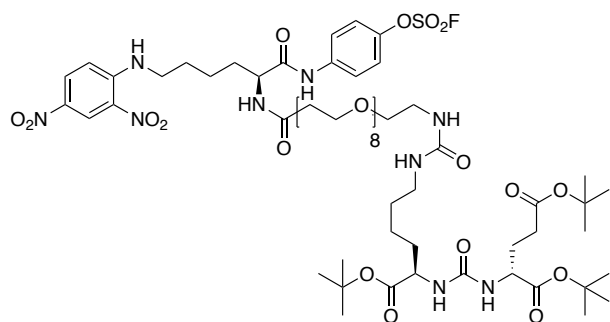


Compound **4E**. DNPLys4amphSO2F

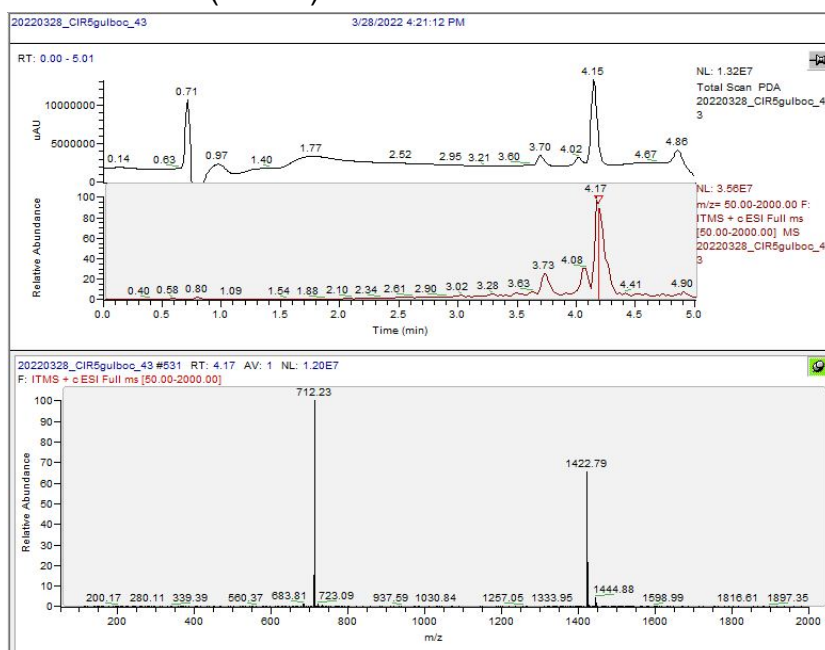
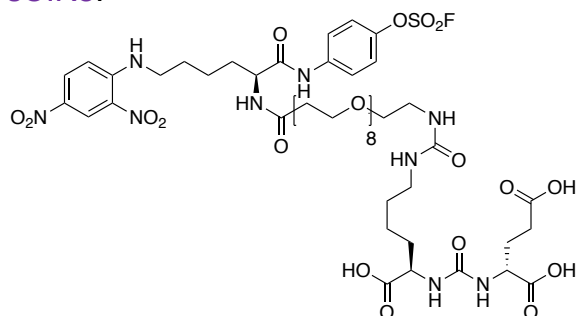


Dissolved in 29.8 mg (0.049 mmol) in 2 mL DCM, then added 0.6 mL TFA. After 2 hours removed solvent and collected 27.3 mg (110%).



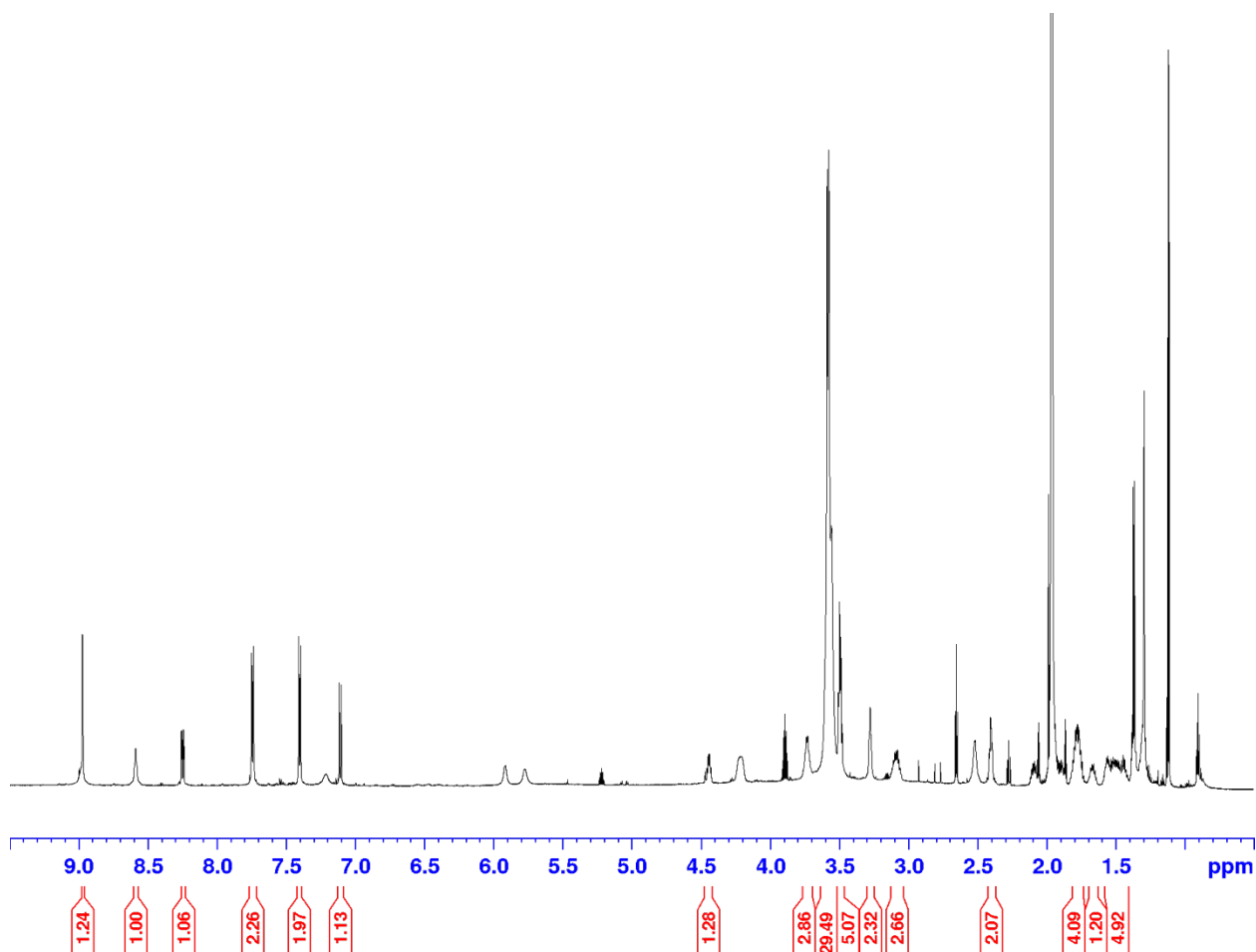
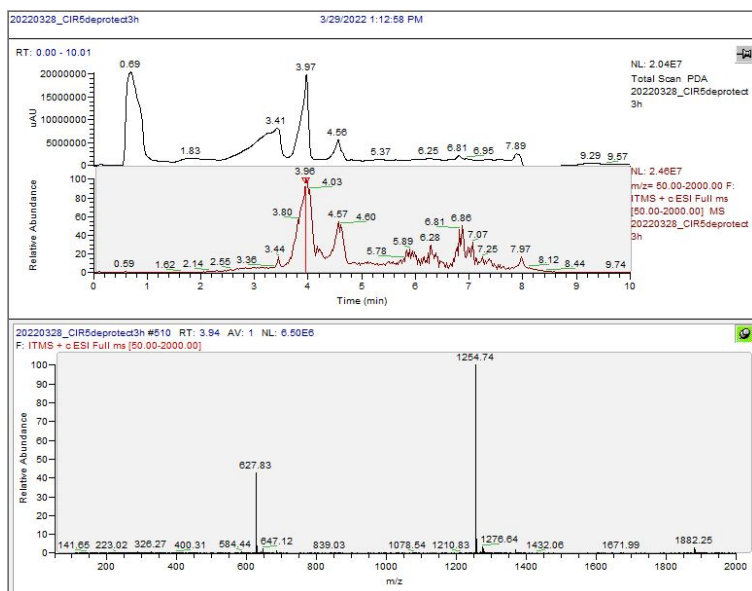
Compound **6E**. DNPLys4amphSO₂Fpeg8GULboc

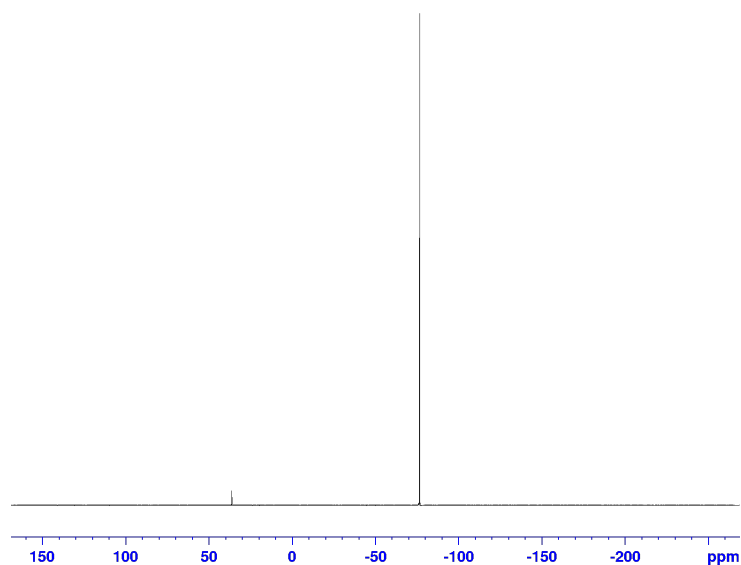
63.6 mg (0.06659 mmol) of Compound **5** was dissolved in 2.5 mL DMF. 39.4 mg (0.1035 mmol) HATU and 23.5 μ L TEA (0.1726 mmol) was added to the reaction. After a few minutes 41.9 mg (0.0863 mmol) Compound **2E** was added to the reaction. 4 hours later solvent was removed, crude material was worked up with EtOAc, washing brine three times. After purification by reverse phase chromatography, 14.2 mg was collected (11.6%).

**sCIR5**.

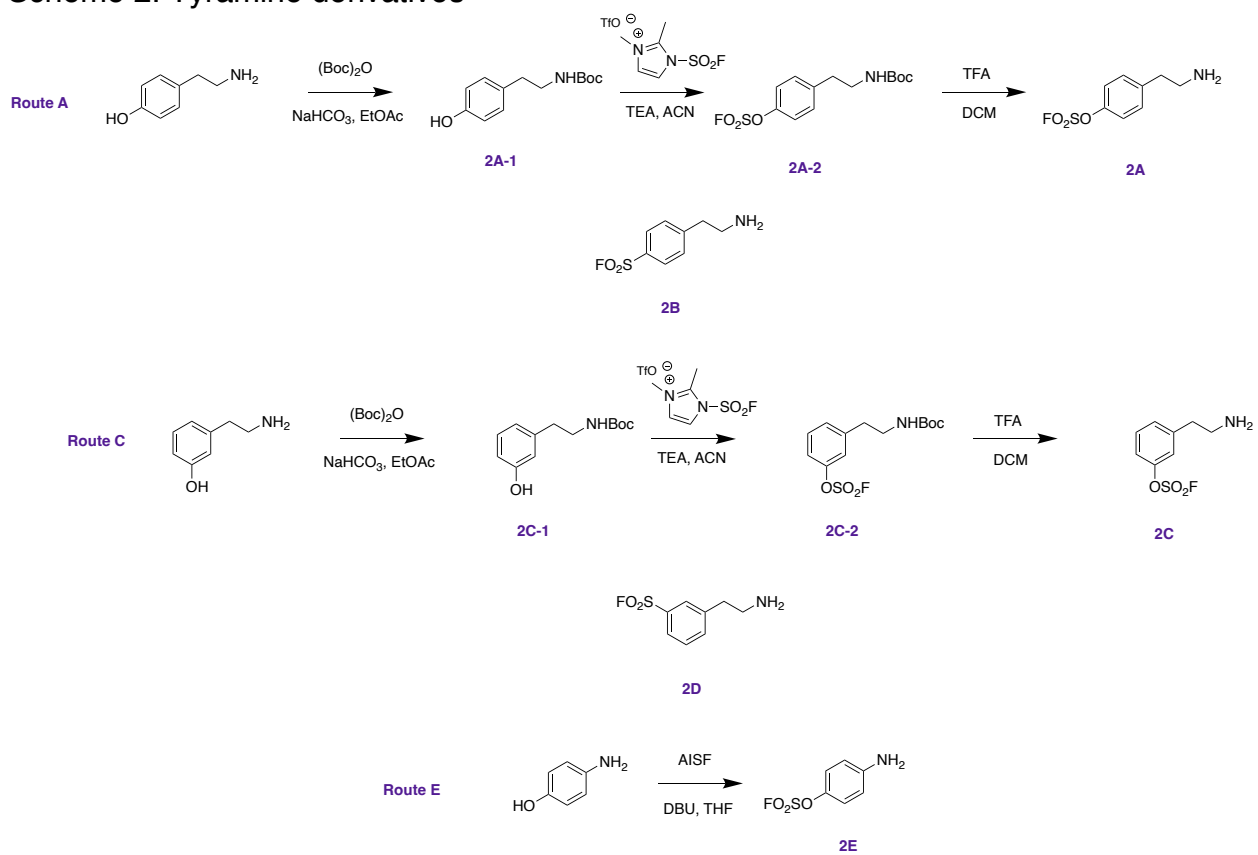
14.4 mg (0.0993 mmol) of Compound **6E** was stirred for 2 hours in 0.6 mL TFA and 2 mL DCM. Solvent was removed *in vacuo* and 14.7 mg was collected (116%). ¹H NMR (700 MHz, CD₃CN) δ 8.96 (d, J = 2.66 Hz, 1H), δ 8.58 (s, 1H), δ 8.24 (dd, J = 4.08 Hz, 1H), δ 7.74 (d, J = 9.17 Hz, 2H), δ 7.40 (d, J = 9.10 Hz, 2H), δ 7.11 (d, J = 9.59 Hz, 1H), δ 4.42 – 4.46 (m, 1H), δ 3.73 (d, J = 6.16 Hz, 3H), δ 3.55 – 3.58 (m, 29H), δ 3.49 (q, J = 5.97 Hz, 5H), δ 3.27 (s, 2H), δ 3.04 – 3.13 (m, 2H), δ 2.39 – 2.41 (m, 2H), δ 1.72 – 1.82 (m, 4H), δ 1.63

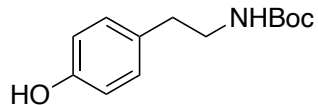
– 1.67 (m, 1H), δ 1.40 – 1.58 (m, 5H), δ 1.29 (s, 5H). ^{19}F NMR (700 MHz, CD_3CN) 36.8 ppm.



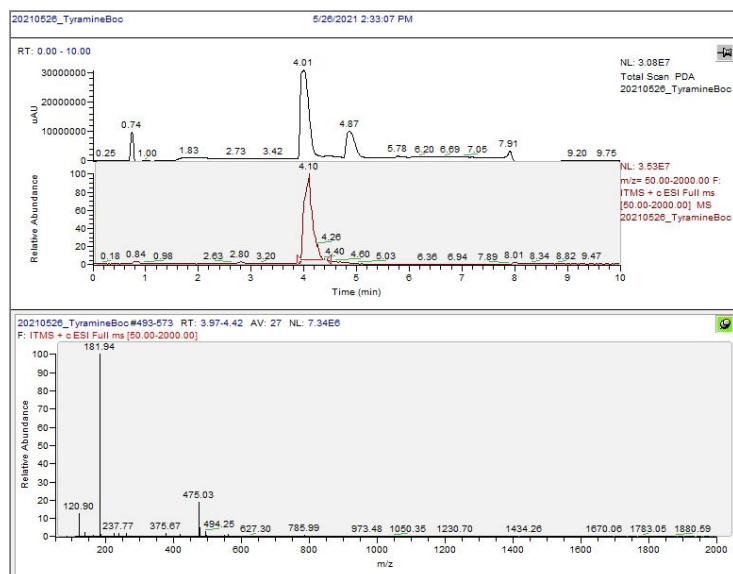


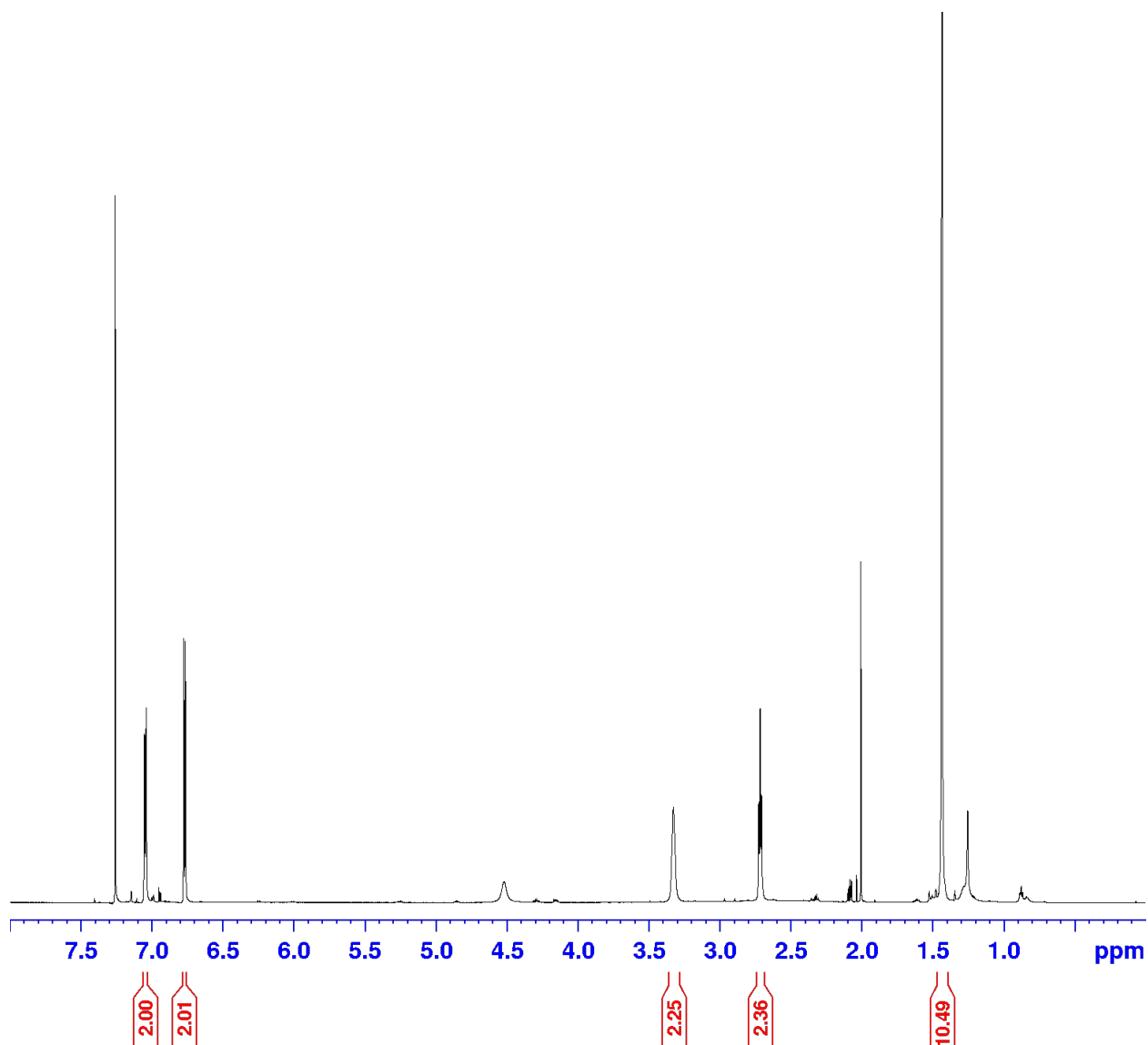
Scheme 2. Tyramine derivatives



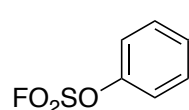
Compound **2A-1**. TyramineBoc

200 mg of Tyramine (1.458 mmol) was dissolved in 5 mL of EtOAc with 477 mg of boc-anhydride (2.187 mmol). The reaction was stirred at room temperature for 5 minutes then sodium bicarbonate (367.4 mg, 4.374 mmol) was added. After 2 hours the reaction was stopped, washed with brine several times, and then purified by EtOAc/Hex with normal phase chromatography. 163.1 mg of product was collected (47.3%). ^1H NMR (700 MHz, CDCl_3) δ 7.05 (d, J = 8.14 Hz, 2H), δ 6.77 (d, J = 8.39 Hz, 2H), δ 3.32 (s, 2H), δ 2.72 (d, J = 6.97 Hz, 2H), δ 2.71 (s, 11H). ^{19}F NMR (700 MHz, CDCl_3) 36.8 ppm.

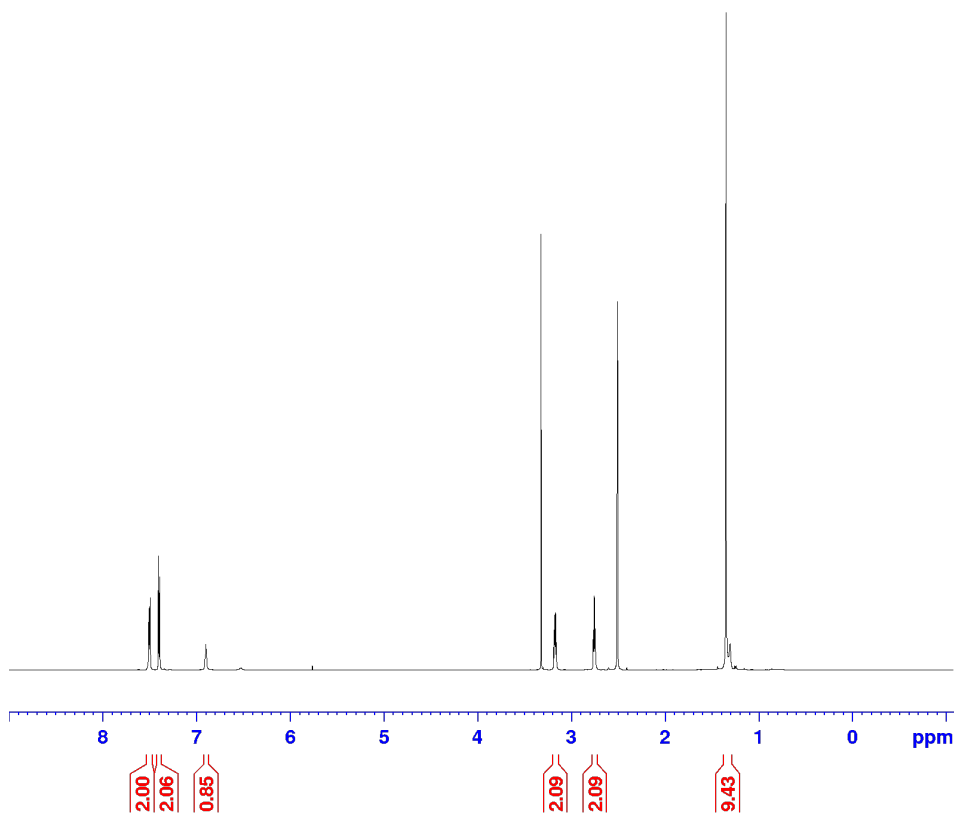
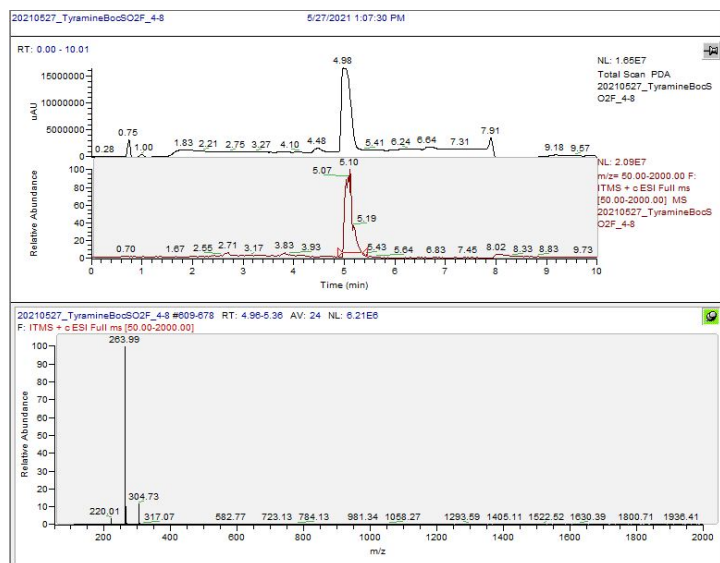


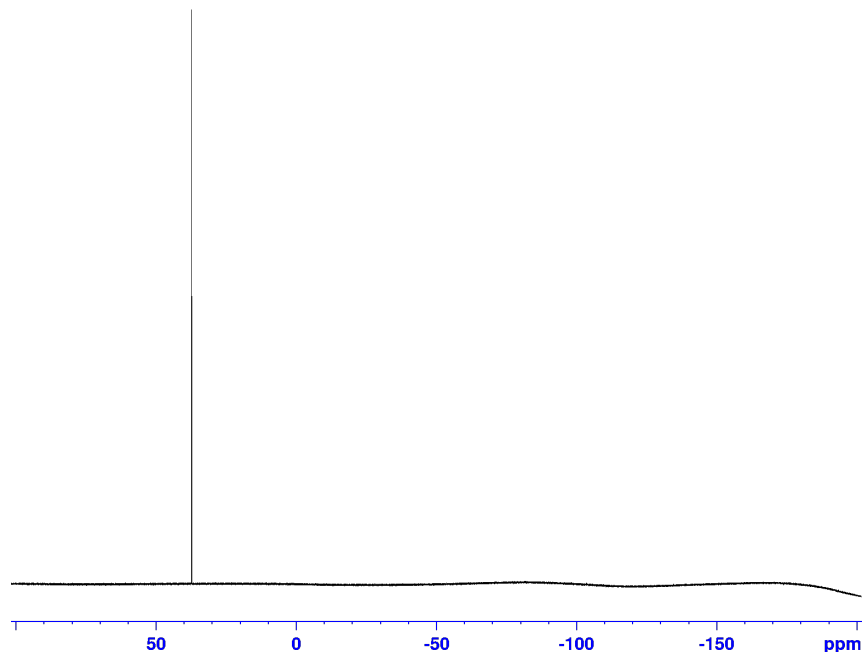


Compound **2A-2**. TyramineBocSO₂F

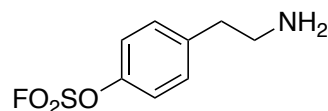


48.3 mg of compound **2A** (0.2035 mmol) was dissolved in 2 mL ACN, along with 42.5 μ L of TEA (0.3052 mmol), and 80.1 mg of 1-(fluorosulfonyl)-2,3-dimethyl-1*H*-imidazol-3-ium trifluoromethanesulfonate (0.2442 mmol). The solution was stirred at room temperature for 1 hour and ACN was concentrated under vacuum. The crude material was purified by normal phase chromatography (DCM/MeOH), to obtain 17.4 mg in 26.8% yield. ¹H NMR (700 MHz, C₂D₆OS) δ 7.50 (d, *J* = 8.47 Hz, 2H), δ 7.40 (d, *J* = 8.65 Hz, 2H), δ 6.89 (t, *J* = 5.34 Hz, 1H), δ 3.17 (t, *J* = 6.66 Hz, 2H), δ 2.75 (t, *J* = 6.66 Hz, 2H), δ 1.34 (s, 9H). ¹⁹F NMR (700 MHz, CD₃CN) 38.1 ppm.

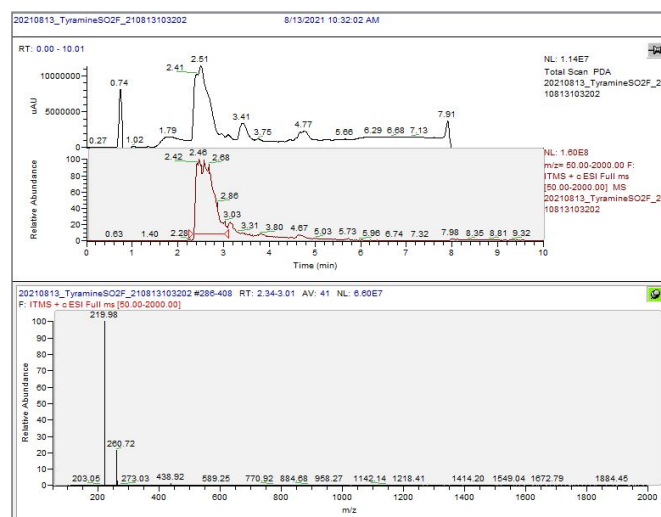


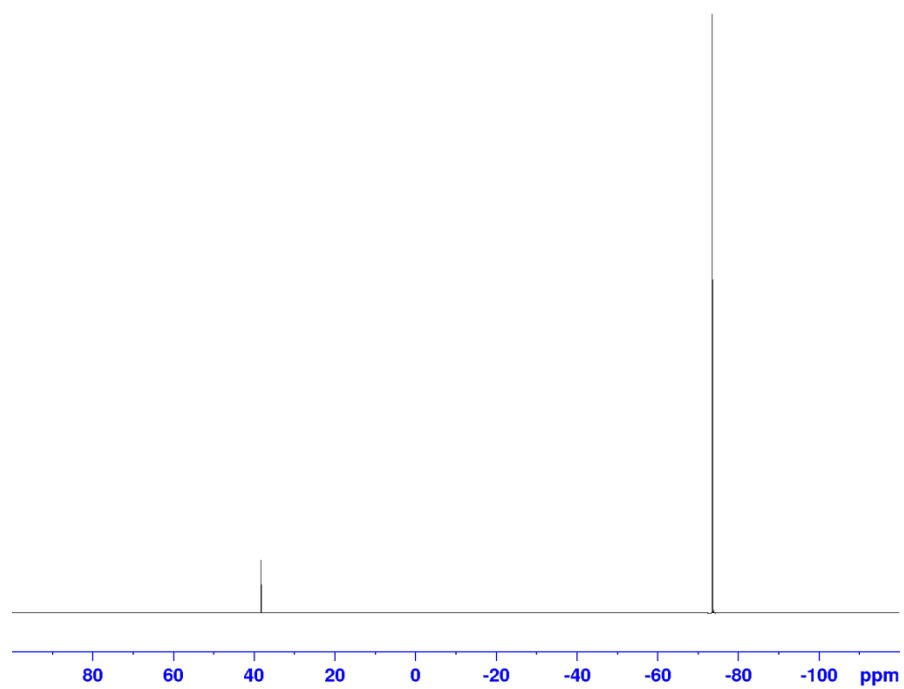
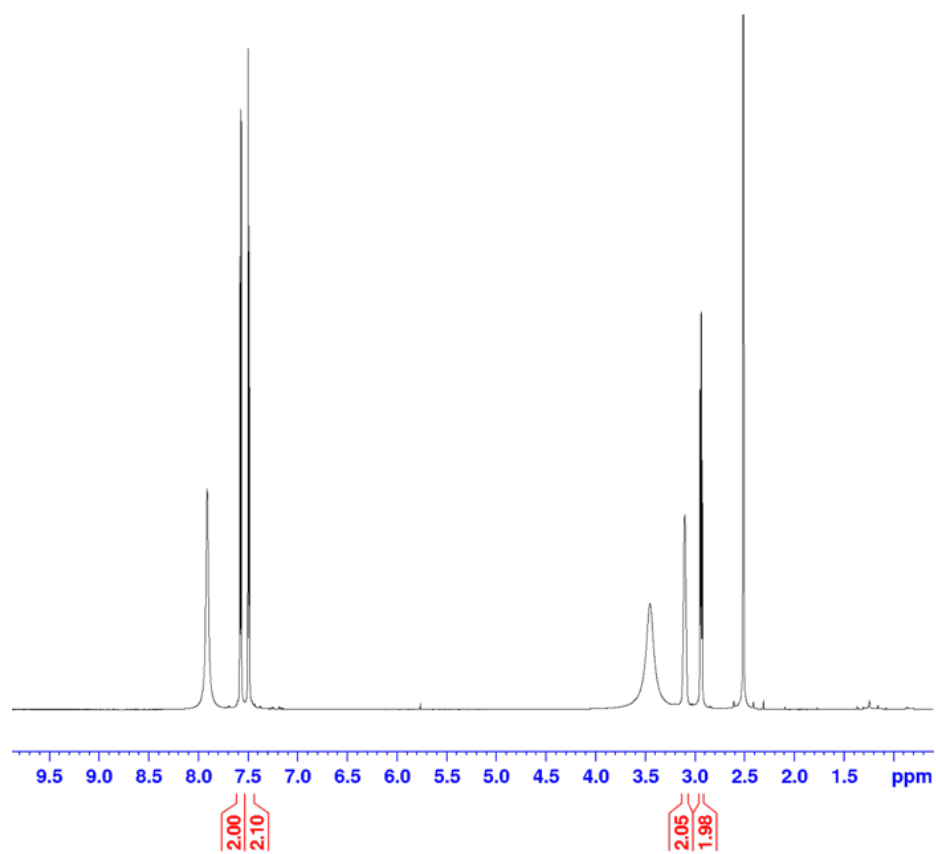


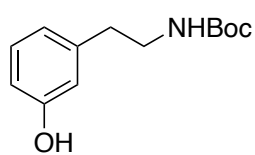
Compound 2A. TyramineSO2F



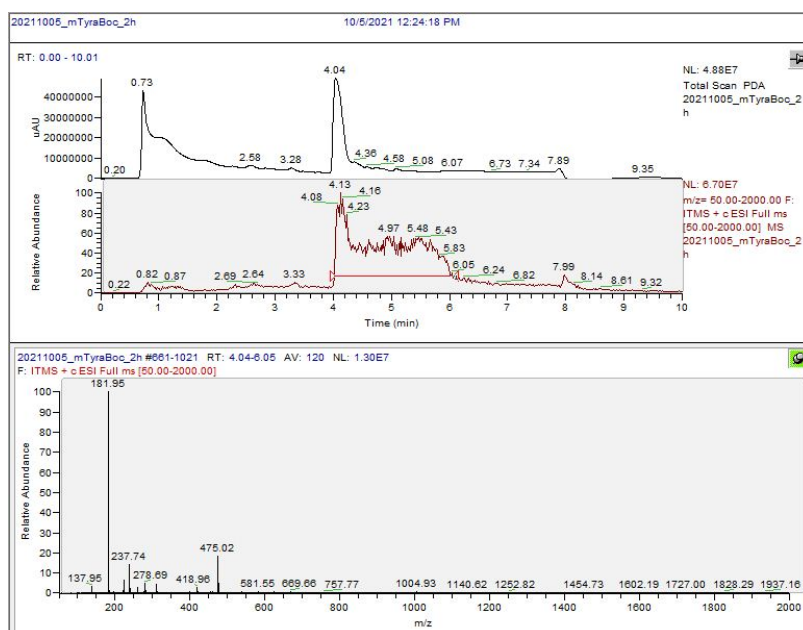
Compound **2A-2** was deprotected by dissolving 62.6 mg (0.1949 mmol) in 1.8 mL DCM and adding 0.2 mL TFA. After stirring the reaction for 2 hours, DCM was reduced under pressure. The resulting solid was re-dissolved DCM and then removed under vacuum three times. Total product obtained was 53.2 mg (124 %). ^1H NMR (700 MHz, CD_3SOCD_3) δ 7.55 (dd, J = 8.61 Hz, 2H), δ 7.47 (dd, J = 8.71 Hz, 2H), δ 6.89 (t, J = 5.34 Hz, 2H), δ 2.91 (t, J = 7.84 Hz, 2H). ^{19}F NMR (700 MHz, CD_3CN) 38.3 ppm.

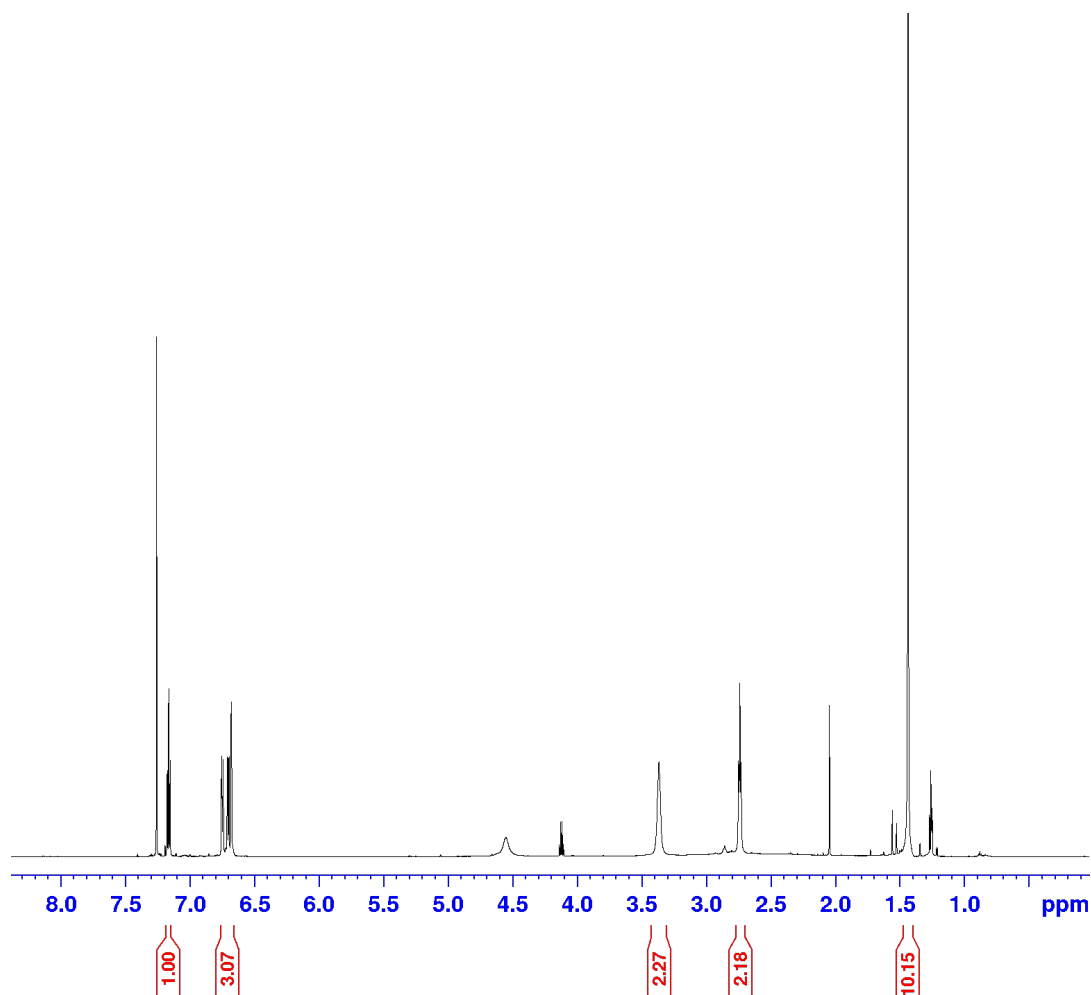




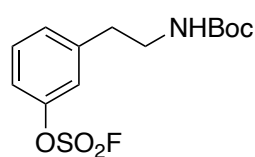
Compound **2C-1**. Tyra(m)Boc

Tyramine (40 mg, 0.2916 mmol) was dissolved in 1-part DMF, 9-parts dioxane (3 mL total). 35 μ L (0.251 mmol) of TEA was added and the reaction was stirred at room temperature for 20 mins. Then 60 mg of boc-anhydride (0.275 mmol) was added, and the reaction was stirred for 2 hours. 1 mL of H₂O was added, and the organic layer was washed three times with brine. After removing the solvent *in vacuo*, the crude material was purified through normal phase chromatography (Hex/EtOAc). 27.1 mg was collected (50% yield). ¹H NMR (700 MHz, CDCl₃) δ 7.16 (dd, J = 7.16 Hz, 1H), δ 6.67 – 6.75 (m, 3H), δ 3.36 (s, 2H), δ 2.73 (t, J = 6.85 Hz, 2H), δ 1.43 (s, 10H).

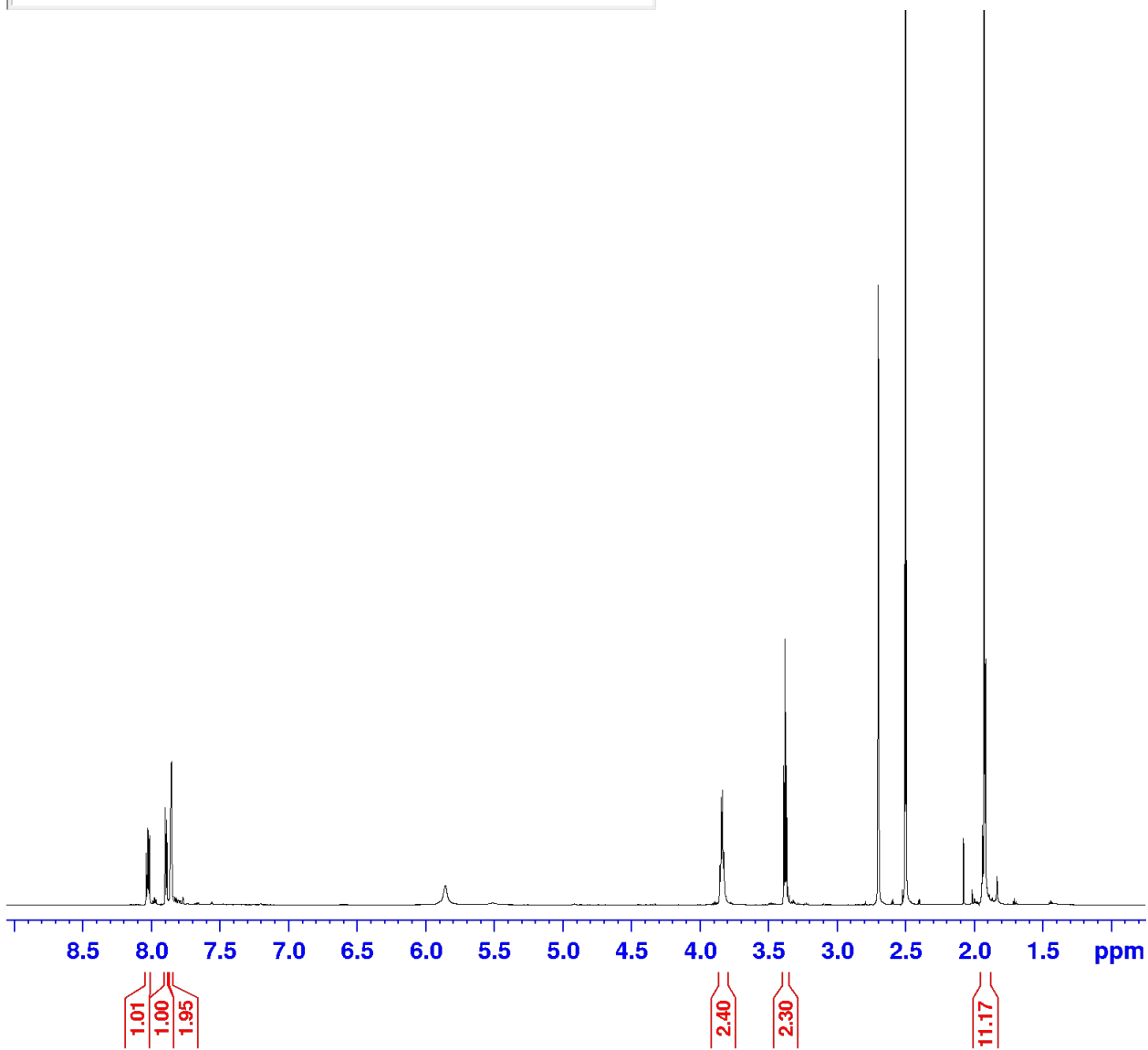
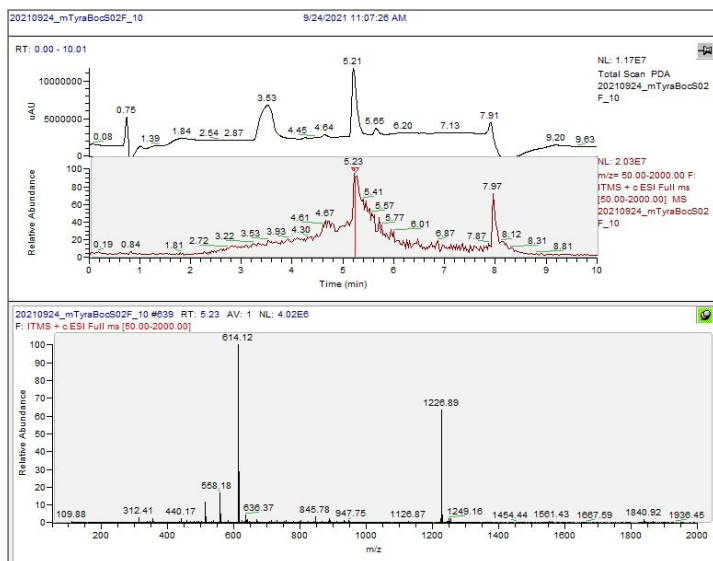


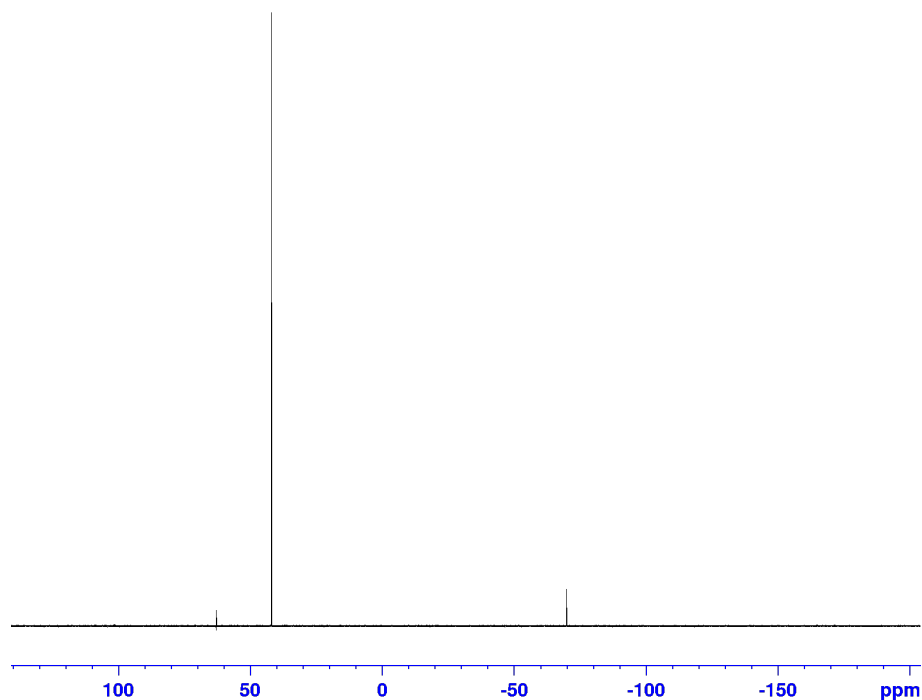


Compound **2C-2**. Tyra(m)BocSO₂F

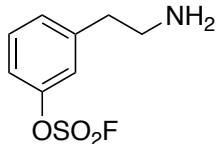


Compound **2C-2** was synthesized by dissolving 30.3 mg of Compound **2C-1** (0.1277 mmol) and 50.3 mg (0.1532 mmol) of 1-(Fluorosulfonyl)-2,3-dimethyl-1*H*-imidazol-3-ium trifluoromethanesulfonate in 2 mL ACN. After adding 26.7 μ L (0.1916 mmol) triethylamine, the reaction was stirred at room temperature for 2 hours. The solvent was removed, and crude material was purified by DCM/MeOH in normal phase chromatography. 18.6 mg was collected, yielding 45.7%. ¹H NMR (700 MHz, CD₃CN) δ 8.02 (t, *J* = 5.54 Hz, 1H), δ 7.89 (d, *J* = 7.70 Hz, 1H), δ 7.85 (s, 2H), δ 3.84 (q, *J* = 6.65 Hz, 2H), δ 3.37 (t, *J* = 6.97 Hz, 2H), δ 1.92 (s, 11H). ¹⁹F NMR (700 MHz, CD₃CN) 42.0 ppm.

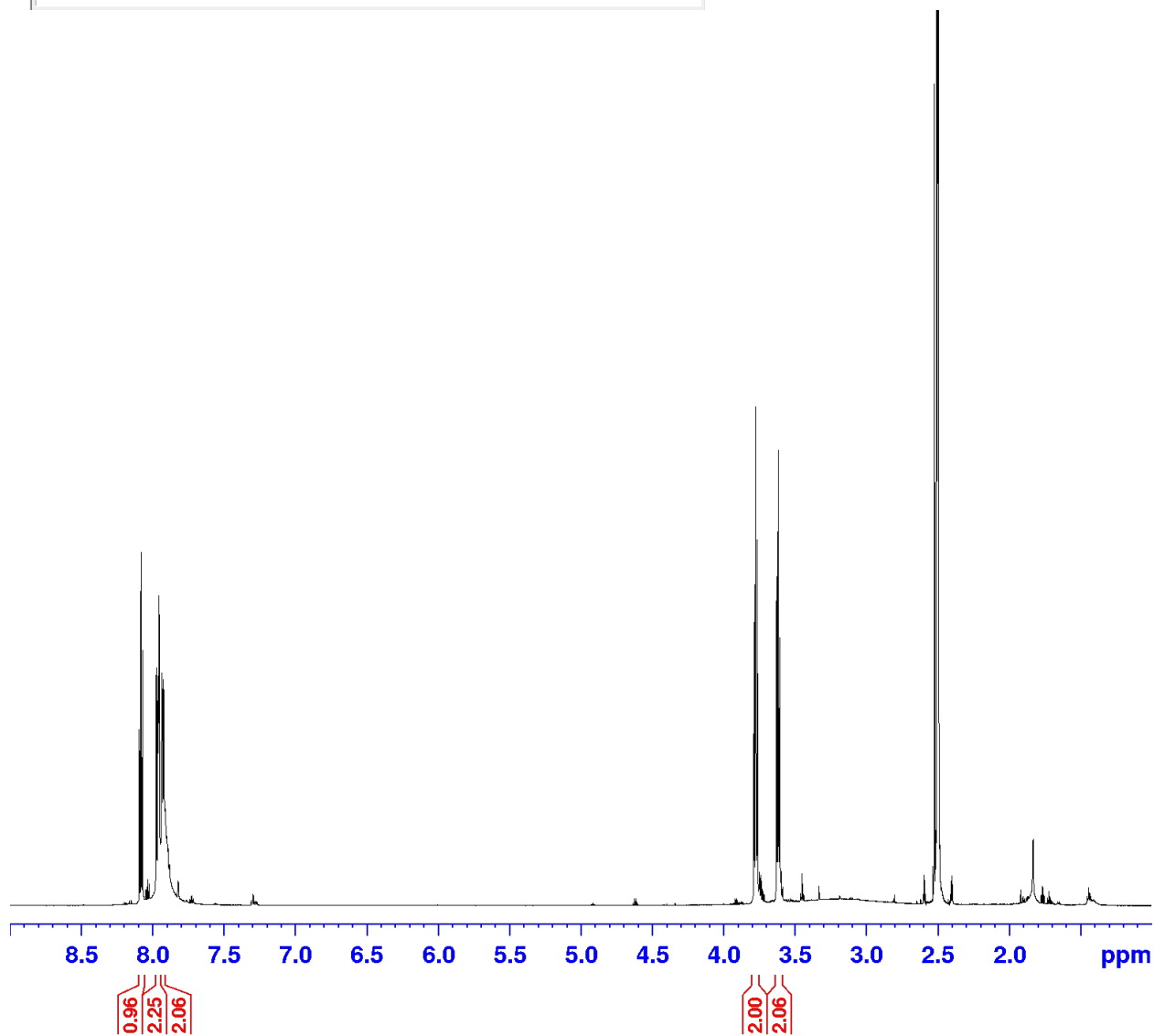
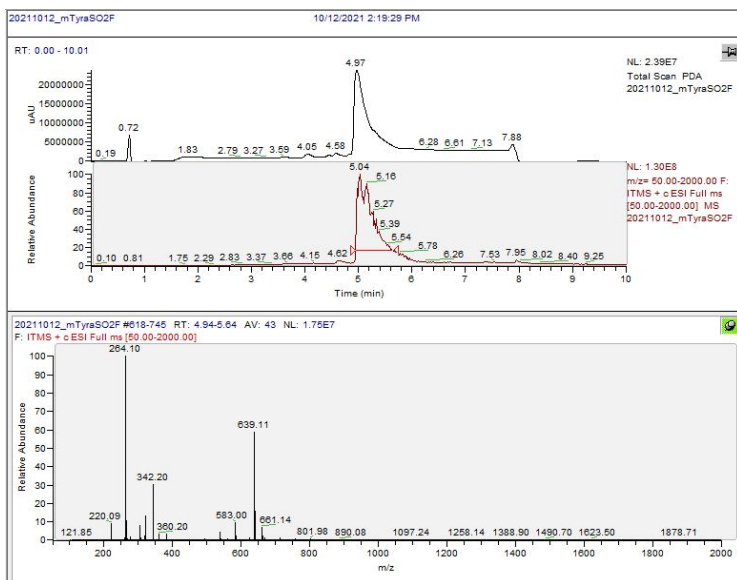


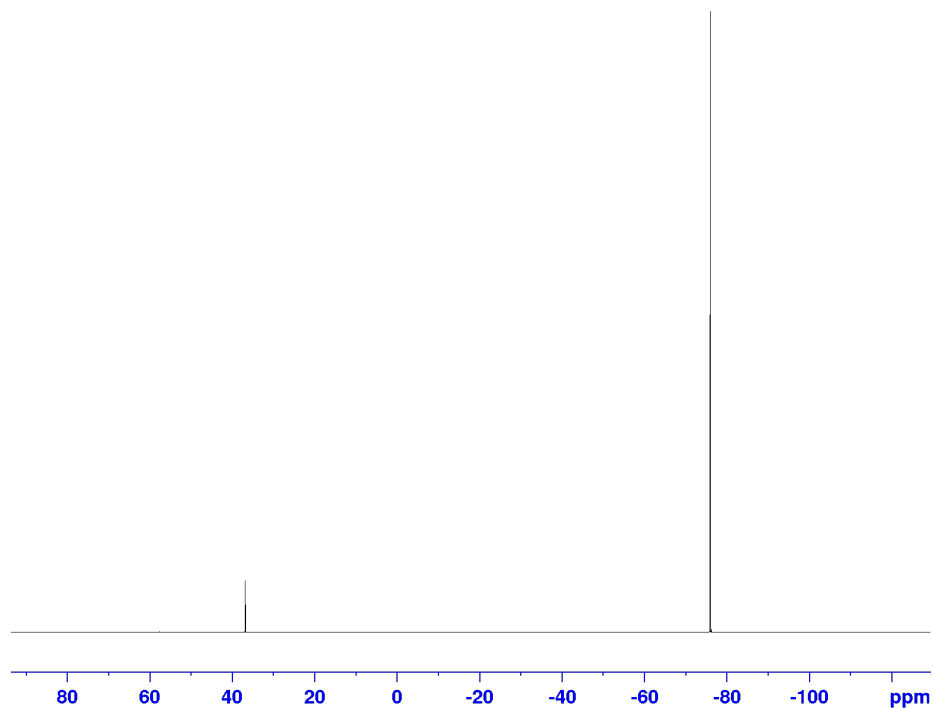


Compound **2C**. Tyra(m)SO₂F

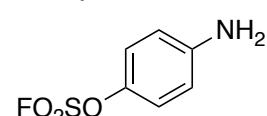


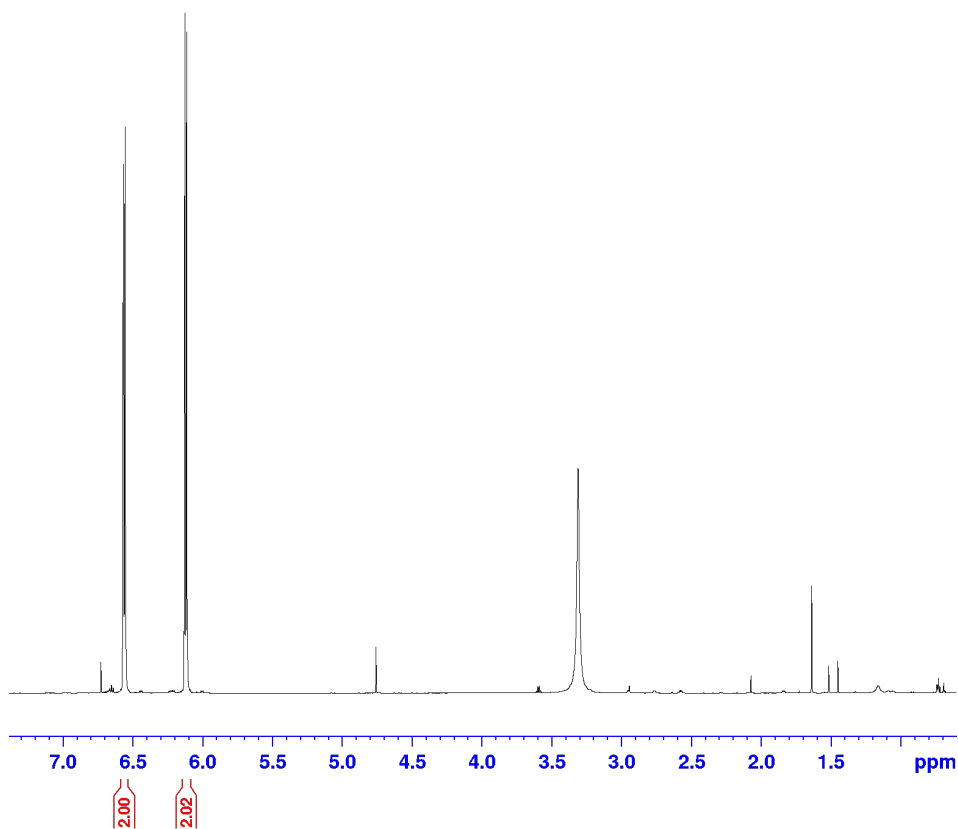
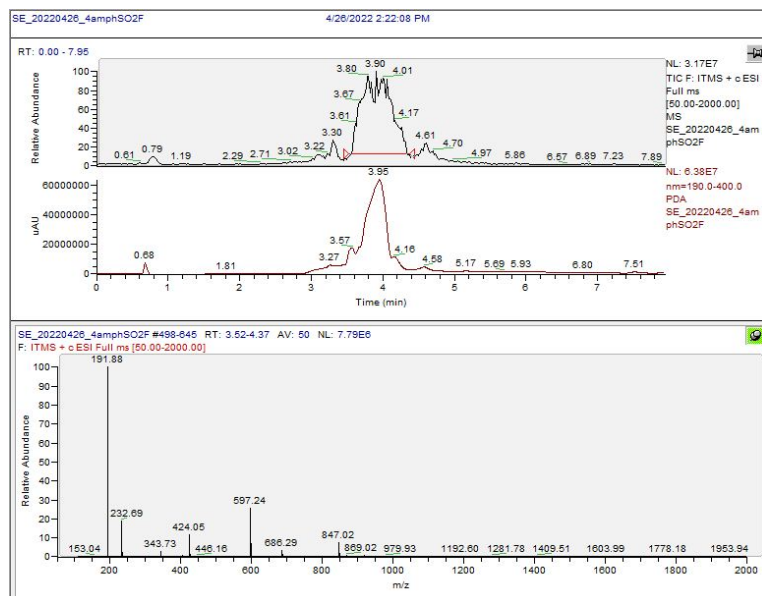
18.6 mg (0.0362 mmol) of Compound **2C-1** was deprotected in 0.4 mL TFA and 1.6 mL DCM. After 1.5 hours, the solvent was removed under vacuum to yield 17.9 mg expected (141 %). ¹H NMR (700 MHz, CD₃SOCD₃) δ 8.08 (t, J = 7.94 Hz, 1H), δ 7.95 – 7.97 (m, 2H), δ 7.92 – 7.94 (m, 2H), δ 3.66 (t, J = 7.59 Hz, 2H), δ 3.61 (t, J = 7.56 Hz, 2H). ¹⁹F NMR (700 MHz, CD₃CN) 63.8 ppm.

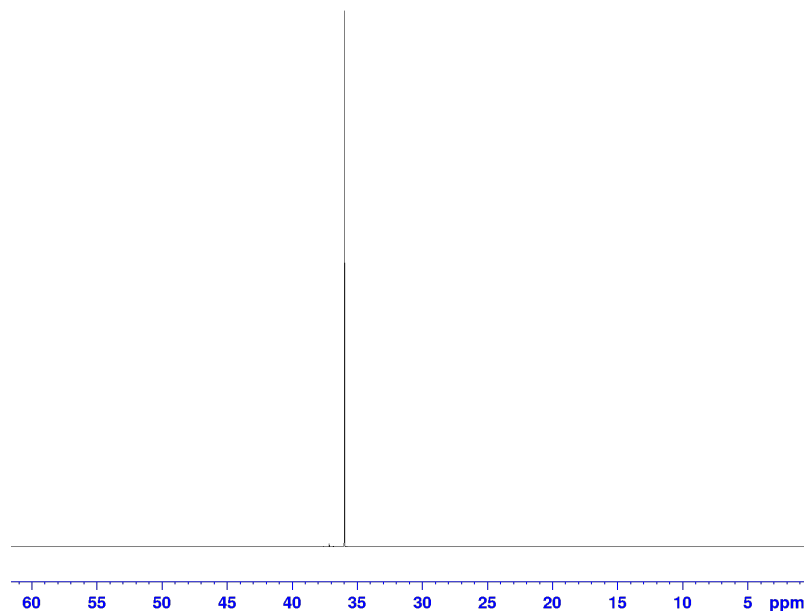




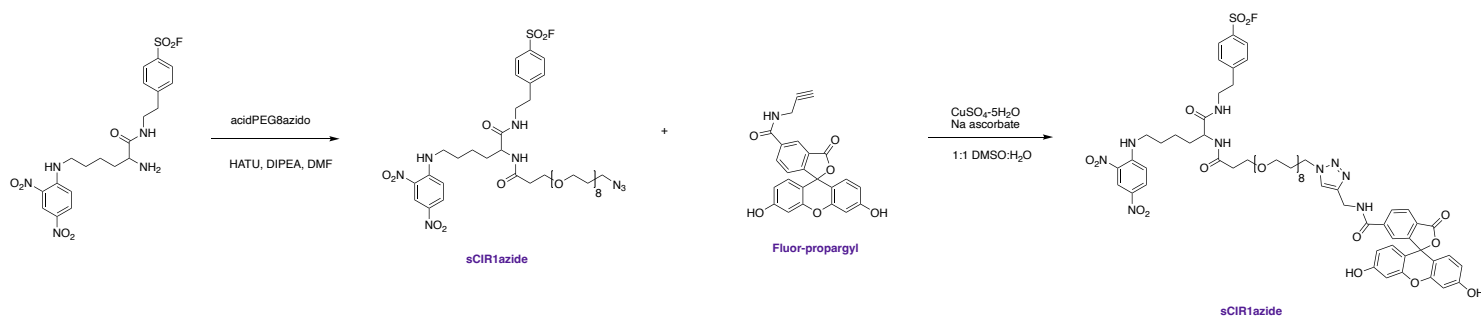
Compound **2E**. 4aminophenolSO₂F


 100 mg (0.916 mmol) of 4aminophenol was dissolved in 2 mL THF. 345 mg of AISF was added (1.09 mmol) along with 300 μL DBU (2.02 mmol). The reaction was stirred for 0.5 hrs then THF was removed. Crude material was purified through normal phase chromatography (DCM/MeOH). Total mass collected was 46.9 mg (26.7 %). ^1H NMR (700 MHz, CD_3SOCD_3) δ 8.82 (d, J = 8.82 Hz, 2H), δ 6.12 (d, J = 4.44 Hz, 2H). ^{19}F NMR (700 MHz, CD_3CN) 36.0 ppm.

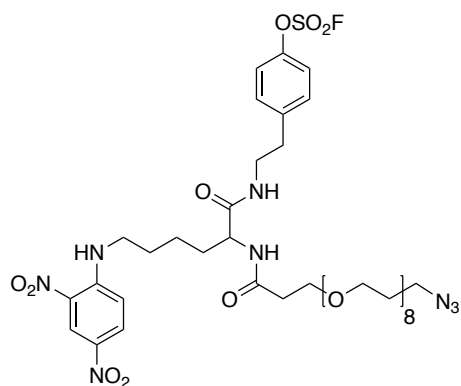




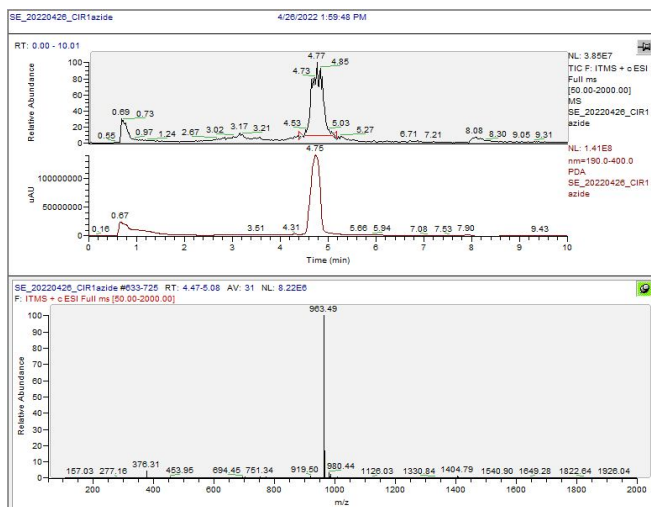
Scheme 3. General synthesis for sCIRfluor derivatives



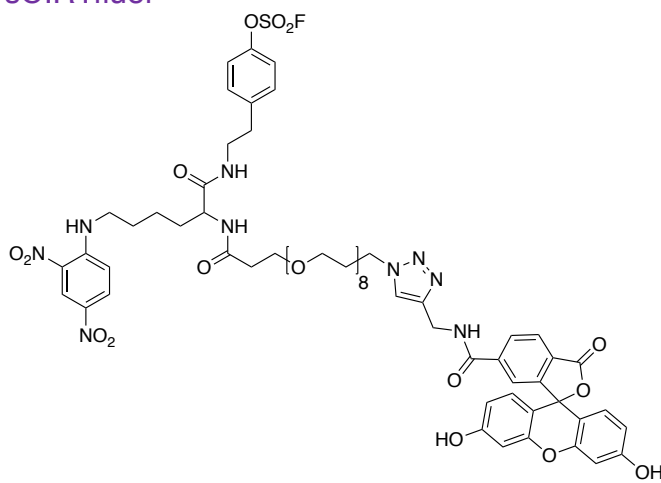
sCIR1azide



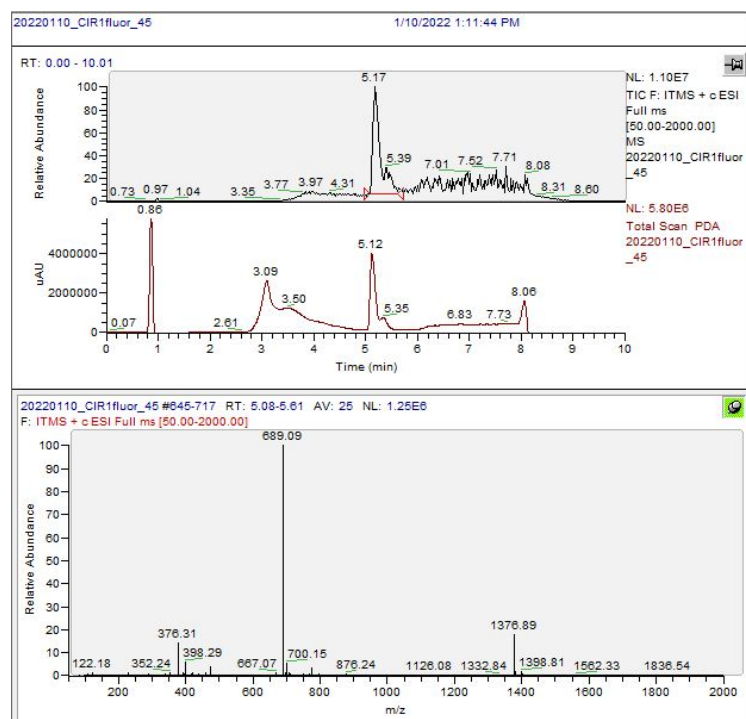
32.8 mg of acidpeg8azido (0.0702 mmol) was dissolved in 2 mL DMF with 33.4 mg of HATU (0.0878 mmol) and 24.5 μ L TEA (0.176 mmol). After a few minutes 30 mg of Compound **4A** (0.0585 mmol) was added to the reaction, and all reagents were stirred together overnight. DMF was removed by adding a small amount of H₂O and excess of EtOAc. After three washes with brine, the crude material was purified by reverse phase chromatography. 18.7 mg was collected, yielding 28% of the theoretical mass.



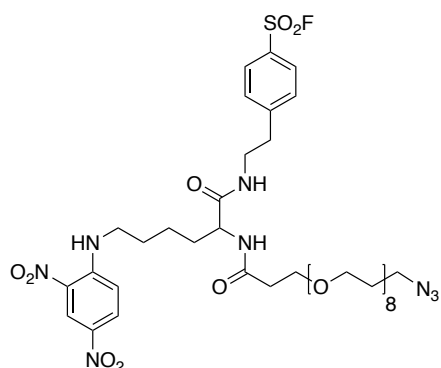
sCIR1fluor



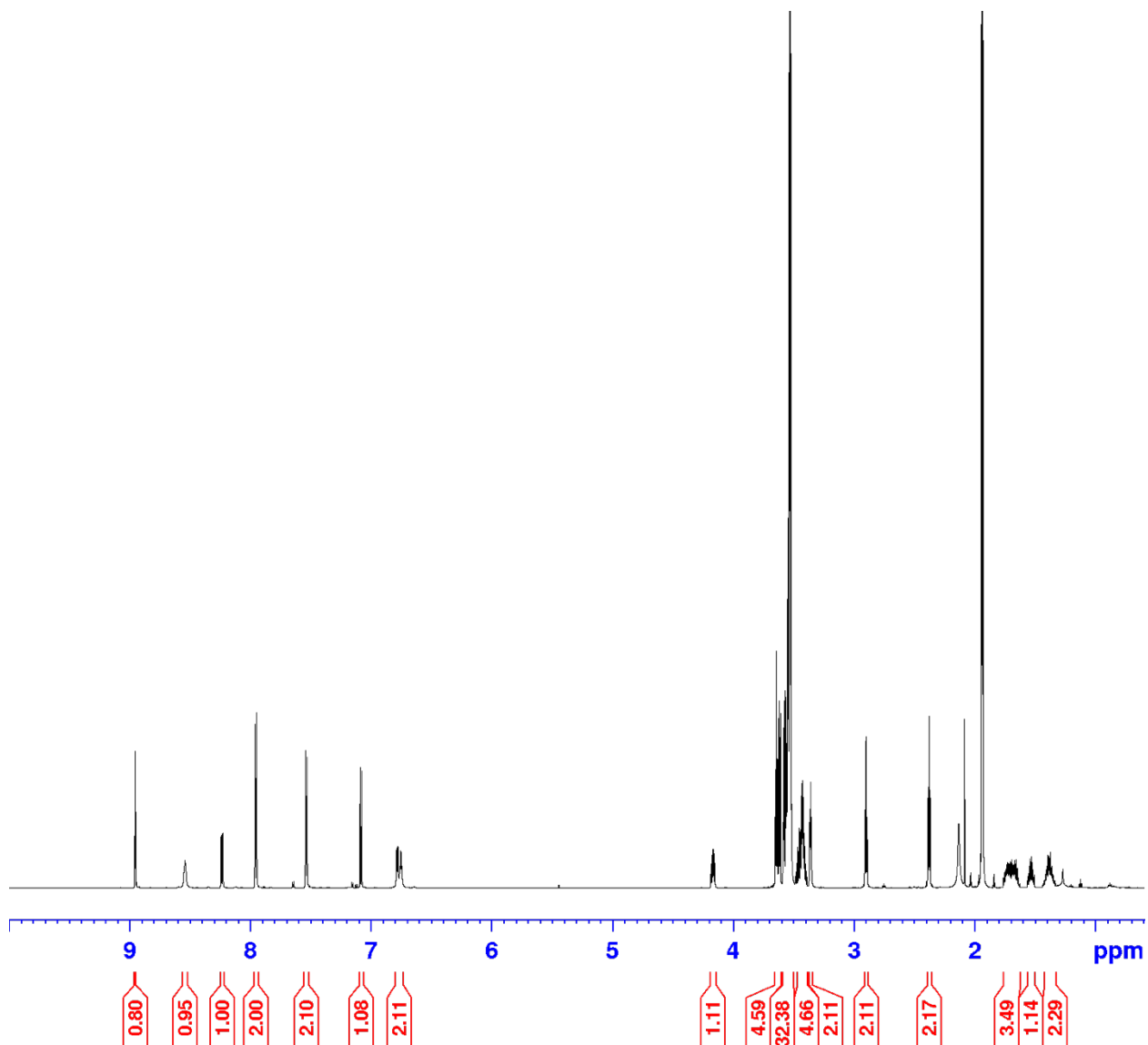
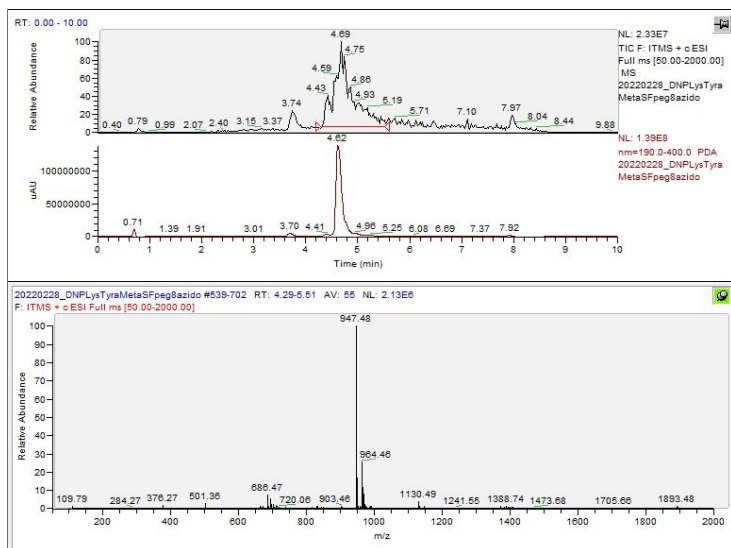
1 mL of DMSO was used to dissolve 21.9 mg of fluor-propargyl (0.053 mmol) and 5 mg CIR1-azide (0.053 mmol). After a few minutes 1 mL of H₂O with sodium ascorbate (0.106 μmol, 21 μg), copper sulfate (0.053 μmol, 13.2 μg), and THPTA (0.053 μmol, 23 μg) was added to the reaction. After stirring for 8 hours, the reaction was frozen at -80 for a few hours. The solvent was lyophilized, and the crude material was purified by reverse phase chromatography. 5.3 mg of product was collected (7.3%).

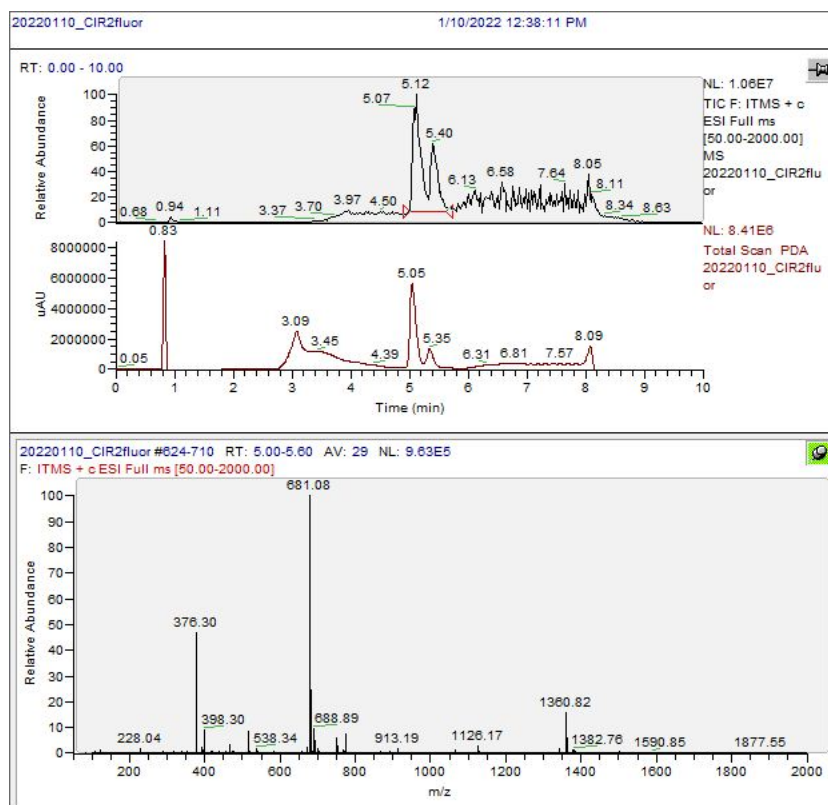


sCIR2azide

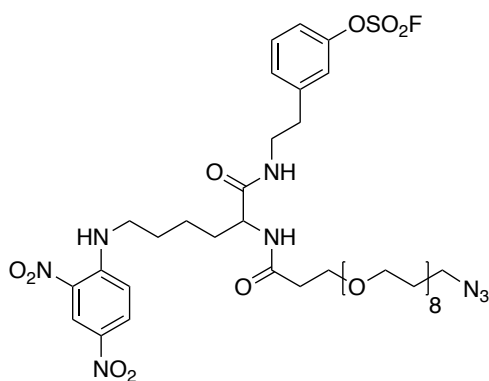


39.9 mg of azidopeg8acid (0.0777 mmol) was dissolved in 2 mL DMF. HATU (35.4 mg, 0.0932 mmol) and DIPEA (27 μ L, 0.1554 mmol) were added to this and the reaction was stirred for a few minutes at room temperature. 39.9 mg of Compound **4B** (0.080 mmol) was added before all reagents were stirred together for 16 hours. DMF was removed under vacuum and the crude material was re-dissolved in EtOAc. After three brine washes, the product was obtained through reverse phase chromatography. 2.3 mg of product was collected (3.1%). ^1H NMR (700 MHz, CD_3CN) δ 8.95 (d, J = 2.70 Hz, 1H), δ 8.54 (s, 1H), δ 8.23 (d, J = 1.84 Hz, 1H), δ 7.95 (d, J = 8.45 Hz, 2H), δ 7.53 (d, J = 8.29 Hz, 2H), δ 7.08 (d, J = 9.61 Hz, 1H), δ 6.74 – 6.78 (m, 2H), δ 4.15 – 4.18 (m, 1H), δ 3.61 – 3.64 (m, 4H), δ 3.50 – 3.59 (m, 32H), δ 3.38 – 3.47 (m, 4H), δ 3.35 (t, J = 4.94 Hz, 2H), δ 2.89 (t, J = 6.81 Hz, 2H), δ 2.37 (t, J = 6.04 Hz, 2H), δ 1.63 – 1.73 (m, 3H), δ 1.50 – 1.55 (m, 1H), δ 1.33 – 1.43 (m, 2H). ^{19}F NMR (700 MHz, CD_3CN) 64.9 ppm.

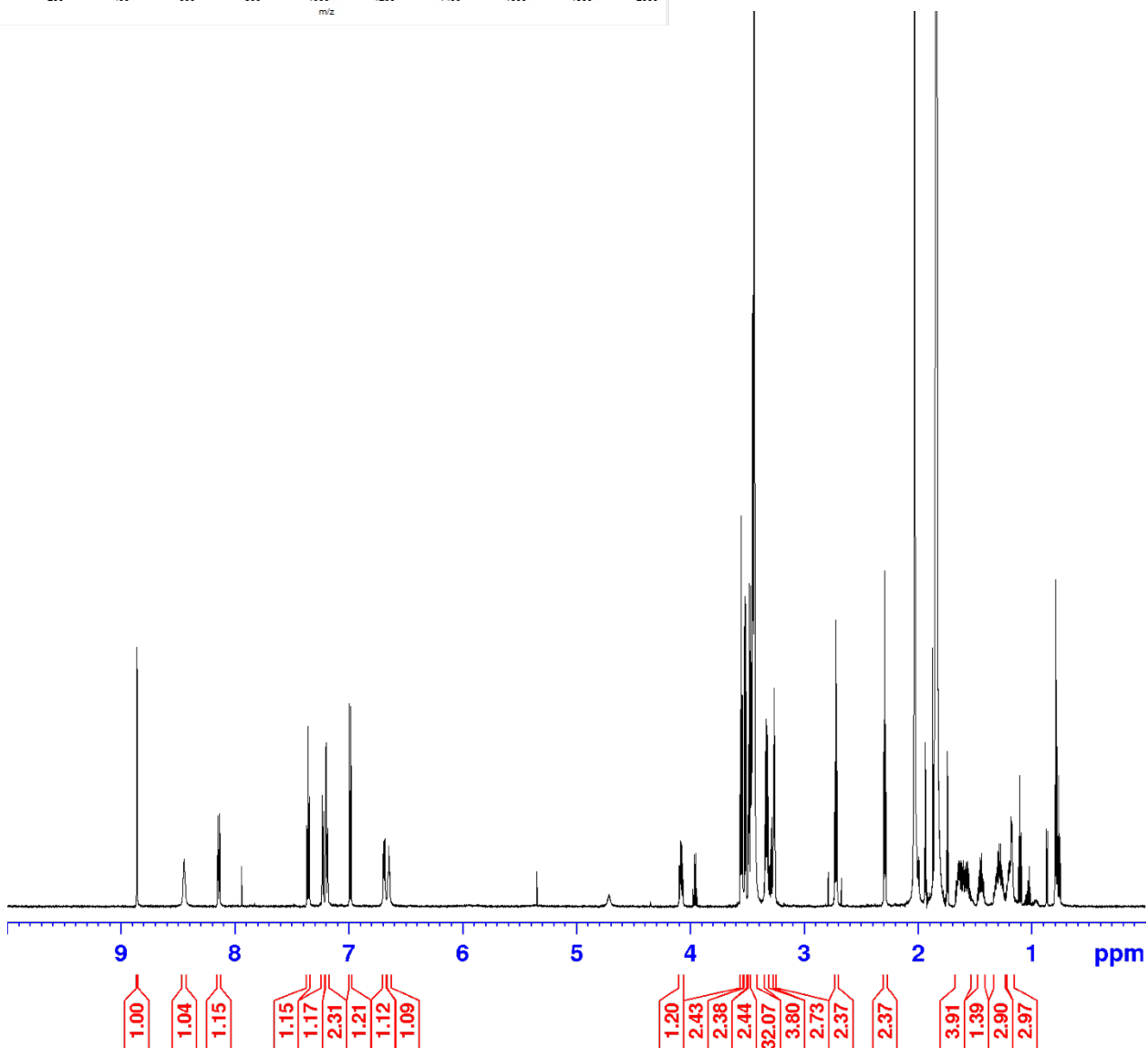
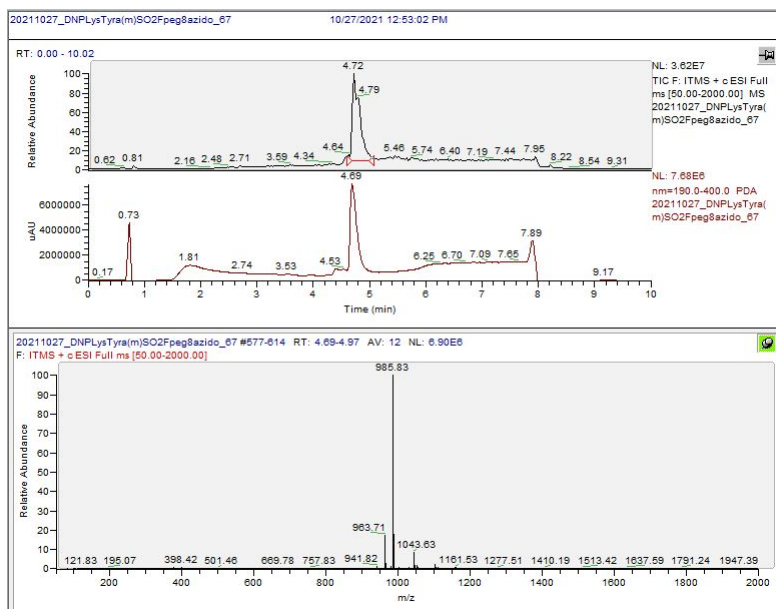


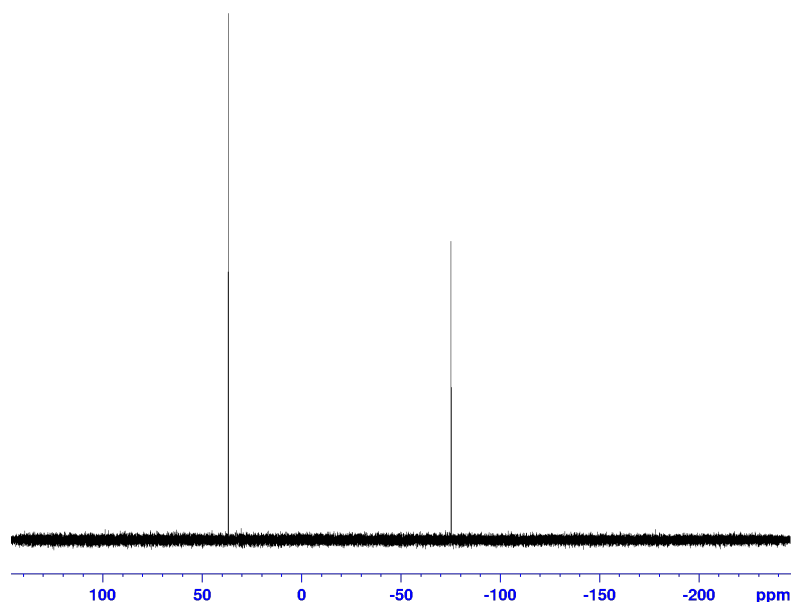


sCIR3azide

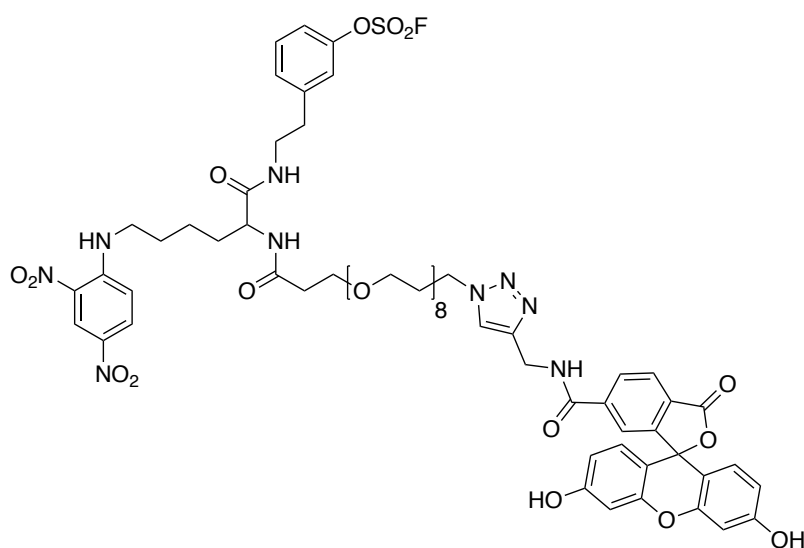


A solution of 13.6 mg azidopeg8acid (0.0292 mmol), 13.3 mg HATU (0.035 mmol), and 7.9 μ L TEA (0.0584 mmol) was made in 2.5 mL DMF. After a few minutes, 15 mg of Compound **4C** (0.0292 mmol) was added to the flask. After stirring overnight, DMF was removed under vacuum. By re-dissolving in EtOAc, washing with brine three times and purifying by reverse-phase chromatography, 3.4 mg (8.5%) was collected. ¹H NMR (700 MHz, CD₃CN) δ 8.86 (d, J = 2.70 Hz, 1H), δ 8.44 (s, 1H), δ 7.35 (t, J = 7.87 Hz, 1H), δ 7.18 – 7.23 (m, 3H), δ 6.89 (d, J = 9.60 Hz, 1H), δ 6.68 (d, J = 7.82 Hz, 1H), δ 6.64 (t, J = 5.79 Hz, 1H), δ 4.06 – 4.09 (m, 1H), δ 3.55 (t, J = 6.03 Hz, 2H), δ 3.52 (t, J = 3.32 Hz, 2H), δ 3.47 – 3.48 (m, 2H), δ 3.43 – 3.47 (m, 32H), δ 3.31 – 3.35 (m, 4H), δ 3.25 – 3.29 (m, 3H), δ 2.71 (t, J = 6.91 Hz, 2H), δ 2.29 (t, J = 6.03 Hz, 2H), δ 1.53 – 1.67 (m, 4H), δ 1.42 – 1.47 (m, 1H), δ 1.23 – 1.32 (m, 3H), δ 1.17 – 1.21 (m, 3H). ¹⁹F NMR (700 MHz, CD₃CN) 36.5 ppm.



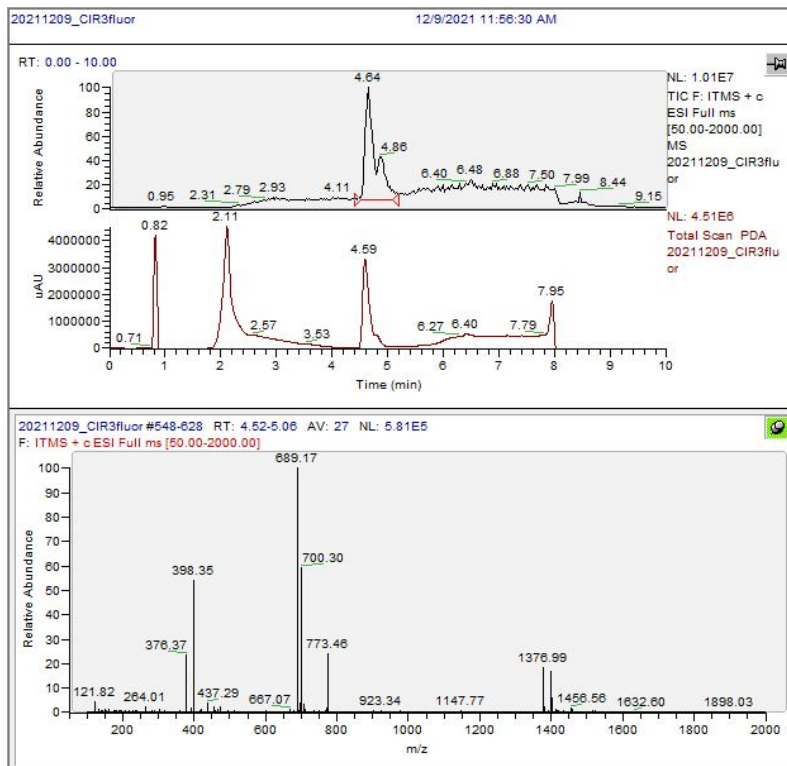


sCIR3fluor

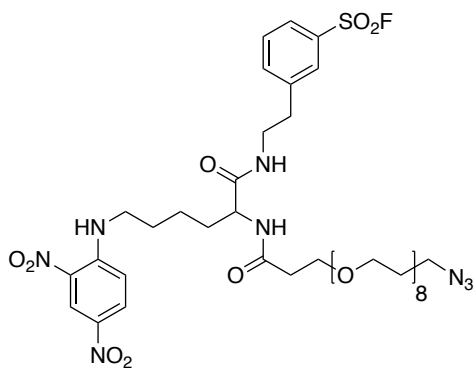


1 mL of DMSO was used to dissolve 9.0 mg of fluor-propargyl (0.0218 mmol) and 2.1 mg CIR3-azide (0.0218 mmol). After a few minutes 1 mL of H₂O with sodium ascorbate (0.0218 μ mol, 4.3 μ g), copper sulfate (0.0218 μ mol, 5.4 μ g), and THPTA (0.0436 μ mol, 18.9 μ g) was added to the reaction. After stirring overnight, the reaction was frozen at -80 for a few

hours. The solvent was lyophilized, and the crude material was purified by reverse phase chromatography. 4.8 mg of product was collected (16.3%).

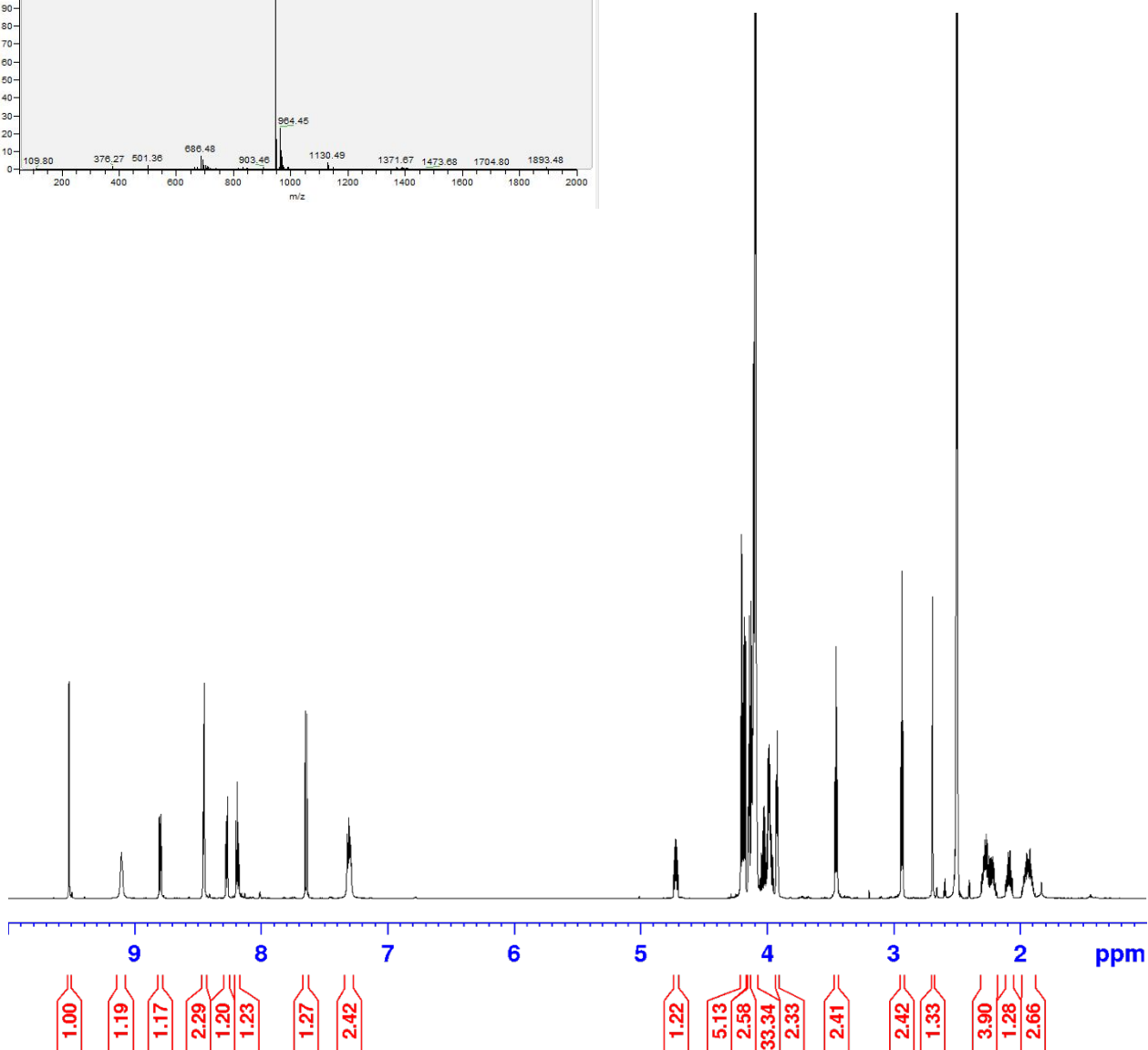
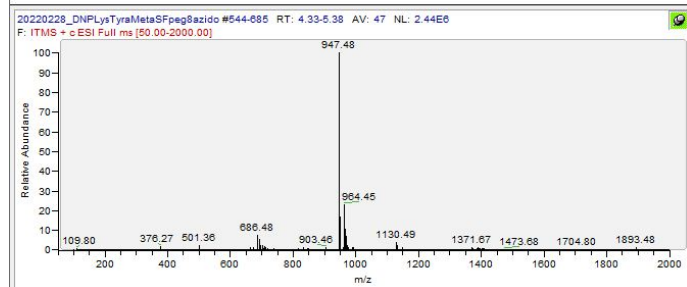
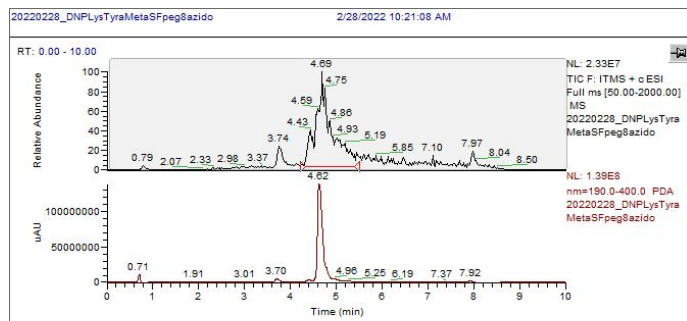


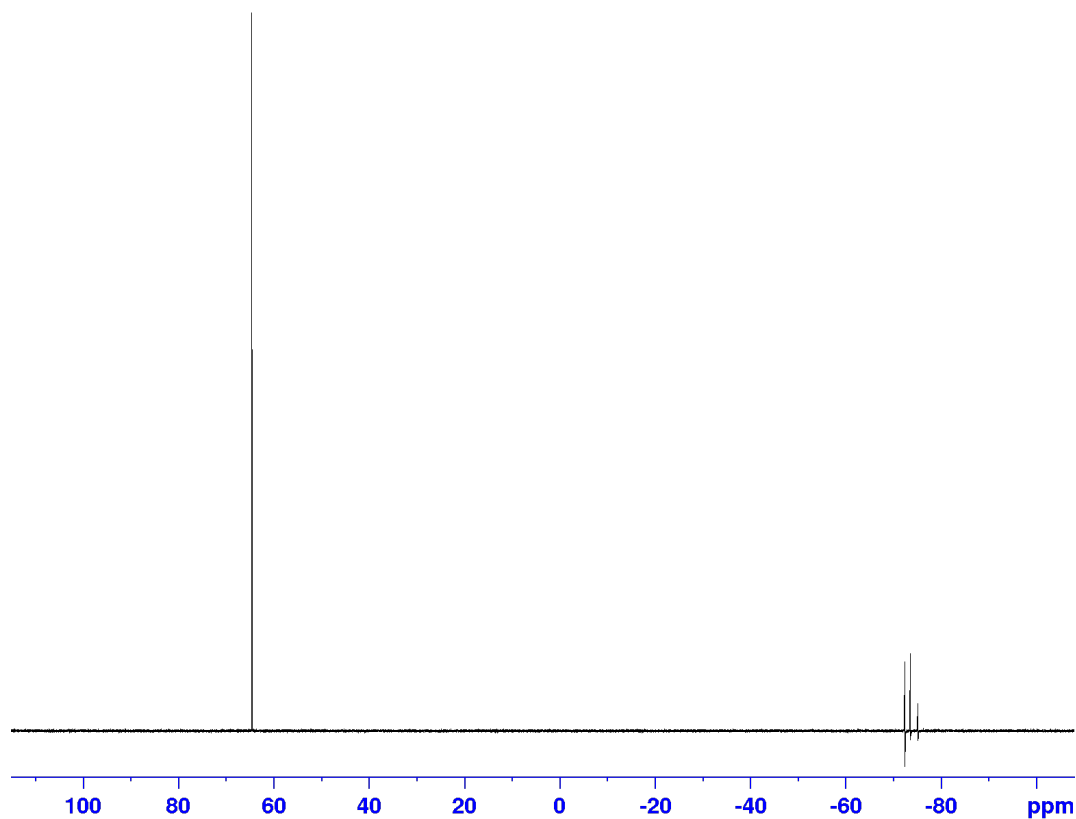
sCIR4azide



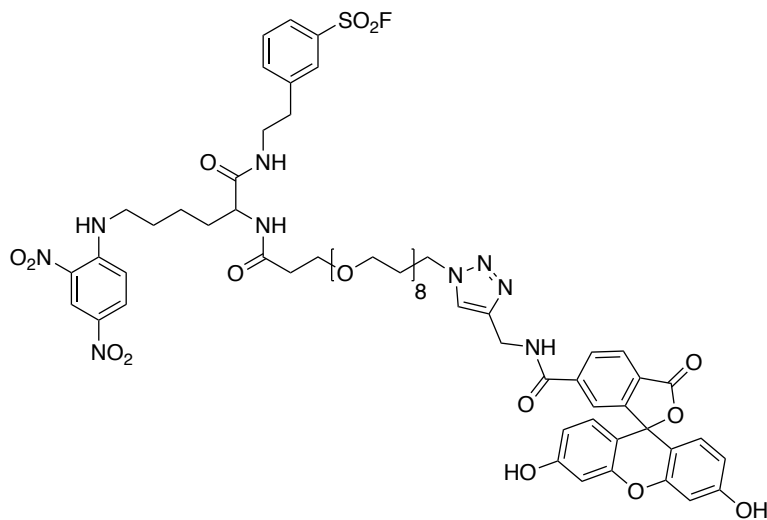
2 mL DMF was used to dissolve 24.9 mg (0.0535 mmol) azidoPEG8acid, 24.4 mg (0.0642 mmol) HATU, and 20 μ L (0.143 mmol) TEA. A few minutes later compound **4D** (26.6 mg, 0.0535 mmol) was added to the reaction before stirring over 18 hours. DMF was washed away by adding a few drops of water to the solution, with 3 mL of EtOAc. With three brine washes and reverse phase purification, 11.4 mg of product was collected (23.2%). ¹H NMR (700 MHz,

CD₃SO CD₃) δ 9.52 (d, J = 2.70 Hz, 1H), δ 9.10 (s, 1H), δ 8.79 (dd, J = 1.82 Hz, 1H), δ 8.45 (m, 2H), δ 8.27 (d, J = 7.74 Hz, 1H), δ 8.18 (t, J = 8.09 Hz, 1H), δ 7.64 (t, J = 9.59 Hz, 1H), δ 7.30 (t, J = 7.26 Hz, 2H), δ 4.72 (q, J = 4.34 Hz, 1H), δ 4.17 – 4.20 (m, 5H), δ 4.13 – 4.14 (m, 2H), δ 4.08 – 4.12 (m, 33H), δ 3.92 (t, J = 4.94 Hz, 2H), δ 3.45 (t, J = 6.77 Hz, 2H), δ 2.93 (t, J = 6.07 Hz, 2H), δ 2.69 (s, 1H), δ 2.20 – 2.29 (m, 4H), δ 2.05 – 2.11 (m, 1H), δ 1.89 – 1.98 m, 2H). ¹⁹F NMR (700 MHz, CD₃CN) 64.9 ppm.



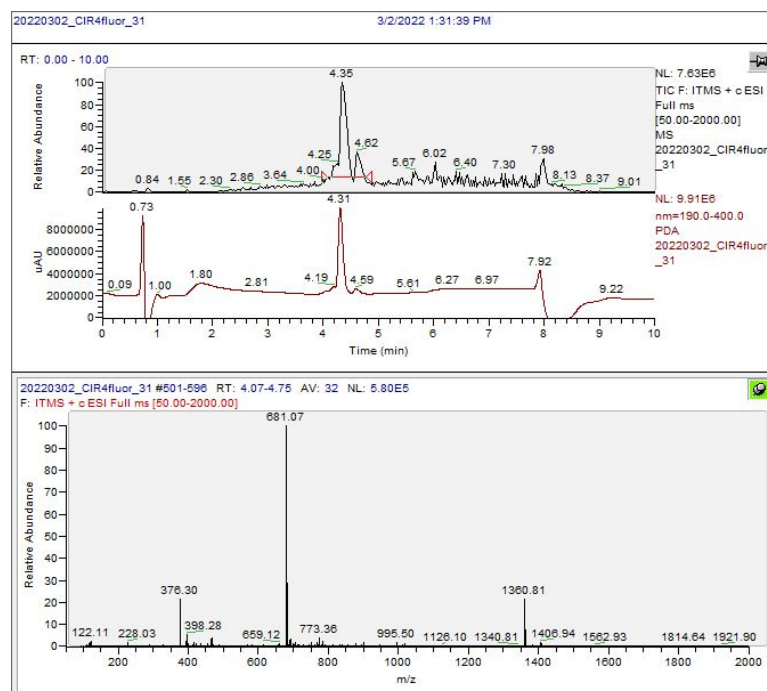


sCIR4fluor 90

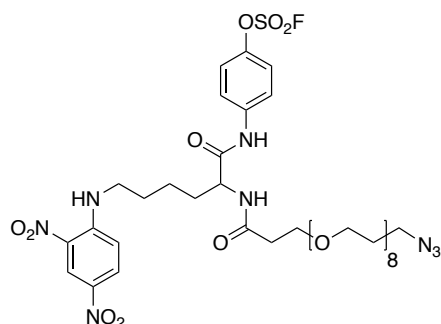


5.7 mg (0.0602 mmol) of CIR4azide and 2.5 mg (0.0602 mmol) of fluor-propargyl was dissolved in 1 mL DMSO and stirred together for a few minutes. Then a pre-mixed solution of 1 mL of H₂O with sodium ascorbate (0.120 μmol, 23.8 μg), copper sulfate (0.062 μmol, 15.4 μg) and THPTA (0.062 μmol, 26.9 μg). These reagents were stirred overnight

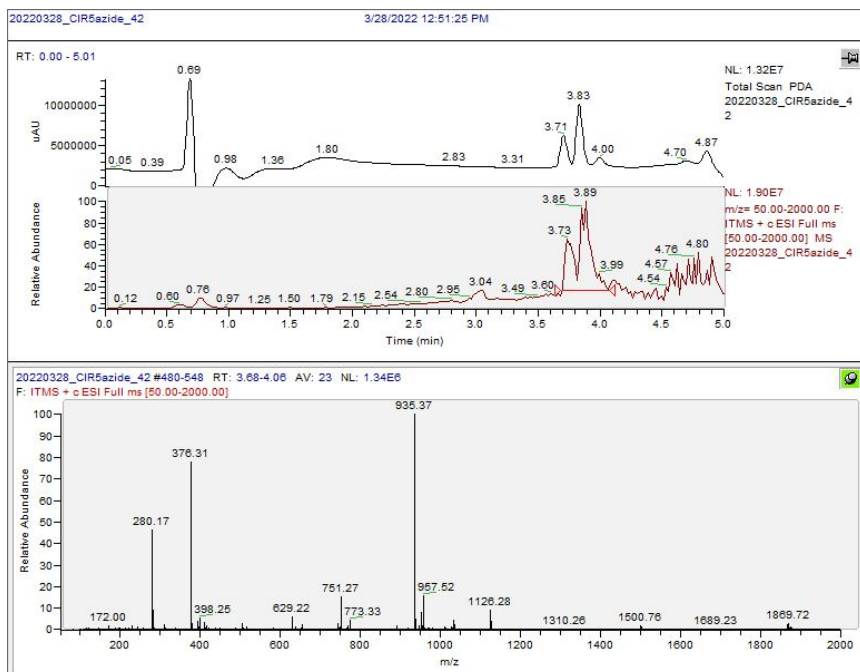
at room temperature, then placed in -80 C for at least 2 hours. The solvent was lyophilized, and the crude material was purified by reverse phase chromatography to yield 2.6 mg (3.2%).

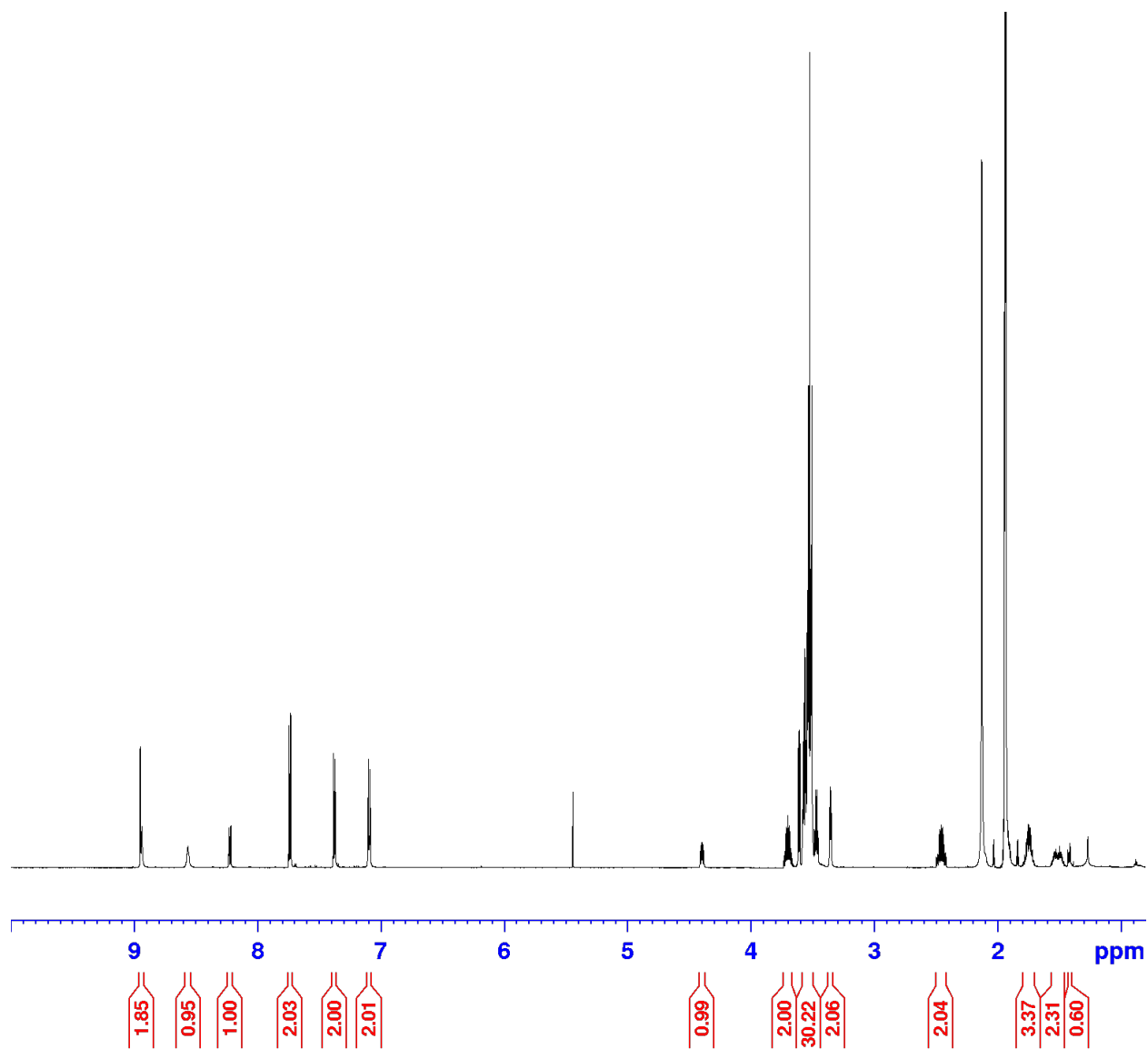


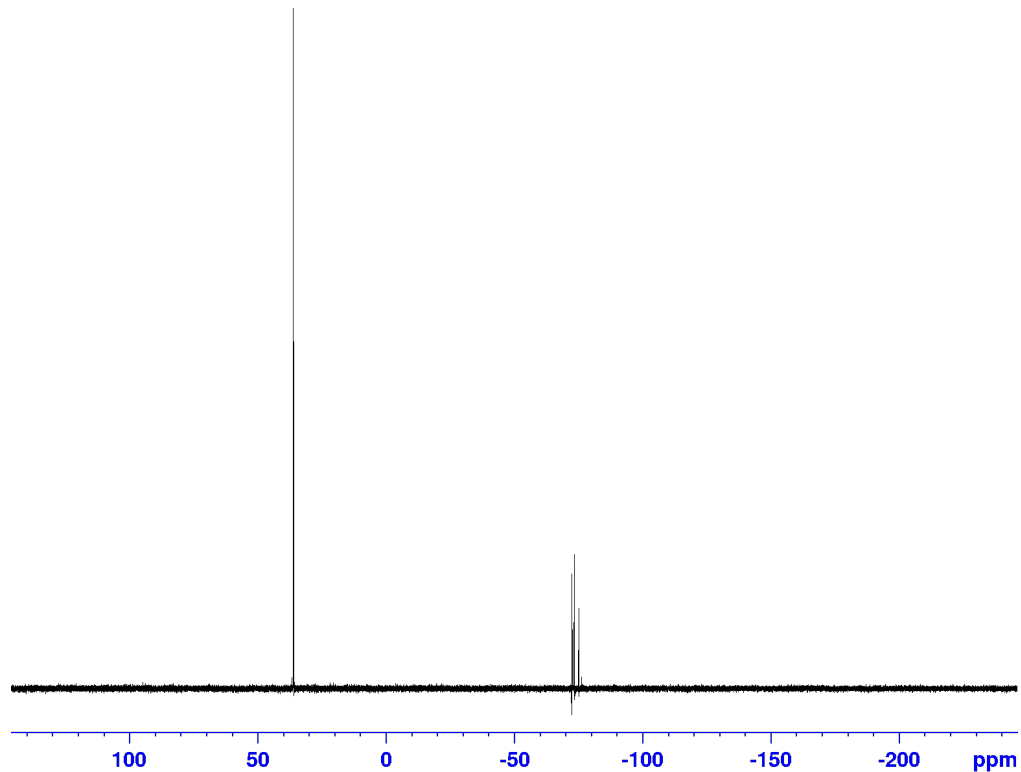
sCIR5azide



This compound was synthesized by combining 10.8 mg of (0.0103 mmol) acidpeg8azido, 4.7 mg (0.1236 mmol) HATU, and 2.87 μ L (0.206 mmol) TEA in 2 mL DMF. 5 mg (0.0103 mmol) of Compound 4E was added to the reaction a few minutes later and all reagents were stirred together overnight. DMF was removed by high pressure vacuum, and the crude material was re-dissolved in ethyl acetate. After washing three times with brine and purifying by normal phase chromatography (DCM/MeOH), 6.0 mg of product was collected (10.7%). ^1H NMR (700 MHz, $\text{CD}_3\text{SO CD}_3$) δ 8.94 (m, 2H), δ 8.56 (s, 1H), δ 8.23 (dd, $J = 1.84$, Hz, 1H), δ 7.74 (d, $J = 9.20$, Hz, 2H), δ 7.37 (d, $J = 9.09$, Hz, 2H), δ 7.09 (d, $J = 9.61$, Hz, 2H), δ 4.39 (m, 1H), δ 3.67 – 3.73 (m, 2H), δ 3.50 – 3.58 (m, 30H), δ 3.35 (t, $J = 4.94$ Hz, 2H), δ 2.41 – 2.49 (m, 2H), δ 1.70 – 1.80 (m, 3H), δ 1.46 – 1.56 (m, 2H), δ 1.40 – 1.42 (m, 1H). ^{19}F NMR (700 MHz, CD_3CN) 35.6 ppm.

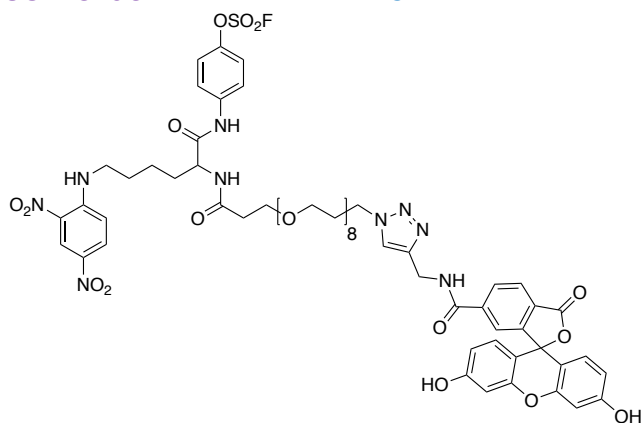






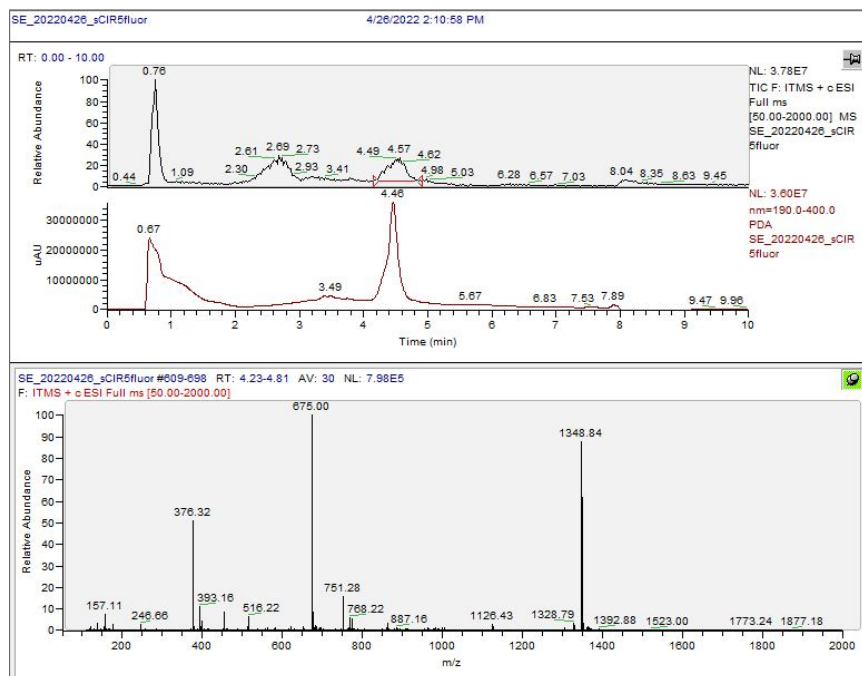
sCIR5fluor

8

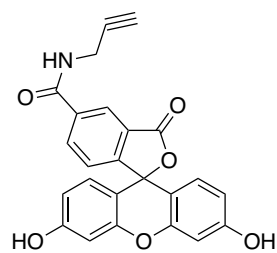


A solution of CIR5azide (6 mg, 0.064 mmol) and fluor-propargyl (2.6 mg, 0.064 mmol) in 1 mL DMSO was stirred at room temperature for a few minutes. 1 mL of H₂O with sodium ascorbate (0.128 μmol, 25.3 μg), copper sulfate (0.064 μmol, 16.0 μg), and THPTA (0.064 μmol, 27.8 μg) was added to the reaction. After stirring overnight, the reaction was frozen at -80 for a few hours. The solvent was

lyophilized, and the crude material was purified by reverse phase chromatography. 1.4 mg of product was collected (16.3%).

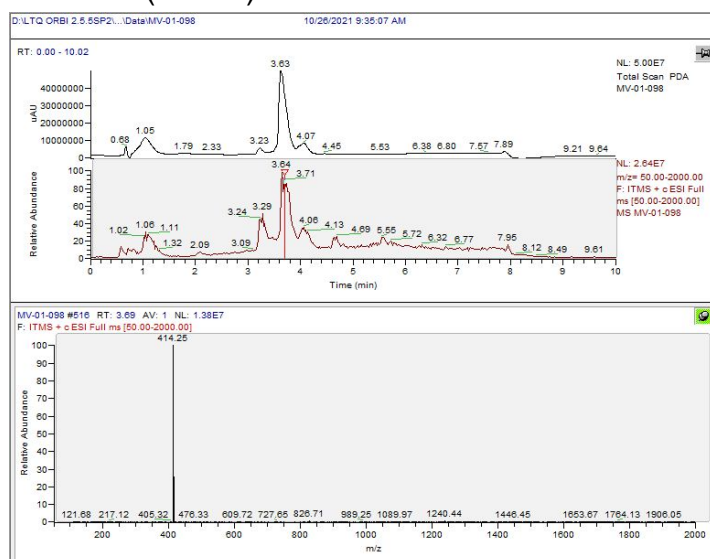


Fluor-propargyl (MV-098)

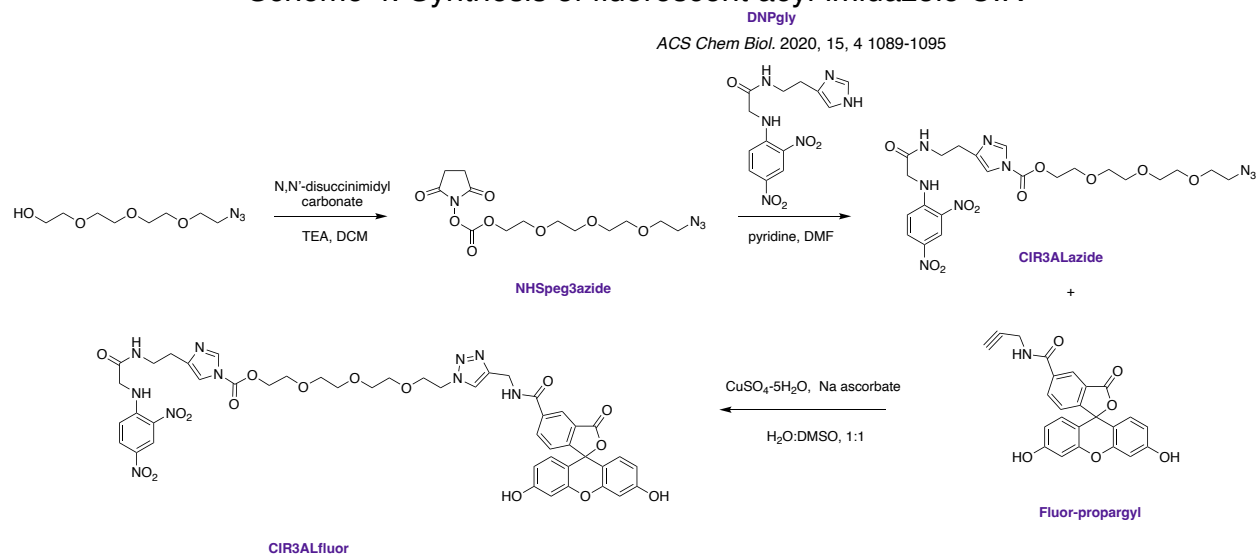


collected (75.7%).

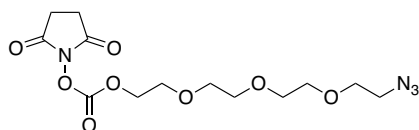
50 mg (0.106 mmol) of Fluorescein-NHS was dissolved in 5 mL DMF, along with propargyl-amine (14 μ L, 0.212 mmol) and sodium bicarbonate (11 mg, 0.127 mmol). The reaction was protected from light and stirred for at least 16 hours. Afterwards, the crude material was dried thoroughly under vacuum. The product was purified by normal phase chromatography (DCM/MeOH) and 33.3 mg was



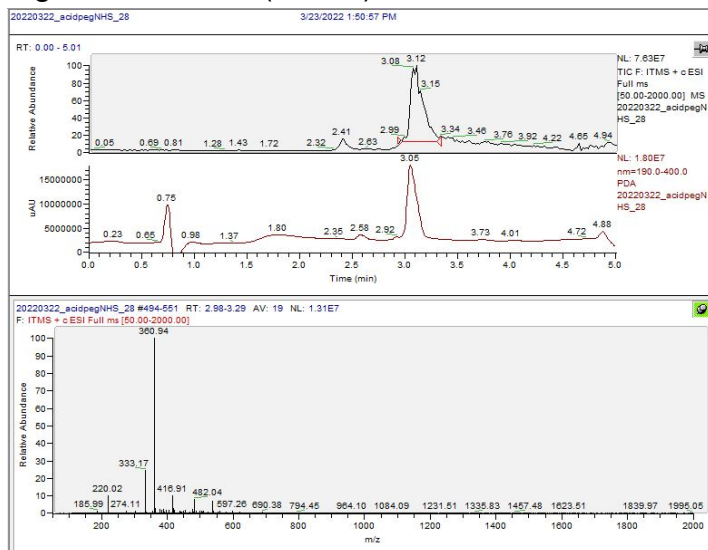
Scheme 4. Synthesis of fluorescent acyl-imidazole CIR



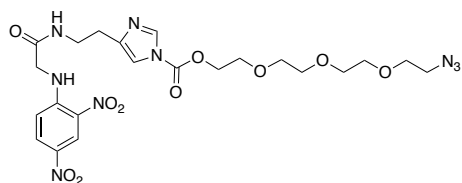
NHSpeg8azide



60.8 mg (0.2775 mmol) of azidepeg3hydroxyl was dissolved in 3 mL DCM along with 85.3 mg (0.333 mmol) of N,N'-disuccinimidyl carbonate, and 58 μ L TEA (0.4163 mmol). After stirring at room temperature overnight, DCM was removed under pressure and the crude material was re-dissolved in EtOAc. The organic layer was washed three times with brine and then purified by reverse phase. 28.2 mg was collected (28.2%).

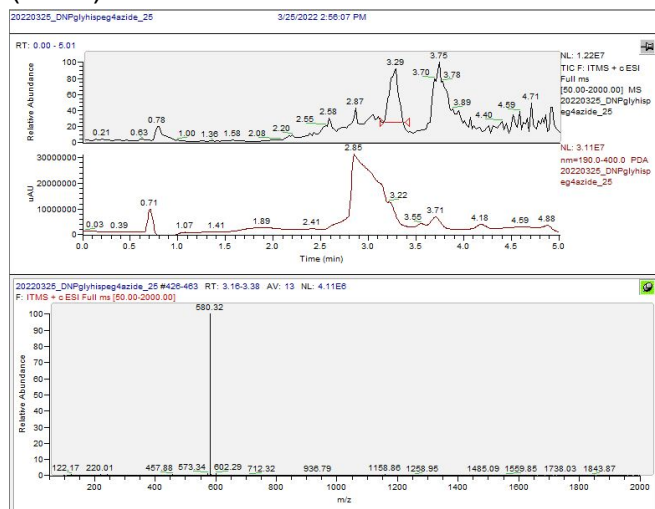


CIR3ALazide

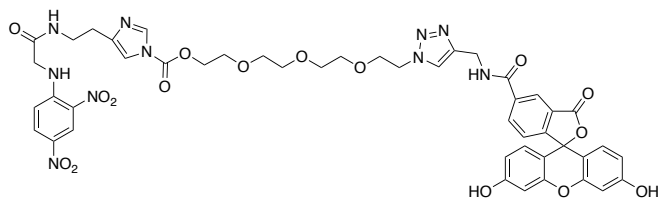


A solution was made with 31.3 mg (0.0936 mmol) of DNPgly, 28.2 mg of **NHSpieg8azide** (0.0783 mmol) and 19 μL of pyridine (0.235 mmol) in 2.5 mL DMF. The reaction was stirred overnight at room temperature and DMF was removed under pressure.

After normal phase purification, the product was dried *in vacuo* and 2.4 mg was collected (5.3%).

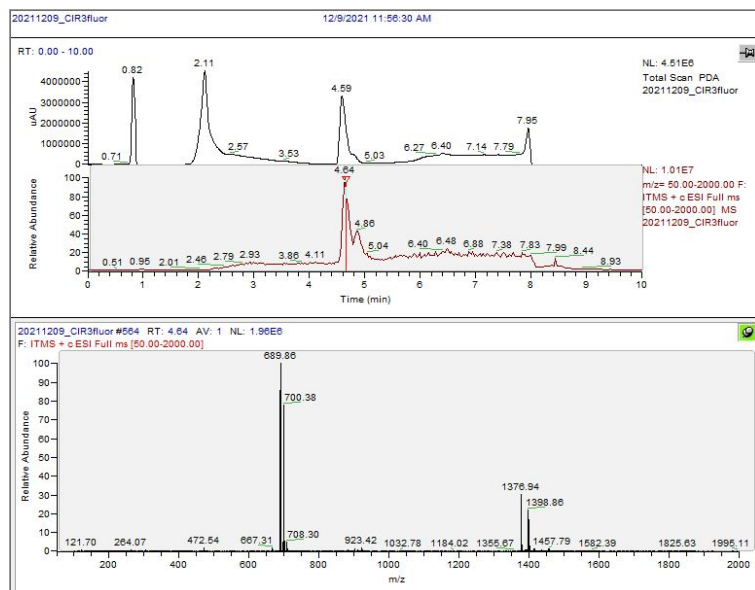


CIR3Afluor

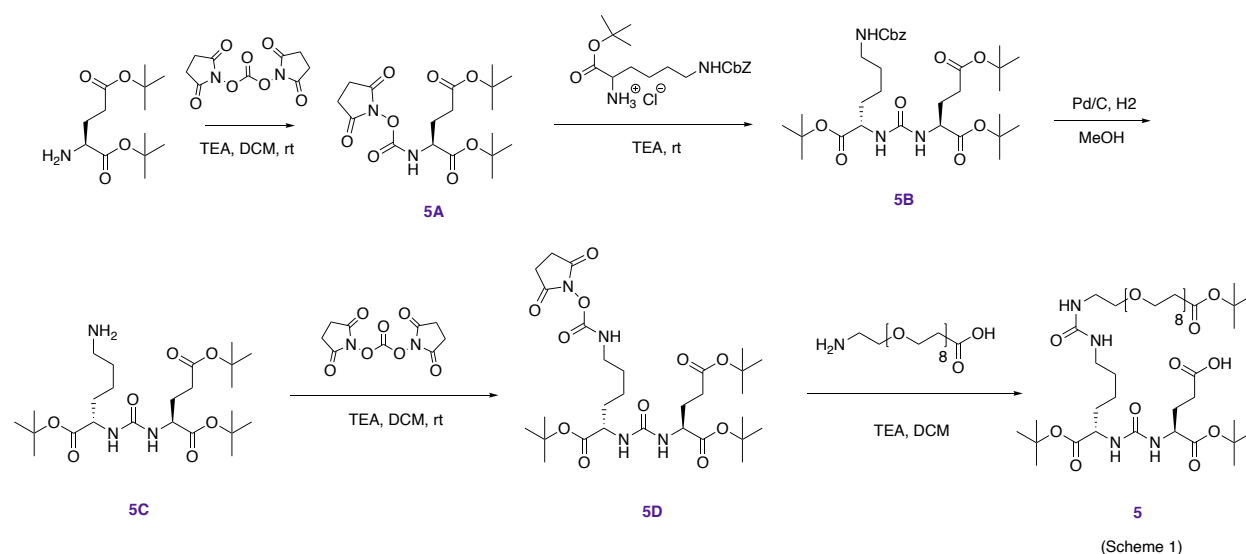


2.4 mg (0.0414 mmol) of CIR3fluor and 1.7 mg (0.0414 mmol) of fluor-propargyl was dissolved in 1 mL DMSO and stirred for a few minutes. A solution of sodium ascorbate (0.0828 μmol , 8.2 μg), copper

sulfate pentahydrate (0.0414 μmol , 10.3 μg) and tris-hydroxypropyltriazolymethylamine (0.0414 μmol , 17.9 μg) in 1 mL H_2O , which was then added to the reaction. The suspension was stirred for 4 hours and then put in -80 C for 2 hours. The solvent was lyophilized, and the crude material was purified by reverse phase chromatography. 2.9 mg of product was collected (70.7%).

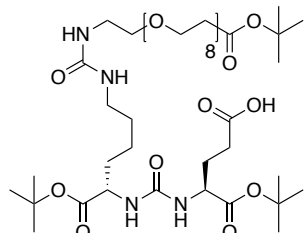


Scheme 5. Synthesis of glutamate derivatives

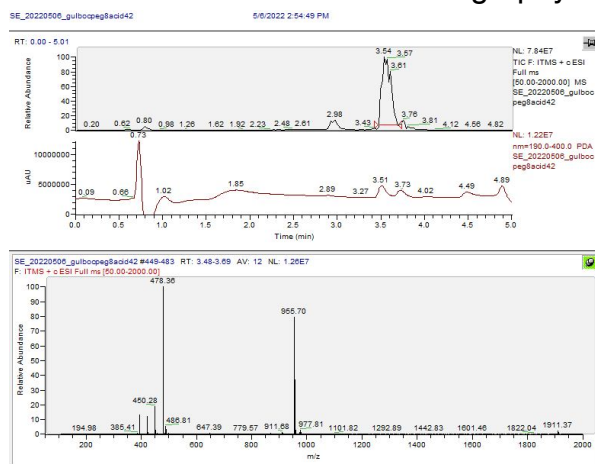


Compounds **5A** to **5D** were synthesized using the experimental methods of *ACS Chem Biol.* 2020, 15, 4 1089-1095

Compound 5. GUL(boc)peg8acid



41.8 mg (0.0665 mmol) of Compound 5D was dissolved in 3 mL DCM, along with 29.3 mg (0.0665 mmol) of aminopeg8acid and 18.5 μ L (0.133 mmol) TEA. This solution was stirred overnight at room temperature, and DCM was removed under pressure. The crude material was purified through reverse phase chromatography. 25.6 mg of product was collected (40.3%).



8.2 Hydrolytic Stability

2-6 mg of each sCIR was dissolved in 0.5-1 mL of 90% PBS/10% D₂O. The sample was analyzed on a Burker 700 MHz spectrometer, collecting fluorine NMR 0-120 hrs after sample preparation. Sulfonyl fluoride (SO₂F) and aqueous fluorine (KF) peaks were integrated and normalized based on trifluoetic acid (TFA) peak set to 1.

Table 5. Preparation of sCIRs for hydrolytic stability studies.

	Preparation	Final concentration (mg/mL)
sCIR1	4.1 mg of sCIR1 was dissolved in 0.75 mL 90% PBS/10% D ₂ O	5.47
sCIR2	2.27 mg of sCIR2 was dissolved in 0.6 mL 90% PBS/10% D ₂ O	3.78
sCIR3	2.3 mg of sCIR3 was dissolved in 0.6 mL 90% PBS/10% D ₂ O	3.83

sCIR4	2.6 mg of sCIR4 was dissolved in 0.6 mL 90% PBS/10% D ₂ O	4.33
sCIR5	6.1 mg of sCIR5 was dissolved in 1 mL 90% PBS/10% D ₂ O	6.1

Table 6. Integration of Fluorine Peaks for sCIR1 stability.

Time (hrs)	Integration of SO ₂ F peak	Integration of Aq. F peak
0	0.4194	0.0581
2	0.4992	0.0539
4	0.5253	0.0839
8	0.4699	0.0546
24	0.4013	0.0725
32	0.4041	0.0841
48	0.3913	0.0745
56	0.4807	0.0743
72	0.4156	0.0763
80	0.4606	0.078
96	0.4659	0.0633
120	0.2926	0.0465
144	0.4967	0.0791
168	0.4429	0.0711
192	0.5065	0.0885
216	0.4909	0.1134
240	0.4629	0.0989

Table 7. Integration of Fluorine Peaks for sCIR2 stability.

Time (hrs)	Integration of SO ₂ F peak	Integration of Aq. F peak
0	0.1396	0.0288
2	0.1376	0.0278
4	0.1227	0.0371
8	0.1282	0.03
24	0.1402	0.0762
32	0.1063	0.0569
48	0.0918	0.096
56	0.0881	0.0942
72	0.083	0.0895
80	0.0823	0.1329
96	0.0628	0.1536
120	0.0669	0.1528

144	0.0628	0.1881
168	0.0652	0.1949
192	0.0665	0.2208

Table 8. Integration of Fluorine Peaks for sCIR3 stability.

Time (hrs)	Integration of SO ₂ F peak	Integration of Aq. F peak
0	0.0561	0.0082
2	0.0648	0.0105
4	0.066	0.0073
8	0.0576	0.0086
24	0.0689	0.009
32	0.0653	0.0078
48	0.0718	0.0111
56	0.0698	0.0091
72	0.0703	0.0108
80	0.0668	0.0141
96	0.069	0.0113
120	0.075	0.0114
144	0.0763	0.012
168	0.0745	0.0121
192	0.0785	0.0133

Table 9. Integration of Fluorine Peaks for sCIR4 stability.

Time (hrs)	Integration of SO ₂ F peak	Integration of Aq. F peak
0	0.0103	-
0.5	0.0101	-
1	0.0113	-
2	0.0123	-
4	0.0099	-
8	0.0145	-
24	0.0109	0.0068
32	0.0095	0.005
48	0.0093	0.008
56	0.009	0.0085
72	0.0085	0.0113
80	0.0116	0.0152
96	0.01	0.0168
120	0.009	0.0252

Table 10. Integration of Fluorine Peaks for sCIR5 stability.

Time (hrs)	Integration of SO ₂ F peak	Integration of Aq. F peak
0	0.0138	0.0017
0.5	0.0128	0.0008
1	0.0133	0.0007
2	0.0139	0.0015
4	0.0157	0.0019
8	0.0153	0.0033
24	0.0145	0.0016
32	0.0164	0.0012
50	0.0162	0.001
56	0.0167	0.0015
72	0.0163	0.0013

8.2 Mass Spectrometry

The monoclonal antiDNP used for PTM analysis was synthesized by the Miller lab at the McMaster Immunology Center. Using a 9.55 μ M antibody stock (in PBS), two samples were prepared and sent to Bioinformatics Solutions Inc. (Waterloo ON) where proteomic analysis occurred. The first sample prepared by incubating equal volumes of 2 μ M antiDNP with 4 μ M of sCIR4fluor for 24 hours. The second sample contained equal volumes of 2 μ M antiDNP with 4 μ M sCIR5fluor incubated for 96 hours. Both samples contained approximately 220 μ g of the monoclonal antibody. Both samples were diluted with PBS, frozen quickly in an isopropanol bath and stored at -80 C before shipping.

The first step of PTM analysis involved reducing a portion of each conjugated sample with PNGase F to remove glycans. 1 unit of PNGase F was used per microgram of protein. After reduction, intact protein samples were dried down and resuspended in 0.1% formic acid for LC-MS analysis. Non-reduced samples were also analyzed by LC-MS in 0.1% formic acid.

To determine the site of modification, a bottom-up MS approach was used. This involved digesting both samples with pepsin (pH 2.3) and trypsin (7.6) at a 20:1 ratio of protein to enzyme. Pepsin digestion was incubated at 37C for 1 hour; trypsin digestion was incubated at 37C overnight. Samples were then dried down and cleaned with C18 tips. Cleaned samples were dried again and resuspended in 0.1% formic acid before performing LC-

MS/MS analysis. Tandem mass spectra of peptide conjugate were manually inspected and mapped to known antibody sequence to confirm site of conjugation.

8.2.1 Sample calculations

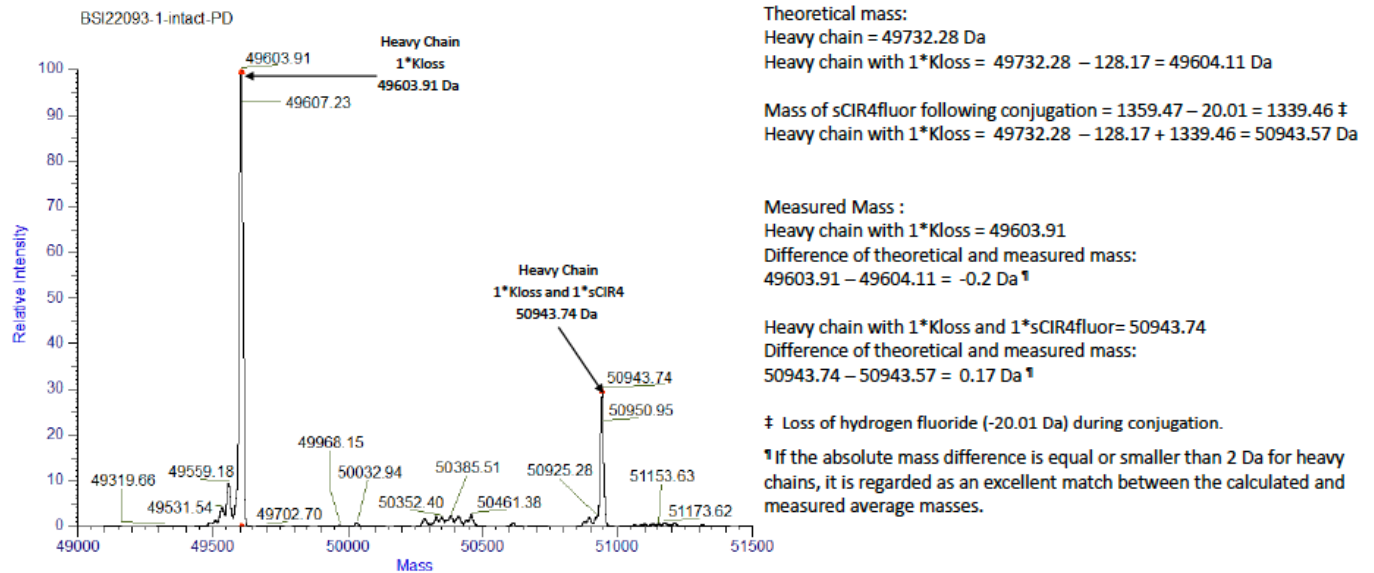


Figure 47. LC-MS analysis and sample calculations for the heavy chain of sCIR4fluor sample after reduction.

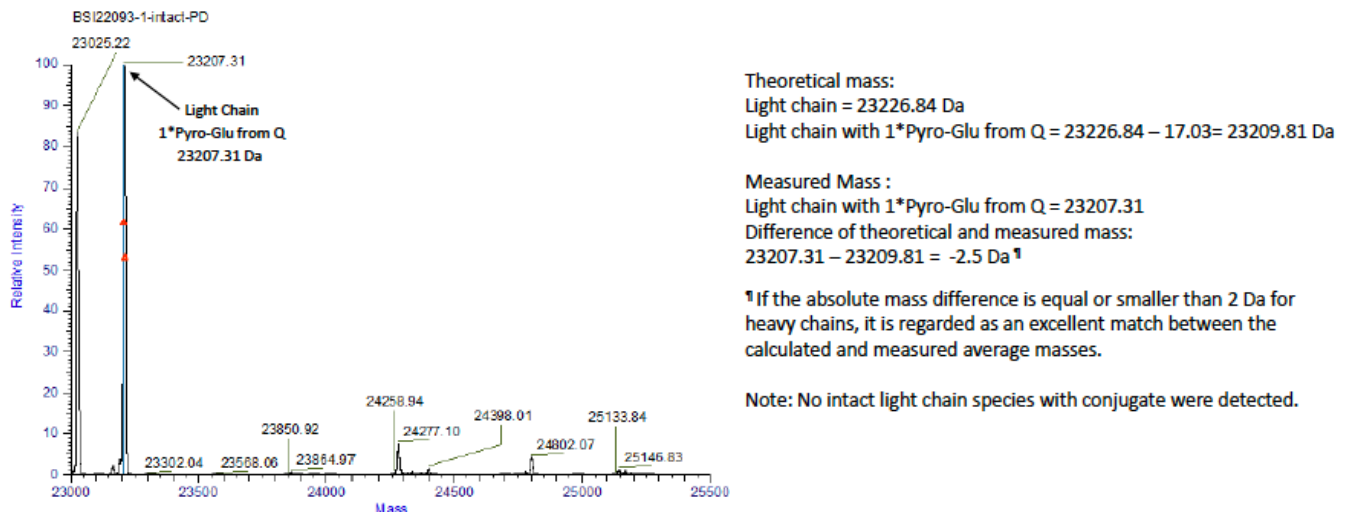
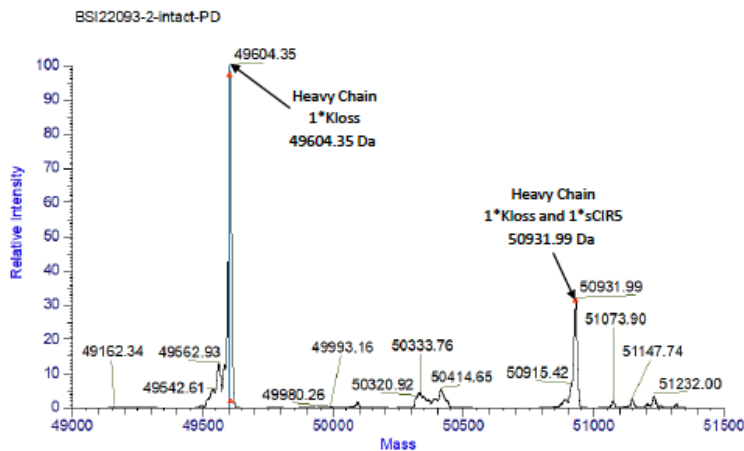


Figure 48. LC-MS analysis and sample calculations for the light chain of sCIR4fluor sample after reduction.



Theoretical mass:

Heavy chain = 49732.28 Da

Heavy chain with 1*Kloss = $49732.28 - 128.17 = 49604.11$ Da

Mass of sCIR5fluor following conjugation = $1347.43 - 20.01 = 1327.42$ Da

Heavy chain with 1*Kloss = $49732.28 - 128.17 + 1327.42 = 50931.53$ Da

Measured Mass :

Heavy chain with 1*Kloss = 49604.35

Difference of theoretical and measured mass:

$49604.35 - 49604.11 = -0.24$ Da ¶

Heavy chain with 1*Kloss and 1*sCIR5fluor = 50931.99

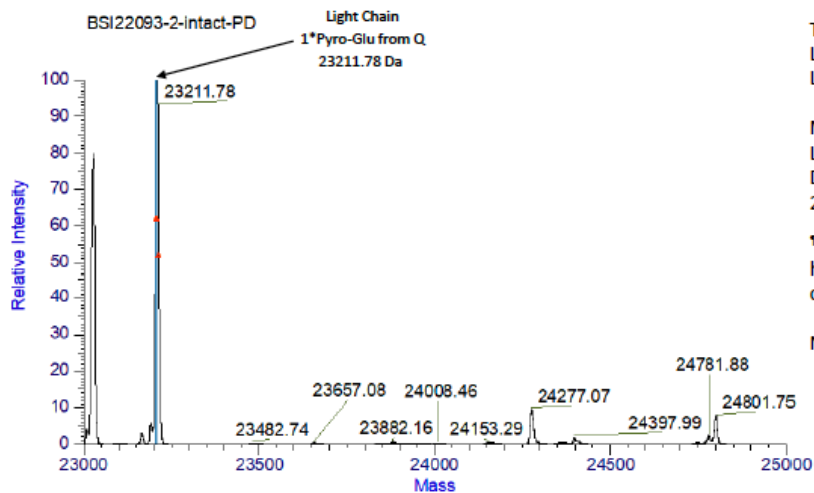
Difference of theoretical and measured mass:

$50931.99 - 50931.53 = 0.46$ Da ¶

¶ Loss of hydrogen fluoride (-20.01 Da) during conjugation.

¶ If the absolute mass difference is equal or smaller than 2 Da for heavy chains, it is regarded as an excellent match between the calculated and measured average masses.

Figure 49. LC-MS analysis and sample calculations for the heavy chain of sCIR5fluor sample after reduction.



Theoretical mass:

Light chain = 23226.84 Da

Light chain with 1*Pyro-Glu from Q = $23226.84 - 17.03 = 23209.81$ Da

Measured Mass :

Light chain with 1*Pyro-Glu from Q = 23211.78

Difference of theoretical and measured mass:

$23211.78 - 23209.81 = 1.97$ Da ¶

¶ If the absolute mass difference is equal or smaller than 2 Da for heavy chains, it is regarded as an excellent match between the calculated and measured average masses.

Note: No intact light chain species with conjugate were detected.

Figure 50. LC-MS analysis and sample calculations for the light chain of sCIR5fluor sample after reduction.

8.3 SDS-PAGE

1 mg of SPE7 C-LAP (1.87 mg/mL) was provided to the Rullo lab by Cyril Barinka's lab at the Institute of Biotechnology of the Czech Academy of Sciences.

Buffer exchange

350 μ L of 1.86 mg/mL SPE7 C-LAP (Buffer: 100 mM Tris, 150 mM NaCl, 5 mM biotin, 5% glycerol) was dialyzed using a Thermo Scientific™ Slide-A-Lyzer™ Dialysis Cassette. The buffer was exchanged with 10 mM HEPES (pH 8) per manufacturer instructions. The next day the samples were removed from the cassette and concentration was determined by measuring absorbance at 280 nm (Thermo Scientific™ NanoDrop™ One Microvolume UV-Vis Spectrophotometers).

SDS-PAGE

An isotype control (human IgG) was from Jackson ImmunoResearch Labs (#009-000-003) prepared at 76 μ M. sCIRs were prepared from DMSO stocks, whose concentration was determined with a standard curve to DNP-gly. 15 μ L of 2 μ M sCIR was incubated with 15 μ L of 4 μ M SPE7 C-LAP or isotype for 0, 1, 2, 4, 8, and 24 hours. Samples were subjected to flash-freezing, before storing at -80 C. On the day of the gel, samples were thawed and 30 μ L of 2X Laemmli buffer was added to each. After two minutes of heating at 95 degrees, 20 μ L of sample was loaded on a Novex™ WedgeWell™ 10-14% Tris-Glycine Gel with 10 μ L of Bio-Rad Precision Plus Protein Unstained Standard (Catalog #161-0363). Gels were run in an Invitrogen mini gel tank at 95V for 15 minutes to ensure stacking. For 30-40 minutes gels were run at 120V until the dye front reached the bottom of the gel. Gels were visualized by a fluorescent laser (Cy-2) at 460V on the GE Typhoon

and densitometric analysis was conducted through ImageJ. Bio-Rad QuickStart™ Bradford 1x dye reagent was used to stain the gels overnight. Protein bands were visualized using Odyssey DLx imaging system.

8.3.1 Intramolecular rate constants

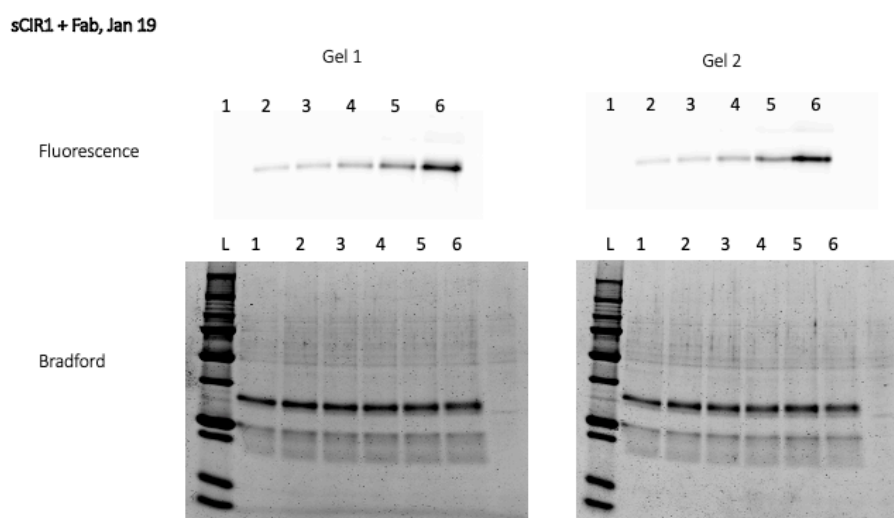


Figure 51. Fluorescent and protein bands of SPE7 Fab incubated with sCIR1. For both gel 1 and 2, L represents the protein ladder and lanes 1 through 6 are sCIR-Fab samples incubated for 0, 1, 2, 4, 8 and 24 hours.

Time (h)	RFU	
0	301.463	421.773
1	1822.675	1849.373
2	2616.388	2505.356
4	4567.906	4590.941
8	8493.333	9636.397
24	19193.516	20787.232

Table 11. Relative fluorescence units of sCIR1fluor samples incubated with SPE7 Fab over 24 hours.

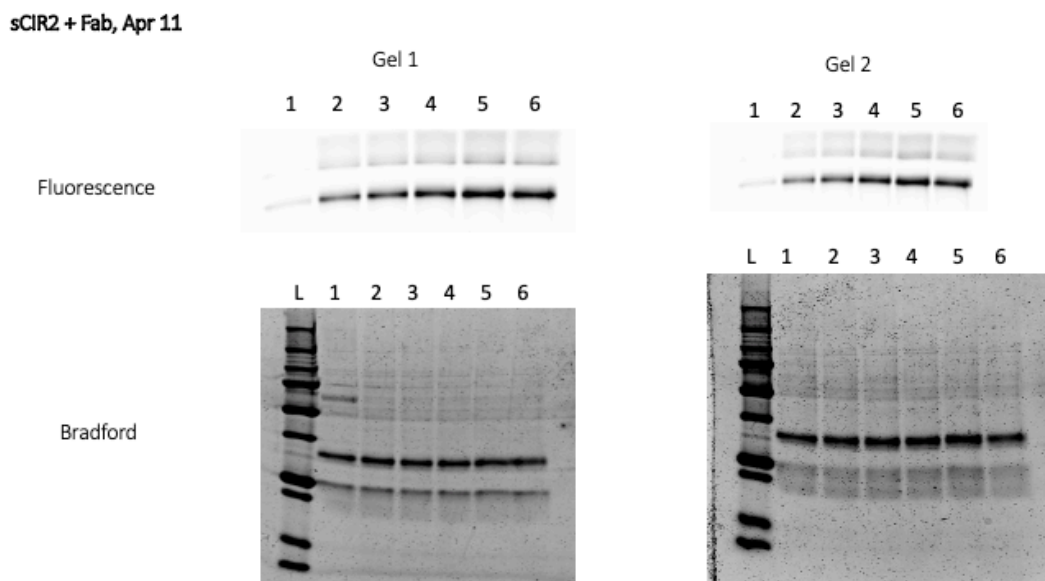


Figure 52. Fluorescent and protein bands of SPE7 Fab incubated with sCIR2. For both gel 1 and 2, L represents the protein ladder and lanes 1 through 6 are sCIR-Fab samples incubated for 0, 1, 2, 4, 8 and 24 hours.

Time (h)	RFU	
0	793.125	1141.088
1	5805.445	6973.725
2	7792.374	10144.9
4	10296.877	13568.889
8	14198.879	18006.349
24	12910.622	15209.46

Table 12. Relative fluorescent units of sCIR2 samples incubated with SPE7 Fab over 24 hours.

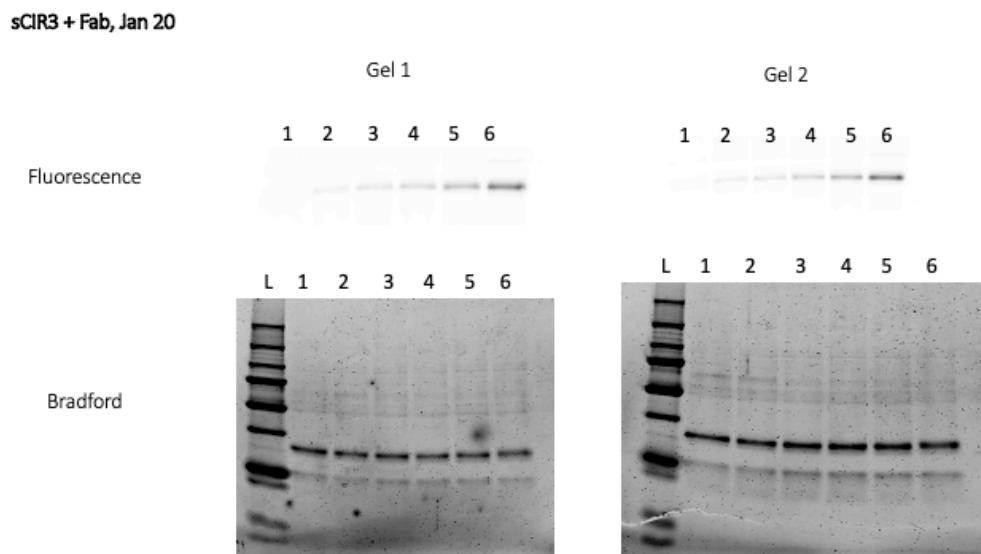


Figure 53. Fluorescent and protein bands of SPE7 Fab incubated with sCIR3. For both gel 1 and 2, L represents the protein ladder and lanes 1 through 6 are sCIR-Fab samples incubated for 0, 1, 2, 4, 8 and 24 hours.

Time (h)	RFU	
0	0	0
1	1239.639	1292.451
2	2121.233	2183.539
4	3891.434	3349.308
8	6584.998	6142.096
24	13682.571	12922

Table 13. Relative fluorescent units of sCIR3 samples incubated with SPE7 Fab over 24 hours.

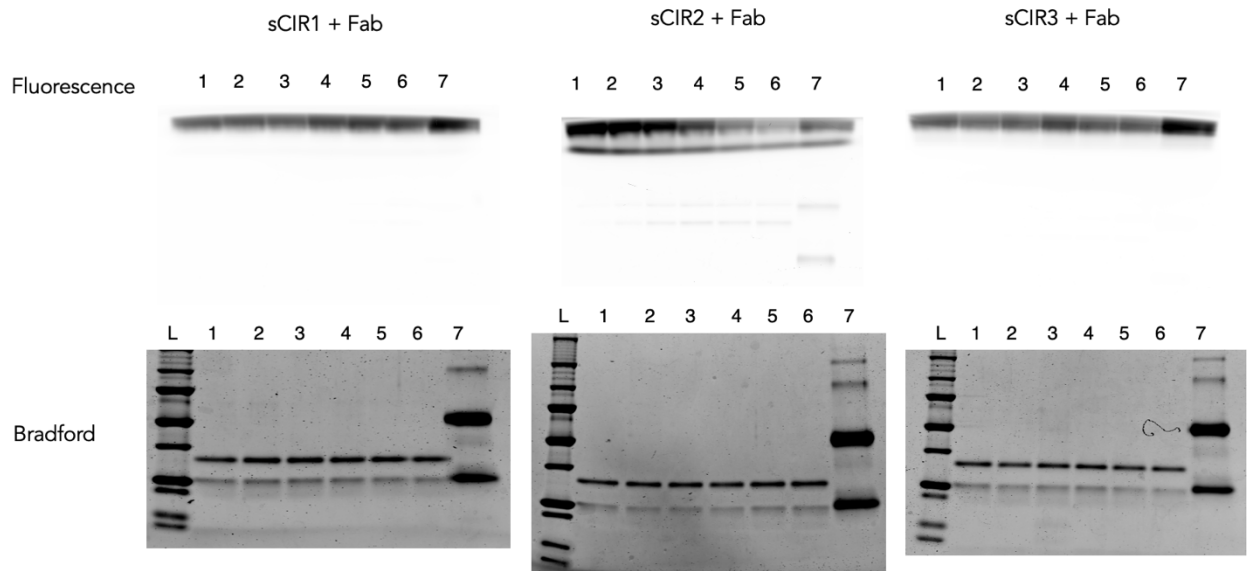


Figure 54. Pre-treatment of DNP-gly with sCIRfluor 1-3 and SPE7 Fab. For both gel 1 and 2, L represents the protein ladder and lanes 1 through 6 are sCIR-Fab samples incubated for 0, 1, 2, 4, 8 and 24 hours, with the isotype control in lane 7.

sCIR4 + SPE7 Fab, Mar 9

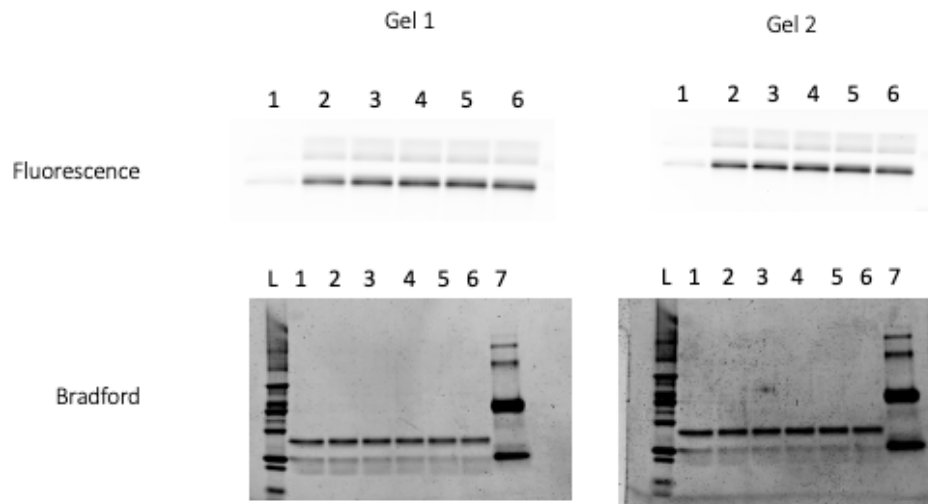


Figure 55. Fluorescent and protein bands of SPE7 Fab incubated with sCIR4.

For both gel 1 and 2, L represents the protein ladder and lanes 1 through 6 are sCIR-Fab samples incubated for 0, 1, 2, 4, 8 and 24 hours, with the isotype control in lane 7.

Time (h)	RFU	
0	1882.826	2180.149
1	14901.005	17499.811
2	19174.984	20466.873
4	19730.53	22110.719
8	19965.78	22750.129
24	19050.358	21030.05

Table 14. Relative fluorescent units of sCIR4 samples incubated with SPE7 Fab over 24 hours.

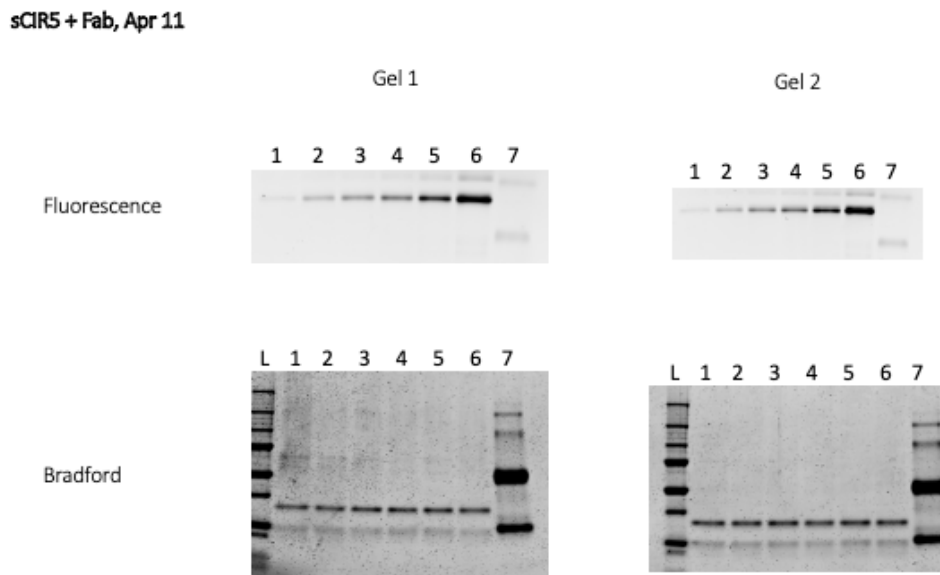


Figure 56. Fluorescent and protein bands of SPE7 Fab incubated with sCIR5. For both gel 1 and 2, L represents the protein ladder and lanes 1 through 6 are sCIR-Fab samples incubated for 0, 1, 2, 4, 8 and 24 hours, with the isotype control in lane 7.

Time (h)	RFU
----------	-----

0	552.606	559.41
1	824.268	788.986
2	1155.62	1052.841
4	1413.291	1305.119
8	2207.866	2059.439
24	4689.258	4450.022

Figure 57. Relative fluorescent units of sCIR3 samples incubated with SPE7 Fab over 24 hours.

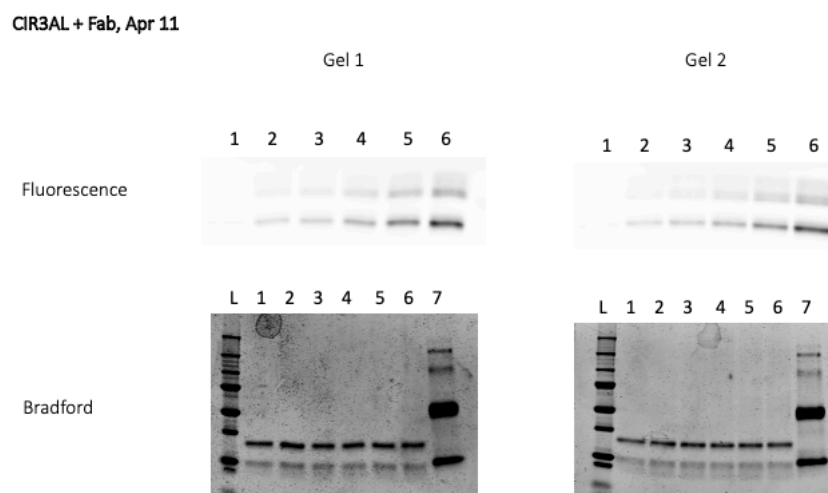


Figure 58. Fluorescent and protein bands of SPE7 Fab incubated with CIR3AL. For both gel 1 and 2, L represents the protein ladder and lanes 1 through 6 are sCIR-Fab samples incubated for 0, 1, 2, 4, 8 and 24 hours, with the isotype control in lane 7.

Time (h)	RFU	
0	0	0
1	2883.619	2888.422
2	4231.821	3878.406
4	6314.939	6386.146
8	10453.849	10934.571
24	18498.242	18232.283

Table 15. Relative fluorescent units of CIR3AL samples incubated with SPE7 Fab over 24 hours.

8.3.2. Intermolecular rate constants

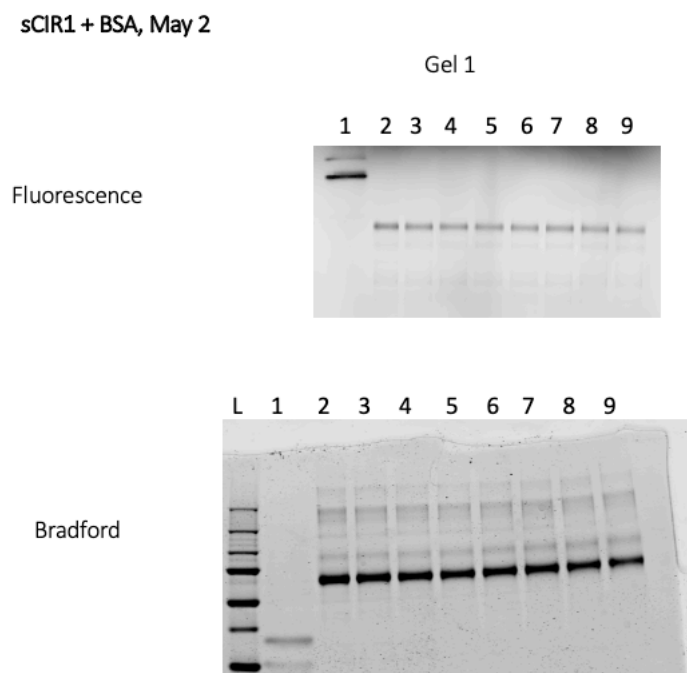


Figure 59. Fluorescent and protein bands of BSA incubated with sCIR1. In the gel L represents the protein ladder, lane 1 contains isotype IgG control, and lanes 2 through 9 are sCIR-Fab samples incubated for 24 hours, 48 hours in duplicate, 72 hours in duplicate, 96 hours, and 120 hours, in order.

Time (h)	RFU	
24	2348.377	
48	2233.79	2196.489
72	2216.057	2005.275
96	2122.722	
120	2153.685	2050.701

Table 16. Relative fluorescent units of sCIR1 samples incubated with BSA over 24 hours.

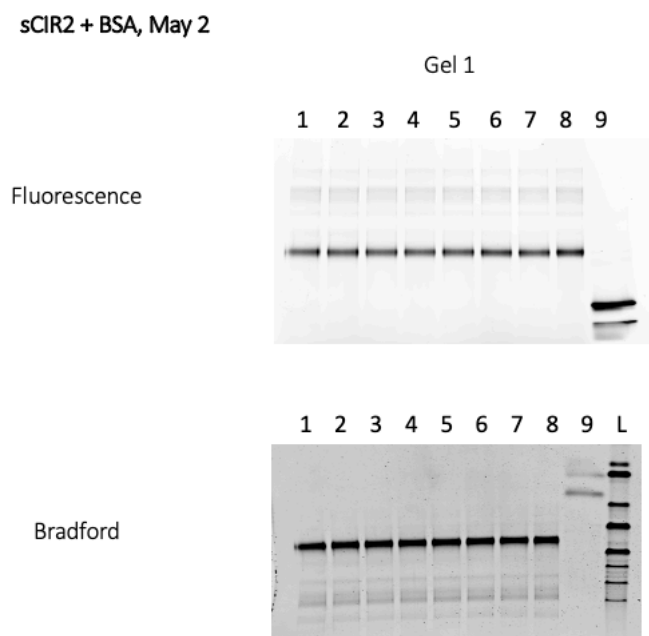


Figure 60. Fluorescent and protein bands of BSA incubated with sCIR2. In the gel L represents the protein ladder, lane 9 contains isotype IgG control, and lanes 1 through 8 are sCIR-Fab samples incubated for 24 hours, 48 hours in duplicate, 72 hours in duplicate, 96 hours, and 120 hours, in order.

Time (h)	RFU	
24	3864.004	
48	3543.19	3718.663
72	3514.766	3308.193
96	3374.625	
120	3625.111	3347.616

Table 17. Relative fluorescent units of sCIR2 samples incubated with BSA over 24 hours.

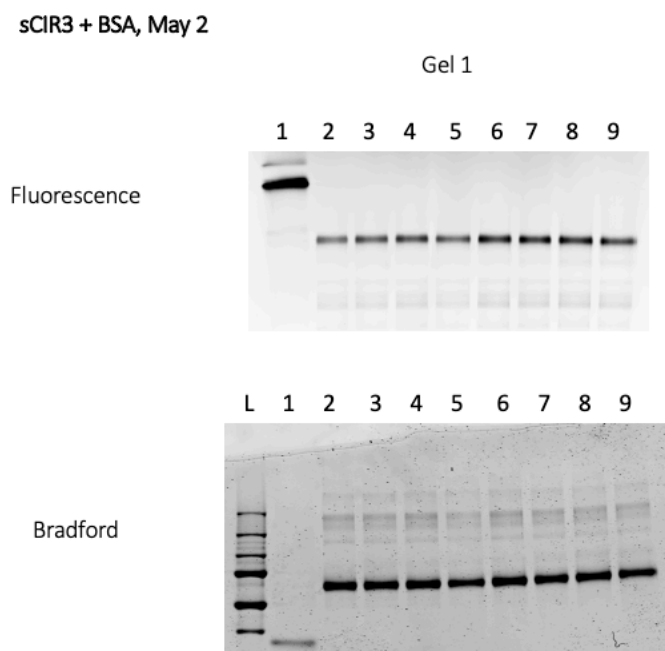


Figure 61. Fluorescent and protein bands of BSA incubated with sCIR3. In the gel L represents the protein ladder, lane 1 contains isotype IgG control, and lanes 2 through 9 are sCIR-Fab samples incubated for 24 hours, 48 hours in duplicate, 72 hours in duplicate, 96 hours, and 120 hours, in order.

Time (h)	RFU	
24	3153.592	
48	4200.22	3778.477
72	5009.671	3733.043
96	4968.803	
120	4536.932	5230.023

Table 18. Relative fluorescent units of sCIR3 samples incubated with BSA over 24 hours.

sCIR4 + BSA, May 2

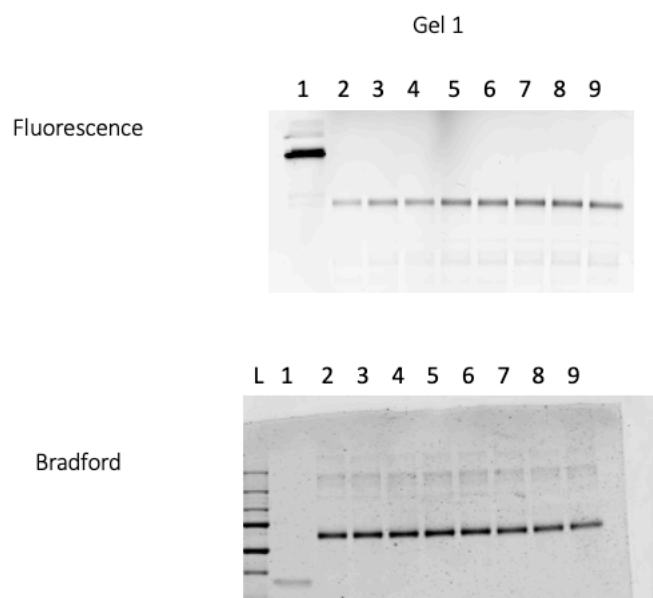


Figure 62. Fluorescent and protein bands of BSA incubated with sCIR4. In the gel L represents the protein ladder, lane 1 contains isotype IgG control, and lanes 2 through 9 are sCIR-Fab samples incubated for 24 hours, 48 hours in duplicate, 72 hours in duplicate, 96 hours, and 120 hours, in order.

Time (h)	RFU	
24	1027.271	
48	1521.732	1472.804
72	2018.173	2077.078
96	2237.858	
120	1964.633	2226.491

Table 19. Relative fluorescent units of sCIR4 samples incubated with BSA over 24 hours.

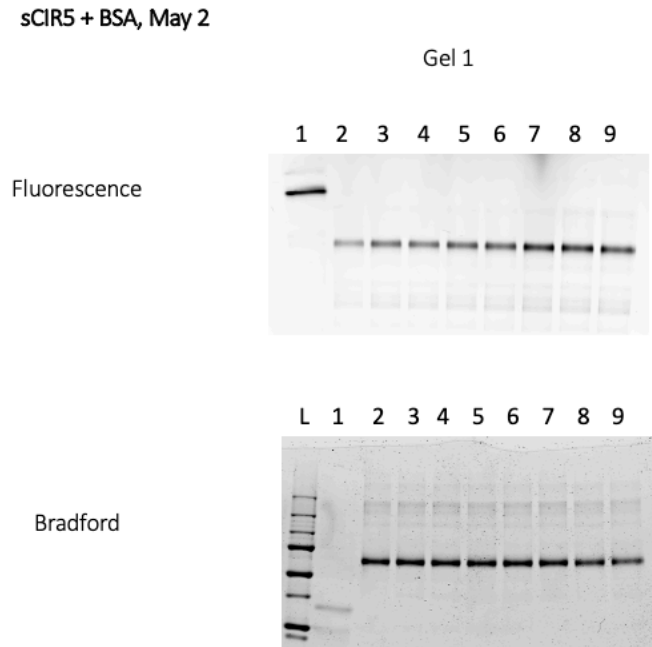


Figure 63. Fluorescent and protein bands of BSA incubated with sCIR5. In the gel L represents the protein ladder, lane 1 contains isotype IgG control, and lanes 2 through 9 are sCIR-Fab samples incubated for 24 hours, 48 hours in duplicate, 72 hours in duplicate, 96 hours, and 120 hours, in order.

Time (h)	RFU	
24	2048.254	
48	3164.528	3040.656
72	3593.691	3825.591
96	5091.643	
120	4899.614	4256.117

Table 20. Relative fluorescent units of sCIR5 samples incubated with BSA over 24 hours.